Guilherme Barreto Arez Coelho

Master in Civil Engineering

Optimization of historic buildings that house artefacts considering climate change

Thesis to obtain the Doctor degree in

Civil Engineering

Supervisor:	Doctor Fernando Manuel Anjos Henriques, Full Professor, FCT-UNL
Co-supervisor:	Doctor Vasco Manuel Araújo Peixoto de Freitas, Full Professor, FEUP

Jury:

President:	Doctor Paulo da Fonseca Pinto, Full Professor, FCT-UNL
Rapporteurs:	Doctor Nuno Manuel Monteiro Ramos, Associate Professor, FEUP
	Doctor Daniel Aelenei, Associate Professor, FCT-UNL
Members:	Doctor Vasco Manuel Araújo Peixoto de Freitas, Full Professor, FEUP
	Doctor Eva Sofia Botelho Machado Barreira, Assistant Professor, FEUP
	Doctor Maria Paulina Santos Forte de Faria Rodrigues, Associate Professor, FCT-UNL
	Doctor Luís Gonçalo Correia Baltazar, Assistant Professor, FCT-UNL

FACULDADE DE CIÊNCIAS E TECNOLOGIA
UNIVERSIDADE NOVA DE LISBOA

December 2020

[Optimization of historic buildings that house artefacts considering climate change]

“Now this is not the end. It is not even the beginning of the end.

But it is, perhaps, the end of the beginning.”

Winston Churchill, November 10, 1942

ACKNOWLEDGEMENTS

A thesis is the responsibility of its author. However, the development of a work of this magnitude is not possible without the help and support of others, whom I would like to thank in the following paragraphs.

Firstly, I would like to thank Professor Fernando Henriques for his supervision of this thesis. I was able to achieve the outlined objectives for this thesis with the help of his pragmatic and constructive observations and comments. Although some might find them demanding, I found them to be very insightful and useful. Hence, the quality of the work presented in this thesis is greatly influenced by him. I would also like to thank his guidance, which started back in 2015 with my master's dissertation and continued to this thesis. I would like to thank him for all his support through this extremely interesting learning period and, at the same time, giving me space to learn and grow. Thank you for believing in me and helping me find my calling.

Secondly, I would like to thank my co-advisor Professor Vasco Peixoto de Freitas for his guidance and advice whenever I needed. I would also like to thank Professor Vasco Peixoto de Freitas for the comments that he made about the work presented here, which greatly helped the development of this document. Finally, I would also like to thank Professor Vasco Peixoto de Freitas for his mentorship and companionship during our visit to Prague for the CESBP conference in 2019, which greatly influenced some sections of this thesis.

Thirdly, I would like to thank Hugo Silva for all the discussions and moments shared through this period of time, but more vividly on its first half. I would also like to thank him the thorough revisions that he did on the work that I prepared, which positively influenced the quality of the work presented here.

Fourthly, I would like to thank the Department of Civil Engineering of the Faculty of Science and Technology for the support provided throughout the preparation of this thesis, more specifically Professor Paulina Faria, Professor Daniel Aelenei and Professor Luís Baltazar. I would also like to thank the support provided by Vítor Silva in the maintenance visits of the monitoring campaign installed in the Jerónimos Monastery and during the experimental works carried out in the laboratories of the department. I would also like to thank Maria da Luz for her assistance with the bureaucracy that I had to deal with during this thesis. Finally, I would like to thank Professor Corneliu Cismasiu for letting me use laboratory 3.14 in DEC, which greatly helped running a great number of simulations in a much shorter period of time.

I would also like to thank the thorough work performed by the reviewers of the manuscripts that I authored or co-authored. I do not know who they are, but their contribution greatly improved the submitted work.

I would like to thank the group of doctoral students from the Civil Engineering Department of FCT for the support and companionship shown throughout this thesis, namely David Manta, Nuno Peres, Naim Majdalani Alexandre Nunes and Gustavo Filipe. I would also like to thank my office colleague, Sara Coimbra for the countless conversations we had concerning building physics. I would also like to thank the friendship shown by “Lisbon's greatest supportive” David Henriques. Finally, I would like to thank all the friendship shown by Hugo Rebelo, who was also doing his PhD thesis at the same time as me, and all the support that he provided

with MATLAB, which greatly helped the development of the final section of this thesis.

I would like to thank the warm welcome I was received during my stay at FEUP in 2017 by the LFC doctoral group as well as during our visit to Prague for the CESBP 2019 conference, Francisca Barbosa, Sílvia Magalhães, Cláudia Ferreira, Mafalda Amorim, Pedro Pereira and Sara Freitas. A special thanks to Teresa Freitas, who was preparing her PhD research when I arrived at FEUP, and who greatly and readily help me with so many things during my stay. I also take the opportunity to thank Professor Ana Guimarães, Professor Eva Barreira and Professor Ricardo Almeida for the companionship shown during CESBP 2019.

I am also grateful to the Foundation for Science and Technology (FCT) for the financial support provided in the form of a doctoral scholarship under the reference PD/BD/127844/2016. I also would like to acknowledge the scientific committee of the doctoral program Eco-CoRe for creating this doctoral program. I also would like to thank the World Monuments Fund (Portugal) and the administrative services of the Mosteiro dos Jerónimos, for their support during the maintenance visits of the monitoring campaign installed in the Church of Santa Maria de Belém, Lisbon. Finally, I also thank the Portuguese Institute for the Sea and Atmosphere, I.P. (IPMA, IP) for providing Lisbon's climate data.

I thank my family for all the support and affection that I felt through my life. In particularly, I would like to thank my brother for the friendship and companionship shared over all these years, but also for showing me the advantage of having an enormous willpower, professionalism, and the meaning of perseverance. To my father, for the example that he has been through all my life, and for showing me that, despite the countless obstacles that life presents us, one should never give up learning. Finally, I would like to thank my mother, for everything that she has done for me over all these years. For her tireless support through my long school life, which of course includes this thesis. Much of what I am today I owe to her.

I also thank my group of long-time friends who helped me manage when work became "too much to handle", namely Carolina Alves, Bruno Lopes, Filipe Franco, Hugo Baldinho, João Arrojado, José Oliveira, J. Diogo Casquinho, Mariana Martins, Noemi Viegas, Nuno Delgado, Nuno Leonardo, Ruben Correia, Raúl Alves, Raquel Fidalgo, Sílvia Costa, and all the others.

Finally, a special thanks to my wife and long-time friend Inês, for all her patience, dedication, motivation and support throughout the course of this thesis.

I dedicate this work to my family,

but specially to my mother, father and grandfather who

showed me the importance of continuously pursuing knowledge.

ABSTRACT

Historic buildings, and the artefacts that are usually kept within these buildings, are a living representation of the past and it is essential to ensure that future generations have access to this heritage. In order to accomplish this, it is necessary to determine the conditions that the buildings are in and, if needs be, to make the required changes in order to preserve our cultural heritage. In addition, the foreseen changes of the indoor climate caused by climate change can endanger the preservation of these artefacts, since they are prone to various types of decay depending on the existing indoor conditions.

One way of counteracting these changes, is the application of passive retrofit measures. However, the guideline was that retrofit measures were hardly ever used in cultural heritage because they could cause the building to lose its authenticity. Nowadays, more and more cases of historic buildings are subject to this type of measures. Indeed, these measures can lead to positive outcomes, such as decreasing the energy consumption of the buildings or mitigating the effects of climate change, but the welfare of the cultural heritage must be ensured before these measured can be applied.

Hence, the main aim of this thesis is to determine the potential of passive retrofit measures in mitigating the negative effects of climate change in the indoor climate of historic buildings, whilst accounting for the artefacts' preservation requirements. For this reason, the indoor climate of a 13th century church in Lisbon was used to develop and validate a whole-building hygrothermal model. Then, the model was run using future weather files to determine the future indoor conditions, which were then assessed using a risk-based analysis and an adaptive thermal comfort model. Finally, the effects of the passive retrofit measures in the building's energy consumption, the artefacts' conservation metrics and the occupants' thermal comfort were assessed.

The future weather files were developed based on the methodology described in standard EN 15927-4 and in *Skartveit and Olseth* model, which divides the global radiation into its direct and diffuse components. In addition, a methodology that aims to make large-sized hygrothermal studies more time-efficient is also presented. This methodology was based in the studies developed in this thesis.

It was shown that the conditions for the preservation of artefacts that are housed in historic buildings will worsen, especially in Mediterranean climates when compared to humid Continental and Oceanic climates. The tested retrofit measures can mitigate, up to a certain extent, the negative effects imposed by climate change in terms of artefacts' conservation requirements. However, the Mediterranean climates do not have the same margin as the other tested climates. In addition, it was also shown that there is a positive outcome of implementing these measures in terms of energy saving potential. These savings will even be higher if these measures are combined with a more adequate relative humidity and temperature setpoint strategy.

Keywords: Cultural heritage, Preventive conservation, Climate change, Computational simulation, Passive retrofit measures

RESUMO

Os edifícios históricos, e os artefactos que geralmente são guardados no interior destes edifícios, são uma representação viva do passado e é fundamental garantir que as gerações futuras também têm acesso ao património cultural. Para isso, é necessário determinar as condições interiores destes edifícios e, se necessário, aplicar as alterações necessárias de forma a promover a preservação do património. Além disso, as mudanças expectáveis dos climas internos causadas pelas alterações climáticas podem pôr em risco a preservação destes artefactos, uma vez que estes são propensos a vários tipos de deterioração consoante as condições internas.

Uma forma de combater as mudanças expectáveis do clima interior deste tipo de edifico é a aplicação de medidas de reabilitação passivas. No entanto, era prática comum a sua aplicação em edifícios históricos ser muito restrita, uma vez que podiam provocar a perda de autenticidade destes edifícios. Actualmente é cada vez mais usual a aplicação destas medidas, que podem ter resultados bastante positivos, como a diminuição do consumo de energia dos edifícios ou a mitigação dos efeitos das alterações climáticas. No entanto, é necessário garantir que o património não sofre danos com a sua aplicação.

O principal objectivo desta tese é determinar o potencial de mitigação dos efeitos negativos impostos pelas alterações climáticas no clima interior de edifícios históricos através do recurso a medidas de reabilitação passivas, tendo em conta os requisitos de preservação dos artefactos. Por este motivo, o clima interno de uma igreja do século XIII em Lisboa foi utilizado para desenvolver e validar um modelo higrotérmico. Numa fase subsequente o modelo foi corrido para ficheiros climáticos futuros de forma a determinar as condições internas futuras, que foram avaliadas recorrendo a uma análise de risco e a um modelo de conforto térmico adaptável. Por fim, foi avaliado o efeito das medidas de reabilitação passivas no consumo de energia do edifício, nas métricas de conservação dos artefactos e no conforto térmico dos ocupantes do edifício.

Os ficheiros climáticos futuros foram construídos com base na metodologia descrita na norma EN 15927-4 e no modelo *Skartveit and Olseth*, que permite subdividir a radiação global na componente directa e difusa. É também apresentada uma metodologia que visa tornar os estudos higrotérmicos com inúmeros casos mais eficiente em termos temporais. Esta metodologia baseou-se estudos desenvolvidos nesta tese de doutoramento.

Ficou demonstrado que as condições de preservação de artefactos guardados no interior de edifícios históricos vão piorar, especialmente em climas mediterrâneos quando comparados com climas húmidos continentais e oceânicos. As medidas de reabilitação passivas testadas podem mitigar, até certo ponto, os efeitos negativos provocados pelas alterações climáticas em termos de conservação de artefactos. No entanto, os climas mediterrâneos não têm a mesma margem que os outros climas testados. Além disso, também foi demonstrado que a implementação destas medidas apresenta um resultado positivo em termos de poupança energética. No entanto, esta poupança será ainda maior se estas medidas forem combinadas com uma estratégia de controlo de temperatura e humidade relativa mais adequada.

Palavras-chave: Património cultural, Conservação preventiva, Alterações climáticas, Simulações computacionais, Medidas de reabilitação passivas

INDEX OF CONTENTS

INDEX OF FIGURES

INDEX OF FIGURES – ANNEX

INDEX OF TABLES

INDEX OF TABLES – ANNEX

NOMENCLATURE AND ABBREVIATIONS

Roman-letter nomenclature

A – Solar azimuth angle (º)

ACH – Air change rate (h^{-1})

c_p – Specific heat capacity, Dry (J/kg.K)

$CV(RMSE)$ – Coefficient of variation of the root mean square error (%)

C_i – Total amount of moisture in zone i (kg)

c_{ext} – External gas concentration (ppm)

c_{int} – Internal gas concentration (ppm)

d – Diffuse fraction (-)

E – Emissivity (-)

Ea – Activation energy (kJ/mol)

eLM – Equivalent Lifetime Multiplier (-)

F_f – Frame factor (-)

Fit – Goodness of fit (%)

G – Rate of the generated gas in the room (m^3/s)

G_{SC} – Solar constant (1367 W/m^2)

g_T – Solar heat gain coefficient (-)

H_i – Total enthalpy in zone i (J)

H_g – Surface global irradiance (W/m^2)

H_{ex} – Extraterrestrial global irradiance (W/m^2)

h – Solar elevation angle (º)

LM – Lifetime multiplier (-)

k – Clearness index (-)

k_1 – Cloudless clearness index (-)

M_w – Molar mass of water (kg/mol)

n – Total number of points across the studied time period or nth day of the year (depending on the equation)

$NMBE$ – Normalized mean bias error (%)

P_v – Water-vapour partial pressure (Pa)

Q – Air volume flow rate through the enclosure (m^3/s)

$\dot{Q}_{Comp,j}$ – Amount of heat that goes through the inner surface of component j into zone i (W)

$\dot{Q}_{HVAC}$ – Amount of heat due to mechanical ventilation (W)

$\dot{Q}_{in}$ – Convective heat sources in zone *i* (W)

$\dot{Q}_{Sol}$ – Amount of short-wave radiation goes through the transparent component into zone *i* (W)

$\dot{Q}_{vent}$ – Amount of heat due to natural ventilation (W)

R – Gas constant (8.314 J/K.mol)

R^2 – Coefficient of determination (-)

RH – Relative humidity (%)

s – Capillary pressure (Pa)

T – Temperature (ºC or K, depending on the equation)

t – Time (s)

U-value – Thermal transmittance (W/m^{2}K)

Uw – Window thermal transmittance (W/m^{2}K)

V – volume of the room (m^3)

w – Water content (kg/m^3)

$\dot{W}_{Comp,j}$ – Moisture flux that goes through the *j* component surface into zone *i* (kg/s)

$\dot{W}_{HVAC}$ – Moisture flow due to mechanical ventilation (kg/s)

$\dot{W}_{in}$ – Moisture production in zone *i* (kg/s)

$\dot{W}_{vent}$ – Moisture flow due to natural ventilation (kg/s)

$X_{i,meas}$ – Measured value of the hygrothermal parameter at the time period *i*,

$X_{i,sim}$ – Simulated value of the hygrothermal parameter at the time period *i*

z – Solar zenith angle (º)

Greek-letter nomenclature

α – Short-wave radiation absorption (-)

σ_3 – Hourly variability index (-)

ε – Porosity (m^3/m^3)

λ_0 – Thermal conductivity, Dry (W/m.K)

μ – Water-vapour diffusion resistance factor (-)

ρ – Bulk density (kg/m^3)

ρ_i – Clear sky index for timestep *i* (-)

ρ_{i-1} – Clear sky index for the timestep prior to *i* (-)

ρ_{i+1} – Clear sky index for the timestep after *i* (-)

φ – Relative humidity (-)

Abbreviations

ASHRAE – American Society of Heating Refrigerating and Air-Conditioning Engineers

AR4 – Fourth Assessment Report

AR5 – Fifth Assessment Report

CCT – Correlated Colour Temperature

CORDEX – Coordinated Regional Climate Downscaling Experiment

CPA08 – Statistical Classification of Products by Activity in the European economic community (2008version)

CRI – Colour Rendering Index

EPS – Expanded polystyrene

EU – European Union

FEMP – Federal Energy Management Program

GCM – Global Climate Model

Gf – Geofísico

GHG – Greenhouse Gas

GDP – Gross Domestic Product

HAM – Heat, Air and Moisture modelling

HMAT – Combine Heat and Moisture Finite Element

HVAC – Heating, Ventilation and Air Conditioning

IEA – International Energy Agency

IM – Meteorological Institute (Instituto de Meteorologia)

IPMA – Portuguese Institute for Sea and Atmosphere (Instituto Português do Mar e da Atmosfera)

IPCC – Intergovernmental Panel on Climate Change

IPI – Image Permanence Institute

IPMVP – International Performance Measurement and Verification Protocol

IR – Infrared radiatian

LED – Light-Emitting Diodes

LIM – Lowest Isopleth for Mould

mae – Mean Absolute Error

mse – Mean Square Error

MRF – Mould Risk Factor

MNAA – National Museum of Ancient Art (Museu Nacional de Arte Antiga)

NOAA ESRL – National Oceanic and Atmospheric Administration Earth System Research Laboratories

OECD – Organisation for Economic Co-operation and Development

PCA – Principal Component Analysis

PI – Performance index

PUR – Polyurethane

RCM – Regional Climate Model

RCP – Representative Concentration Pathway

St-Ch – St. Cristóvão church

SPM – Summary for Policymakers

SRES – Special Report on Emission Scenarios

TAR – Third Assessment Report

US – United States

UTC – Coordinated Universal Time

UV – Ultraviolet radiation

WMO – World Meteorological Organization

XPS – Extruded polystyrene

Chemical compounds

CH_3COOH – Acetic acid

CH_4 – Methane (*$TgCH_4/yr$* for emissions and *ppb* for atmospheric concentrations)

CO_2 – Carbon dioxide (*GtC* or *PgC* for emissions and *ppm* for atmospheric concentrations)

He – Helium

H_2S – Hydrogen sulphide

NO_2 – Nitrogen dioxide ($\mu g/m^3$)

N_2O – Nitrous oxide

O_3 – Ozone ($\mu g/m^3$)

$PM_{2.5}$ – Fine particles ($\mu g/m^3$)

PM_{10} – Coarse particles ($\mu g/m^3$)

SF6 – Sulphur hexafluoride

SO_2 – Sulphur dioxide ($\mu g/m^3$)

1. INTRODUCTION

1.1. Research motivation and background

Historic artefacts are a pillar of society since they are a "living" representation of the past and, therefore, have great heritage value, which makes them irreplaceable. In addition, so that future generations also have access to these priceless objects, it is necessary to ensure that the interior climate of the buildings that house them is adequate in terms of conservation.

Usually, these objects are housed in museums, libraries, archives, churches and galleries. In most cases these buildings are classified as historic buildings, which means that they have their own history and can have great heritage value. For example, the *National Museum of Ancient Art* (MNAA), which holds the largest collection of ancient art in Portugal nowadays, is installed, since its creation in 1884, in the old Alvor palace built in the 17th century at the bidding of the first Count of Alvor after his return from India. Due to their heritage value there is an additional difficulty to ensure the quality of the indoor climate since they are protected by law, but also because most of these buildings were not initially built to exhibit or store artefacts. Hence, they had to go through adaptations over the years to fulfil the required conditions to host artefacts. Nonetheless, these changes should be thoroughly analysed prior to application.

It is also important to highlight the great heritage value of most historic buildings, which sometimes makes them the most valuable component of the collection. Hence, it is necessary to ensure that the present use of these buildings, such as the number of people associated to mass tourism, does not damage their state of preservation. Additionally, it is expected that climate change will worsen the capacity of the indoor climate to preserve artefacts adequately, as well as cause the deterioration of historic buildings. Thus, this study is a relevant matter so that preventive conservation is promoted.

However, due to the complexity of all these concerns, they must be addressed individually. First, it is necessary to check if the current indoor conditions are harmful or not to the housed collection. This step can be performed using a risk-based analysis, which depending on the type of housed collection, checks the risk of mechanical, chemical and biological decay occurring dependent on the indoor conditions. The driving forces of these three processes are relative humidity and temperature, which can be determined through a multi-sensor and long-term monitoring campaign.

Secondly, and if the indoor conditions are harmful to the collection's welfare, it is necessary to implement measures so that the indoor climate becomes suitable to house the collection. In addition, bearing in mind that this type of building is protected by law, a thorough analysis of the effects on the indoor climate in terms of conservation metrics, thermal comfort and energy consumption must be performed prior to the application of any type of measure. Furthermore, due to the already mentioned negative effects of climate change, it is also interesting to analyse the effects that the selected retrofit

measures will have in the future, since although the retrofit measure might not be necessary nowadays, they can become necessary in the future, or even to optimize the select retrofits to future needs.

This complex analysis can be developed using a whole building hygrothermal model of the case-study. However, in order to be reliable, the model has to be thoroughly validated against the measured indoor conditions. The validation of this type of models is a highly time-consuming process, mostly due to the lack of information regarding the materials and techniques used to construct the case-study, but also due to the large number of inputs necessary to build a reliable model (e.g. current outdoor weather conditions, building geometry and respective building element hygrothermal characteristics, internal gains loads and respective schedules, natural and mechanic ventilation, among others). Nonetheless, it is possible to develop such models for historic buildings resorting to the help of a sensitivity analysis.

The main research gaps detected from a literature review carried out concerning the hygrothermal behaviour of historic buildings with high thermal inertia that house artefacts are presented in the following bullet list. Nonetheless, other minor research gaps are mentioned throughout this thesis.

- There is a wide gap in the knowledge regarding the hygrothermal behaviour of high thermal inertia buildings that house artefacts, mainly for temperate climates (e.g. Lisbon's climate), since most of the existing studies deal with case-studies situated in humid continental climates.
- The validation of many whole-building thermal and hygrothermal models in literature is to some extent lax, since some of the authors validate the models in relation to short-term monitoring, others authors use statistical parameters to assist in the model's validation process that are not adequate; and most of the times the soil/slab interface temperature is a parameter that is not mentioned in many of the hygrothermal models in literature, among other shortcomings.
- The effects of climate change in the indoor climate of historic buildings in terms of its influence in the artefacts' conservation metrics, the visitors' thermal comfort and the buildings' energy consumption has not been addressed sufficiently in literature.
- The potential of passive retrofit measures to improve the indoor climate in terms of thermal comfort and conservation metrics, as well as to decrease the building's energy consumption, whilst taking into account the changes due to climate change has not been sufficiently studied in historic buildings that house artefacts.

1.2. Research aims

This research intends to develop even further the existing knowledge concerning the hygrothermal behaviour of buildings with high thermal inertia. It also aims to develop a methodology that selects the most appropriate retrofit measures for historic buildings that house artefacts. This methodology will take into account the three key parameters that affect the management of this type of buildings, namely the artefacts' conservation metrics, the visitors' thermal comfort and the building's energy consumption. Furthermore, this methodology will also take into account the changes that the indoor climate is going

to suffer in the future due to the negative influence of the anthropogenic greenhouse gases emissions. Ultimately, this option will allow to plan the best course of action for these buildings.

Considering all these goals, the development of a reliable whole-building hygrothermal model of a historic building was defined as a priority. This option is mostly due to the uniqueness of each historic buildings, which is why they are protected under-law, and enforces the concept that any type of change that is seen fit to be apply to this type of buildings, such as increasing the number of visitors substantially or installing a new ventilation system, needs to be thoroughly analysed first, and only if the outcome of this analysis is positive, can it be applied to the building. The use of a validated whole-building hygrothermal model allows to perform this type of analysis with great detail without jeopardizing the building itself, because it is based on a non-intrusive methodology, i.e. it measures the indoor conditions using multiple sensors and uses the recorded data to develop the building's model.

However, the model's reliability is extremely dependent on the robustness of the validation process. Hence, these models are developed based on extensive monitoring campaigns that measure indoor conditions. Subsequently, the gap between the measured and simulated indoor conditions is shortened using several statistical that analyse the difference. These models can analyse most of the parameters that influence the hygrothermal behaviour of a building, such as the substantial increase of visitors, the effect of climate change, indoor temperature and relative humidity setpoints that account for outdoor conditions, and the use of historic buildings to house and store artefacts, among many others. For this reason and for the fact that it does not jeopardize the welfare of the buildings, it is clear the usefulness of these models. Nonetheless, their development is a challenging endeavour.

The case-study selected for this research was St. Cristóvão church in Lisbon, which is a good example of a high thermal inertia building due to its thick limestone walls and low window/wall area ratios. In addition, the building is naturally ventilated and does not have any type of climate control system, which are important facts because they reduce the uncertainty associated to the model's validation process considerably, since most of the software cannot account for the precise influence of the climate control systems. The variability of both the indoor conditions and the outdoor conditions in the vicinity of the church were already determined using a long-term and multi-sensor monitoring campaign, namely in terms of air temperature and relative humidity.

In order to identify the most appropriated adaptations for this type of buildings it is helpful to first determine how the outdoor conditions are going to change in the future. This was already determined by the many developed future scenarios that encompass the *Intergovernmental Panel on Climate Change* (IPCC) assessment reports, which are continuously being updated due to the ever-new knowledge reached by the scientific community. Secondly, it is important to determine how the indoor climate of historic building will change, so that truly useful adaptations can be implemented. This can be determined using a validated hygrothermal model of a case-study coupled to the respective future

weather file, which are based on previously mentioned future scenarios. Nonetheless, the variability of both the indoor and outdoor conditions should be assessed and quantified using statistical parameters, because it allows to explain why certain indoor hygrothermal behaviours will occur in these buildings.

In addition, the future indoor conditions can also be used to assess how the artefacts' conservation metrics, the visitors' thermal comfort and the building's energy consumption are going to evolve in the future, whilst taking into account the international standards and guidelines that preconize the ranges of the indoor conditions that mitigate the risks of artefacts decay. Analysing the evolution of these three key parameters will greatly help the search for the most appropriate adaptations for this type of buildings. Whilst the artefacts conservation metrics must be assessed using a risk-based analysis, the thermal comfort can be assessed either using an analytical model, or an adaptive method, but both parameters depend on the indoor conditions.

Passive retrofit measures can have a great potential to mitigate the effects of climate change on the indoor climate. To select the most adequate retrofit measures for each case-studied, whilst taking into account climate change and the three previously stated parameters, it will be necessary to test repeatedly.

Based on the many hygrothermal simulations performed to achieve the aims of this thesis, which took a large amount of time to perform, a methodology that makes large sized hygrothermal studies more time-efficient is presented. This methodology is based on several techniques that reduce the time consumed to either prepare the simulations, run the simulations or process the obtained results.

In summary, the main aim of this thesis is to determine the potential that passive retrofit measures have in mitigating the negative effects of climate change in the indoor climate of historic buildings that house artefacts. As consequence of the developed work, a whole-building hygrothermal model for a 13th century church was developed and validated against its measured indoor conditions, a fast and reliable methodology to build weather files was created in MATLAB and a methodology that considerably reduces the time spent to perform large-sized hygrothermal studies was developed.

1.3. Thesis layout

This thesis is organized in eight chapters, including the present chapter that outlines the research motivation and background, as well as its main aims. The remaining chapters will be briefly presented.

The second chapter, named *Literature review,* consists of a brief overview of the challenges that this research aims to address. Secondly, the climate monitoring procedures, the climate conservation and thermal comfort tools, as well as the indoor climate limiting standards for cultural heritage are addressed. Thirdly, the assumptions behind the climate change IPCC scenarios are addressed. Finally, several of the monitoring campaigns of historic buildings that exist in literature are reviewed, as well as the application of passive retrofit measures to improve the indoor climate of historic buildings.

The third chapter, named *Whole-building hygrothermal modelling using WUFI,* consists of a more

detailed review of the WUFI software, namely the necessary outdoor weather file, the building materials properties and the considered internal gains. In addition, the validation work that the software has been through over the years, as well as the software disadvantages are addressed. Finally, a review of the statistical parameters mainly used to help in the development of computational models is performed. A methodology that reduces the time spent to perform large sized hygrothermal studies is presented.

The fourth chapter, named *Validation of hygrothermal models of historic buildings*, establishes a validation process for historic buildings based on annual indoor conditions using a simulation software. The indoor conditions of a 13th century church in Lisbon were used. i.e. St. Cristóvão church. The model accuracy was assessed by comparing the simulated and measured temperature and water-vapour pressure, and quantified using the coefficient of determination, coefficient of variation of the root mean square error, normalized mean bias error and goodness of fit. In addition, a simplified model was developed using tested simplifications in order to decrease the simulation time significantly.

The fifth chapter, named *Impact of climate change on artefacts kept in cultural heritage buildings and the thermal comfort of the visitors*, studies the effects of climate changes on the free floating indoor climate of heritage buildings and on the conservation of artefacts and thermal comfort of visitors. For this purpose, the validated hygrothermal model of St. Cristóvão church in Lisbon coupled with climate change weather files was used to obtain the future indoor conditions. The obtained indoor climates were assessed using a statistical analysis based in several indices, a risk-based analysis and an adaptive thermal comfort model. The simulations were performed for several climate types.

The sixth chapter, named *The Impact of climate change in cultural heritage: from energy consumption to artefacts' conservation and building rehabilitation*, consists of quantifying the energy consumption associated to three different setpoints strategies and respective financial cost, as well as their future trend to demonstrate the positive outcome of passive retrofit measures. These will be responsible for decreasing the building's energy consumption and mitigating the effects of climate change in artefacts' preservation. A validated whole-building hygrothermal model of a historic building coupled to climate change weather files was used to obtain the expected future indoor conditions for three types of climates, which were also assessed using a risk-based analysis.

The seventh chapter, named *Performance of passive retrofit measures for historic buildings that house artefacts viable for future conditions*, consists on the study of the performance of several types of retrofit measures in historic buildings that house artefacts by considering climate change. To accomplish this endeavour, a validate hygrothermal model of a 13th-century church is used coupled with future weather files, which were built using the EN 15927-4 methodology and the *Skartveit and Olseth* model, and a global risk-assessment methodology based on damage functions.

The eighth chapter, named *Conclusions*, lists the main conclusions reached with the research reported in this thesis, as well as presenting some suggestions for future research.

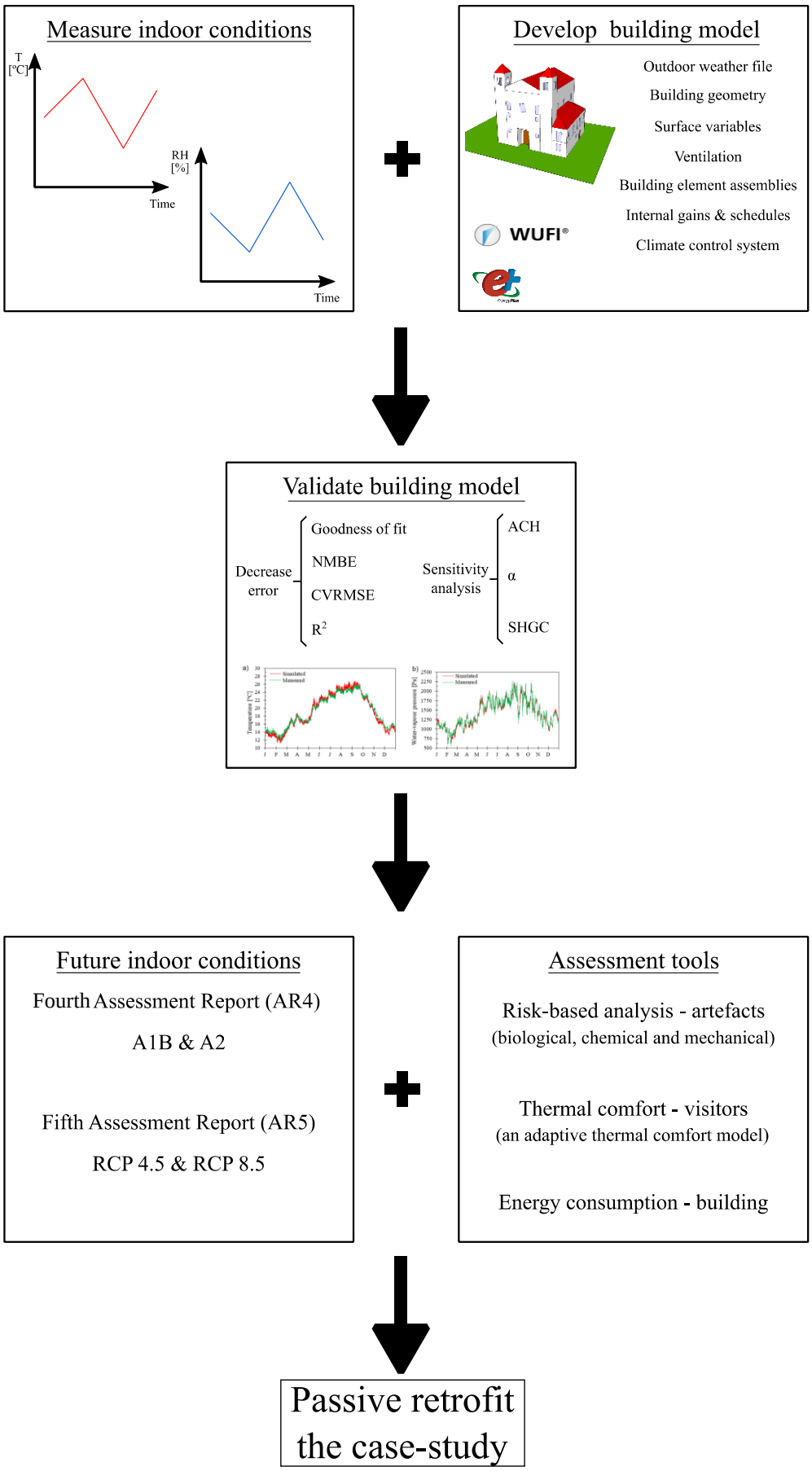

Figure 1.1 – Thesis outline. The measured indoor conditions correspond to the monitoring campaign described in Ref. [250]

2. LITERATURE REVIEW

2.1. Introduction

The deterioration of historic objects is a continuous and irreversible process [136]. In the buildings that exhibit and store such objects, namely, museums, galleries, archives, churches and libraries, it is necessary to ensure certain conditions to delay the deterioration processes, as much as possible. The conditions necessary to preserve the objects vary according not only with each collection, but also within the collection.

Over the past few years, the analysis of the indoor climate of historic buildings for cold climates has increased. Even the European standard that limits the indoor air temperature and relative humidity of buildings that house artefacts was based on studies performed for cold climates [90]. On the other hand, there are few studies that thoroughly analyse the hygrothermal behaviour of historic buildings in temperate climates, when compared with the ones that exist for cold climates [250].

The studies performed in these buildings need to be the less intrusive possible due to their great heritage value. Hence, many of the studies performed nowadays are based on climate monitoring, which normally uses a multi-sensor grid for long periods of time [51]. Subsequently, the indoor climate is assessed using a risk-based analysis, which determines the risk of mechanical, biological or chemical decay depending on the recorded indoor temperature and relative humidity [178].

If the indoor conditions are averse to the preservation of historic artefacts, it is necessary to implement changes that guarantee an adequate indoor climate. However, it must be taken into account that historic buildings are protected by law and any major intervention is always confronted with great opposition. Thus, the selection process of the set of improvement measures that is applied to this type of building is of key importance. The selected set of measures should be subject to a detailed analysis prior to its application, since they can lead to irrecuperable damages if not adequately chosen [224].

This analysis can be performed using hygrothermal models, which have to be thoroughly validated against the measured indoor conditions so that the model's outputs are reliable [66]. These models allow the identification of the consequences of the proposed changes without endangering the welfare of the building, since they are based on a non-invasive procedure, which is a substantial advantage.

For the monitoring campaign to record the variability of the indoor climate in historic buildings, certain requirements have to be ensured. *Camuffo* [51] advocates that the monitoring campaign should have a minimum duration of one complete year to include the seasonal fluctuations in its recordings and, if possible, the monitoring should be extended for another year or two to rule out possible anomalies that might occur during the monitoring period. Hence, the validation of hygrothermal models for this type of buildings should also be based on a long-term period. However, this is not the case for the vast majority of the literature (e.g. [245,104]), thus making it very hard to develop reliable models.

The choice of the statistical parameters used to validate the computational model plays a key role in the model's validation process [195,160]. If the statistical parameters do not represent reality accurately, it

is not possible to converge to a real model. Most of the existing literature either makes a visual comparison between the simulated and measured variable for short durations (e.g. [245]) or uses an insufficient set of statistical parameters (e.g. [58]). The soil/slab interface temperature, which is a parameter that considerably influences the hygrothermal behaviour of a building [66], is also one of the model inputs that is not mentioned in the development of many of the existing models in literature.

The development of reliable hygrothermal models validated by recorded climate conditions from historic buildings allows the analysis of several parameters that influence the building's hygrothermal behaviour, such as: analysing the effect of a set of rehabilitation measures on buildings [108], studying the effects of the climate control strategy [157], identifying the influence of the mechanical ventilation system on the indoor climate [125], studying the effects of moisture buffering materials [15], studying the characteristics of the building's surroundings [31] or assessing the effect of visitors on the building [40]. It is also possible to assess the influence of climate change on the building and, consequently, on the indoor climate [172].

It is important to be aware that the weather conditions will change in the future [132,133], mainly due to anthropogenic contributions of carbon dioxide (CO_2) [196]. Consequently, the indoor climate of historic buildings, which are substantially influenced by the outdoor climate, can undergo significant changes and put artefacts at risk [128,67]. Hence, it is of the utmost importance to analyse the effect of climate change in the artefacts, to find ways to keep both the artefacts and the building safe.

2.2. Indoor climate of historic buildings

This subchapter starts by briefly addressing the main concerns while monitoring the indoor climate of historic buildings. The second subchapter deals with the tools used to assess the quality of the indoor climate in terms of artefact conservation and human thermal comfort. Lastly, the major international standards and guidelines that limit the indoor climate to preserve artefacts are addressed.

2.2.1. Climate monitoring

In order to characterize the indoor climate of a building thoroughly, researchers normally resort to a multi-sensor grid, since they are non-intrusive for the building. In historic buildings, this grid usually monitors at least the indoor temperature and relative humidity, but it can also monitor additional variables, such as the CO_2 concentration (e.g. [274]) or indoor pollutants (e.g. [53]), among others. However, several aspects have to be taken into account to make an adequate record.

In a monitoring campaign the position of the sensors must be carefully chosen in order to accurately explain the indoor climate differences both in plan as in height. In addition, their location must be out of the influence of unwanted sources, such as sources of radiation, air flow through open doors/windows and heat loss through the envelope [128,51,169,131,253,193]. Moreover, there are those that perform a pre-monitoring campaign with a short-term duration to determine the best location for the sensors [105]. For outdoor sensors it is also important to account for the influence of rain in addition to the already

mentioned unwanted sources [232].

It is also important to define the length of the monitoring campaign and its recording frequency, since the monitoring campaign has to be long enough to record the indoor environment variability completely and the recording frequency has to allow the proper reconstruction of the indoor environment with the minimum number of values. *Camuffo* [51] states that monitoring campaigns should last at least one complete year and have a recording frequency of 10 minutes. EN 15757 [90] follows the same line of thought since it states that in order to define the historical climate of an object it is necessary to perform a long-term measuring campaign of at least one year with a recording frequency of one hour or less.

In order to choose an appropriate sensor for each monitoring campaign there are several factors that must be considered, such as the compatibility of the sensor with the ambient conditions, its measuring range, resolution, accuracy, response time, drift and compatibility with the recording instrument, but its cost is also a decisive factor [51]. Another aspect that has to be taken into account is the uncertainty of the sensors, which has to be within certain limits – for temperature it is required that the uncertainty is lower than 0.5 ºC, but it is desirable that it is lower than 0.2 ºC [91], and for relative humidity it has to be lower than 3 %RH [92]. Further information concerning this topic can be found elsewhere [51].

More recently, Arduino based sensors have been more and more used in climate monitoring of historic buildings [169,184,33,246,147,248]. This has been occurring due to their much lower cost when compared to the traditional ones [248], but also due to their open-source nature, which allows a greater flexibility [248]. Ultimately, these advantages offer the possibility of performing an accurate monitoring campaign at a lower cost. For example, Silva et al. [248] installed a long-term monitoring campaign in the church of the Jeronimos Monastery in Lisbon using this type of sensors, which allowed them to save up to ca 230€ per sensor when compared to the traditional sensors. However, there are still some mistrust concerning the accuracy of these sensors. Hence, several authors have showed that their accuracy is as good as the traditional ones by performing extensive experimental campaigns (e.g. [246,248]).

2.2.2. Climate quality assessment tools

This subchapter includes several statistical parameters that quantify the variability of both indoor and outdoor meteorological conditions, as well as three distinctive materials risk assessment tools - biological, mechanical and chemical, for four different artefacts - paper, panel paintings, furniture and wooden sculptures. Lastly, the analytical and the adaptive thermal comfort models are addressed.

2.2.2.1. Tools to analyse the variability of climate conditions

Due to the key influence of the outdoor climate on the indoor climates, and in order to explain certain hygrothermal behaviours that occur in buildings, it is of the utmost importance to analyse the meteorological conditions accurately.

WUFI is equipped with a very interesting tool that quickly assesses the outdoor temperature and relative

humidity both in terms of hourly values and monthly moving averages, as well as the distribution roses of the global radiation and the wind-driven rain [292]. However, these parameters are not enough to carry out a thorough analysis of the outdoor climate. Hence, this subchapter presents additional parameters that were used in this research to analyse the outdoor climates, namely: *monthly moving averages*, *seasonal cycles*, *short-term fluctuations* and *yearly normals*. The standard parameters, such as the annual average, the percentiles or the max/min values, are not presented in this subchapter, since it is believed that due to their calculation simplicity it is not necessary to describe them.

The *monthly moving average* consists on calculating an average with values corresponding to 15 days prior and 15 days after the central value *i* [90]. Note that the moving average can be calculated for any of the hygrothermal variables, namely temperature (ºC) or relative humidity (%).

$$X_i = \frac{1}{n+1}\sum_{i-0.5\cdot n}^{i+0.5\cdot n} X \qquad 2.1$$

Where X_i corresponds to the 30-day moving average centred on *i*, *n* corresponds to the number of data over the considered period (*n* corresponds to 720 since hygrothermal modelling normally deals with hourly data) and *i* corresponds to the centre point.

The *seasonal cycles* are evaluated using the maximum variation of the monthly moving average temperature ($\Delta\overline{T}_{seasonal}$) and relative humidity ($\Delta\overline{RH}_{seasonal}$). These variations are determined by the difference between the maximum value and the minimum value of the monthly moving average:

$$\Delta\overline{T}_{seasonal} = max\left(\overline{T}_{i,seasonal}\right) - min\left(\overline{T}_{i,seasonal}\right) \qquad 2.2$$

$$\Delta\overline{RH}_{seasonal} = max\left(\overline{RH}_{i,seasonal}\right) - min\left(\overline{RH}_{i,seasonal}\right) \qquad 2.3$$

The *short-term fluctuations* are determined using equations 2.4 and 2.5:

$$\Delta T_i = T_i - \overline{T}_{i,seasonal} \qquad 2.4$$

$$\Delta RH_i = RH_i - \overline{RH}_{i,seasonal} \qquad 2.5$$

Where ΔT_i and ΔRH_i are the short-term fluctuations for temperature and relative humidity, T_i and RH_i are the respective hourly values of temperature and relative humidity, and $\overline{T}_{seasonal}$ and $\Delta\overline{RH}_{seasonal}$ are the monthly moving averages of temperature and relative humidity.

Another interesting parameter to assess a large amount of data is the *annual normals* concept, which is determined by averaging the twelve monthly normals [289]. Usually, this concept is used for 30-year intervals. The *monthly normals* are calculated using the following equation:

$$Z = \frac{\sum_{i=1}^{n}\overline{X}_i}{n} \qquad 2.6$$

Where *Z* is the monthly normal, $\overline{X}$ is the monthly mean average and *n* is the number of months within

the selected period (usually, varies between 25 and 30). Note that the annual normal cannot be calculated if either three-consecutive values are missing or if either more than five year-months in total are missing.

2.2.2.2. Risk-based analysis

This subchapter includes three distinctive materials risk assessments: biological, mechanical and chemical, for four different artefacts: paper, panel paintings, furniture and wooden sculptures. In order to assess the materials' behaviour to the variation of the indoor conditions it is necessary to calculate its *response time*. This parameter was developed by *Martens* [178] and it consists in the amount of time that an object takes to get to 95 % of the end value in case of a RH step change, i.e. reflects how fast a material reacts to the variation of the indoor climate:

$$RH_{response,i} = \frac{a \cdot RH_i + a^2 \cdot RH_{i-1} + a^3 \cdot RH_{i-2} + a^4 \cdot RH_{i-3} + \ldots + a^n \cdot RH_{i-(n-1)}}{(a/(1-a))} \quad 2.7$$

Where $RH_{response,i}$ is the object response in RH at instant i (%), RH_i is the room relative humidity at instant i (%) and a is the response factor (-), which is calculated using the following equation [178]:

$$a = e^{\frac{-3 \cdot \Delta t}{\tau response}} \quad 2.8$$

Where a is the response factor (-), Δt is the time interval between two consecutive points (s) and $\tau_{response}$ is the response time (s). Note that if the response time ($\tau_{response}$) is much larger than the time interval between points (Δt), then equation 2.7 can be simplified to the following form [178]:

$$RH_{response,i} = \frac{RH_{response,i-1} + RH_i/(n/3)}{(1 + 1/(n/3))} \quad 2.9$$

Where $RH_{response,i}$ is the object response in RH at instant i (%) and n is the number of data points in the response time (-). Table 2.1 presents the respond time and respective relevant responds for the analysed objects [178]. Note that these values correspond to intact objects. Hence, and if deterioration has already occurred, the respond time will decrease [178].

Table 2.1 – Respond time and respective relevant responds for panel painting, lacquer box and wooden sculptures [178]

Object	Relevant response	Response time
Panel painting	Surface response just under oil paint	4.3 days
	Full response of entire panel	26 days
Lacquer box	Full response of entire lacquer box	40 days
Wooden sculptures	Surface response	10 hours
	Sub-surface response causing maximum stresses	15 days

2.2.2.2.1. Chemical risk

Although chemical decay is a slow process, all organic materials are vulnerable to it, especially paper. Its speed is proportional to temperature and relative humidity, i.e. the higher the temperature and relative humidity, the faster will chemical decay occur. The damage in the material is caused by chemical reactions (namely, hydrolysis and oxidation), which take place within the material and depend primarily on the temperature and secondly on its moisture content. Michalski [186] states that for each 5 K drop, the chemical lifetime of most chemical sensitivity materials doubles. The life expectancy for the several types of chemical sensitivity materials can be consulted elsewhere [188,187].

The amount of moisture within a hygroscopic material increases with the RH by adsorption processes in the hygroscopic region [163]. Initially, there is only one layer of water molecules, but due to the increase of RH, the number of layers will increase as well. This will lead to the increase of the thickness of the sorbate film. As the film thickness increases, the external water molecule layer will be less controlled by the porous wall and more available for chemical reaction (namely, hydrolysis). This is the reason why it is necessary to reduce the RH where the chemical sensitivity materials are housed, as much as possible.

The chemical decay is assessed using the *lifetime multiplier* concept, which was developed by Michalski based on the Arrhenius equation [186], and reflects for how much time the object remains usable by comparison to standard conditions, i.e. 20 ºC and 50% RH. The activation energy necessary for the reactions to start occurring is 100 kJ/mol for paper (i.e. cellulose) and 70 kJ/mol for the other materials (i.e. varnish) [178].

$$LM_x = \left(\frac{50\ \%}{RH_x}\right)^{1.3} \cdot e^{\frac{E_a}{R}\left(\frac{1}{T_x+273.15}-\frac{1}{293.15}\right)} \quad 2.10$$

Where LM_x is the lifetime multiplier at point x (-), RH_x is the surface relative humidity at instant x (%), E_a is the activation energy (J/mol), R is the gas constant (8.314 J/Kmol) and T_x is the temperature at instant x (ºC). The *equivalent Lifetime Multiplier* can be used to quantify the chemical risk under a single value [253]. This is beneficial for this research, because it allows the assessment of the variation of the chemical decay throughout a large period of time more easily:

$$eLM = 1\Big/\left(\frac{1}{n}\cdot\sum_{x=1}^{n}\left(\frac{1}{LM_x}\right)\right) \quad 2.11$$

Where *eLM* is the *equivalent Lifetime Multiplier* (-), *n* is the number of data points in considered period (-) and LM_x is the lifetime multiplier at instant x (-).

2.2.2.2.2. Biological risk

Many of the artefacts that are housed in buildings, such as museums, are vulnerable to fungal growth,

especially those that are composed by at least one organic material, but also inorganic materials with organic films [197]. For fungal to grow it is necessary to attain certain values of relative humidity and temperature, but it is also necessary that the substrate has nutrients [244]. These three conditions have to be met simultaneously and must endure for a specific period of time for mould growth to occur. Due to the risk that mould presents to artefacts conservation it is of key importance to cease this process. This can be achieved by first knowing the conditions under which mould growth occurs and secondly acting appropriately.

Sedlbauer [244] developed a two phase method, known as *isopleth model*, that allows the study of the mould growth based on relative humidity, temperature and substrate. This model includes four types of substrates: category 0 – optimum culture medium, category I – Bio-utilizable substrates, category II – Substrates with porous structure and category III – Inert substrates. Substrate category III is disregarded because it is assumed that mould will only form if there is severe soiling [244].

In the first phase, one determines the time needed for the spores to became active. Secondly, and once they are active, the rate of the mould growth is determined. For the first phase the *Spore germination* graph is used (Figure 2.1a), in which spores became active fungi when the *Lowest Isopleth for Mould* (LIM) is surpassed. The germination time decreases as temperature and relative humidity increase.

In the second phase, the speed of the fungi growth is determined using the *Mycelium growth rate* graph (Figure 2.1b). If the active fungi die, the germination process has to start all over again. It is also important to bear in mind that the maximum RH in which there is no mould growth varies according to the type of climate (while in temperate regions the RH should remain below 70 %, higher values maybe permitted in cold regions [51]).

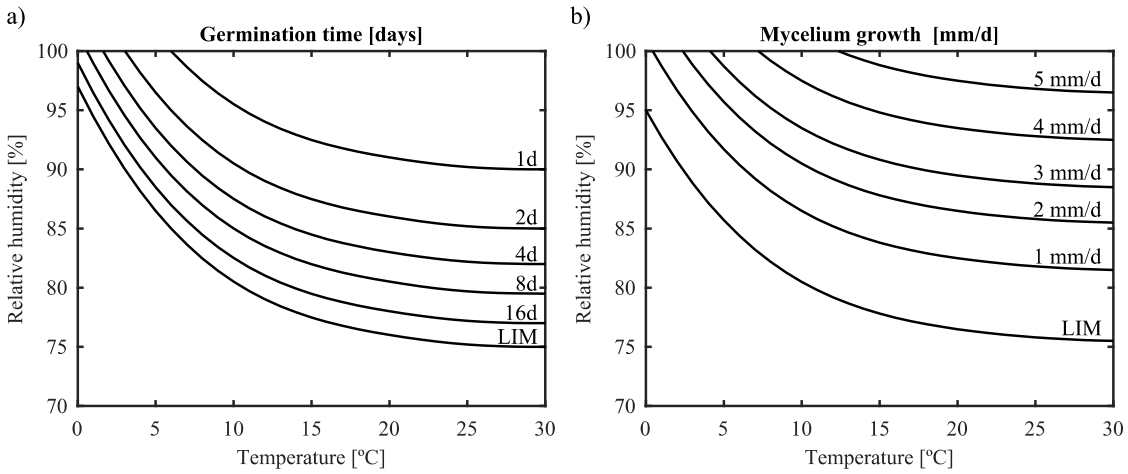

Figure 2.1 – Spore germination (a) and Mycelium growth (b) for the substrate category I (adapted from Ref. [244])

In order to quantify the biological risk under a single value, the *mould risk factor* (MRF) was calculated. The MRF is the sum of the time contributions to spore germination of each set of temperature and relative humidity that overcomes the respective LIM. This is done by summing the reciprocal of the corresponding germination time. For example, for a hourly set of values, if for a given instant the isoline

16 days is surpassed its contribution to MRF is 1/(16 days x 24 hours) = 0.0026. Note that this contribution corresponds to hourly frequencies and for different frequencies the contribution to MRF changes (see, for example, Ref. [251]). The spores became active fungi when the MRF reaches 1.

According to IPI metrics [197], if the MRF is lower than 0.5 there is little or no risk of mould growth. It is important to bear in mind that due to MRF restrictions (namely, the possibility of the active fungi dying), the MRF value can vary throughout the considered period. This leads to the fact that the assessment should be focussed on the maximum values and not necessarily in the final value. Another advantage of this factor, which is important for this specific research, is the fact that a single value allows to assess the risk of mould growth throughout a large period of time more easily.

2.2.2.2.3. Mechanical risk

All hygroscopic organic materials are susceptible to mechanical decay, which is a process that is mainly governed by relative humidity. The variation of relative humidity will lead to the variation of the moisture content of these materials, which will cause the material to shrink if relative humidity decreases or swell if relative humidity increases. Additionally, and if the material has internal or external restraints, it will cause stresses within itself, which may eventually result in its cracking.

Hygroscopic composite objects are the most susceptible to mechanical decay, since their constituents have different moisture expansion coefficients and therefore will shrink/swell at different rates, thus causing indoor restraint. In most hygroscopic materials, the lowest dimensional change occurs at 50 %RH, whilst the highest occur in the extremes [181].

Mechanical decay can be caused by uneven moisture distribution within the object (e.g. in a thick object, the moisture content of the surface can differ significantly from the moisture content of the core) or by uneven dimensional changes between the substrate and surface layer (namely, in painted panels).

This research follows a validated methodology of mechanical decay assessment [178], and analyses the dimensional change of furniture, sculptures and panel paintings, whose constituents have to be analysed individually – i.e. wood substrate and pictorial layer (Figure 2.2).

For furniture, the mechanical decay is assessed using an adapted version of Bratasz *et al.* [44] graph, in which the x-axis corresponds to the annual average of relative humidity and the y-axis corresponds to the surface response to relative humidity. For sculptures, the mechanical decay is assessed using an adapted version of Jakiela *et al.* [144] graph, in which the x-axis corresponds to the sub surface response to relative humidity and the y-axis corresponds to the surface response to relative humidity.

The mechanical decay in the wood substrate and the pictorial layer of painted panels have to be assessed using two different methods. The mechanical decay of the wood substrate is assessed using an adapted version of Mecklenburg's *et al.* [181] graph in which the x-axis corresponds to the object full response to relative humidity and the y-axis corresponds to the surface response to relative humidity. On the other

hand, the mechanical decay of the pictorial layer is assessed using Bratasz's *et al.* [45] graph. A more detailed explanation of these methods can be found elsewhere [178].

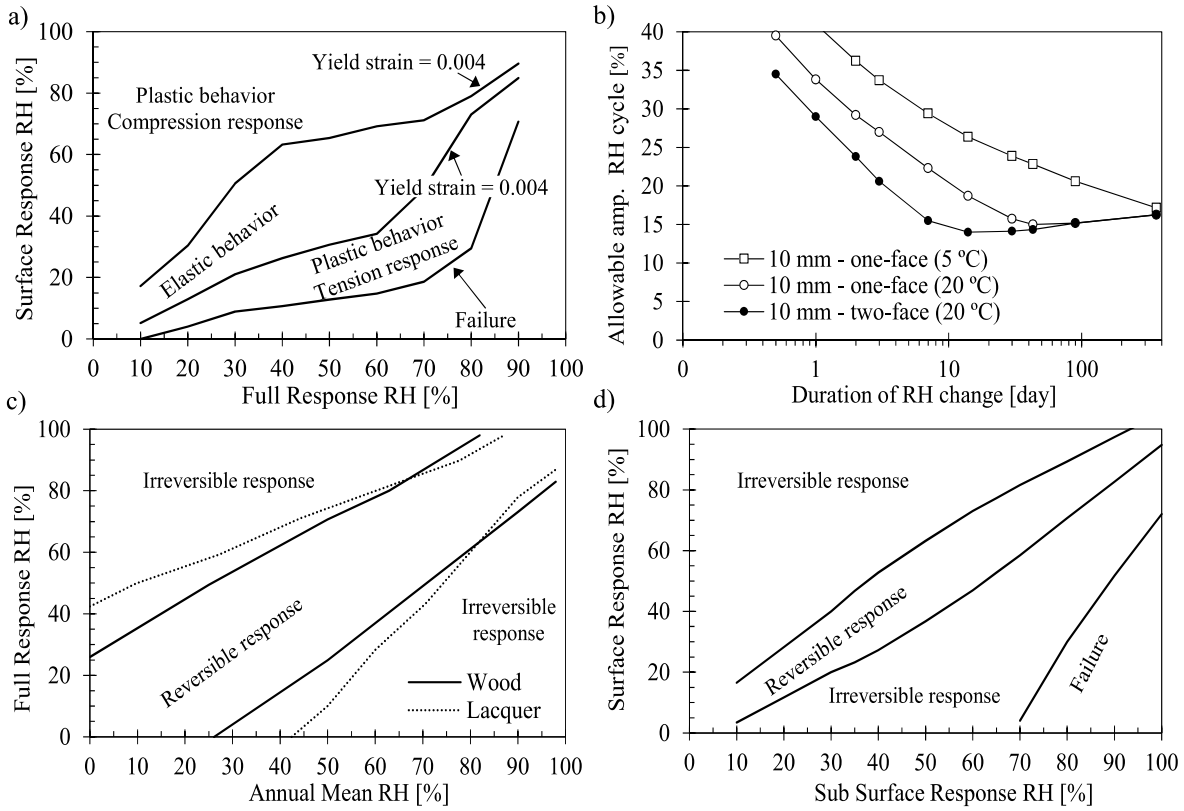

Figure 2.2 – Mechanical decay assessment for: a) wood substrate of the panel painting [181], b) pictorial layer of the panel painting [45], c) wood furniture [44] and d) wood sculptures [144]

2.2.2.3. Thermal comfort

Visitors are crucial for the continuity of buildings that exhibit artefacts because they are a major source of revenue. Hence, it is important that the management of the indoor climate in these building also takes the comfort of the visitors into account.

The human thermal sensation can either be assessed using an analytical method, such as the Predicted Mean Vote (PMV) and the Predicted Percentage Dissatisfied (PPD) [106], or using an adaptive thermal comfort model, such as the one developed in ASHRAE Research Project 884 [73], which was later on included in ASHRAE 55 [4] with some adaptations.

The PMV/PPD model has suffered several updates over the years and it is still one of the most used thermal comfort models in literature nowadays. These indices are included in several international standards concerning human thermal comfort, such as ASHRAE 55 [4] and ISO 7730 [137].

Another reason why the PMV/PPD model is normally used in literature is due to the fact that the literature concerning the thermal comfort in museums or galleries is scarce [154]. The PMV/PPD indices can be calculated using, for example, a MATLAB routine based on the code presented in ISO 7730 [137], which is advantageous when analysing a great number of cases. However, de Dear *et al.* [73]

demonstrated that although the PMV/PPD model is valid for buildings with HVAC-systems, it is not suitable to assess the indoor climate of naturally ventilated buildings.

The adaptive method of ASHRAE 55 [4] can have either an 80 % acceptability limit (Figure 2.3a) or an 90 % acceptability limit, which is used when a higher level of comfort is sought [4]. This method is valid for natural ventilated buildings without HVAC systems, in which occupants can adapt their clothing to the climate conditions, and the activity level is near-sedentary [4], i.e. varying between 1.0–1.3 met. Furthermore, this method accounts for local thermal discomfort effects, clothing adaptation and indoor air speed adaptation [4]. The outdoor air temperature is obtained using a 7-day exponential weighted running average of the daily averages of the outdoor temperature [4].

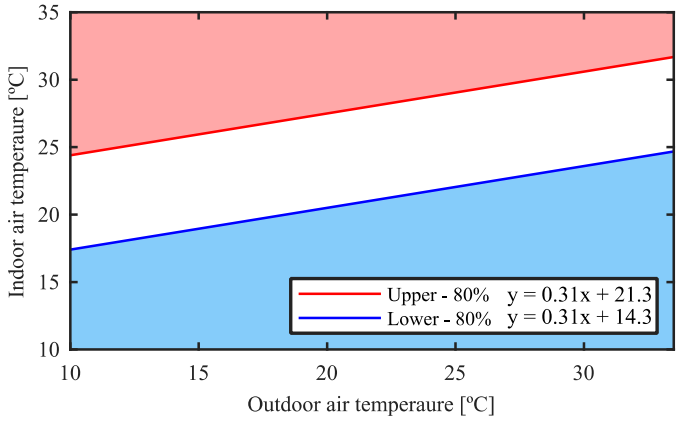

Figure 2.3 – ASHRAE 55 adaptive thermal comfort model for an acceptability limit of 80 % [4]

2.2.3. Limiting indoor climate

Due to the importance of maintaining historic artefacts safe, many standard and guidelines that aim to reduce or mitigate the risk of deterioration, by limiting the variance of the indoor temperature and relative humidity, have been developed over the years. For instance, Gary Thomson developed a guideline in which the buildings are divided in two classes (Table B.1): class 1, which aims to mitigate most deterioration risks by varying the indoor conditions within a more stringent range; and class 2, which aims to avoid major deterioration risks whilst keeping costs to a minimum [264]. Class 1 is recommended for major museums since they have the financial capacity to guarantee the recommended indoor conditions.

Another important guideline, which aims at mitigating the risks of artefacts deterioration, is the ASHRAE guideline [5], which was first introduced in the ASHRAE Handbook – HVAC Applications in 1999. This guideline is centred in a five permissible class system in which the strictness in terms of indoor conditions lessens from the first class (class AA) to the last class (class D) (Table B.2). In other words, the energy spent to ensure the setpoints preconized by the guideline will decrease, but at the same time the risks of deterioration will increase. The first two-classes are not recommended for historic buildings due to problems induced by condensation, hence the recommended classes for high inertia historic buildings are B, C or D [5].

On the other hand, in Europe the current standard that deals with the preservation of artefacts is standard EN 15757 [90]. This standard aims to mitigate the mechanical risk induced by the indoor conditions to hygroscopic materials by maintaining the historical climate. The standard is based on the definition of the historical climate using a long-term monitoring campaign and, on the assumption, that if the artefact is subject in the future to the same conditions as in past, then the risk of mechanical damage is low. However, if the measured climate is not stable, then the 14 % largest short-term fluctuations, i.e. the 7 % most dangerous fluctuations in dryness and wetness [51], must be excluded.

There are also two other European standards worth mentioning: PAS 198 [48] and UNI 10829 [84]. The first aims to slow down, as much as possible, the deterioration of artefacts by choosing appropriate setpoints for the indoor conditions, namely in terms of temperature, relative humidity, and light; but also reduce the effects of indoor pollutants. However, this standard always takes into account the energy consumption necessary to maintain each set of indoor conditions [48].

The second standard limits the range within which the indoor temperature and relative humidity can vary to guarantee the preservation of the housed artefacts. This Italian standard encompasses several classes of objects in which the seasonal cycles and the short-term fluctuations of the indoor temperature and relative humidity are limited according to the requirements of each object [84].

More recently, Silva et al. [250,252] developed a two-class guideline that aims to mitigate the risk of deterioration of artefacts housed in historic buildings for temperate climates (Table B.3). This guideline limits the variance of the indoor temperature and relative humidity in terms of seasonal and short-term fluctuations with a more stringent class 1, which is meant for buildings with important and permanent collections, and a more flexible class 2, which is meant for less resourceful buildings. This guideline was partially based on UNI 10829 [84], in the ASHRAE specification [5] and on EN 15757 [90]. A detailed review of these standards and guidelines is presented in Ref. [226].

2.3. Outdoor climate

It is known that the outdoor climate can play a prominent role in the variance of the indoor climate [6]. In order to explain certain hygrothermal behaviours that occur in the building, it is of great importance to analyse the outdoor climate. It is also very important to analyse how the outdoor climate is going to evolve in the future so as to predict how the indoor climate is going to evolve.

This subchapter briefly addresses the evolution of the emissions of greenhouse gases into the atmosphere since 1990 until 2017, because they are one of the main causes for climate change. Secondly, the changes that Lisbon's climate has suffered in the past years are addressed. Finally, the several scenarios encompass in IPCC's reports that describe how the world can evolve in the future are also addressed. The last three assessment reports are addressed, i.e. third, fourth and fifth assessment reports.

2.3.1. Emission of greenhouse gases

The emission of greenhouse gases into the atmosphere caused by anthropogenic activities is greatly responsible for the changes the outdoor climate will suffer in the future [196]. The two main contributors for these emissions worldwide are the United States (US), since the US are responsible for more than 40 % of the total GHGs emissions of the OECD members [201]; and China, which is also responsible for a large amount of GHGs emissions, which have been increasing abruptly over the past years. China even surpassed the US emissions in 2005 turning it into the main producer of greenhouse gases worldwide from then onwards (Figure 2.4).

Nonetheless, the European Union (EU) has also a key contribution to the overall GHGs emissions (Figure 2.4). The European Union is responsible for more than one third of the GHGs emitted by the OECD members, i.e. 5,600,000 tonnes of CO_2-equiv per year [201]. However, this amount has been steadily decreasing over the past years (Figure 2.4), mostly due to the efforts made by the EU parliament in promoting a more environmentally friendly society by establishing demanding, but necessary, goals to its member states to reduce the GHGs emissions of the European Union [88].

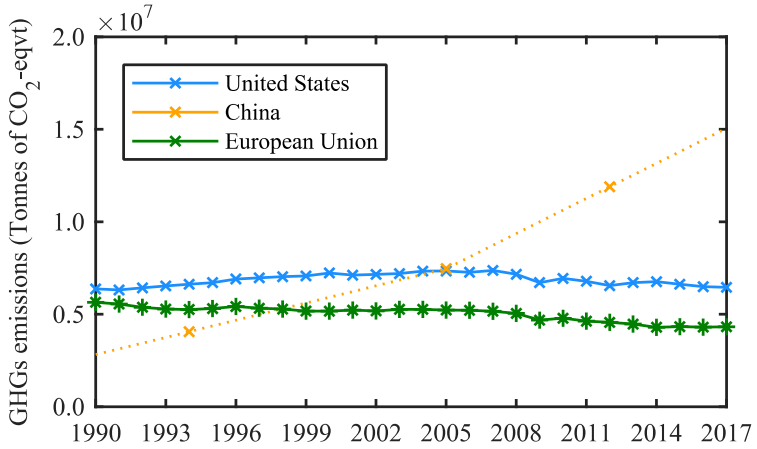

Figure 2.4 – Greenhouse gases emissions (in tonnes of CO_2-equivalent) for the United States, China and the European Union between 1990 and 2017 [201]. The OECD database only has three values for China (1994, 2005 and 2012), hence, the remaining years were determined through interpolation and extrapolation

Nevertheless, the magnitude of GHGs emissions is still quite alarming [201]. The main European contributors are Germany (21.5 %), the United Kingdom (11.2 %), France (11.1 %), Italy (10.1 %), Poland (9.8 %), Spain (8.1 %) and the Netherlands (4.6 %) (Figure 2.5). It is obvious that if these environmentally friendly policies are to be successful, they must be followed by all EU member states, especially by these seven countries. In addition, there are two other non-European countries that have a very significant contribution to the continent overall emissions amount, i.e. Russia (ca 2,150,000 tonnes of CO_2-equiv) and Turkey (ca 500,000 tonnes of CO_2-equiv).

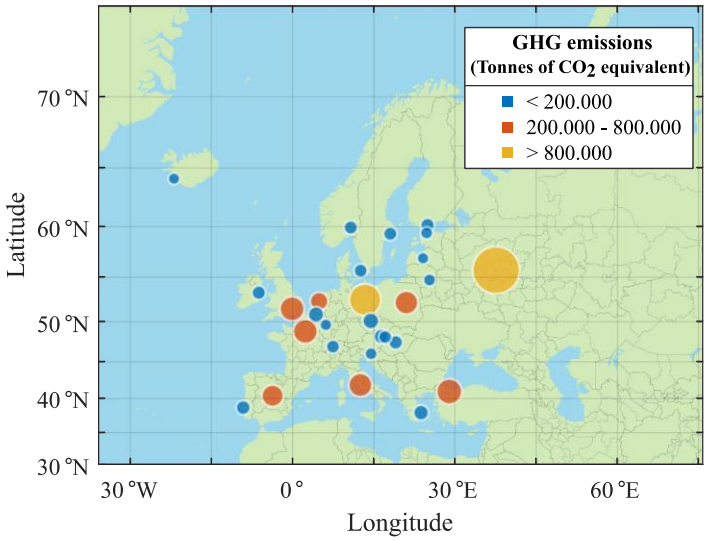

Figure 2.5 – Greenhouse emissions throughout Europe in tonnes of CO_2 equivalent in 2017 [201]. Countries emission are divided in three levels: level 1 - annual emissions of GHGs lower than 200.000, level 2 - annual emissions of GHGs between 200.000 and 800.000, level 3 - annual emissions of GHGs higher than 800.000

A great part of the greenhouse gases emissions in Europe is caused by electricity related consumptions, i.e. more than 400.000.000 tonnes of CO_2 in 2017, which corresponds to 9 % of the overall sum, as well as the building construction sector, i.e. more than 330.000.000 tonnes in 2017, which corresponds to 7 % of the overall sum (Figure 2.6). These values have been decreasing since 2008 [101].

However, private households are even a larger contributor to the GHGs emissions, which were responsible for the emission of more than 830.000.000 tonnes of CO_2 in 2017, which corresponds to 19 % of the overall sum. These numbers show the key importance of the building sector on the overall emissions of greenhouse gases in Europe. Thus, demonstrating the crucial need to intervene in this sector in order to perform a significant reduction of the GHGs emissions in the European Union.

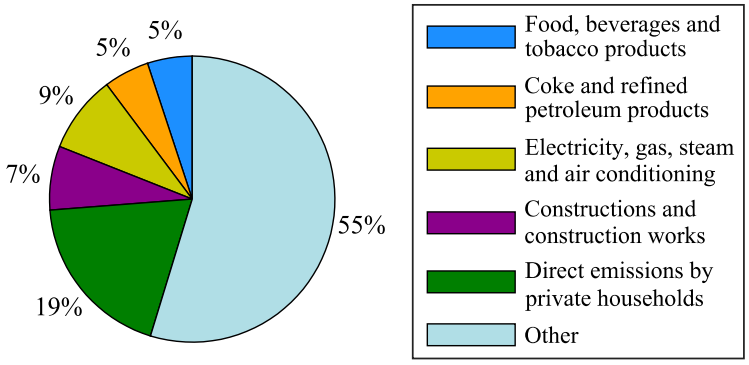

Figure 2.6 – Greenhouse gases emissions distribution in accordance with the activities defined for the CPA08 in Europe in 2017 [101] with the four most pollutant activities, the direct emissions caused by private households and the “other” section, which includes all the remaining activities (Table C.1)

2.3.2. Situation in Lisbon, Portugal

As was stated before, the changes suffered by the environment over these past years have been greatly caused by the emission of greenhouse gases due to anthropogenic activities. For example, in Lisbon, which is a coastal city and the largest city in Portugal with over 2.8 M people [214], it is expected that

the annual precipitation decreases. On the other hand, it is also expected that the number of extreme phenomena with extreme rains will increase, the droughts will become more frequent and more severe, and both the air temperature and the average sea level will rise [50].

2.3.2.1. Temperature and precipitation

In order to study the changes in the outdoor climate over the past years in Lisbon, three sets of temperature and precipitation were analysed: 1951–1980, 1970–2000 and 2005–2015. The first set was supplied by the old *Meteorological Institute* (now IPMA) and used by *Henriques* [122] to analyse the variability of the outdoor climate in eight climate representative cities of Portugal – Bragança, Porto, Portalegre, Lisboa, Beja, Faro, Ponta Delgada (Açores archipelago) and Funchal (Madeira archipelago). The second set was obtained from IPMA website [142] and the third set was supplied by IPMA for other projects [66]. Although, the third set does cover the required 25–30 years [289] and only includes 11-years' worth of data, the obtained results are representative of a more recent climate in Lisbon.

Overall, the mean temperature in Lisbon considerably increases from 1951–1980 to 1970–2000, with the difference amounting to +4.0 ºC (Figure 2.7). The only month in which the average temperature corresponding to 1970–2000 is not higher than the average temperature of 1951–1980 is May (-0.3 ºC). The highest increases occur in March (+0.8 ºC) and in December (+0.7 ºC). The same observation can be made whilst comparing the values that correspond to 1951–1980 and 2005–2015, i.e. the mean temperature considerably increases throughout the whole year (Figure 2.7). The difference amounts to +7.7 ºC and the highest increases occur in April (+1.1 ºC) and in December (+1.0 ºC).

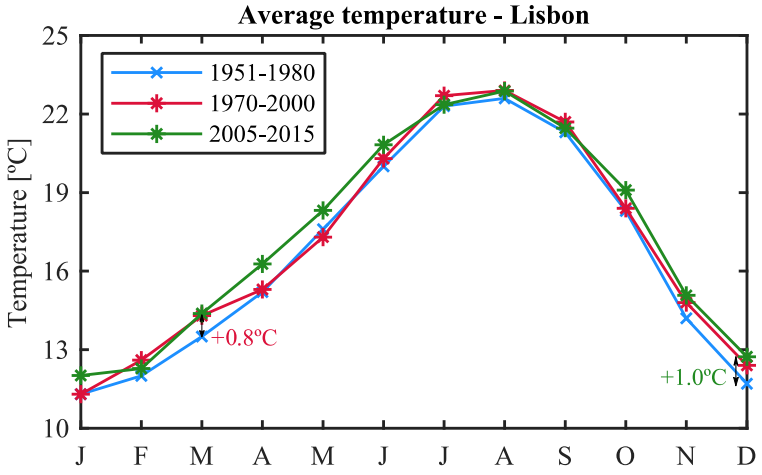

Figure 2.7 – Normals of the average outdoor temperature for three periods: 1951-1980 (used in Ref. [122]), 1970-2000 [142] and 2005-2015 (used in Ref [66])

The precipitation accumulated difference between 1951–1980 and 1970–2000 is approximately -52 mm, which means that the precipitation in Lisbon has decreased significantly from 1951–1980 to 1970–2000 (around 7 %). The highest difference occurred in March with a decrease of ca -50 mm (Figure 2.8). However, the difference in January (-25 mm), February (-18 mm) and December (-15 mm) is also considerable. On the other hand, the precipitation increases substantially in May (+12 mm) and April

(+11 mm), but it is not enough to compensate the decrease that occurs on the other months.

When comparing 1951–1980 and 2005–2015 the difference in terms of precipitation is even higher (Figure 2.8), i.e. the precipitation decreases ca -127 mm, around 16 % when compared to the 1951–1980 value. The most significant decreases occur in March (-43 mm), December (-42 mm) and January (-40 mm). On the other hand, the precipitation increases substantially in October (+23 mm) and November (+20 mm) and slightly in September (+5 mm), but once again these increases are not enough to compensate the decreases of precipitation that occur in the other months of the year.

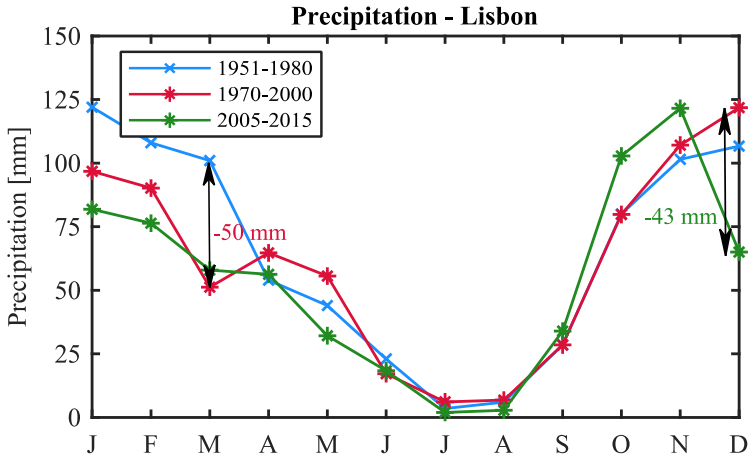

Figure 2.8 – Precipitation normals for three periods: 1951-1980 (used in Ref. [122]), 1970-2000 [142] and 2005-2015 (used in Ref [66])

In addition, the average monthly maximum and minimum were compared for the periods of 1951–1980 and 1970–2000. It is visible that the difference of the maximum temperatures is not as substantial as one would expect (Figure 2.9). The temperature accumulated difference amounts to +1.2 ºC, with the largest differences being reached in March (+0.9 ºC), December and February (+0.5 ºC). On the other hand, the difference between both periods is much more significant for the minimum temperatures, with the 1970–2000 period always corresponding to higher temperatures, except for January (Figure 2.10). Its accumulated difference amounts to +6.9 ºC, with the largest differences being reached in July and December (+0.9 ºC), closely followed by August and September (+0.8 ºC).

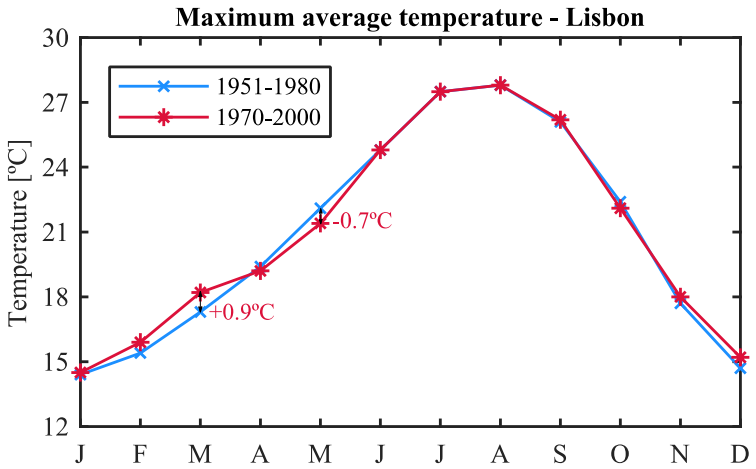

Figure 2.9 – Normals of the maximum outdoor temperatures for two periods: 1951-1980 [122] and 1970-2000 [142]

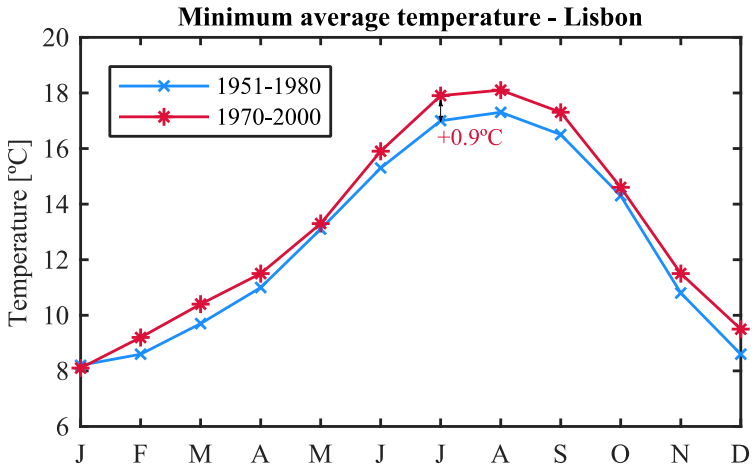

Figure 2.10 – Normals of the minimum outdoor temperatures for two periods: 1951-1980 [122] and 1970-2000 [142]

2.3.2.2. Airborne pollutants

Pollutants, which exist in several states of matter and can either have an anthropogenic or natural origin [260], are one of the main threats to artefacts conservation [5]. This is due to their capacity to hasten other decay processes when coupled with certain levels of temperature and relative humidity [5], but because they can also be responsible for the deterioration itself (see Annex D). *Tétreault* [260] defines three ways in which pollutants can reach artefacts: 1) pollutants are carried by air (typically known as *airborne pollutants*), 2) pollutants are passed from an object to another one through physical contact, and 3) pollutants are already part of the object or are produced by chemical reactions. The main focus of pollutants studies in artefacts conservation is the first type of transmission [260].

Although, there is a large number of airborne pollutants, only a few have been proven to be harmful to artefacts, namely [260,207,228,5]: acetic acid (CH_3COOH), hydrogen sulphide (H_2S), nitrogen dioxide (NO_2), ozone (O_3), sulphur dioxide (SO_2) and fine particles (i.e. particles with aerodynamic diameter smaller than 2.5 µm). *Tétreault* [260] also defines water-vapour as a key airborne pollutant because it causes physical and chemical damage, but also due to its capacity to heighten other decay processes.

Due to the negative consequences that these airborne pollutants have on the indoor climate of museums and similar buildings and, subsequently, on the housed artefacts, their variance over the past 24 years – 1995 to 2018 – in several locations in Lisbon was analysed (Figure 2.11). The used data was obtained by QualAR project [216], which is a project mainly financed by the European Union, whose aim is to help in the decision making process concerning the air quality in Portugal by monitoring pollutants [215]. The monitoring campaigns did not start in 1995 in all zones, nor did they all last until 2018.

The analysed airborne pollutants in this research were nitrogen dioxide (NO_2), ozone (O_3), sulphur dioxide (SO_2) and fine particles ($PM_{2.5}$), since they are the key damaging pollutants in the museum environment [260,207,228,5]. Furthermore, the Directive 2008/50/EC of the European Parliament [202] established limit-values and target-values for these airborne pollutants to improve the air quality for human health and vegetation throughout the European Union (Annex E).

Directive 2008/50/EC [202] established that the nitrogen dioxide (NO_2) should be assessed using two parameters, so that human health is protected, namely the *hourly values* and the *annual average*. Whilst the first cannot overcome the 200 µg/m^3 limit more than 18 times a year, the second must not be higher than 40 µg/m^3. The failure of any of these two conditions makes the climate unbefitting for human presence and, consequently, leads to the need of applying measures that improve the air quality.

The hourly values of the 33 monitored zones (Figure 2.11a) were assessed over a period of 24 years in terms of number of times the 200 µg/m^3 limit is overcome in each year (Figure 2.12a). If this sum is higher than 18, then the zone' air quality has to be improved. This figure shows that at the beginning of the analysed period the limit-value was overcome ca 550 times in *Avenida da Liberdade* (one of the main avenues of Lisbon) and ca 420 times in *Avenida Casal Ribeiro* (located in a highly populated zone of Lisbon), which shows the poor air quality of the city at the time. However, the air quality in terms of these parameter has been improving over the years for all monitored zones, except for *Avenida da Liberdade* that amounts to more than the 18/year-limits in more than one occasion – 2005–2011, 2014–2015 and 2017–2018.

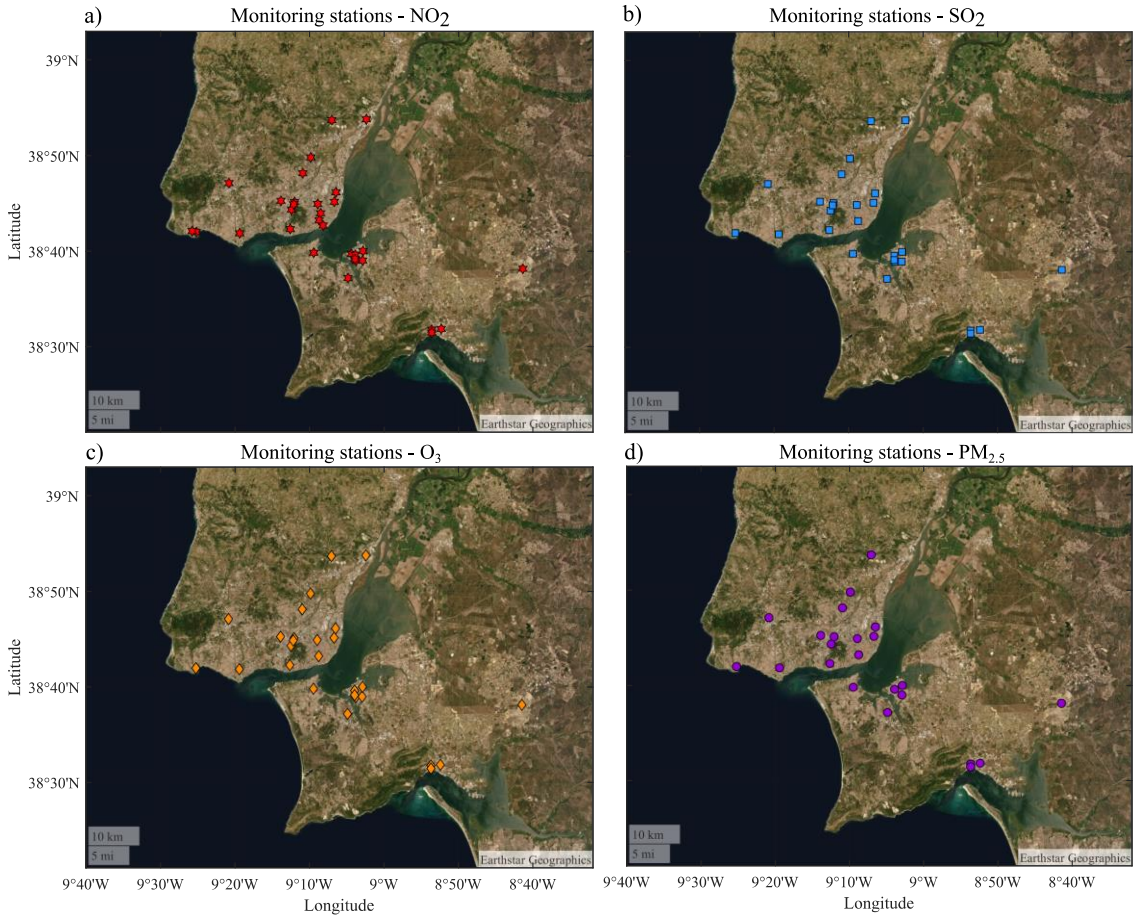

Figure 2.11 – Location of the QualAR stations that monitored the nitrogen dioxide (NO_2) – 33 zones (a), the sulphur dioxide (SO_2) – 29 zones (b), the ozone (O_3) – 29 zones (c) and fine particle matter ($PM_{2.5}$) – 26 zones (d) concentration

Although the number of times the NO_2 concentration is higher than the limit-value has clearly improved, the same cannot be said for the annual average. In fact, more zones have higher values than the limit-

value (Figure 2.12b), in opposition to the number of zones where the hourly NO_2 concentration is higher than the limit-value. Once again, *Avenida da Liberdade* is the overall worst case. Although its annual average decreases, it is still far from the limit. These observations are worrisome in terms of human health, since long-term exposure to high levels of NO_2 concentration can cause the decrease of lung function and the increase of respiratory problems [300].

These values reflect what is happening outdoors, which indirectly affects the conservation metrics indoors, depending on the building's ventilation behaviours [5]. There are several models in literature that accurately determine the indoor concentration of a pollutant [228], but in order to have an idea of the indoor concentration, one can use the "100, 10, 1" rule purposed by *Tétreault* [261] that states that a pollutant's indoor concentration will be 10 % of its outdoor concentration. If the annual moving average of *Avenida da Liberdade* in 2017 (i.e. 58.9±2.6 µg/m^3) is multiplied by this percentage, this means that the annual moving average of the indoor NO_2 concentration is 5.9 µg/m^3, which means that the NO_2 susceptible artefacts would start showing signs of decay in 5 years [260]. This observation shows the key importance in addressing air pollution in big cities in order to safeguard both human health and artefacts.

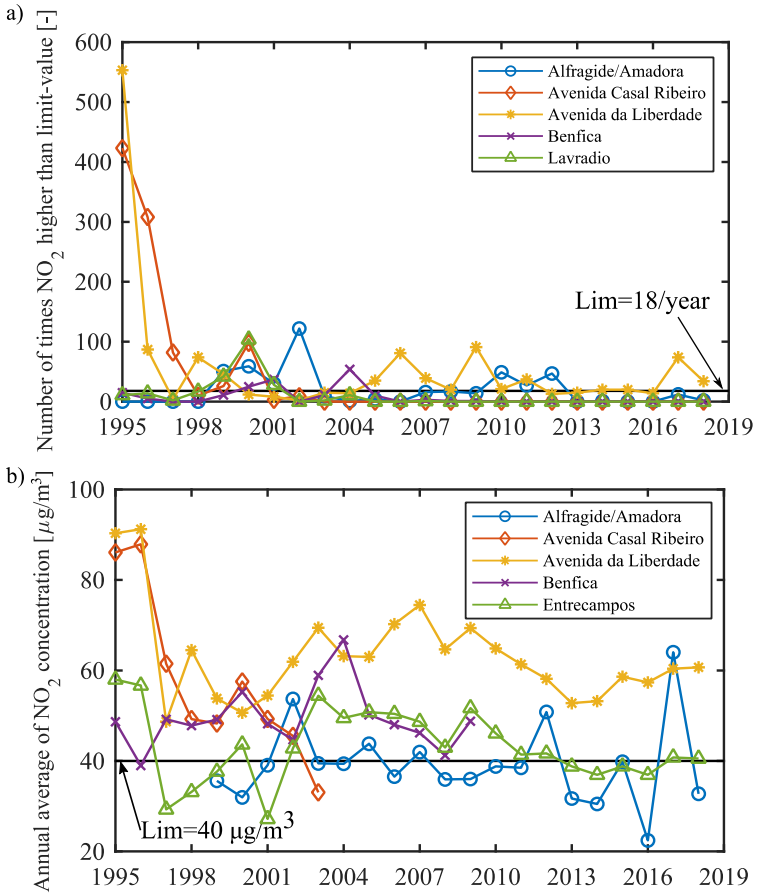

Figure 2.12 – Number of times the NO_2 concentration is higher than the limit-value 200 µg/m^3 (a) and annual NO_2 concentration average (b) for the five worst cases in Lisbon's metropolitan area. The first parameter should only occur, at most, 18 times a year, whilst the annual average should not surpass the 40 µg/m^3 [202]

The *Sulphur dioxide* (SO_2) was analysed in terms of *hourly values* and *daily averages*, since these are

the two parameters in terms of SO_2 concentration that have to be controlled in order to guarantee human health [202]. Whilst the first cannot overcome the 350 µg/m^3 limit more than 24 times a year, the second cannot exceed the 125 µg/m^3 more than 3 times a year [202]. By failing one of these two conditions the climate is classified as unbefitting for human presence and the application of air quality improvement measures is required. Long-term exposure to high levels of SO_2 can cause respiratory illness symptoms, as well as the increase of respiratory illness frequencies [287].

The hourly values of the 29 monitored zones (Figure 2.11b) were assessed over a period of 24 years by determining the number of times the 350 µg/m^3 limit is overcome in each year (Figure 2.13a). The only two zones that did not comply with the first SO_2 concentration requirement were *Hospital Velho* and *Lavradio*. Whilst *Hospital Velho* only overcame the 350 µg/m^3 limit more than the allowed 24 times in 1996, *Lavradio* overcame this limit in 1999, 2001–2003 and 2007–2008. Afterwards, the monitoring campaign stopped in *Lavradio*. In addition, the obtained results for the *daily averages* supported these observations, since the only two zones that did not satisfy the limit-values for the *daily averages* were *Hospital Velho* and *Lavradio* for the same years (Figure 2.13a).

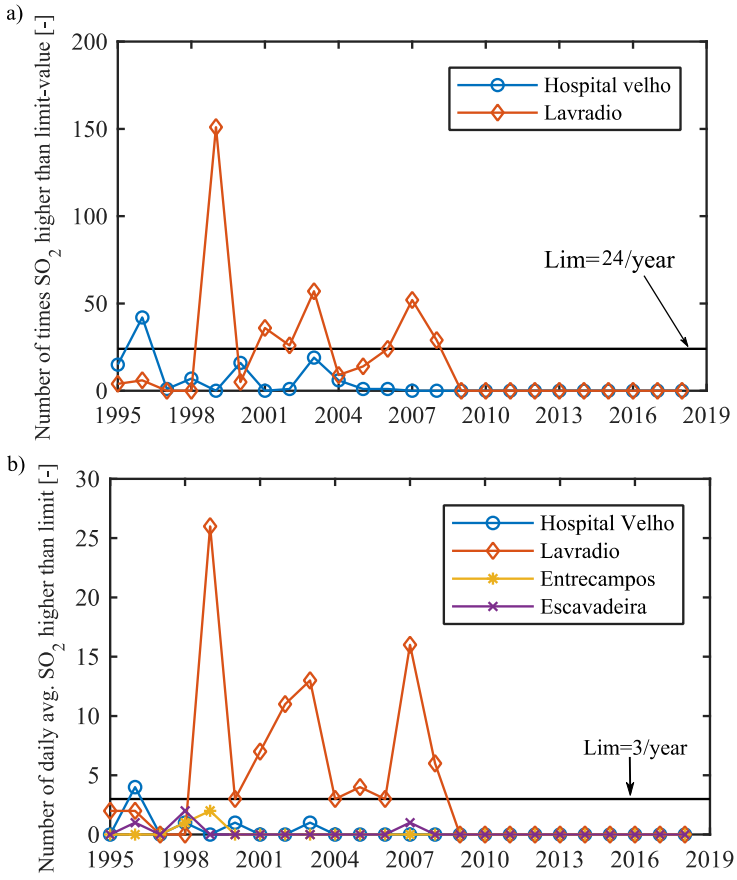

Figure 2.13 – Number of times the hourly SO_2 concentration is higher than the limit-value 350 µg/m^3 (a) and the number of times the daily average of SO_2 concentration is higher than the limit-value 125 µg/m^3 (b) for the worst cases in Lisbon's metropolitan area. The first parameter should only occur, at most, 24 times a year, whilst the daily average should not surpass the limit-value more than 3 times a year [202]

The *Ozone* (O_3) concentration in Lisbon's metropolitan area was analysed in terms of *maximum eight-hours daily averages*, since this is the parameter established by Directive 2008/50/EC [202] that has to

be checked to assess the air quality in terms of O_3 concentration. The parameter can overcome the target-value (120 µg/m^3), at the most, 25 days in average for a period of 3 years [202]. If this requirement is not guaranteed, then the zone is classified as unbefitting for human presence and it is necessary to implement air quality improvement measures.

The hourly values of the 29 monitoring zones in Lisbon's metropolitan area (Figure 2.11c) were assessed over a period of 24 years in terms of the number of times the 120 µg/m^3 limit is overcome in each year. This limit cannot be overcome more than 25 days/year for a three-year average. Figure 2.14 shows that the air quality has improved in some of the zones, but most of the years the values are higher than the 25/year limit, with *Chamusca* being the worst case. This is quite worrisome in terms of human health since long-term exposure to high levels of O_3 concentrations can be responsible for asthma, the decrease of lung function growth, lung cancer and, consequently, the increase of the mortality rate [300].

If *Tétreault's* "100, 10, 1" rule [261] is applied to the annual moving average for 2017 of *Chamusca* (i.e. 71.1±2.1 µg/m^3), this would mean that the annual moving average of the indoor O_3 concentration would be below ca 7.1 µg/m^3. By taking Table 2 in *Tétreault* [260] into account, this would mean that the O_3 susceptible artefacts would start showing signs of decay in less than four years. Once again, showing the importance of addressing air pollution.

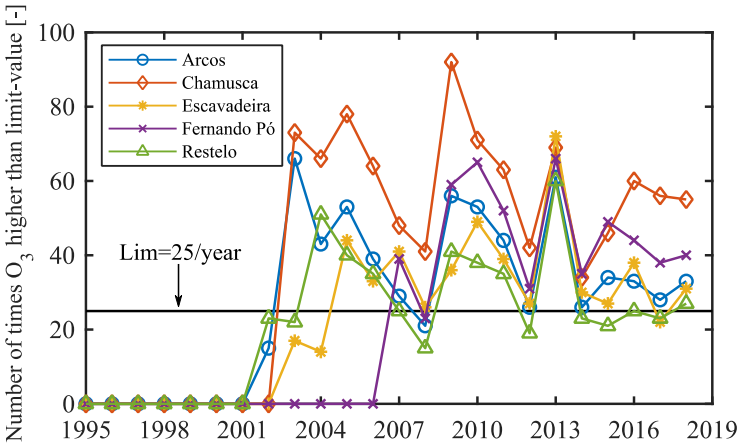

Figure 2.14 – Number of times the maximum daily eight-hour mean of the O_3 concentration is higher than the limit-value (120 µg/m^3) for the five worst cases in Lisbon metropolitan area. This should only occur, at most, 25 times a year in a three year average [202]

Lastly, the *fine particles matter* ($PM_{2.5}$) concentration in Lisbon's metropolitan area was analysed in terms of *annual average*, since this was the parameter established by Directive 2008/50/EC [202]. However, contrary to the other three already addressed airborne pollutants, $PM_{2.5}$ did not have a limit-value at the time of the development of this directive, but instead it had target-values since at the time the threshold below which human health was guaranteed was not yet identified [202]. Nonetheless, it is important to stress that $PM_{2.5}$ has a substantial negative effect on human health [202] and should be thoroughly monitored, since long-term exposure to this pollutant can result in the reduction of life expectancy, due to the increase of cardio-pulmonary problems, as well as lung cancer mortality [300].

The hourly values of the 26 monitoring zones in Lisbon's metropolitan area (Figure 2.11d) were assessed over a period of 18 years in terms of annual average in each year. This limit cannot overcome the target-value 25 µg/m^3. Figure 2.15 shows that this limit is guaranteed for all of the selected cases, which is quite reassuring. In addition, there is a general decrease of the $PM_{2.5}$ concentration over the years, except for *Entrecampos* at the second part of the decade (i.e. 2014–2017). The only zone that has a higher value than the target-value is *Fidalguinhos*. However, only one year of data is available, which is not representative enough to assess this zone's situation properly.

If *Tétreault's* "100, 10, 1" rule [261] is applied to the annual moving average for 2017 of *Entrecampos* (i.e. 17.8±5.3 µg/m^3), this would mean that the annual moving average of the indoor $PM_{2.5}$ concentration would be below ca 1.8 µg/m^3. Taking Table 2 in *Tétreault* [260] into account, this would mean that the $PM_{2.5}$ susceptible artefacts would start showing signs of decay in approximately nine years. Once again, this result shows the importance of addressing air pollution in terms of artefacts conservation.

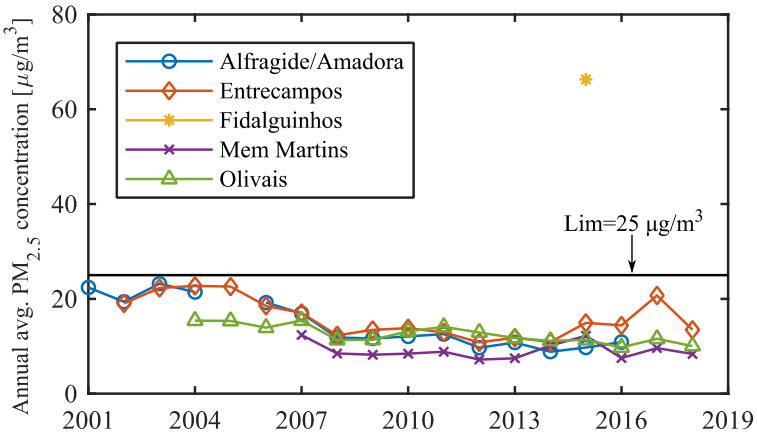

Figure 2.15 – Annual $PM_{2.5}$ concentration average (µg/m^3) for the five worst cases in Lisbon's metropolitan area. The annual average should not surpass the 40 µg/m^3 limit according to Directive 2008/50/EC [202]

2.3.3. Climate change

Nowadays climate change is one of the key challenges faced by mankind, since it will greatly influence the environment, human health and both global and local economy [284]. Furthermore, these changes will also affect the durability of buildings negatively [18]. However, due to the variability of all the factors that affect the emission of greenhouse gases (GHG) and, consequently, the outdoor climate, it is necessary to describe the different ways in which the outdoor climate might evolve.

For this purpose, the *Intergovernmental Panel on Climate Change* (IPCC) developed several scenarios that are grounded on different assumptions. Based on a multi-model methodology, the variance of the outdoor meteorological conditions was determined for all scenarios of the 3rd Assessment Report (TAR). Their driving forces are the demographic and socio-economic developments, as well as the technological evolution [196]. Prior to this report, the IPCC had already developed two others, namely the *First Assessment Report* (FAR) [301] in 1990 and the *Second Assessment Report* (SAR) [127] with the IS92 scenarios in 1995. Despite their interest, these reports will not be discussed because they are outdated.

Due to the need to reflect the updates suffered by climate change modelling, since scientific knowledge is constantly progressing, there is a need to produce new assessment reports that reflect these advances periodically. Hence, the assessment report that was developed after TAR was the 4th Assessment report (AR4), in 2007. This AR used some of TAR's scenarios – A2, A1B and B1. These three scenarios were updated due to the scientific progress that occurred during the years between both reports. More recently, the outdoor conditions were determined in accordance with the scenarios of the 5th Assessment Report (AR5), named *Representative Concentration Pathway* (RCP).

The assumptions behind the three more recent assessment reports will be briefly addressed in the following subchapter. More detailed information about them can be found elsewhere, i.e. TAR [196], AR4 [302] and AR5 [303]. In addition, the next assessment report is expected to be released between 2021–2022 [141], i.e. 6th Assessment report (AR6).

2.3.3.1. Effects of climate change in cultural heritage

The changes that the outdoor climate will suffer in the future will affect historic buildings negatively [18]. UNESCO World Heritage Report 22 [288] points out the major impacts of climate change in cultural heritage (Table 2.2). Amongst all the impacts mentioned by this document, the following impacts standout for historic buildings: physical changes of porous building materials and corrosion of metals due to *moisture change*; deterioration of facades due to thermal stress and freeze-thaw/frost damage induced by the *temperature change*; penetrative moisture into porous building materials and deterioration of surface due to *wind pattern changes*. These risks demonstrate the urgency in studying climate change in order to safeguard our cultural heritage.

Due to the great risks that climate change poses to cultural heritage there have been two European research projects that focus on analysing the effects of climate change on cultural heritage, namely: *NOAH's Ark* project [229], and *Climate for Culture* project [172]. The *NOAH's Ark* project aimed to fill the gap of the effects of climate change in cultural heritage buildings. Thus, European risk-based maps, which outline the risks of decay in cultural heritage in the future, were created [229].

The *Climate for Culture* research project focused on the study of the effects of climate change on the decay process of artefacts housed in historic buildings. A methodology based on computational models of the case-studies, future outdoor weather files and damage functions was used to assess the future risks for the collections. This methodology has been used in several other studies that analyse the future indoor conditions using computational models of historic buildings (e.g [18,129,128,130,131,218,266]).

For instance, Huijbregts et al. [128] concluded that an increase of both the indoor temperature and relative humidity is expected, and that in terms of the conservation of artefacts there is no location in Europe that is safe from some sort of decay, with each zone having its respective risks [129,130]. More recently, Rajčić et al. [218] determined that an increase of the risk of both mechanical and biological decay is expected in Croatia, while Turhan et al. [266] determined that an increase of the risk of chemical

decay and a decrease of the thermal comfort are expected in Turkey, due to the increase of the indoor temperature. Hence, it can be said that climate change will increase the risks of biological, chemical and mechanical decay to a different extent depending on the location.

Table 2.2 – Climate change risks and consequent impacts in cultural heritage buildings (table adapted from UNESCO World Heritage Report 22 [288])

Climate indicator	Risk	Impact
Moisture change	- Flooding - Intense rainfall - Changes in water-table levels - Changes in soil chemistry - Changes in humidity cycles - Increase in time of wetness - Sea-salt chlorides	- Physical changes to porous building materials and finishes due to rising damp - Crystallisation and dissolution of salts caused by wetting and drying affecting standing structures, archaeology, wall paintings, frescos and other decorated surfaces - Erosion of inorganic and organic materials due to flood waters - Relative humidity cycles/shock causing splitting, cracking, flaking and dusting of materials and surfaces - Corrosion of metals
Temperature change	- Diurnal, seasonal, extreme events (heat waves, snow loading) - Changes in freeze-thaw and ice storms, and increase in wet frost	- Deterioration of facades due to thermal stress - Freeze-thaw/frost damage - Damage inside bricks, stones, ceramics
Wind	- Wind-driven rain - Wind-transported salt - Wind-driven sand - Winds, gusts and changes in direction	- Deterioration of surfaces due to erosion - Penetrative moisture into porous cultural heritage materials
Climate and pollution	- pH precipitation - Changes in deposition of pollutants	- Stone recession by dissolution of carbonates - Blackening of materials - Corrosion of metals

2.3.3.2. Intergovernmental Panel on Climate Change assessment reports

2.3.3.2.1. Third assessment report

Due to the large variability of its driving forces, it is quite difficult to determine exactly how the world will evolve in 100 years from now. Hence, IPCC developed several evolution scenarios to cover the possible ways in which the world can evolve. Each of these scenarios is based on different assumptions in terms of society's development, more precisely in terms of technological, demographic and socio-economic development [196]. For the 3rd assessment report (TAR, 2001), the following six scenarios were developed, which are subdivided into four families: A1F1, A1B, A1T (family A1); A2; B1; and B2 (Figure 2.16). Each scenario has different levels of emission of gases that cause the anthropogenic

radiative forcing[1], e.g. CO_2, CH_4 [196], since they are based on different assumptions.

In total, 40 scenarios were developed for the 3rd assessment report (Figure 2.16). Furthermore, six of these scenarios were chosen to represent each family, which are known as "marker scenarios": AIM (A1B scenario), MiniCAM (A1F1 scenario), MESSAGE (A1T scenario); ASF (A2 scenario); IMAGE (B1 scenario) and MESSAGE (B2 scenario). These scenarios were chosen because the SRES team found them to be the ones that best represent the initial quantifications of each family storyline [134]. Moreover, these scenarios do not include additional climate policies as, for example, the emission targets established by the Kyoto Protocol or United Nations Framework Convention on Climate Change [196].

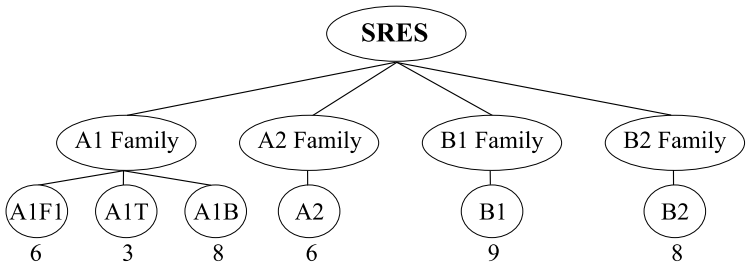

Figure 2.16 – Scenario families for TAR and respective number of developed scenarios (adapted from Ref. [196])

Although all greenhouse gases evolution is important, carbon dioxide is the main contributor for the radiative forcing [196]. All these scenarios are based on the fact that the variation of CO_2 emissions will greatly depend on the total energy consumption and energy supply structure [196]. Figure 2.17b shows the predominant type of energy in each scenario/year, since it is obtained by subtracting the amount of energy that has fossil sources to the amount of energy that has non-fossil sources. Hence, if the result is negative, then the focus for that scenario and that year is fossil technologies. In contrast, if the result is positive, then the focus is non-fossil technologies for that scenario and that year.

The A1 family is based on the assumptions of a fast economic growth (Figure 2.17c red, blue and green), the increase of the world's population, as well as the introduction of new and more efficient technologies [196]. The world's population will rapidly grow until mid-century and then will decline until 2100 (Figure 2.17a red, blue and green). The distinction between the three scenarios in family A1 – A1F1, A1B and A1T – lays in the evolution of the fuel powered technologies. Whilst scenario A1F1 is based on the intensive development of fossil fuel technologies (Figure 2.17b, red), the A1T is based on a non-fossil fuel technology development (Figure 2.17b, blue).

These assumptions will mean a steeply increase of the CO_2 emissions until 2080 for scenario A1F1, only refraining at the end of the century (Figure 2.17d, red). On the other hand, for scenario A1T there is a substantial increase of the CO_2 emissions in the beginning of the 21st-century, but the CO_2 emissions will steeply decrease after 2050 (Figure 2.17d, blue). Lastly, A1B scenario is based on the balanced development of both types of technologies (Figure 2.17b, green). These assumptions will mean a

[1] Difference between the amount of radiation absorbed by earth (emitted by the sun) minus the amount of energy emitted.

substantial increase of the CO_2 emissions in the beginning of the century. However, after 2050 the CO_2 emissions will steeply decrease due to the structural changes of the energy sector (Figure 2.17d, green).

Scenario A2 is based on a heterogeneous world in which its population continuously increases (Figure 2.17a, yellow) and in the assumption that fossil fuels remain the main source of energy (Figure 2.17b, yellow). These assumptions will mean a significant increase of the CO_2 emissions from the beginning of the 21st-century until 2100 (Figure 2.17d, yellow).

Scenario B1 has an evolution of the world's population very similar to the trend of the A1 family (Figure 2.17a, orange), but this scenario is also defined as having a fast change in the economic structure, since it will become service and information orientated. Subsequently, the material consumption will decrease [134]. In addition, this scenario is centred on clean and resource-efficient technologies, focusing on global solutions [134]. Due to these assumptions, the CO_2 emissions will initially increase, but mid-century they will steeply decrease, attaining the lowest value of the six scenarios (Figure 2.17d, orange).

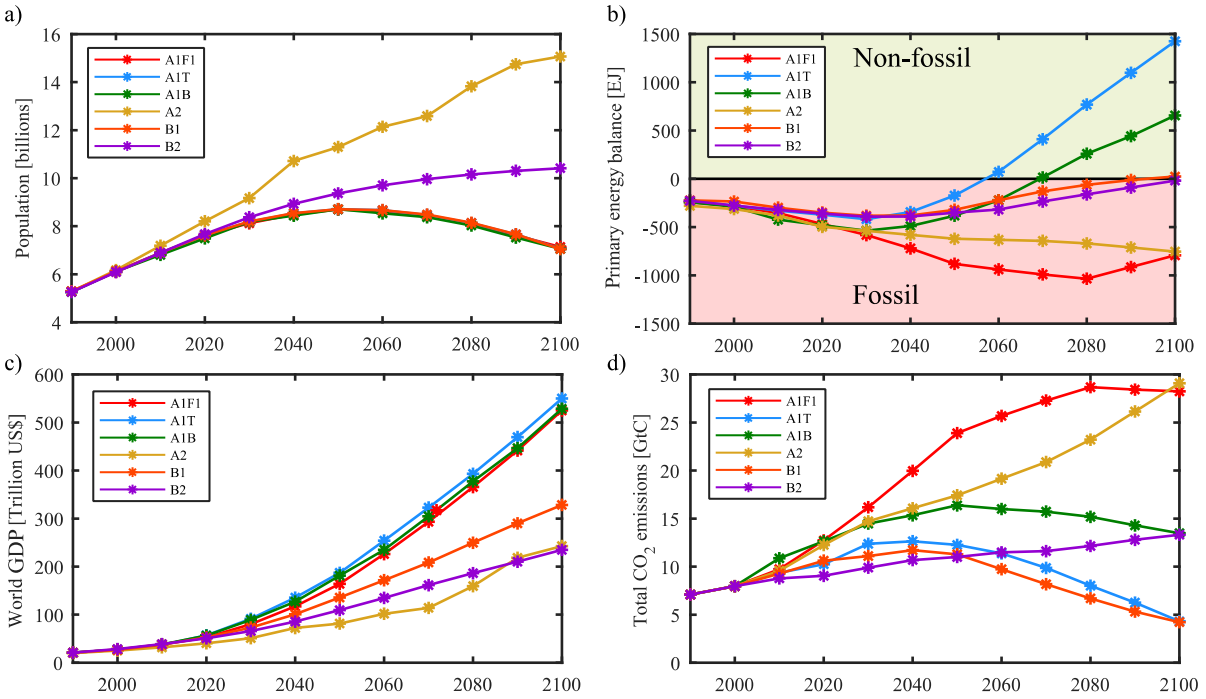

Figure 2.17 – Evolution of the world's population (a), balance between the primary energy for fossil sources and non-fossil sources (b), world's gross domestic product in trillions of US$ (c) and total carbon dioxide emissions in gigatons of carbon (d) between 1990 and 2100 for the six representative scenarios: A1F1, A1T, A1B; A2; B1 and B2 [258]

Finally, scenario B2 is based on the assumption of a gradual increase in the world's population (Figure 2.17a, purple), but to a lower extent than scenario A2. This scenario is also based on an intermediate level of economic development, a slower but a more diverse technological change than scenario B1 and family A1, focusing more on the local and regional level [134]. These assumptions will lead to a relatively constant increase of the CO_2 emissions across all the analysed period (Figure 2.17d, purple).

Overall, the six scenarios can be divided into three groups in terms of the magnitude of the radiative forcing that they induce to the outdoor climate [134]: low-radiative forcing – scenario **B1** and **A1T**;

mid-radiative forcing – scenario **A1B** and **B2**; and high-radiative forcing – scenario **A2** and **A1F1**.

2.3.3.2.2. Fourth assessment report

In 2007, the *Intergovernmental Panel on Climate Change* (IPCC) used some of the scenarios that were developed for the *Special Report on Emission Scenarios* (SRES) to assess the future variability of the world's meteorological conditions for the fourth assessment report (AR4) – B1, A1B and A2. Moreover, the scenarios descriptions for AR4 were the same as for TAR's [304], but the scenarios suffered updates due to the scientific progress that occurred during the six years between the reports.

For instance, access to a larger and more comprehensive amount of data, which had a wider geographical coverage; to more sophisticated data analysis methods and to a more extensive study on the uncertainty ranges allowed a better understanding of how the climate is going to change both in terms of space and time. This data was obtained using a larger number of models than in TAR, which are more complex and simulate climate changes more faithfully [304]. Additionally, the *Summary for Policymakers* (SPM) also summarized the main changes the climate has suffered in the recent years [304], namely:

- significant increase of the atmospheric concentration of CO_2, CH_4 and N_2O
- increase of air temperature and ocean temperature, as well as the surface water-vapour content (see subchapter 3.4.2.1 in Ref. [302])
- melting of glaciers and icecaps, which contributes to the increase of sea level
- increase of precipitation in some zones of the world – eastern parts of North and South America, northern Europe and northern and central Asia, but its decrease in other regions – Mediterranean, southern Africa and Sahel, as well as some regions of southern Asia
- more intense and longer droughts, particularly in the tropics and subtropics, but increase of the frequency of heavy rains events in most land areas
- changes in extreme temperature – cold days/nights and frost are less frequent, and hot days/nights and heat weaves are more common

In addition to the increase of ocean temperature, the oceans also absorb more than 80 % of the heat that is added to the system. This causes the seawater to expand and, consequently, contributes to the increase of sea level. For more detailed information about these topics consult chapter 3 in Ref [302].

The effects of each climate change scenario will differ from scenario to scenario since their forcing also differs. However, only the climate changes induced by scenario A1B and A2 in Europe will be addressed, since these two scenarios will be used in subsequent chapters. Nonetheless, the effects on the climate for the other scenarios can be consulted elsewhere [302].

Scenario A1B and A2 are based on certain scenarios drives that affect the outdoor conditions in Europe differently. In terms of temperature it is foreseen that the annual temperature will increase for all Europe

[302]. In contrast, the effect of climate change in precipitation will differ from region to region. For instance, both the annual precipitation and the number of precipitation days will decrease for the Mediterranean regions [302]. On the other hand, the precipitation will increase in winter and decrease in summer for central Europe [302]. The risk of drought in these two regions will increase in summer [302]. Distinctively, the annual precipitation and the extremes of daily precipitation will increase in the northern European regions [302]. Additionally, the snow season is likely to shorten in all Europe [302].

2.3.3.2.3. Fifth assessment report

A new set of climate changes scenarios were developed in the scope of the 5th Assessment Report [303], named *Representative Concentration Pathway* (RCP). However, these scenarios differ from the previous ones since the methodology applied to their development changed from a *sequential process*, which was used until AR4 and took about 10 years to be fully developed [238], to a *parallel process*. This change was carried out so that the time it takes to develop these scenarios decreases substantially, but also to couple the socio-economic drives and the changes in the outdoor climate more successfully [238].

The AR5 scenarios were based on a *parallel process* that instead of starting off with thoroughly characterized socio-economic storylines (which were used to generate future emissions scenarios and then climate scenarios [239]), they started off with a limited number of radiative forcing *pathways* that were *representative* of the emissions scenarios that existed in literature and the resulting ranges of GHGs *concentrations* were wide enough to produce clearly different climate change projections [239]. The novelty of this methodology is the fact that the climate scenarios and the socio-economic scenarios are developed parallelly, thus reducing the time it would take to develop these two phases [239]. Further information about the novelty of this process can be found elsewhere [238,239,303].

The RCPs describe four different ways in which the greenhouse gases and the air pollutants emissions, the atmospheric concentrations and the changes of land use can evolve in the future, namely [63]: RCP 2.6 (stringent mitigation scenario), RCP 4.5 and RCP 6.0 (two intermediate scenarios), RCP 8.5 (high GHGs emissions). These scenarios were named according to their total radiative forcing in 2100 (Figure 2.18). However, contrary to the SRES scenarios some of the RCPs scenarios included future climate polices [303]. Whilst RCP 2.6 is a mitigation scenario that includes this sort of policies to reduce the GHGs emissions, so that the increase of the global temperature is lower than 2 ºC relative to 1750 (i.e. pre-industrial age); the RCP 6.0 and RCP 8.5 are baseline scenarios that do not include these policies, thus reaching a higher level of GHGs emissions [63].

In addition, there is a correspondence in terms of radiative forcing between the scenarios of the 4th and 5th assessment reports, namely scenario RCP 4.5 is close to scenario B1, whilst scenario RCP 6.0 is close to scenario A1B and scenario RCP 8.5 is close to scenario A2 (Figure 2.18). However, this sort of correspondence does not necessarily mean the similarity of their respective GHGs emissions (Figure

F.1 for CO_2 and CH_4, which are the biggest contributors for the anthropogenic radiative forcing [259]) or their concentrations (Figure F.2, which also correspond to CO_2 and CH_4). Furthermore, the span of the radiative forcing for the RCP scenarios is much wider than the span for these three SRES scenarios, mainly due to RCP 2.6 (Figure 2.18).

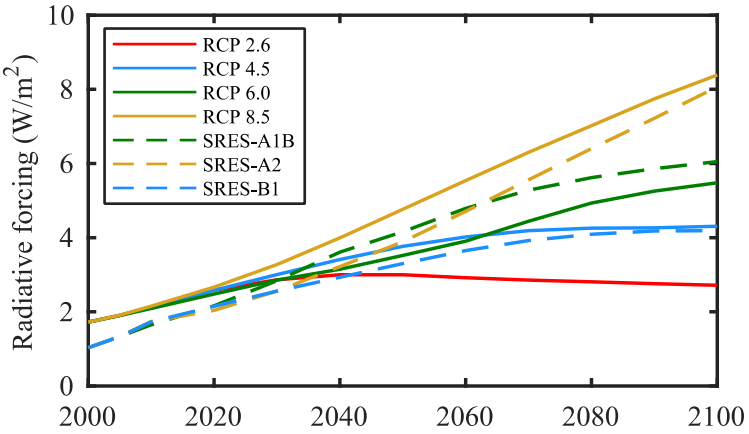

Figure 2.18 – Radiative forcing between 2000–2100 for the three SRES scenarios and four RCPs scenarios, namely: RCP 2.6 (IMAGE RCP3-PD [279,280]), RCP 4.5 (MiniCAM [256,61,285]), RCP 6.0 (AIM [116,124]) and RCP 8.5 (MESSAGE [222])

Both this new approach and the several other updates that were implemented in the modelling of the RCPs scenarios, due to the constant scientific progress, led to more robust climate change scenarios. Nonetheless, the climate change projected by the RCPs scenarios is similar to the one projected by the SRES scenarios for Europe both in terms of patterns and magnitude [305], namely:

- Increase of the global temperature all over Europe, but to a bigger extent in southern Europe during summer, as well as in northern Europe during winter
- Decrease of precipitation in southern Europe, and its increase in northern Europe
- Increase in the number of heat waves, droughts and heavy precipitations events
- Increase of the global mean sea level, as well as extreme sea level events (e.g. storms)
- Slight increase of the extreme wind speed during winter in central and northern Europe, and its slight decrease in southern Europe

2.4. Hygrothermal monitoring of historic buildings: case-studies

It is possible to highlight some studies, namely those performed in religious buildings that can be used to understand the natural response of heritage buildings and to contribute for future measures to control the indoor climate effectively. For example, Bratasz *et al.* [47] performed a monitoring campaign of the indoor climate of the church of Saint Maria Maddalena to evaluate the dimensional changes in its wooden altarpiece, which allowed to study how the constituents of the wooden altarpiece components behave according to the variation of the indoor climate conditions. Camuffo *et al.* [54], through a long-term monitoring campaign, studied the effects of replacing a warm-air heating system for a friendly-

heating system in two Italian churches – Saint Maria Maddalena and Saint Stefano di Cadore. San Juan Bautista Church in Talamanca de Jarama in Spain was monitored for 13-months to study how natural ventilation, human presence and the installed heating system affected the indoor climate and the buildings envelope [275,276]. Camuffo *et al.* [52] reconstructed the historical climate that a 15th century wooden bookcase was subjected for 500 years to define to which extend the indoor climate can be changed without inducing mechanical decay. Bertolin *et al.* [37] applied the same line of thought to a different case-study, namely an old choir installed in S. Giustina monastery in Padua, Italy. It is also worth pointing out the important work performed by the following monitoring campaigns in religious buildings [117,26,112,28,274].

The monitoring campaigns developed in Cathedral of Valencia, Spain [118,299]; St. Cristóvão church, Lisbon [250,251]; Saint Michael Archangel church, Poland [46] and Santa Maria Maggione Basilica, Italy [55,46], can be highlighted since they correspond to studies of non-heated historic buildings. García-Diego *et al.* [118] installed in 2007 a monitoring campaign in Cathedral of Valencia in Spain that included several sensors in the plaster layer (layer that supports the frescos), in the adjoining walls and also throughout the whole cathedral, and carried out a preliminary assessment based on the recorded data to determine if the frescos of the Spanish cathedral were endangered. Four years later and using the data recorded until then, Zarzo *et al.* [299] carried out a second assessment that validated the *principal component analysis* (PCA) as a preventive tool for culture heritage.

Silva *et al.* [250] performed a monitoring campaign in a 13th century church (St. Cristóvão) in Lisbon, Portugal. Using the recorded data, they developed a methodology adequate for historic buildings in temperate climates that aims to mitigate the physical damage induced by the environment in artefacts. The results of this campaign were also used to perform a thorough assessment in terms of biological, chemical and mechanical risk induced by the indoor conditions. This allowed the evaluation of the effects caused by the values of temperature and relative humidity imposed by each of the studied standards [251]. Bratasz et al. [46] proposed a method to mitigate the climate-induced physical damage by cutting the 16 % largest fluctuations. Then, this method was tested in three churches to encompass the main factors that influence the indoor climate of a historic building. Two of these churches were non-heated – Saint Michael Archangel church in Poland, and Santa Maria Maggione Basilica in Italy. This latter case-study had already been subjected to a monitor campaign by Camuffo *et al.* [55] with the aim to preserve its ancient mosaics and frescos.

The work performed in Malatestiana library in Italy [105], Classense library in Italy [12] and Necip Paşa library in Turkey [232] on non-heated libraries is also worth addressing. Fabbri *et al*. [105] performed a monitoring campaign of the Malatestiana Library in Cesena, Italy. Since its construction, in the 15th century, the indoor climate has been controlled by opening/closing the library windows. Andretta *et al.* [12] monitored the indoor conditions of the Classense library in Ravenna (Italy) during a summer period and a winter period to corelate the indoor conditions with the outdoor conditions. They also compared

the recorded indoor conditions against the recommended values by standard UNI 10586 [85] for libraries using the performance index (PI). Sahin *et al.* [232] performed a one year monitoring campaign of the Necip Paşa library in Turkey to assess if the indoor conditions presented biological, chemical and mechanical risk for the housed artefacts. They concluded that the application of passive measures should have priority over the installation of an HVAC system, due to the natural behaviour of the building.

2.5. Retrofit of historic buildings

Nowadays, one of the most used outputs of monitoring campaigns is the validation of thermal or hygrothermal models to perform thorough analysis of the several parameters that influence the building's behaviour (e.g. [66]). These models are validated against the measured indoor conditions in order to accurately represent reality. These models allow the thorough analysis of several parameters, such as the effects of applying improvement measures prior to their implementation (e.g. [281]), the effects of climate change in the indoor climate [172] or the effect of altering the setpoint strategy (e.g. [154]). The number of validated models of historic buildings has increased lately [66], which shows its usefulness in the preservation of cultural heritage buildings and their collections.

Due to their high heritage value, retrofit measures, such as the application of a thermal insulation layer in the exterior walls or the installation of mechanical systems, are always faced with a lot of adversities [203]. Hence, these measures have to be thoroughly studied and their effects quantified before application. This is one of the reasons why the development of computational models is such a useful tool for historic buildings. Nonetheless, these models have to be validated against the indoor conditions so that they can replicate reality accurately. This is a difficult task to perform, especially for historic buildings [66].

Due to the difficulty in implementing these measures, historic buildings are more susceptible to the effects of climate change [129,167]. Additionally, and as pointed out by *Lucchi* [175], preventive conservation is the best course of action to reduce the energy demand in a sustainable way without jeopardizing the artefacts welfare and human comfort. Hence, and taking into account climate change, it is fundamental to develop preventive conservation methodologies.

Sometimes, in order to achieve a proper indoor climate for the preservation of artefacts it is necessary to adopt passive or active measures or even a combination of both. For example, Muñoz-González *et at.* [194] studied several of these options to improve the indoor climate of a 17th century church in Seville (Spain) and Sciurpi *et al.* [243] studied several windows replacing options and different solar shadings for the "La Specola" Museum in Florence in Italy to improve the conservation metrics of the indoor climate. Both these studies used computational models to assess the improvement measures viability.

Retrofit measures aim to guarantee a proper indoor climate for the conservation of the housed artefacts without compromising the energy consumption of the building [234]. In the past few years, these measures have been subject to a significant number of studies that test their performance in historic

buildings having today's sustainability concerns in mind (e.g. [25,22,190,231,72,193,225,194]). In addition, these measures can also be important to ensure that these buildings are still around in the future [282].

However, their viability is greatly dependent on the outdoor climate [205], which means that a thorough study of the effects of each measure has to be developed in each specific case to ensure that they lead to an improvement of the indoor climate quality and not the opposite. This type of study is even more important for historic buildings that house collections due to these buildings' specific characteristics and the fact that most of them were not initially built to house artefacts. An inadequate retrofit measure might even threaten the collection welfare or might lead to irreparable damages in the building [224].

3. WHOLE-BUILDING HYGROTHERMAL MODELLING USING WUFI

This chapter has been partly published in the following reference: G.B.A. Coelho, H.E. Silva, F.M.A. Henriques, *Development of a hygrothermal model of a historic building in WUFI®Plus vs EnergyPlus*, in: **4th Central European Symposium on Building Physics (CESBP 2019)**, Prague, Czech Republic, 2019. doi:10.1051/matecconf/20192820207

3.1. Calculation methodology

Several software have been used to develop computational models of historic buildings to study either the thermal or the hygrothermal behaviour of the building [179]. However, WUFI®Plus is one of the most known software to develop studies concerning the hygrothermal behaviour of buildings, thus, making it an adequate choice for the work performed in this research. There are several examples of the application of this software to study the effects of different parameters in the hygrothermal behaviour of historic buildings, such as churches [18,86,13,87,19,177], palaces [39,177], museums [162,217] and other types of historic buildings [149,152].

The following subchapter shortly addresses the calculation equations used by WUFI®Plus in its hygrothermal mode, the software validations as well as the software disadvantages. More detailed information about the WUFI®Plus software can be found elsewhere Ref. [14].

WUFI®Plus is indeed a powerful hygrothermal simulation software that determines the indoor temperature and relative humidity for each zone of the model by taking into consideration the heat and moisture transfer that occurs through components, which is induced by the boundary conditions; the gains/losses due to natural and/or mechanical ventilation and the gains/losses due to internal heat or moisture sources/sinks, i.e. people, lights and equipment. The temperature and relative humidity for each zone is obtained by calculating the coupled heat and moisture balance equations [14]:

$$\frac{\partial H_i}{\partial t} = \sum_{j=1}^{n} \dot{Q}_{Comp,j} + \dot{Q}_{Sol} + \dot{Q}_{in} + \dot{Q}_{vent} + \dot{Q}_{HVAC} \quad 3.1$$

$$\frac{\partial C_i}{\partial t} = \sum_{j=1}^{n} \dot{W}_{Comp,j} + \dot{W}_{in} + \dot{W}_{vent} + \dot{W}_{HVAC} \quad 3.2$$

Where H_i is the enthalpy of the air in zone *i* (J), *t* is time (s), $\dot{Q}_{Comp,j}$ is the amount of heat from the inner surface of component *j* into zone *i* (W), $\dot{Q}_{sol}$ is the amount of radiation that goes through the transparent components into zone *i* (W), $\dot{Q}_{in}$ is the amount of convective heat in zone *i* (W), $\dot{Q}_{vent}$ is the amount of heat due to natural ventilation (W), $\dot{Q}_{HVAC}$ is the amount of heat due to mechanical ventilation (W), C_i is the amount of moisture in the air of zone *i* (kg), $\dot{W}_{Comp,j}$ is the moisture flux from the inner surface of component *j* into zone *i* (kg/s), $\dot{W}_{in}$ is the moisture production in zone *i* (kg/s), $\dot{W}_{vent}$ is the moisture flux due to ventilation (kg/s) and $\dot{W}_{HVAC}$ is the moisture flux due to mechanical ventilation (kg/s).

The heat and moisture transfer that occurs through opaque components is based on *Künzel*'s [163] one-dimensional simultaneous heat and moisture transfer model, in which the variables are the temperature and relative humidity. For the transparent components WUFI®Plus calculates the amount of heat that goes across a window through transmission based on the window's thermal transmittance and emissivity, and the amount of incident solar radiation that manages to go through the window based on a direct solar heat gain coefficient, a diffusive solar heat gain coefficient and the frame section.

The ventilation in buildings can be either induced by physical effects, i.e. natural ventilation, or by using a mechanical equipment. WUFI®Plus takes into consideration both these types of ventilation in the heat and moisture balance equations. The internal heat and moisture gains or losses due to living beings and/or equipment are also taken into consideration in the heat and moisture balance equations. A detailed explanation about these behaviours and their calculation methodologies can be found elsewhere [14].

In order for WUFI®Plus to perform at its full capacity [75,292], the following parameters have to be defined (Figure 3.1):

- Basic materials' properties – bulk density (kg/m^3), porosity (-), specific heat capacity (J/kg.K), thermal conductivity (W/m.K), and water-vapour diffusion resistance factor (-);
- Advanced materials' properties – moisture storage function, liquid transport coefficient (m^2/s), moisture-dependent thermal conductivity (W/m.K) and resistance factor (-), temperature-dependent thermal conductivity (W/m.K) and enthalpy (J/kg);
- Outdoor weather file (in hourly time steps preferably) – wind speed (m/s) and wind direction (º), normal rain (mm), global and diffuse radiation (W/m^2), air temperature (°C), relative humidity (-), atmospheric pressure (hPa). If radiation cooling is to be account for in the simulations, then the weather file must also have the long-wave atmospheric radiation (W/m^2) and cloud index (-) both also in hourly time steps [292];
- Detailed schedule of the internal sources – building's occupancy schedule, illumination and equipment use.
- Surface variables – heat transfer resistances (calculated depending on the wind characteristics if needed), short-wave radiation absorption, long-wave emissivity, shading factor, solar gain, water-vapour transfer coefficients, additional water vapour diffusion resistance factor (for surface coatings if needed), rain load coefficients and rain absorption coefficient (if rain load is considered)
- Building geometry and disposition – surfaces orientation and dimension, building's volume and floor area, windows and doors placement

If the case-study has direct contact with soil, then it is also necessary to input the soil/slab interface temperature [292]. For window elements, it is necessary to define the window's thermal transmittance (W/m^{2}K), the frame factor (-), the short-wave radiation average (-) and the long-wave radiation emissivity (-) [292].

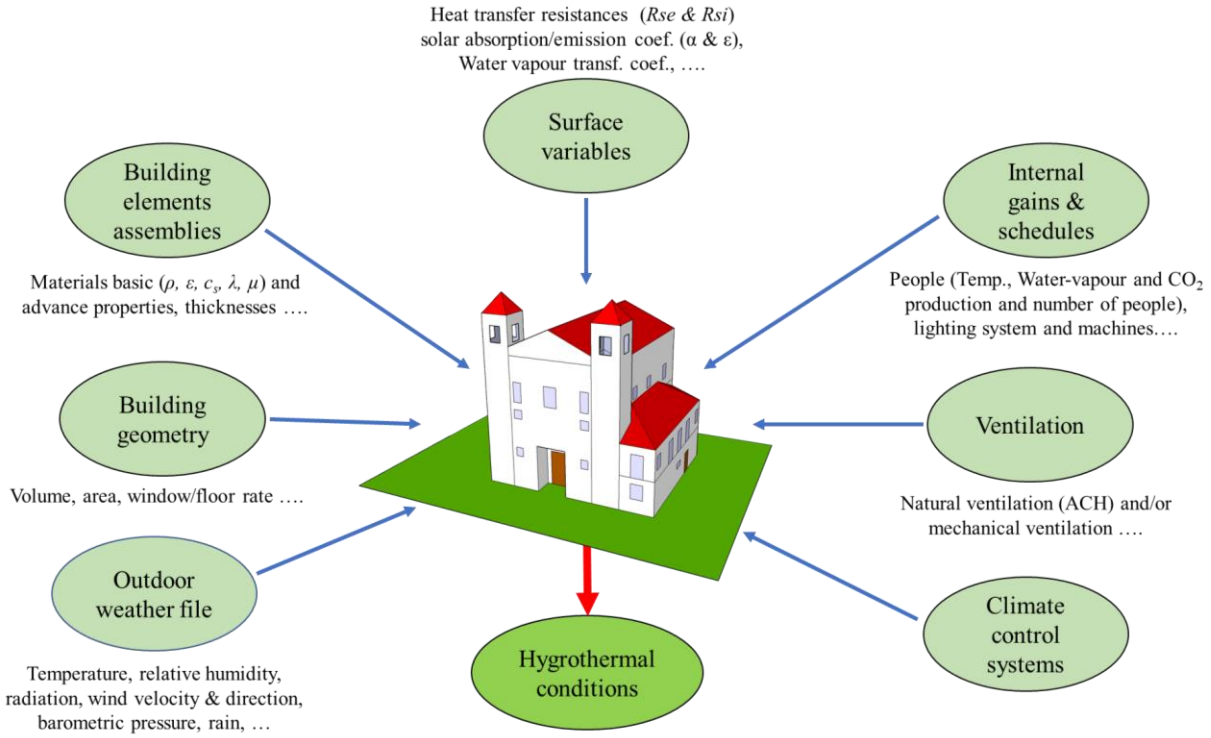

Figure 3.1 – Outline of the necessary inputs necessary for WUFI®Plus to run at its full capacity

3.2. Software inputs

This subchapter briefly addresses the inputs necessary for WUFI®Plus to solve the coupled heat and moisture balance equations, i.e. data describing the outdoor and indoor climate, the basic and advanced properties of the materials that make up the constructive element; the internal gains in terms of people and illumination. More detailed information about these topics can be found elsewhere [14].

3.2.1. Weather files

In hygrothermal modelling, the outdoor boundary conditions are defined using a weather file that is based on measured meteorological data. This data is typically registered in open spaces, such as airports fields, so that the equipment is unaffected by the influence of other buildings/objects [138].

The meteorological data in hourly time steps that WUFI requires to perform at its full capacity are the following [75,292]: wind speed (m/s) and wind direction (º), normal rain (mm), direct and diffuse radiation (W/m^2), air temperature (°C), relative humidity (-), atmospheric pressure (hPa). If the radiation cooling is to be account for in the simulations, then the weather file must also have the long-wave atmospheric radiation (W/m^2) and cloud index (-) both in hourly time steps [292].

If the case-study is a building, then WUFI needs the soil/slab interface temperature [292]. Another important input for the software is the ventilation, which can be determined by monitoring the indoor carbon dioxide concentration [27]. Additional to WUFI's incorporated weather file database, there are several other that have sets of weather files that can be used to run hygrothermal simulations in WUFI [292], for example, EnergyPlus online database [83], LNEG's excel climatic data [174] and Meteonorm

program [185], amongst other.

3.2.1.1. Soil/slab interface temperature

Although soil/slab interface temperature is a key input in whole-building hygrothermal simulations, it is not very often mentioned in the models' description (e.g. [104]). However, since WUFI®Plus cannot simulate this interface temperature it has to be either monitored or determined using another software. EnergyPlus [81] can determine the interface temperature using the *Slab pre-processor*, through *Detailed Ground Heat Transfer* field; or *Ground Domain* through one of the three available models to determine the undisturbed ground temperature: *Finite Difference, Kusuda-Achenbach* and *Xing.* All these methods need both the soil and slab properties, i.e. λ, ρ and c_p; and additional data is needed to determine the interface temperature.

The interface temperature can also be determined using the methodology of Standard EN ISO 13788 [93] or, for more complex cases, the methodology of Standard ISO 13370 [94], or even a sine curve. The interface temperature can also be rudimentarily determined by subtracting 2 ºC to the indoor monthly average [267].

The *Detailed Ground Heat Transfer* needs the monthly indoor average temperature for the twelve months of a year, the area/perimeter slab ratio and the slab thickness [268]. A disadvantage of this method is the fact that it requires the average indoor temperature for each month of the year. However, this can be overcome by conducting a preliminary simulation and then using the output average indoor temperature for each month in the second simulation. The *Kusuda-Achenbach* method [164] assumes that the earth temperature can be determined by a simple harmonic time function, which is valid for heat transfer through the soil/slab interface. This method only requires the soil surface temperature average and respective amplitude, and the day with the lowest surface soil temperature.

Xing [296] developed a one-dimensional numerical model to determine the ground temperature through a full surface heat balance by using some of the outdoor conditions, i.e. incident short-wave radiation on a horizontal surface, air temperature and relative humidity as well as wind speed. However, Xing et al. [297] also stated that for most engineering challenges it was not necessary to use such a complex model. Therefore, a simpler model that only required a few parameters, i.e. the annual soil temperature average, two temperature amplitude and two-phase shift, was developed, i.e. the two-harmonic analytical model.

The *Finite Difference* method is a one-dimensional implicit finite difference heat transfer model based on *Xing* [296] model assumptions and on *Lee* [170] numerical methods that uses the weather file to determine the daily boundary conditions averages and requires the soil moisture content volume fraction, soil moisture content volume fraction at saturation and evapotranspiration ground cover [269].

The sine curve determines the soil/slab interface temperature using the mean annual temperature and its

amplitude, as well as the day with the highest temperature. Choosing this option offers better results since they can be fitted to the real case. However, since the model is fitted to these conditions it cannot be applied to other outdoor conditions. As a result, this option is restrictive since it cannot be used under different conditions or in other situations.

3.2.1.2. Carbon dioxide concentration

A room's *Air Change per Hour* (ACH) is normally determined through the release and, subsequent, monitoring of the concentration values of the tracer gas in the room. The used gas should be non-toxic, chemically stable, not absorbable or adsorbable by building materials, have a density close to the air and a low concentration in the atmosphere. The most common used gases are nitrous oxide (N_2O), sulphur hexafluoride (SF_6), carbon dioxide (CO_2) and helium (He) [27].

The mass balance equation is obtained by subtracting the amount of gas that leaves the room to the amount of gas that enters the room plus the amount of gas that is generated in the room:

$$V \cdot \frac{\partial c_{int}}{\partial t} = G + Q \cdot (c_{ext} - c_{int}) \quad 3.3$$

Where V is the volume of the room (m^3), c_{int} is the internal gas concentration (ppm), t is the time (s), G is the rate of the generated gas in the room (m^3/s), Q is the air volume flow rate through the enclosure (m^3/s) and c_{ext} is the external gas concentration (ppm). There are three different methods to determine the ACH of a room using an inert gas: c*oncentration decay method*, *constant tracer injection method* and *constant concentration method*. Of the three methods, the concentration decay method is the most commonly used method [27].

The *concentration decay method* consists on injecting the tracer gas into the room and allowing it to mix with air inside the room. After achieving equilibrium, the concentration of the tracer gas is monitored using an appropriate detector during a suitable period of time.

Assuming that there is no production of the gas inside the room and that its concentration in the atmosphere is low (e.g. SF_6), the ACH of the room can be obtained using the following equation [3]:

$$ACH = -ln\left(\frac{c_{int,t}}{c_{int,0}}\right) \cdot \frac{1}{t} \quad 3.4$$

On the other hand, if the gas' concentration in the atmosphere is not negligible (e.g. CO_2), the ACH of the room has to be calculated using the following equation [209]:

$$ACH = -ln\left(\frac{(c_{int,t} - c_{ext})}{(c_{int,0} - c_{ext})}\right) \cdot \frac{1}{t} \quad 3.5$$

If during the experimental campaign, the external gas tracer concentration is not recorded for any type of reason, it is possible to assume that its value is equal to the internal gas concentration in steady-state,

i.e. when the variation of the internal gas concentration is less than 2 % for at least 1 hour [191].

The *constant tracer injection* method is quite similar to the concentration decay method, except for the fact that when the equilibrium is achieved the gas tracer will still be pumped into the room at a constant rate, and both the pump rate and the concentration are monitored throughout the test [27]. The c*onstant concentration method* relies in maintaining a constant level of the gas tracer concentration during all the test by controlling the gas injection rate [27]

3.2.2. Hygrothermal properties of building materials

WUFI divides the building materials properties in two major categories [292]: the basic properties, which are indispensable for the program, but are easily determined or found in literature; and the advance properties, which can be left out whilst inputting building materials into the database. However, by leaving out these properties, WUFI will not perform to its fullest, which means that not all the heat and moisture processes that WUFI considers will be taken into account in the simulation [113]. Hence, the results will be far from reality.

3.2.2.1. Basic properties

The basic properties include bulk density (kg/m^3), porosity (m^3/m^3), specific heat capacity (J/kg.K), thermal conductivity of the building material in dry state (W/m.K), and water vapour diffusion resistance of the building material in dry state (-). These five properties will be shortly addressed in the following subchapters. In addition, the individual procedures to determine these properties are thoroughly described, for example, in Delgado et al. [75] or Krus [161].

3.2.2.1.1. Bulk density

The bulk density of a building material, which is presented in kg/m^3, is obtained by dividing the mass of the sample by its respective volume. WUFI uses this material's property to transform the specific heat capacity by mass (J/kg.K) into the specific heat capacity by volume (J/m^3.K) by multiplying the first for the material's bulk density [113]. The specific heat capacity by volume is used in the heat transport equations, more precisely in the enthalpy calculations. The bulk density of a building material is obtained using the following equation:

$$\rho_{bulk} = \frac{m}{V_{total}} \qquad 3.6$$

Where ρ_{bulk} is the bulk density of the building material (kg/m^3), m is the mass of the sample (kg) and V_{Total} is the volume of the sample (m^3).

3.2.2.1.2. Porosity

The porosity of a material is the ratio of the volume of voids per the total volume of the sample. Its values can either be presented in m^3/m^3 or in percentage. This property allows to determine the

maximum water content of the building material by simply multiplying its value for the bulk density of water [113]. As it is known, the latter varies with the temperature [146], however, WUFI® does not take this variance into account and assumes that the bulk density of the water is 1000 kg/m^3. Since in most of the simulations, the water content does not surpass the saturation water content (i.e. limit which is inferior to the maximum water content), it is possible to estimate the value of the maximum water content. The porosity of a building material is obtained using the following equation:

$$\Psi = 1 - \frac{\rho_{bulk}}{\rho_{true}} \quad 3.7$$

Where ψ is the porosity (m^3/ m^3), ρ_{true} is the true density (kg/m^3) and ρ_{bulk} is the bulk density (kg/m^3). Building materials can either be classified as having: *open porosity*, in which there is communication between the voids and, therefore, the circulation of fluids within the material is possible (e.g., air, moisture); and *closed porosity*, when there is no connection between the voids, hence there is no circulation of the fluids within the material (i.e. impermeable materials). Most of the building materials have open porosity [115].

3.2.2.1.3. Specific heat capacity

The specific heat capacity by mass (J/kg.K) is the amount of energy necessary so that one kilogram of the building material in dry state increases its temperature by one degree Kelvin. On the other hand, the specific heat capacity by volume (J/m^3.K), which was previously mentioned, is the amount of energy necessary so that one cubic meter of the material increases its temperature by one degree Kelvin.

The advantage of using the specific heat capacity by mass is the fact that it depends on the chemical composition of the material, and not on its porosity [113]. Since the specific heat capacity by mass refers to the material in its dry state, the software will account for the enthalpy changes caused by moisture in its various states, i.e. liquid, vapour and solid.

3.2.2.1.4. Thermal conductivity

The thermal conductivity (W/m.K) is the amount of energy that goes through a unit of thickness of the material for a temperature differential of one degree Kelvin. In WUFI, the thermal conductivity refers to the building material in dry state. However, the contribution of the latent heat of evaporation must be subtracted from the amount of total energy because it is already accounted elsewhere in the heat transport equation. The influence of moisture in this property is also considered by the software (subchapter 3.2.2.2.3).

3.2.2.1.5. Water vapour diffusion resistance factor

The diffusion of water vapour in a porous medium faces a resistance distinct from that encountered in the environment. This distinction results from the material characteristics. This behaviour is

characterized by the vapor diffusion resistance factor. This factor shows that the diffusion resistance in the porous medium is superior to that of the environment and refers to the material in its dry state.

3.2.2.2. Advance properties

The advanced properties include the moisture storage curve (kg/m^3), the liquid transport coefficient for suction (m^2/s) and the liquid transport coefficient for redistribution (m^2/s), the dependency of the thermal conductivity to moisture (W/m.K) and the dependency of the water-vapour diffusion resistance factor to moisture (-).

3.2.2.2.1. Moisture storage curve

The majority of the materials used in civil engineering is hygroscopic [115], which means that that they have the capacity to store moisture and that moisture can travel through them. Consequently, this type of materials can be greatly influenced by the border conditions. Hence, it is of key importance to establish a relationship between the border conditions and the amount of moisture within the building materials. The moisture storage curve establishes the correspondence between the value of water content for the selected building material to each value of relative humidity.

The concept that quantifies the moisture within a building material is the water content since it quantifies the moisture regardless of its physical form. Moisture can exist within a building material in its three forms, namely solid, liquid and vapour. However, it is only transported in either its vapour state (named *diffusion flux*) or in its liquid stated (named *capillary flux*). Whilst the diffusion flux is governed by the water-vapour pressure, the capillary flux is governed by the water content.

The moisture storage curve is divided in three regions: hygroscopic, capillary (or super-hygroscopic depending on the literature [163]) and supersaturated (Figure 3.2). The hygroscopic region is composed by a molecular adsorption zone and a capillary condensation zone. Initially, the water molecules attach to the walls of the pores, thus forming a single layer of water molecules. When it reaches approximately a relative humidity of about 20 %, adjacent layers to the single layer are created, thus reducing the cross-section of the pore channels. This behaviour is named multi-molecular adsorption and occurs until approximately 40 % of relative humidity. Depending on the material properties, concave menisci, in which condensation occurs for values inferior to 100 %RH; or convex menisci, in which condensation occurs for value higher than 100 %RH, are created within the pores.

The hygroscopic region is characterized by the transport of moisture in the vapour phase, and its inferior limit is the water content of the material in dry state and its superior limit is the free water saturation (≈ 95 %RH). On the other hand, the capillary region is mainly characterized by the transport of moisture in liquid state. Consequently, there is a gradual reduction of the cross-section of the pore channels until it reaches the free water saturation (≈ 100 %RH), and water-vapour diffusion stops occurring.

The free water saturation corresponds to the maximum amount of moisture a building material can store

under normal conditions. Depending on the building material, there may be air pockets in its constitution, which can lead to a higher water content than the free water saturation. For example, the pores that are not interconnected are not filled with moisture under normal conditions, only in supersaturated region are these pores filled with moisture. This limit is only achieved under special conditions, i.e. when the building material is subject to an overpressure or when it is submerged for a considerable period of time. This domain is usually neglected in the moisture storage curve since it is not possible to establish a relationship between the increase in water content and a constant relative humidity.

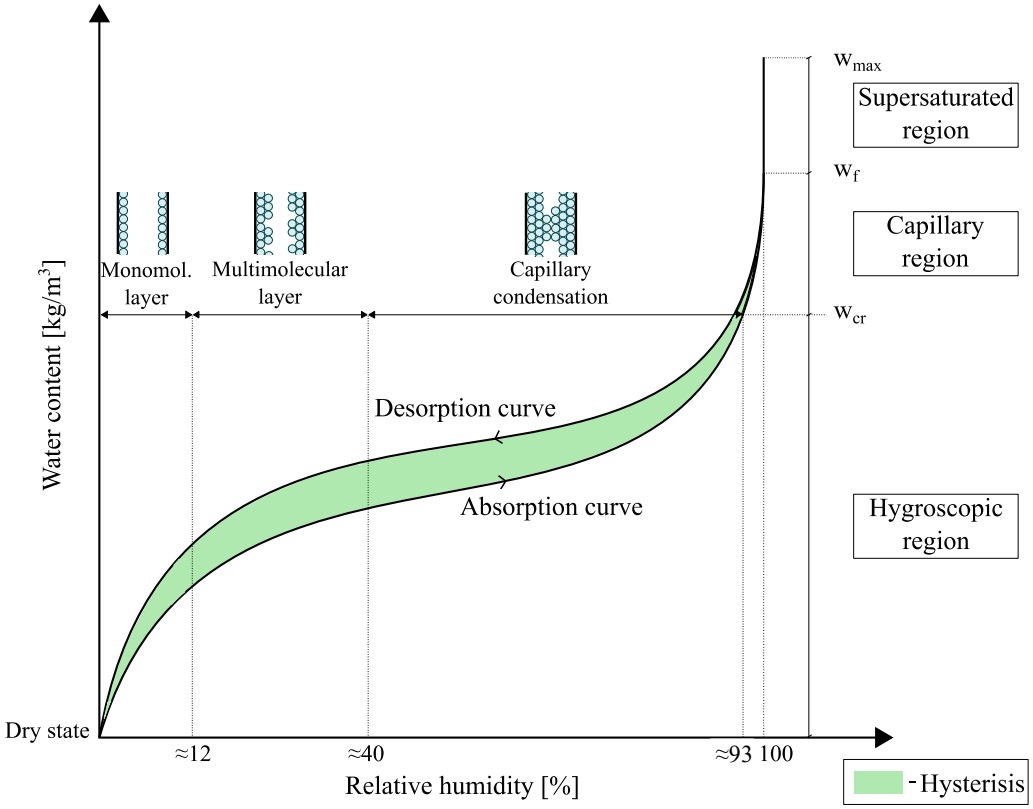

Figure 3.2 – Example of a moisture storage function for a building material (adapted from Ref. [115,123])

In the hygroscopic region (i.e. between the material in its dry state and approximately 93 %RH), the moisture storage curve is either determined by the desiccator method or by the climate chamber method [139]. Both methods obtain an adsorption curve, since they are based on the methodology of determining the mass of the specimen that is under controlled temperature and relative humidity conditions until the specimen reaches an equilibrium with the boundary climate. However, it is not possible to determine the moisture storage curve in the capillary region using either of these two methods, because both the salts and the climatic chamber cannot attain relative humidity above 93%.

Hence, an alternative technique named *pressure plate method* [161,200], which was initially created to characterize soils, is used to determine the moisture storage curve in the capillary region. This technique consists on applying a pressure to saturated specimen until they reach the equilibrium, and,

subsequently, determining the amount of expelled moisture. Based on Kelvin's law it is possible to correspond the applied pressure to a certain relative humidity value, and with the amount of expelled moisture it is possible to determine the water content for each level of applied pressure (equation 3.8). Contrary to the procedures applied to determine the hygroscopic curve, which obtains an adsorption curve, the pressure plate method obtains a desorption curve.

$$\varphi = e^{\left(-\frac{s \cdot M_w}{\rho_w \cdot R \cdot T}\right)} \quad 3.8$$

where φ is the relative humidity (-), s is the capillary pressure (Pa), M_w is the molar mass of water (kg/mol), R is the gas constant (J/kg.mol) and T is the temperature (K). Alternatively, to the pressure plate method it is possible to use the *mercury porosimetry method*, which in spite of being faster, having a greater precision and covering a greater range of pore radius, depicts a picture far from the real situation, since it does not use water to perform the procedure as *pressure plate method* [161].

3.2.2.2.2. Liquid transport coefficient

In the hygroscopic region, the liquid conduction coefficient is obtained using the following equation:

$$D_\varphi = P_{v,sat} \cdot \delta \cdot \left(\frac{1}{\mu^*(\varphi)} - \frac{1}{\mu}\right) \quad 3.9$$

Where D_φ is the liquid conduction coefficient (kg/m.s), $P_{v,sat}$ is the saturation vapour pressure (Pa), δ is the water vapour permeability of stagnant air (kg/m.s.Pa), μ* is the fictious water vapour diffusion resistance factor (-) and μ is the water vapour diffusion resistance factor of the building material in its dry state (-). The water-vapour diffusion resistance factor of the building material corresponds to material in its dry state (i.e. 3 to 50 % relative humidity), whilst the fictious water vapour diffusion resistance factor corresponds to high relative humidity values (i.e. 50 to 90 % relative humidity).

In the capillary region, the liquid conduction coefficient is obtained using both the moisture storage curve and the liquid transport coefficient. In addition to the difficulty in determining the liquid transport coefficient, this parameter varies with the amount of moisture within the building material. Hence, WUFI uses a simplified method to determine the liquid transport coefficient based on the water absorption coefficient building material, on its free water content and water content.

The liquid transport coefficient depends on the characteristics of the building material, but it also depends on the conditions of the boundary climates. WUFI uses one of two liquid transport coefficients depending on the conditions of the boundary climates, i.e. whether rain hits the building element or not. WUFI uses the *liquid transport coefficient for suction* when the building material is subjected to an interrupted supply of water and, consequently, the surface of the building material is completely wet. Suction will be dominated by the larger pores, since they have a minor resistance.

On the other hand, when the building material is not subjected to an interrupted supply of water, the

moisture within the building material is redistributed and WUFI uses the liquid transport coefficient for redistribution. The redistribution process of moisture is dominated by the smaller pores, since there is no continuous supply of water, the amount of moisture within the building material will decrease, which means that the smaller pores (higher capillary pressure) will extract the moisture within the large pores (smaller capillary pressure).

Since redistribution is governed by the smaller pores, which have a greater flux resistance, and suction is governed by the larger pores, which have a minor flux resistance, these processes will occur at different velocities. Normally, the redistribution coefficient is smaller than the suction coefficient [113].

Since the liquid transport coefficient has not been measured for a significant number of building materials, WUFI determines this coefficient for suction using the following equation [113]:

$$D_{ws} = 3.8 \cdot \left(\frac{A}{w_{sat}}\right)^2 \cdot 1000^{\left(\frac{w}{w_{sat}}\right)-1} \quad 3.10$$

Where D_{ws} is the liquid transport coefficient for suction (m^2/s), A is the water absorption coefficient ($kg/m^2s^{0.5}$), w_{sat} is the free water content (kg/m^3) and w is the water content (kg/m^3).

The liquid transport coefficient for suction increases with water content. However, the previously mentioned equation cannot be used in the supersaturated region, since there is no relationship between the water content and the liquid transport coefficient. On the other hand, the redistribution coefficient is assumed to be one decimal of the suction coefficient in the capillary domain [163].

3.2.2.2.3. Thermal conductivity dependent on the moisture content

Hygroscopic building materials have the capacity to store fluids within, such as moisture. The amount of moisture will affect the thermal conductivity of the building material, since its increase is associated to the replacement of the existing fluid within the building material. The replacement of air that has a thermal conductivity of 0.025 W/m.K [235] for moisture that has thermal conductivity of 0.6 W/m.K at 10 ºC [235], will mean an increase of the thermal conductivity of the hygroscopic material.

The thermal conductivity dependent on the moisture content is determined using the following linear equation, whose initial value is the thermal conductivity of the building material in its dry state:

$$\lambda = \lambda_0 \cdot \left(1 + \frac{b \cdot w}{\rho_{bulk}}\right) \quad 3.11$$

Where λ is the thermal conductivity of the building material (W/m.K), λ_0 is the thermal conductivity of the building material in its dry state (W/m.K), b is the thermal conductivity supplement (%/M.-%), w is the water content within the building material (kg/m^3) and the ρ_{bulk} is the bulk density of the building material in its dry state (kg/m^3). The thermal conductivity supplement accounts for the increase in percentage of the thermal conductivity in accordance to the percentual increase of the moisture mass.

The thermal conductivity supplement value depends on the characteristics of the building material [163].

3.2.2.2.4. Water vapour diffusion resistance factor dependent on moisture content

In experimental measurements, the values referring to the diffusion of water vapour and those referring to the surface diffusion are not separated, which means there will be a reduction of the diffusion resistance, i.e. the water-vapour diffusion resistance factor will decrease accordingly. This reduction, which occurs at high relative humidity values, means that this factor is dependent on the moisture content [113].

WUFI has two methods to account for this dependency [113]: the first considers that this factor is constant and adjusts the liquid transport coefficients to account for the surface diffusion accordingly; the second uses a water-vapour diffusion resistance factor that depends on moisture. In both methods, and for water content values higher than the free water saturation, the water-vapour diffusion resistance factor decreases with the increase of water content until it reaches zero, which corresponds to the maximum water saturation [113]. This decrease of the water-vapour diffusion resistance factor shows the difficulty of vapour diffusion occurring at high relative humidity values, since even the larger pores are filled with moisture.

3.2.3. Internal gains

The indoor climate is influenced by many variables, such as the outdoor climate and the building envelope, as well as the occupants, lighting system and equipment (these last three variables are commonly referred to as *internal gains*) [6]. Internal gains can be responsible for an increase/decrease of the indoor heat load, moisture load or CO_2 concentration. The effect that each source has on the indoor climate depends on the type of source. For instance, humans are responsible for the increase of temperature, humidity level and CO_2 concentration, whereas a computer is solely responsible for the increase of the indoor temperature.

The internal gains that are usually considered whilst developing hygrothermal/thermal models are human beings, lighting system and the building's electric equipment. Since the focus of this research is historic building that exhibit/store artefacts, the contribution to the internal gains load of the electric equipment is almost non-existent when compared, for example, to an office. Thus, its contribution to the indoor climate of historic buildings will be neglected henceforth.

3.2.3.1. People

People have a key influence on the hygrothermal behaviour of buildings, as well as its indoor air quality, since each person produces sensible and latent heat, and CO_2. In addition, a person can also be responsible for carrying air pollutants inside the building, which can accelerate the deterioration process of the artefacts [207].

While the fraction of latent heat is responsible for the instantaneous increase of water-vapour

concentration in a space, the sensible heat fraction is absorbed and stored by the surrounding materials. It is estimated that between 20–60 % of the emitted sensible heat assumes the radiation form, which depends on several aspects, such as clothing, mean radiant temperature and air velocity [262]. This heat is dissipated by *radiation* from the body surface to the surrounding surfaces, *convection* from the body surface and respiratory act to the surrounding air, and *moisture evaporation* from the body surface and respiratory act to the surrounding air [56]. The sensible heat emitted by a person is split in its radiation and convection portion according to a person's clothing, performed activity, mean radiant temperature and air velocity.

The heat generated by a human body, which usually performs at ca. 37 ºC [56], varies according to a person's characteristics – i.e. gender, diet, age and physical attributes, as well as the performed activity. It is usually referred to as *metabolic rate*, which can be presented in either met or W/m^2 (1 met = 58.2 W/m^2 [180]). There are several standards worldwide that have metabolic rates for numerous activities, such as ASHRAE Fundamentals [7], ISO 8996 [140], ASHRAE 55 [4], EN 13779 [95] or ISO 7730 [137].

However, there is no consensus in the scientific community concerning metabolic rates for museums and churches. The values used in literature differ substantially among authors and usually vary between 1.0 and 2.0 met. For example, Bellia *et al.* [34], who analysed the operating costs of several HVAC systems using a computational model of a modern museum, assumed a total heat gain per person of 147 W with 85 W being sensible heat and 62 W being latent heat (this corresponds to ca. 1.4 met considering a surface body area of 1.8 m^2 [140]). Ascione *et al.* [24], who analysed air diffusion equipment resorting to computational modelling, adopted a metabolic rate of 1.5 met/person. Ferdyn-Grygierek [108,110], who studied the implications of the temperature scheme and several ventilation systems on a museum's energy consumption, assumed that each visitor would be responsible for 75 W of sensible heat (50 % was emitted by convection and the other 50 % by radiation) and 55 W of latent heat, which means a total heat of 130 W (this corresponds to ca. 1.2 met considering a surface body area of 1.8 m^2 [140]). Kramer *et al.* [154], who studied the energy-saving potential of several setpoint strategies using a simulation model of the Hermitage Amsterdam museum, assumed that each visitor was responsible for 100 W (this corresponds to ca. 1 met considering a surface body area of 1.8 m^2 [140]).

Furthermore, Karyono *et al.* [148], who aimed at widening the scope of the typical thermal comfort studies, assumed that in the studied cathedral the visitors would have a metabolic rate of 1.0 met (which corresponds to *seated, relaxed* [140]) and in the museum it would vary between 1.0 (which corresponds to *seated, relaxed* [140]) and 1.2 met (which corresponds to *standing, at rest* [140]). Balocco *et al.* [29], who modelled an 11^{th} century church in Florence, assumed that each visitor emitted 75 W of sensible heat and 55 W of latent heat, which means a total heat of 130 W (this corresponds to ca. 1.2 met considering a surface body area of 1.8 m^2 [140]). Camuffo *et al*. [54], who tested a heating system in two churches in Italy, considered that the metabolic rate of a person varied from 1.0 met (*seated, quiet*

person [4]), 1.2 met (*standing, relaxed person* [4]), 1.5 met (*singing* [4]) and 2.0 met (*walking* [4]). Finally, Aste *et al.* [26], who studied several heating strategies for churches using the Basilica di Collemaggio as a case study, assumed a total heat load of 108 W per person (this corresponds to ca. 1 met considering a surface body area of 1.8 m^2 [140]).

3.2.3.2. Light

Light is a key environment factor in conservation, since it can cause irreversible damages to artefacts [96]. Light also plays a major role in the indoor climate stability and energy demand of buildings [210]. Nonetheless, light is a necessity for human beings, since it is necessary to have the appropriate illuminance in order to perform any activity adequately. This value differs according to the type of activity, as well as the person who is performing it and the space where the activity takes place.

Indoor spaces can either be illuminated by daylight or by artificial sources. By combining the use of daylight, while its intensity is suitable for the activity that the person is performing, together with artificial light, when the daylight intensity is no longer suitable, is more energy efficient. The amount of daylight that manages to enter a building varies according to the building location, architecture, surroundings and also season and sky condition. Daylight is also preferable to artificial light due to health and comfort reasons [20].

However, in museums the use of daylight is limited by the collection conservation requirements. Artificial light is usually preferable to natural light since it is easier to control, thus decreasing the possibility of surface deterioration [264]. The lighting limits will greatly depend on the collection requirements, since the artefacts can either be sensitive (e.g. silk) or insensitive to light (e.g. stone sculpture) [264,136]. Nevertheless, the required light to observe an object differs according to the visitors' characteristics (such as, age), the object's characteristics (such as, luminance) and the surroundings [51].

Lighting the indoor spaces is indeed one of the greatest conservation's paradigm. It must be appropriate so that the visitors enjoy their visit, but at the same time it must be as low as possible to decrease the light damage magnitude [136]. It is not sufficient just to limit the light intensity to avoid any risk because surface damage is a cumulative process. The best course of action to preserve these objects is to illuminate them using the lowest lighting level necessary for viewing and only for the required period of time [51].

In the museum environment, the radiation spectrum that deteriorates artefacts consist of ultraviolet radiation (300–400 nm), visible radiation (400–760 nm) and infrared radiation (>760 nm). Whilst the first two types of radiation are a source of concern due to the photochemical damages, the latter can be responsible for heating artefacts, which can lead to internal stress.

Ultraviolet radiation (UV), which corresponds to the highest levels of photon energy, can be responsible for the yellowing of the materials and even their disintegration (typically occurs for higher photon

energy than 3 eV [77]). On the other hand, visible light is responsible for the fading of colours (typically occurs between 2 and 3 eV [77]). Standard CEN/TS 16163:2014 [96] states that the intensity of UV in museums for display lighting has to be lower than 75 μW/lm.

Radiant heating can also jeopardize the objects welfare, since the increase of the surface temperature will eventually lead to internal stress. This happens because the surface and subsequent layers are not at the same temperature, therefore, they will expand at different rates. On the other hand, when the object is no longer under the direct effect of the light beam, the surface temperature decreases and only later on does the subsequent layers' temperature decrease, which causes internal stress. This expansion/contraction cycle is harmful to the object and its magnitude increases when the artefact is composed by two or more materials. Thus, to perverse the artefacts, it is necessary to reduce, as much as possible, the portion of UV, visible and IR radiation that manage to reach the artefacts.

3.2.3.2.1. Indoor illumination

The lighting level is either presented in terms of lighting power per area (W/m^2) or by the level of lighting required for the space (lux). The recommended lighting power density (LPD) for museums is 11.3 W/m^2 for the exhibition area [8], 11.0 W/m^2 for the restoration/conservation areas and 9.0 W/m^2 for the storage area [6].

On the other hand, CIBSE Guide A [262] presents the recommended illuminance according to the type of building and the level of lighting required. The values are 200 lux for the display area and 50 lux for the storage area of museums. Standard EN 12464-1 [97] also presents the recommended illuminance for various types of buildings according to the developed activity. However, in the specific case of museums it is stated that illuminance must be determined according to the display requirements without presenting any single value.

Museums have used many types of lamps to light their rooms due to the evolution of the light industry throughout time – incandescent (tungsten and halogen), metal halide, fluorescent and solid-state (namely, LED). Their properties are quite different (Table 3.1) and, consequently, the increase of surface temperature that they cause is also quite different. This is shown by Camuffo [51] by subjecting a black aluminium surface to four light beams with 500 lux for 80 minutes – ca. 0 ºC for a fluorescent lamp, ca. 0.8 ºC for a metal halide lamp, ca. 2.1 ºC for a halogen incandescent lamp and ca. 3.1 ºC for a tungsten incandescent lamp.

The *colour rendering index* (CRI) is the comparison of an object colour caused by the tested light source, to the object colour under a reference light source. It varies from 0 to 100, which means that the light emitted spectrum is continuous, just like daylight. In order to provide the visitors with the best colour experience in a museum, the lamps should produce a continuous spectrum, as close as possible to daylight [51]. *Luminous efficacy* is obtained through the quotient of luminous flux (lumens) by power (watt) and expresses how successfully a light source produces visible light. The *correlated colour*

temperature (CCT) quantifies the feeling transmitted by the light source to the human eye. A value below 3300 K gives the feeling of a warm light, between 3300 and 5300 K an intermediate light and above 5300 K gives the feeling of a cold light [97]. Visitors prefer a warm light in museums [77].

Table 3.1 – Comparison of the characteristics of each type of lamp used in museums throughout time

Type of lamp	Source	Colour rendering index [-]	Luminous efficacy [lm/W]	Correlated colour temperature [K]	Lifetime [h x 10^3]
Tungsten incandescent	[51]	≈ 100	10–15	2700	0.75–1.5 [77]
	Benefits: Continuous spectrum, warm tonality Drawbacks: Requires Anti-UV filter, large IR emission, large heat dissipation, high energy consumption				
Halogen incandescent	[51]	≈ 100	20	3200	2–2.5 [77]
	Benefits: Continuous spectrum, warm tonality, slightly higher luminous efficacy and lifetime than tungsten incandescent lamps Drawbacks: Requires Anti-UV filter, large IR emission, large heat dissipation, high energy consumption				
Metal halide	[51]	≈ 95	70–90	3000–6000	6–20 [120]
	Benefits: Continuous spectrum, wide range of colour temperature, greater luminous efficacy than incandescent lamps Drawbacks: Requires a warm-up period, uses mercury vapour to produce light				
Fluorescent	[51]	80–98	50–90	3000–5000 [264]	6–12 [77]
	Benefits: Cold tonality, low IR dissipation, wide range of colour temperature Drawbacks: Requires Anti-UV filter, discontinuous spectrum; uses mercury vapour to produce light				
White LED	[96]	≈ 80	70–95	3000-6000	50
	Benefits: High efficiency, low energy consumption, low UV and IR emission, long lifetime Drawbacks: Requires combination of lights to produce white light, discontinuous spectrum, initial cost				

LED lamps have a higher luminous efficacy than for example halogen lamps, which means that for the same amount of light, a lower electric power is used. In addition to this energy saving, the need for cooling also decreases since the process on which LED lamps are based attain lower temperatures. It is common to assume that for every 3 watts of saved energy in lighting, 1 watt of cooling energy is also saved [77].

The electric energy used by a luminaire is converted into light and heat. The amount of electric energy that is transformed into light differs according to the type of lamp [56,51], but the luminaire itself has a

key influence in this division, due to its effect on the radiant and convective heat ratio [262]. Heat is dissipated from the luminaire to the surrounding surfaces through radiation and convection, and to the adjacent materials through conduction. The emitted radiant heat, which can cause discomfort for visitors, is absorbed by the surrounding surfaces and stored by the materials, which means that it cannot be immediately considered in the cooling load [262].

3.2.3.2.2. Light conservation limits

It is possible to divide materials in two groups in terms of light damage: sensitive (organic materials) and insensitive (mineral materials). The former group is divided in three classes: low sensitive (e.g. undyed leather), medium sensitive (e.g. tapestries) and high sensitive to light (e.g. silk). Hence, the requirements of the lighting system will differ according to the type of the displayed artefacts.

CIE 157:2004 [136] and CEN/TS 16163:2014 [96] limit lighting system in terms of exposure, illuminance and exposure time according to the type of artefact (Table 3.2). Due to the reciprocity law, if the illuminance decreases, it is possible to increase the exposure time without overcoming the exposure limit. On the other hand, if the exposure time is reduced, the illuminance can be increased.

Although mineral materials do not require a limit of illuminance, since they are insensitive to light, the illuminance of the rooms where they are displayed must not differ substantially from the illuminance of the rooms with sensitive materials. Otherwise, visitors will feel discomfort when moving from a room with light insensitive materials to a room with light sensitive materials. Thomson [264] states that for a room with light insensitive materials the maximum illuminance should be 300 lux.

Table 3.2 – Exposure, illuminance and exposure time limits according to the type of object. Adapted from CIE 157 [136]

Category	Limiting exposure [lux.h/year]	Limiting illuminance [lux]	Limiting exposure time [h/year]
1.Insensitive	No limit	No limit	No limit
	Examples: Most metals, stone, most, stone, most glass, genuine ceramic, enamel, most minerals		
2. Low sensitive	600 000	200	3 000
	Examples: Oil and tempera painting, fresco, undyed leather and wood, horn, bone, ivory, lacquer, some plastics		
3. Medium sensitive	150 000	50	3 000
	Examples: Costumes, watercolours, pastels, tapestries, prints and drawings, manuscripts, miniatures, paintings in distemper media, wallpaper, gouache, dyed leather and most natural history objects, botanical specimens, fur and feathers		
4. High sensitive	15 000	50	300
	Examples: Silk, colorants, newspaper		

Druzik and Michalski [77] present the rate of colour change in materials due to the light for each of the

four material categories and according to the illuminance. This parameter has a wide range of values within each material category, but it also varies substantially for different illuminance and between different material categories (Table 3.3). The rate of colour change due to light allows the evaluation of the indoor lighting conditions in terms of material's conservation. For a low light sensitive material subject to an illuminance of 200 lux, the colour change will start to show in 77–1707 years with lighting being used during 8 hours a day for 7 days a week.

However, limiting the exposure is not sufficient to guarantee the welfare of objects. It is also necessary to analyse the spectrum of the artificial light source [220]. CIE 157:2004 [136] presents the relative damage potential, which is based on the damage potential of the CIE Illuminant A, for different correlated colour temperature. The damage potential is the quotient between the effective irradiance and the illuminance. Additionally, CEN/TS 16163:2014 [96] presents the typical relative damage potential for specific light sources normally used in museums with and without filter. The lowest values are obtained for the LED lamp. The use of an edge filter reduces the relative damage potential for both the tungsten-halogen and fluorescent lamps. For fluorescent and LED lamps the lower the CCT, the lower the relative damage potential. This parameter helps deciding which type of lamp should be used in museums [283].

Table 3.3 – Number of hours it takes for the materials to start showing noticeable fade according to the illuminance (adapted from [77]).

Sensitivity level	Number of years before "just noticeable fade" occurs		
	50 lux	150 lux	500 lux
Low sensitivity	300 – 7000 years	100 – 2000 years	30 – 700 years
Medium sensitivity	20 – 700 years	7 – 200 years	2 – 70 years
High sensitivity	1.5 – 20 years	6 months – 7 years	52 days – 2 years

3.2.3.2.3. Lighting power density in computational models

In whole-building hygrothermal models, the internal gains due to lighting are taken into account by the *lighting power density* (LPD). This parameter has a key influence in the indoor conditions of building and, consequently, in the building's energy consumption.

Despite the importance of lighting in conservation and energy consumption in museums, there is no consensus in the scientific community. Ascione *et al.* [21] used a LPD of 20 W/m^2 in a model of a 1200 m^2 modern museum to study several measures aiming to reduce the energy consumption of the building's mechanical systems. Balocco *et al.* [30] developed a thermal model of a museum in Florence to guarantee the necessary temperature and relative humidity values for the conservation of the housed artefacts and thermal comfort using a constant air flow system coupled to radiant panels, several rooms

were modelled, which in turn had different internal gains and a LPD between 15 and 20 W/m^2. Janssen *et. al.* [145] considered a LPD of 5 W/m^2 for a hygrothermal model of a 3180 m^2 museum storage in Vejle (Denmark) to analyse the applicability and efficiency of full passive conditioning for this type of buildings. Ferdyn-Grygierek [108] used a LPD of 40 W/m^2 to study the influence of the temperature and relative humidity setpoints on the energy demand of a Polish museum. Sciurpi *et. al.* [243] used LPD of 7.02 and 9.5 W/m^2 for two simulated room of the "La Specola" museum in Florence to study measures to reduce the overheating during the Summer.

Kramer et al. [158], studied the thermal comfort in museums by taking into account the PMV-model and the adaptive comfort guidelines imposed conditions, as well as the building's envelope characteristics. They analysed their effects on the building's energy consumption using a LPD of 9 W/m^2. In a state-of-the-art museum installed in a 17th century building, Kramer et al. evaluated in [154] and in [156] the energy-saving potential of several setpoints strategies by taking into account degradation risks (using damage functions) and the thermal comfort (using an adaptive temperature guideline), and secondly on the capacity to predict energy accurately using an *Integral Building Energy Simulation* model and a *Zone Air Building Energy Simulation* model using the same 9 W/m^2.

3.3. Software validation

A positive aspect about WUFI®Plus is the fact that it is a computational software that has been subject to several important updates in the past years [49,16,208] and it is continuously being subject to updates [295]. This is a crucial aspect for research because this makes the software up to date in terms of modelling.

Another key aspect of this software was its validation. Normally the results obtained by the software are either compared against experimental results or against another software that has already been validated. Since the mathematical algorithm used by WUFI®Plus to calculate the hygrothermal behaviour of building assemblies is based on *Künzel*'s model, this section of the software is already validated because Künzel validated it in its PhD thesis [163].

WUFI®Plus has additional models that also have to be validated when compared with WUFI®Pro [113]. Hence, in 2003 Holm et al. [126] compared the performance of WUFI®Plus against TRNSYS in terms of heating energy and indoor temperature using a two-story building made out of prefabricated AAC elements. The obtained results were similar, which validated the thermal part of WUFI®Plus. In addition, the authors also compared the performance of WUFI®Plus against an experimental setup to validate the hygric part of WUFI®Plus. The values calculated by WUFI®Plus were similar to the relative humidity values measured in the experimental setup, which validated the hygric part of WUFI®Plus.

More recently, Antretter et al. [17] compared the performance of WUFI®Plus separately. Whilst the thermal part of WUFI®Plus was tested resorting to the cases presented in standard VDI Guideline 6020 [277] and ASHRAE standard 140 [9]. The results obtained from WUFI®Plus were similar to the values

presented in these standards. The hygric part of WUFI®Plus was tested by comparison against the measured results from a moisture buffering experiment, in which a ceramic interior tile was analysed. A model of the climate chamber, which was used to test the specimen, was developed in WUFI®Plus. The comparison was divided in a two-step procedure in which the authors first compared the RH results without the specimen and then compared the results with the specimen. In both cases, the WUFI®Plus results were similar to the measured values.

In addition, WUFI®Plus was included in the IEA Annex 41 project [227], which tested the performance of a set of whole-building hygrothermal software. Although, the authors of the project did not identify the results associated to each software, the overall results were quite good for all tested software. All these comparisons showed that WUFI®Plus simulates the hygrothermal behaviour of buildings reliably.

WUFI®Plus performance was also compared with other software using buildings that house artefacts. For example, Schmidt et al. [242] compared the performance of a model developed in WUFI and TRNSYS based on measured data with the aim of thoroughly studying the retrofit project of Schack-Gallery Munich. The obtained results showed that both software are appropriate tools for this kind of projects. Coelho et al. [68] developed the same model of St. Cristóvão church in both WUFI®Plus [292] and EnergyPlus [81] to see how much the results would differ. They compared each model outputs against the measured indoor conditions using four statistic indices: the *coefficient of determination* (R^2), the *coefficient of variation of the root mean square error* (CV(RMSE)), the *normalized mean bias error* (NMBE) and the *goodness of fit* (fit). More details about these statistic indices are presented in subchapter 3.5.

The obtained values show that both software appropriately model the hygrothermal behaviour of St. Cristóvão church. Table 3.4 summarizes the obtained values of the four selected indices concerning temperature and water-vapour pressure. In terms of goodness of fit the WUFI®Plus model attains a significantly higher temperature fit, as well as a higher water-vapour pressure fit when compared to the EnergyPlus model. Although the EnergyPlus model does not surpass the imposed limit, the obtained value is very close to the limit, which makes it acceptable. WUFI®Plus higher accuracy might be due to the fact that a sensitivity analysis to determine some of the inputs is carried out, something that is not done in EnergyPlus. The same inputs were used in both models since the aim of this subchapter is to test the same model in both software.

The obtained CV(RMSE) and NMBE for both models are lower than the demand values by IPMVP [80] for the model to be validated (especially, CV(RMSE) which is ca. 4 times lower than the imposed limit). On the other hand, the R^2 is not an appropriate index to compare both software, since the obtained values are very high.

Table 3.4 – R^2, CV(RMSE), NMBE and goodness of fit for temperature (T) and water-vapour pressure (P_v) of the models developed in WUFI®Plus and EnergyPlus

Software	R^2 [-]		CV(RMSE) [%]		NMBE [%]		Fit [%]		
	T	P_v	*T*	P_v	*T*	P_v	*T*	P_v	*Avg.*
WUFI®Plus	0.99	0.97	3.2	4.4	2.7	3.4	84.8	81.7	**83.2**
EnergyPlus	0.99	0.96	4.1	5.5	3.5	4.1	80.4	76.5	**78.5**

Figure 3.3 displays the annual variation of the indoor temperature and water-vapour pressure of the monitoring campaign data and the simulated values for both models. Although the models' outputs do not perfectly overlay the recorded data, they have a very similar variability, which shows that the obtained values from both models are acceptable.

The model of St. Cristóvão church was developed in the hygrothermal mode of WUFI®Plus and using the Combine Heat and Moisture Transfer (HAMT) in EnergyPlus. It is noteworthy that both the hygrothermal mode and the HAMT mode are based on Künzel's [163] governing equations for the simultaneous calculations of heat and moisture transfer in building materials [269].

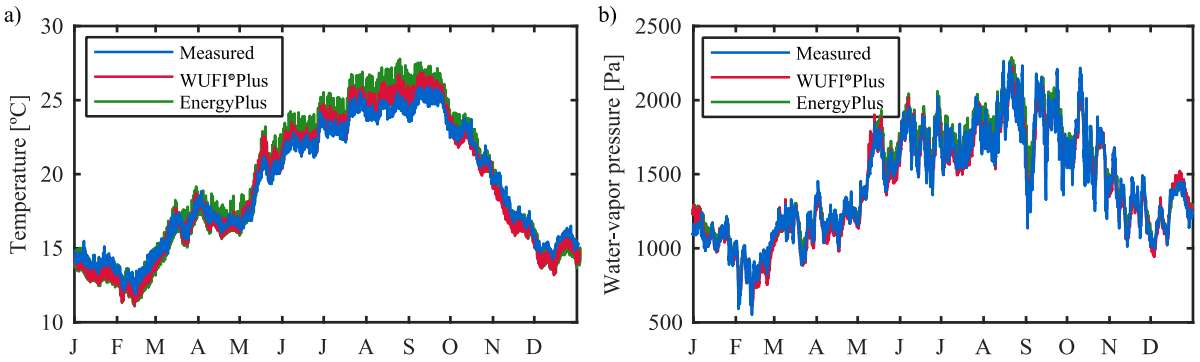

Figure 3.3 – Simulated WUFI®Plus and EnergyPlus and measured indoor temperature (a) and water-vapour pressure (b) of St. Cristóvão church

Both software have been extensively validated by their developing teams and also by independent studies. This fact is of extreme importance since it gives credibility to the software and, consequently, the obtained results. Plus, both software are continuously being updated to account for more thermal/hygric behaviours that influence buildings, but also to increase their accuracy and fix bugs. Nonetheless, some differences stand out between these software, which will influence the users' choice when modelling the behaviour of a building.

While WUFI®Plus has always been a hygrothermal software, i.e. calculates the simultaneous and coupled heat and moisture transport in building elements, whereas EnergyPlus was developed for energy simulations. EnergyPlus suffered an update to take into account the simultaneous heat and moisture transport with HAMT, which uses the same equations as WUFI [269]. The disadvantage is that hygrothermal simulations take more time to run in EnergyPlus than in WUFI®Plus.

Since EnergyPlus is a free software, that makes it much more used than WUFI®Plus. This means a greater number of Q&A forums (e.g. Unmet Hours [273]) and a greater number of tutorials (e.g. the Big ladder website [41], the manuals developed by the labEEE [165]). These documents, in addition to the very detailed documentation of the software itself [82] are fundamental when the user is leaning how to use the software. Among other parameters, EnergyPlus is much more complete in terms of climate control systems than WUFI®Plus, which only has five possible systems.

Due to the difficulty of introducing the geometry of the case-study in EnergyPlus it is advisable to use other software, such as the free OpenStudio plug-in [2] or DesignBuilder [76]. WUFI®Plus also has this drawback when the user is using the vertices introducing methodology for complex building geometries, but it also has alternatives, such as the SketchUp plug-in or the Revit conversion software [292].

Ultimately, the choice between the two software will greatly depend on the aims of the study. If the thermal and hygric behaviour are important for the study (as it is for the study described in this thesis), then it is advisable to use WUFI®Plus. However, if the hygric behaviour is negligible and the climate control systems are important for the study, then it is advisable to use EnergyPlus.

It is also possible to develop your own code, which has the great advantage of fitting to the purpose of the study more precisely than commercial software do. However, this can be a very time-consuming process, which will increase with complexity of the problem (e.g. if the simulation is only 1D or otherwise occurs in 2D/3D, or if the simulations only models the thermal behaviour of the case-study or otherwise if it also models its hygric behaviour). In addition, it is also of key importance to validate the code either against experimental data or standards provided values, so that the results are reliable. Another drawback is the fact that they cannot keep up with the development of commercial software, because they are usually developed by small teams, whereas commercial software are developed by much larger teams.

3.4. Software disadvantages

Although WUFI®Plus is a state-of-the-art hygrothermal simulation software, it cannot take all the factors that influence a building into account and, therefore, the following assumptions were made [14]:

- In each zone both the temperature and relative humidity are constant. Therefore, when choosing the model's zones, it is important to know how the indoor climate varies within the building
- The simultaneous heat and moisture transfer in building components is based on *Künzel's* model [163] and, consequently, has the same limitations as that model, namely:
    - The hysteresis in the moisture storage function is disregarded [290]
    - The software does not account for the following processes: convection in heat and in water vapor transport; rising damp due to gravity, hydraulic flow due to pressure differences, electrokinetic, and osmosis in the transport of moisture in the liquid phase

    - Dependency between salts and moisture transport in liquid phase is not considered
    - The interface between two capillary active building materials is considered as ideally conducting, when in fact there is normally a transfer resistance in this zone [114]
    - The enthalpy flow that results from the transport of moisture in the liquid phase caused by a temperature differential is ignored, e.g. low temperature rainwater does not cool to surface of the building element
    - The heat transfer coefficients are either constant or are determined using a simple equation that depends on the wind characteristics
- The radiation is equally distributed in the components' surfaces
- The materials' aging process is not considered, since the software does not take the changes that properties suffer throughout the course of time into account
- The outdoor climate is not influenced by the building

3.5. Models' accuracy

Many hygrothermal models of historic buildings in literature evaluate the model's accuracy by visual comparison between the simulated and the measured values for each of the selected hygrothermal variables (e.g. [40,152]). Although this visual comparison is of key importance in the validation process, the additional use of statistical parameters gives the model's developers a quantitative notion of how well the model simulates the behaviour of the real building.

Other authors use statistical parameters to assist the validation process of whole-building models. For example, in addition to the visual comparison Ferreira *et al*. [111] used the annual average, the standard deviation and the minimum and maximum of the difference between the measured and simulated values to validate an hygrothermal model of a museum at Oporto. Pisello *et al*. [213] and Pernetti *et al.* [212] used the statistical parameters proposed by ASHRAE guideline 14:2002 for the validation process of thermal models [10], with the coefficient of determination also being used in the latter paper. Kramer *et al*. [160] used the mean square error, mean absolute error and goodness of fit to validate several hygrothermal models of historical buildings.

These statistical parameters were structured in three levels (Table 3.5), where $X_{i,meas}$ is the measured value of the hygrothermal parameter at the time period i, $X_{i,sim}$ the simulated value of the hygrothermal parameter at the time period i, n the total number of points across the studied period of time (i.e. 8760 since it corresponds to one year worth of hourly values) and $\overline{X}_{meas}$ the average of the measured values of the hygrothermal parameter during the studied time period.

Table 3.5 – Accuracy parameters used to validate the models found in literature.

Level	Designation	Equation	Example
1st	Annual average	$\bar{X} = \frac{\sum_{i=1}^{n} X_i}{n}$	[111]
	Standard deviation	$\sigma = \sqrt{\sum_{i=1}^{n}(X_i - \bar{X})^2 / n}$	
	Minimum and maximum		
2nd	Coefficient of determination	$R^2 = 1 - \left[\sum_{i=1}^{n}\left(X_{i,meas} - X_{i,sim}\right)^2 \Big/ \sum_{i=1}^{n}\left(X_{i,meas} - \bar{X}_{meas}\right)^2 \right]$	[212,213]
	Coefficient of variation of the root mean square error	$CV(RMSE) = \left[\left[\sum_{i=1}^{n}\left(X_{i,meas} - X_{i,sim}\right)^2 \Big/ (n-p) \right]^{1/2} \Big/ \bar{X}_{meas} \right] \times 100$	
	Normalized mean bias error	$NMBE = \left[\sum_{i=1}^{n}\left(X_{i,meas} - X_{i,sim}\right) \Big/ \left((n-p) \times \bar{X}_{meas}\right) \right] \times 100$	
3th	Mean square error	$mse = \sum_{i=1}^{n}\left(X_{i,meas} - X_{i,sim}\right)^2 / n$	[195,160]
	Mean absolute error	$mae = \sum_{i=1}^{n}\left\lvert X_{i,meas} - X_{i,sim}\right\rvert / n$	
	Goodness of fit	$fit = \left[1 - \frac{norm\left(X_{i,meas} - X_{i,sim}\right)}{norm\left(X_{i,meas} - \bar{X}_{meas}\right)} \right] \times 100$	

The ASHRAE guideline 14:2002 [10], the IPMVP protocol [80] and the FEMP guideline [107] limit some of these statistical parameters for the validation of whole-building thermal/hygrothermal models with hourly data (Table 3.6). These are just guideline values and the lower the CV(RMSE) and NMBE are, the higher the accuracy of the developed model will be.

Table 3.6 – Limits of the statistical parameters used to validate models

Accuracy parameter	Values	Source
R^2	0.75	IPMVP [80]
CV(RMSE)	20 %	IPMVP [80]
	30 %	ASHRAE 14 [10] & FEMP [107]
NMBE	5 %	IPMVP [80]
	10 %	ASHRAE 14 [10] & FEMP [107]

3.6. Making large-sized hygrothermal simulation studies more time-efficient

The emission of greenhouse gases (GHGs) into the atmosphere caused by anthropogenic activities is greatly responsible for the changes the outdoor climate will suffer in the future [196]. Climate change is one of the key challenges that mankind faces nowadays, since it will greatly influence the environment, human health and the world's economy [284].

The European Union (EU) has a key contribution to the overall GHGs emissions since it is responsible for more than one third of the GHGs emitted by the OECD members, i.e. 5,600,000 tonnes of CO_2-equiv per year [201]. This amount has been steadily decreasing over the past years, mostly due to the efforts made by the EU Parliament in promoting a more environmentally friendly society by proposing demanding goals, which aim to reduce the GHGs emissions of the European Union [88].

In Europe, the building sector has a significant contribution to the amount of GHGs emitted. Evidently, that this is due to construction of buildings, but also due to the several activities that are performed within the buildings [101]. In the scope of the CPA08 classification, the GHGs emitted by the construction sector corresponded to more than $3.3x10^8$ tonnes of CO_2-equiv in 2017 (7 % of the total emissions), while the energy sector corresponded to more than $4.0x10^8$ tonnes of CO_2-equiv (9 % of the total emissions) and the private households corresponded to more than $8.3x10^8$ tonnes of CO_2-equiv (19 % of the total emissions). If the goals of the Paris Agreement are to be achieved [206], then it is necessary to reduce, as much as possible, the portion of the GHGs emitted by the building sector.

One way of reducing the GHGs emissions caused by the building sector is to design more efficient buildings using, among other means, simulation software like EnergyPlus [81] or WUFI®Plus [292]. This kind of software allows to thoroughly assess the performance of each building assembly in new buildings or the impact of each retrofit measure for existing buildings [11], which allows to choose the best course of action for each case-study while taking into account the goal of reducing the GHGs emissions [119]. On the scope of buildings, climate change will have a negative effect on their durability [18].

Studies that use this kind of software have the drawback of requiring a large number of simulations so that the analysis is thorough and accurate. This situation is even more time-consuming if the study is performed using the hygrothermal mode. The choice between using the thermal mode or the hygrothermal mode will depend on the goals of the study. For example, Huijbregts et al. [128] developed hygrothermal computational models of two museums located in The Netherlands and in Belgium to study how artefacts will fare in the future. The use of these hygrothermal models coupled with future weather files allowed to obtain the future indoor conditions. Since the deterioration processes that affect the artefacts are dependent on both temperature and relative humidity [178], it is only natural that the authors developed hygrothermal models.

Several studies that use either thermal or hygrothermal models to conduct a thorough analysis of the

indoor climate can be found in literature. For example, Muñoz-González et al. [193] constructed a model of San Francisco de Asís church based on the results of the monitoring campaign that they installed to study retrofit opportunities for Spanish churches while taking into account the building's energy consumption, the occupants' thermal comfort and the preservation of the artefacts; and Kramer et al. [155] that analysed the energy impact of four typologies of buildings among 20 European cities using a model that they developed for the Hermitage Amsterdam museum [154,156]. Nonetheless, the time needed to perform these studies is very substantial, and it will greatly increase with complexity of the analysis [69].

The validation of these models, though a time-consuming process, is a crucial task if their outputs are to be reliable [66]. A prior task that can also be greatly time-consuming is the insertion of the building geometry in the simulation software. Fortunately, WUFI®Plus has three different options to introduce the geometry, namely: 3-D editor, SketchUp import and gbXML Import. The 3-D editor consists in inputting the vertices of each surface manually and then uniting them to build each surface. This is a very time-consuming way of introducing the geometry and gives way to inconsistencies for more complex geometries. On the other hand, the SketchUp import and gbXML import are a much more efficient way of introducing the geometry, since the case-study is designed in software that are aimed for that purpose. The gbXML import can have a key importance for new project, since it allows the use of building geometries developed in Revit by performing the proper conversion [292].

There are several software that simulate the thermal or/and the moisture behaviour of buildings in literature [227,74]. The Annex 41 project of the International Energy Agency (IEA) [227,286] assessed the performance of many of these software in its CE0 and CE1 exercises, namely: BSim, Clim2000, Delphin, EnergyPlus, ESP-r + NPI, IDA ICE, HAMFitPlus, HAMLab, HAM-Tools, PowerDomus, SPARK, TRNSYS, WUFI®Plus, and Xam. Most of these are commercial software that are available to the public [74]. The overall results were quite good for all tested software, both in terms of thermal and moisture modelling, which showed their great capacity in simulating the thermal and moisture behaviour of buildings.

Among the many previously mentioned software, the simulations reported in this subchapter were run in WUFI®Plus since it is one of the most known software where studies concerning the hygrothermal behaviour of buildings have been developed, but mainly due to the fact that it has been extensively validated over the years, it has been continuously subjected to updates and because it accounts for several of the behaviours that affect the thermal and moisture behaviour of buildings [291,294].

This subchapter presents a methodology that aims to decrease, as much as possible, the time required to develop large sized hygrothermal simulation studies, thus making this type of studies more time-efficient. Several techniques were used to minimize the time required for the first three stages of simulation studies, i.e. simulation setup, simulation run and results processing. In order to show the

benefits of using this methodology, three examples in which it is applied are presented. The obtained time savings using this methodology are reported, whilst comparing with a more traditional way of performing simulations.

3.6.1. Methodology

The aim of this subchapter is to develop a methodology that may considerably reduce the time necessary to perform large sized hygrothermal simulations, thus making them more viable. Hence, a methodology was developed based in several techniques that aim to reduce the required time at three levels, namely in the *simulation setup*, the *simulation run* and the *results processing*. The methodology will be thoroughly explained in the following subchapter, and its benefits will be shown in three examples.

Simulation studies can be divided in four steps (Figure 3.4): 1) setting up the simulations inputs; 2) performing the simulations; 3) processing the obtained results in figures or tables; 4) assessing the results and writing conclusions. The duration of each of these steps will greatly depend on the aim of the performed study. The purpose of this procedure is to minimize the time taken to perform each of the first three stages:

Step 1 (*Simulation setup*) – The time spent on this step can be reduced drastically by automatically inserting the inputs, for example, using an external software, such as MATLAB or OCTAVE. In WUFI®Plus, the users can save the project as a mwp file (traditional way of saving files in WUFI®Plus), or as a xml file. This latter type of file allows to the change its parameters, such as the thickness of a material or the location of the outdoor climate weather file, by resorting, for example, to a code that is developed for that purpose [64]. This step has a very substantial time saving effect on simulation studies that are subdivided in several computers. In addition, this step also decreases the possibility of human error, since the inputs are automatically introduced, thus eradicating monotonous tasks.

Step 2 (*Simulation run*) – The time spent on this step can be reduced by performing the simulations resorting to batch mode, which allows to run the simulations sequentially, and by dividing the simulations through several computers. This measure can lead to the increase of the individual simulation time, if the computers are not modern, but it ultimately decreases the overall simulation time. For example, Coelho et al. [69] initially used a computer equipped with Intel(R) Core(TM) i5-8500 CPU @ 3.00 GHz and 16 GB of RAM to perform the hygrothermal simulations (henceforth known as PC#1), which took between 1h to 1h30 to run depending on the outdoor climate. Alternatively, they used a set of 20 computers equipped with Intel(R) Core(TM) i5-650 CPU @ 3.20 GHz and 4 GB of RAM (henceforth known as PC#2) to run the same simulations and took at least 3h. However, the overall simulation time, i.e. the sum of all the individual simulation time, is much lower in the 20 PC#2 than in the PC#1. Taking into account the previously mentioned simulations run time for PC#1, and, if it is run, for example,

20 simulations in PC#1, this would mean that the overall simulation time would take between 20 to 30h depending on the outdoor climate. On the other hand, if the same number of simulations are run divided between the 20 PC#2, the overall simulation time is around 3h, which means a reduction of 85-90% of the overall simulation time.

Step 3 (*Result processing*) – The time spent on this step can be substantially decreased if instead of using the traditional excel spreadsheets, a software that is aimed for numerical calculation is used, as for example MATLAB or OCTAVE. Evidently, that the users will spend time developing the code for the analysis that they aim to perform. However, if the code is developed taking into consideration that it might be adapted to assess a larger number of simulations or a large number of inputs in the future, the time it takes to make this change is compensated when compared to perform the same task in excel spreadsheets. This step gains importance with the growing complexity of the analysis and decreases the time taken to perform the same analysis for other sets of simulations very considerably when compared to excel spreadsheets.

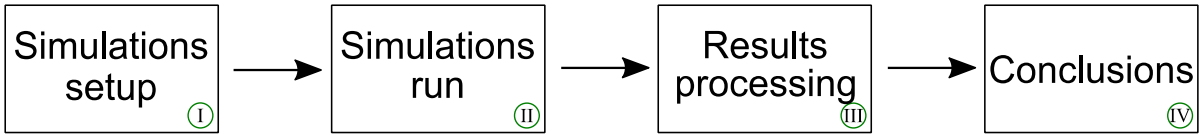

Figure 3.4 – Scheme of the four stages of simulation studies

Alternatively to using a set of several computers as mentioned previously, it is possible to use a single computer, but it has to be a rather powerful one to compensate the performance of the individual computers. With WUFI®Plus, which has the drawback of only performing the simulations sequentially, the computer has to be powerful enough to, at least, perform each simulation in 9 mins in order to compensate the performance of the set of computers used by Coelho et al. [69]. However, these powerful computers are considerably more expensive than the typical office/personal computers (e.g. [183]).

3.6.2. Application of the time-saving methodology

In order to show the benefits of this methodology, three examples of its application are presented below. The first determines the variation of the energy consumption in the future for historic buildings that house artefacts. The second determines the effect that a set of retrofit measure will have on the artefacts' conservation requirements while considering climate change. The last example, which is the most complex, presents the results of a detailed analysis of retrofit measures for historic buildings that house artefacts.

3.6.2.1. Case-study

The examples that are presented in this subchapter are based in a case-study, i.e. St. Cristóvão church, which is a 13th century church that is located in the vicinity of St. Jorge Castle in Lisbon (Figure 3.5). The church has thick mortared limestone walls, single-glazed windows and a ceramic tile roof, and does

not have any type of climate control system [250]. The church, which is naturally ventilated, is composed by several compartments with the largest ones being the nave, the mortuary and the sacristy. Overall, the church has a volume of 5250 m^3, and the window per floor area ratio is 0.12.

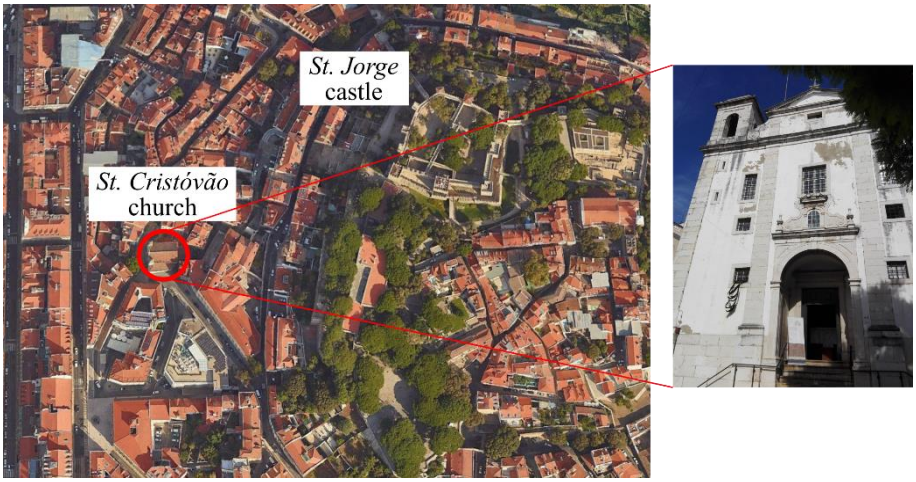

Figure 3.5 – Location (a) and façade (b) of St. Cristóvão church, Lisbon

The church was subjected to a long-term monitoring campaign from November 2011 to August 2013 that used several sensors to determine the quality of the indoor climate in terms of artefacts conservation [250,251]. Subsequentially, the recorded data was used in the validation process of computational models of the church [66,68]. The outdoor temperature and relative humidity in the vicinity of the church were monitored to build an outdoor weather file, which was then used to run the church models [66]. More information about the campaign or the model can be found elsewhere [250,66].

St. Cristóvão model was calibrated using four statistical indices, and the measured temperature (T) and water-vapour pressure (P_v), namely: coefficient of determination *(R^2* – 0.99 for T and 0.97 for P_v [66]), normalized mean bias error *(NMBE* – 2.7% for T and 3.4% for P_v [66]), coefficient of variation of the root mean square error *(CV(RMSE)* – 3.2% for T and 4.4% for P_v [66]), and goodness-of-fit *(fit* – 84.8% for T and 81.7% for P_v [66]). Considering the values that exist in the models published in literature, the obtained values for St. Cristóvão model are quite good, which validates this model [66]. The results of this validation can be seen in Figure 4.13, which presents the measured and simulated indoor temperature and water-vapour pressure for St. Cristóvão.

3.6.2.2. Variation of the energy consumption in historic buildings that house artefacts while considering climate change

In order to assess the energy consumption in historic buildings that house artefacts for the two types of climate control strategies that exist in literature [69], a total of 665 simulations were carried out in WUFI®Plus. The study included five climates (Figure 3.6) – Lisbon and Seville (Mediterranean climates), Prague and Oslo (Humid continental climate) and London (Oceanic climate); two IPCC scenarios – A1B (mid radiative forcing [134]) and A2 (high radiative forcing [134]); and three climate

control strategies – Thomson [264] (constant-value methodology), and ASHRAE [5] and FCT-UNL [250] (dynamic methodologies). In sum, there were nine weather files for each IPCC scenario plus one reference weather file, which allowed the comparison of the evolution of the energy consumption in historic buildings that house artefacts between the two IPCC scenarios.

Running all those simulations in just PC#1 would take more than 730 hours – i.e. 30 days of continuous simulation, which would make it impractical timewise. Instead of performing this study on just PC#1, the simulations were divided among 20 computers. This resulted in the decrease of the overall time spent on step 3) by 62 %, i.e. it decreased from 730 to 280 hours. Each simulation that is run in a PC#2 will take more time than if it was run in PC#1, but what matters for the purpose of the study is the overall time, which is substantially reduced as was previously reported.

In addition, instead of taking ca. 9 hours in processing the obtained data (which will greatly depend on the analysis that is perform), the data was assessed and presented in the form of the three figures shown in Ref. [69] in 20 seconds. Evidently it takes time to develop the original code, but it is rather easy to adapt code in programs like MATLAB. Moreover, if the code is initially built with the notion that it can be used for other analysis in the future, it is much easier to perform the necessary adaptations and, consequently, the time required to perform these adaptations will be rather low.

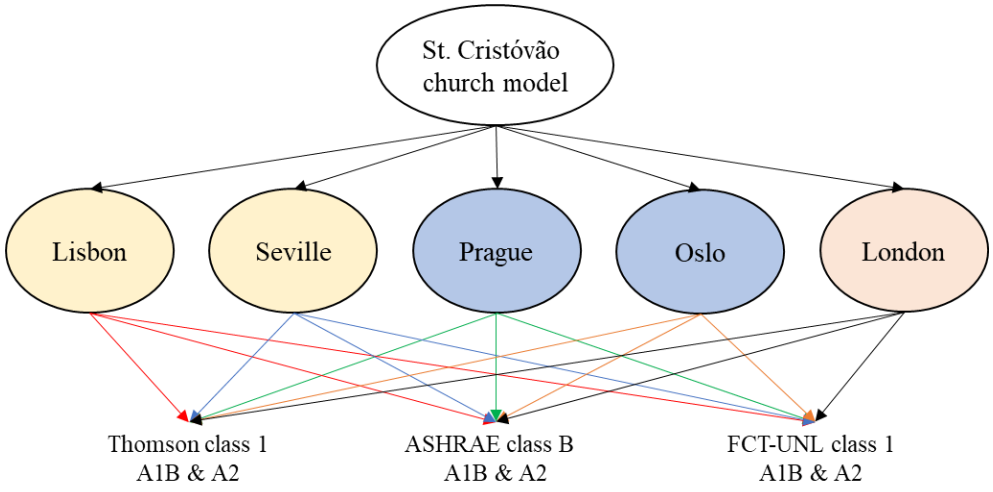

Figure 3.6 – Scheme of the developed simulations to assess the variability of the energy consumption in the future for five climates, two IPCC scenarios and for three climate control strategies (Thomson, ASHRAE and FCT-UNL). Analysis developed in chapter 6.

Lastly, it is also important to point out the time that is spent performing similar analysis. For instance, whilst assessing and presenting the data obtained for Thomson and ASHRAE guideline, MATLAB takes ca 4.5 seconds for each figure [69], which means a total of less than 10 seconds. If the traditional excel spreadsheet methodology were to be developed for the same purpose it would take 3 hours for each analysis, i.e. 6 hours in total. This is mostly due to the fact that because of the large amount of data that is generated and assessed (each of the figures presented in Ref. [69] corresponds to more than 800,000 values), it will be necessary to subdivide the data in several spreadsheets, so that excel can manage this

amount of information straightforwardly. This procedure will require the manual update of the individual excel spreadsheet whenever new data is added, which will considerably increase the time necessary to sort out the data for analysis.

3.6.2.3. Performance assessment of four representative retrofit measures in terms of artefacts conservation while considering climate change

Due to the alterations that climate change will have in the indoor climate of historic buildings that house artefacts [67], a set of four representative passive retrofit measures were tested to see if they could mitigate the changes in the artefacts' conservations metrics (Figure 3.7) – interior insulation system (R1), external thermal plaster (R2), insulation of the ceilings (R3) and replacement of the windows (R4) [69]. The two most demanding climates of the set of climates presented in the previous example were tested – i.e. Seville (Mediterranean climate) and Oslo (Humid continental climate), since the indoor climate is dependent on the outdoor climate; two IPCC scenarios were selected – A1B (mid radiative forcing [134]) and A2 (high radiative forcing [134]); and two climate control strategies – Thomson [264] (a constant-value methodology), and FCT-UNL [250] (a dynamic methodology), as representative of the two typologies of standards/guidelines that exist in literature [226].

For each of the retrofit measures, nine weather files for each IPCC scenario plus one reference weather file were run, i.e. 19 simulations. In addition, a case without any retrofit measure for the same weather files was run. This allowed to identify the changes that the application of the selected retrofit measures had in the indoor climate in terms of artefacts conservation metrics – i.e. biological, chemical and mechanical decay [178]. In total, 760 simulations were run in WUFI®Plus to perform this analysis, which would take ca 950 hours to run in PC#1, i.e. almost 40 days of continuous simulation. Instead, the simulations were subdivided in the set of 20 PC#2, which resulted in a decrease of 34 % of the simulation run time, since it dropped from 950 to 627 hours, which although considerable, is lower than the example presented in subsection 3.6.2.2. This is mostly due to the weather files, which will influence the simulation run time due to the additional hygrothermal processes prompted in colder climates [14].

In this example, the stage of the results processing is even more important because the performed analysis is more complex than the one described in subsection 3.6.2.2. While the numerical process in 3.6.2.2 boils down to the sum of the individual HVAC system needs – i.e. heating, cooling, humidification and dehumidification, which depends on the indoor climate and the climate control strategy preconized values; the numerical processes included in this example are much more complex. First, because instead of just performing one analysis to determine the energy consumed in the future like in subsection 3.6.2.2, in this example the indoor climate is assessed using three different analysis that assess the risk of decay in artefacts – i.e. biological decay using the isopleth method [244], chemical decay using the equivalent lifetime concept [186,251] and mechanical decay in which the method varies according to the material [181,44,144,45]. Second, because in subsection 3.6.2.2 the mathematical

operation just adds values, while in this example the obtained values are compared against sets of values for each timestep, which takes much more time to perform.

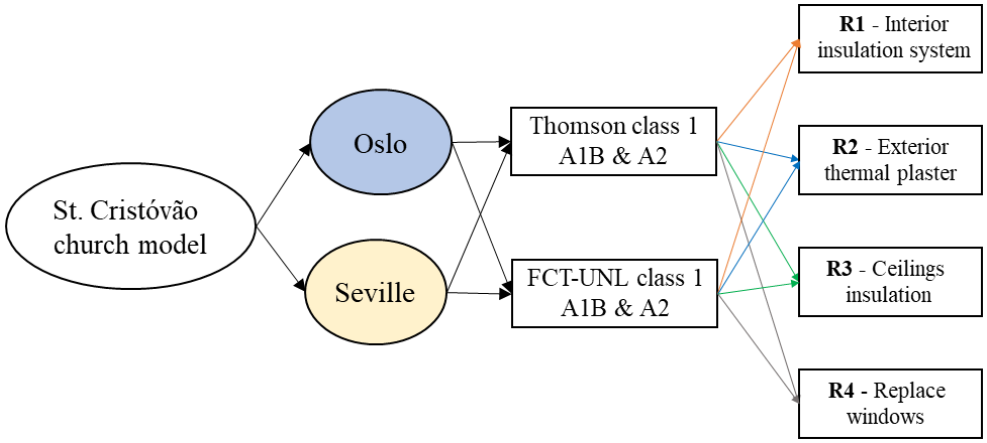

Figure 3.7 – Scheme of the developed simulations to assess the performance in terms of artefacts conservation of four types of retrofit measures for historic buildings that house artefacts in two climates and for two climate control strategies. Analysis developed in chapter 6.

Instead of taking ca. 19 hours in processing the obtained data using the traditional methodology (ca 9.5 hours for each climate), the data was assessed and presented in the form of the figures shown in Ref. [69] under 9 hours (ca 4.5 hours for each climate) using MATLAB. The benefits of using this type of software is more obvious when performing similar analysis in which the necessary adaptations will only take a few minutes to perform, whereas in the traditional methodology this could take up to several hours, depending on the complexity of the analysis. In addition, the use of MATLAB has the advantage of performing the work independently from the user, contrary to the traditional methodology in which the updates have to be performed manually. This means that while MATLAB is assessing data, the user can develop other tasks.

3.6.2.4. Detailed analysis of a set of retrofit measures for historic buildings that house artefacts

The third example corresponds to the thorough analysis of the application of passive retrofit measures in historic buildings that house artefacts while considering climate change [64]. The effect of each of these passive retrofit measures was assessed in terms of artefacts' conservation metrics to see if they could mitigate the changes caused by climate change – i.e. interior insulation systems, external thermal plaster, insulation systems of the ceilings/roofs, and the replacement of the window system [64]. The study included five climates – Lisbon and Seville (Mediterranean climates), Prague and Oslo (Humid continental climate) and London (Oceanic climate); two of the newest IPCC scenarios were selected – RCP 4.5 (intermediate GHG emissions [63]) and RCP 8.5 (high GHG emissions [63]). The future indoor conditions were obtained using the model of St. Cristóvão church coupled with the developed RCP weather files for two moments in time, i.e. near future and far future [64]. The historical values work as a reference for the future weather files.

Overall, 1350 simulations were run in WUFI®Plus to perform this analysis (Figure 3.8), which would

take ca 1485 hours to run in PC#1, i.e. 62 days of continuous simulation. Instead, the simulations were once again subdivided for the set of 20 PC#2, which resulted in a decrease of 62 % of the simulation run time, since it dropped from 1485 to 567 hours. The saved-time in data processing is similar with what was presented in subsection 3.6.2.3, since the analysis are similar in nature, i.e. the same three analysis to assess the risk of decay in artefacts are used to assess the performance of each retrofit measure.

Another problem that gained emphasis due to the subdivision of the simulations among several computers was the time taken to setup the simulations to run. This procedure is normally performed manually, which takes a considerable amount of time to perform and it will depend on the number of simulations that are assigned to each computer. For instance, if each of the 20 PC#2 were assigned 20 simulations to run, then the time spent to setup all the 400 simulations would be almost 7 hours. It took around 20 minutes to set each computer in Ref. [64] since this included the inputting of the necessary data for the model to run properly, as well as to check if the inputs were well introduced in the model.

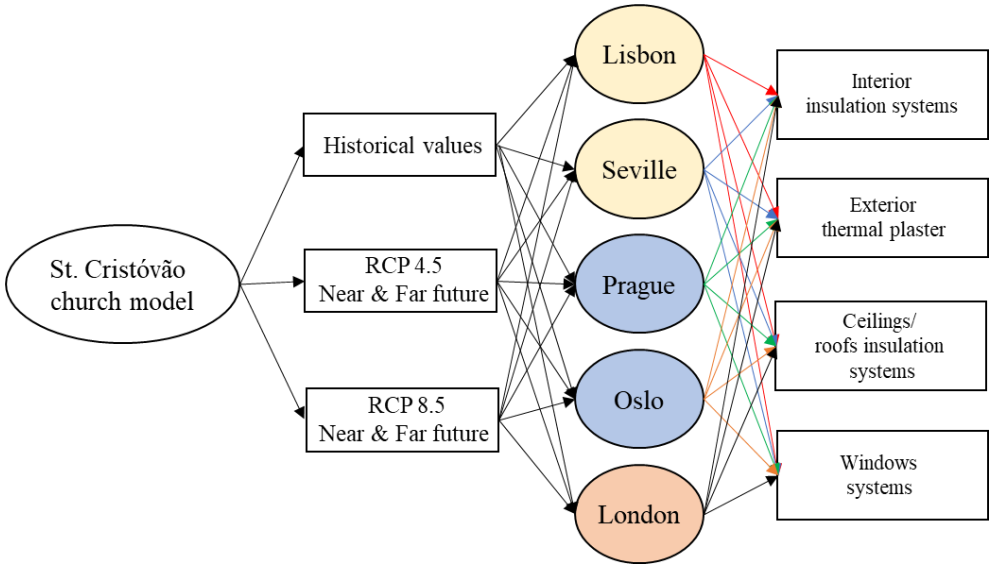

Figure 3.8 – Scheme of the developed simulations to assess the performance of four types of retrofit measures in historic buildings that house artefacts for five climates and two IPCC scenarios in the near future and far future in terms of artefacts conservation metrics. Analysis developed in chapter 7.

In order to decrease the amount of time taken by this procedure, an original code that automatically sets the inputs in the WUFI model was written in XML language. The WUFI model is saved as a xml file, instead of the typical mwp file, and then it is changed using either MATLAB or Octave. This procedure allows to save a large amount of time when performing changes in existing simulations, and facilitates the process of creating new simulations considerably, which is fundamental for large sized hygrothermal simulation studies. Furthermore, this development decreases the probability of human error, since the software user no longer has to perform the same monotonous procedure for a large number of simulations.

Instead of taking the 20 minutes to set each computer, the simulations were setup in 2.5 seconds. The

time it would take to setup the 400 simulations will decrease from ca 7 hours to ca 50 seconds. Overall, this means that the time it would take to setup the 1350 simulations manually would be ca 23 hours, since the XML code cuts this time to seconds, the simulations overall run, and setup time would drop 62%, i.e. from 1542 to 584 hours. The larger the number of simulations included in the performed analysis is, the more effective becomes this time-saving procedure.

In order to show the advantages of the methodology presented herein more straightforwardly, the time savings discussed throughout this section were summarized in Table 3.7. Based on the values presented in this table it is visible that setting up the simulations becomes negligible in terms of time consumption. A task that takes, at least, half a day to perform manually, only takes at most 3 minutes to perform using a software like MATLAB.

The data processing becomes almost non-time consuming, although the extent of the time savings will depend on the analysis that has been performed. By replacing the traditional way of processing the data for a software like MATLAB the data processing in subsection 3.6.2.2 drops from taking 9 hours to complete to only ca. 20 seconds (i.e. almost a 100 % drop), but on the other hand, the duration of the data processing task in subsection 3.6.2.3 only decreases ca 53%. Nonetheless, the data processing in this type of software is independent once it starts, so the time it takes to perform this task can be used to develop other tasks. Finally, the simulation run time also decreases substantially, i.e. varying from 34 to 62 %, but this decrease will greatly depend on the aims of the analysis, more specifically, in terms of outdoor climates (subsection 3.6.2.3).

Table 3.7 – Time savings achieved using the developed methodology for the examples presented in subsection 3.6.2.2, 3.6.2.3 and 3.6.2.4, respectively

Example			1	2	3
Number of simulations			665	760	1350
Step 1	Simulation setup duration	Manually	11 h	13h	23 h
		MATLAB	1 min	2 min	3 min
		Time savings	99.8%	99.7%	99.8%
Step 2	Simulation run time	PC#1	730 h	950 h	1485 h
		20 PC#2	280 h	627 h	567 h
		Time savings	61.6%	34.0%	61.8%
Step 3	Data assessment duration	Excel	9 h	19 h	34 h
		MATLAB	20 s	9 h	17 h
		Time savings	99.9%	52.6%	51.1%
Overall duration		Traditional	750 h	982 h	1542 h
		New	280 h	636 h	584 h
		Time savings	63%	35%	62%

4. VALIDATION OF HYGROTHERMAL MODELS OF HISTORIC BUILDINGS

This chapter has been partly published in the following reference: G.B.A. Coelho, H.E. Silva, F.M.A. Henriques, Calibrated hygrothermal simulation models for historical buildings, Building and Environment. 142 (2018) 439–450. doi:10.1016/j.buildenv.2018.06.034.

4.1. Introduction

Historic buildings are a living representation of our past and it is our duty to ensure that future generations have access to their heritage. Nowadays a substantial number of historic buildings house collections. Consequently, certain levels of temperature and relative humidity must be guaranteed in these buildings so that the artefacts are kept safe and at the same time to ensure human comfort. It is important to bear in mind that most of these buildings were not designed for this purpose, therefore it can be difficult to guarantee such indoor conditions.

In order to guarantee such indoor conditions, powerful mechanical systems have traditionally been used. However, nowadays these systems are continually questioned owing to their high energy expenditure, and consequent high financial and environmental costs. This change of approach has opened the way to other solutions (such as, passive rehabilitation techniques [234]) that can lead to energy reduction. However, the potential of the passive system is largely dependent on the outdoor conditions, as well as the building's characteristics (e.g. wall assemblies) [234]. In addition, hygrothermal improvements of heritage buildings are not always possible without sacrificing authenticity [203]. At the same time it is also important to study strategies for climate control, which are based on energy savings but also take the local climate, collections or comfort needs into account [253].

The first step to promote the safety of the housed artefacts is to conduct a thorough monitoring of the building's indoor conditions, over a sufficient period of time, in order to assess if the present conditions are suitable or not for the preservation of the objects [251,241]. Should the conditions not be adequate for the preservation of the artefacts, the necessary changes will have to be implemented to ensure a more suitable environment.

However, one of the downsides of using the monitored climate, which usually does not cover more than one year, is the fact that it cannot take into account years with different climates, to evaluate future scenarios of climate changes and the impact of hygrothermal improvement measures. The use of simulation models is an important tool for the microclimatic analysis of cultural heritage, since it allows to test possible retrofits and/or different climate control strategies with a high level of confidence, as in [108], for example. Additionally, computer simulations are non-intrusive for occupants and buildings [298], which is important for historic buildings.

The models must be validated against the building's indoor conditions so that they can reliably simulate its hygrothermal behaviour [173,224,57,168]. The combined use of several statistical parameters and the use of more than one compared variable (e.g. temperature and water-vapour pressure) should lead to a more reliable model [195,160]. Poorly calibrated or uncalibrated models assume an even greater importance for historic buildings, since any measurement based on such models may lead to irreparable damage to the building [224]. The more robust the hygrothermal model, the closer simulation outputs will be to reality.

The thermal and hygrothermal models of historic buildings found in literature are used for several different types of analysis, which shows how valuable this type of research tool is. For example, Huijbregts et al. [128] modelled and validated rooms in two museums in order to assess how the climate change would affect the artefacts' welfare. Wang et al. [281] developed a thermal model of the National Gallery of Edinburgh to study several low energy solutions for its renovation project. Kramer et al. [154] analysed the potential for energy saving of several setpoints strategies using a validated hygrothermal model of a museum, damage functions and an adaptive temperature guideline. Ferdyn-Grygierek et al. [110] modelled a Polish museum to evaluate the impact of several ventilation systems in its energy consumption. Sciurpi et al. [243] developed a thermal model of the "La Specola" museum to evaluate the strategies of replacing windows and the use of different solar shadings. Kramer *et al*. [155] developed a setpoint calculation algorithm that takes into account both the collection´s and the visitors' requirements and used the algorithm to analyse the energy demand in museums.

However, there are also models that are not validated against the indoor conditions, or their accuracy is only assessed by visual comparison between the simulated and measured values for each of the hygrothermal variables. The use of statistical parameters gives the model's developers a quantitative notion of how well the model simulates the behaviour of the real building. Some authors use statistical parameters to assist the validation process of whole-building models. For example, Ferreira *et al*. [111] used the annual average, the standard deviation and the minimum and maximum of the difference between the measured and simulated values to validate a hygrothermal model of a museum at Oporto in addition to the visual comparison. Pisello *et al*. [213] and Pernetti *et al.* [212] used the statistical parameters proposed by ASHRAE guideline 14:2002 for the validation process of thermal models [10], with the coefficient of determination also being used in the latter paper. Mustafaraj *et al.* [195] used simultaneously the goodness of fit, mean absolute error, mean squared error and coefficient of determination to validate thermal models of an office in London. Kramer *et al*. [160] also used the mean square error, mean absolute error and goodness of fit to validate several hygrothermal models of historic buildings.

Although whole-building hygrothermal models are valuable as a research tool, it is quite difficult to develop them for historic buildings due to the lack of information about the building materials, as well as the techniques that were used in the building, the ventilation rates, occupancy schedules and soil/slab interface temperature. Most often, only the building's architecture and surface materials are known, and due to their heritage value it is difficult to conduct the necessary characterization tests.

A simulation model of a 13th century church in Lisbon – St. Cristóvão church, was developed using the software WUFI® Plus [292] with the aim of establishing a methodology for the calibration and validation process of hygrothermal models, specifically for historic buildings, based on annual indoor conditions. Hence, the whole-year indoor conditions monitored in the church [250,251] were used to validate the model against the measured data. The hygrothermal accuracy of the simulations was assessed by

comparing the measured and simulated temperature and water-vapour pressure using four statistic indices, namely the coefficient of determination (R^2), the coefficient of variation of the root mean square error (CVRMSE), the normalized mean bias error (NMBE), and the goodness of fit (fit).

To overcome the usual difficulties in simulation studies, the following parameters were studied the influence of the outdoor climate by testing four different weather files for Lisbon; and the temperature of the interface between the soil and slab by testing six different methodologies for determining such temperature. To calibrate the model, a sensitivity analysis was carried out for three parameters – air change rate, solar heat gain coefficient of windows and short-wave radiation absorption coefficient, performing a total of 48 simulations. Finally, four simplifications of the validated St. Cristóvão church model were tested to reduce the simulation time while guaranteeing the accuracy of the model.

4.2. Methodology

4.2.1. Case study

For the purposes of the current study, a hygrothermal model of St. Cristóvão church in Lisbon was developed. The church is a 13th century building, classified as a national monument and is located on the slopes of St. Jorge's Castle in Lisbon, Portugal. The church is approximately 5250 m^3 in volume and it is made up of a nave (ca. 286 m^2), a funeral home to the south (ca. 93 m^2), a sacristy to the north (ca. 71 m^2), two towers (ca. 9 m^2 each) and an annex at the end of the nave (ca. 11 m^2). A photo of the southern façade and the horizontal plan of the church can be seen in Figure 4.1 and in Annex G. The church is naturally ventilated and does not have a climate control system.

The building has been widely studied by Silva and Henriques [250,251], who conducted a microclimatic monitoring of the church from November 2011 to August 2013 in which the temperature and relative humidity were recorded with 10 minutes intervals. A set of 17 thermocouples type T with an accuracy of ± 0.5 ºC and a probe RHT2nl of Delta T with an accuracy of ± 0.1 ºC and ± 2% RH was connected to a Delta T data logger to monitor the indoor climate of the main room. In addition, two data loggers HOBO U12-013 with an accuracy of ± 0.35 ºC and ± 2.5 % RH were used: the first one installed on the northern pulpit and the other on the northern tower to measure the outdoor conditions. Owing to technical issues, some of the thermocouples did not record data during the whole period, which in parallel with the differences between the types of sensors and the manufacturers of the data loggers justified the use of the data collected by the two HOBO, as reported in [250,251]. The location of the devices is shown in Figure 4.1.

The recorded data can be seen in Figure 4.2 for 2012 in which the light coloured lines represent the 10-minute records and the bold lines the 30-day running average to evaluate the seasonal trends. The analysis of the graphs allows to conclude that the interior climate follows the fluctuations of the exterior, although the seasonal cycles evidenced a certain damping and delay caused by the thermal inertia of the building. These indoor data were used to validate the simulation results. Since the relative humidity is a

variable that depends on the partial-pressure of water vapour and temperature, in this work the analysis of the hygrometric state of the air was made using water-vapour pressures. As this is a simulation study, this approach avoids the error replication in the calibration process and in attesting the accuracy of the models. A detailed analysis of the interior climate of the building can be seen elsewhere [250,251].

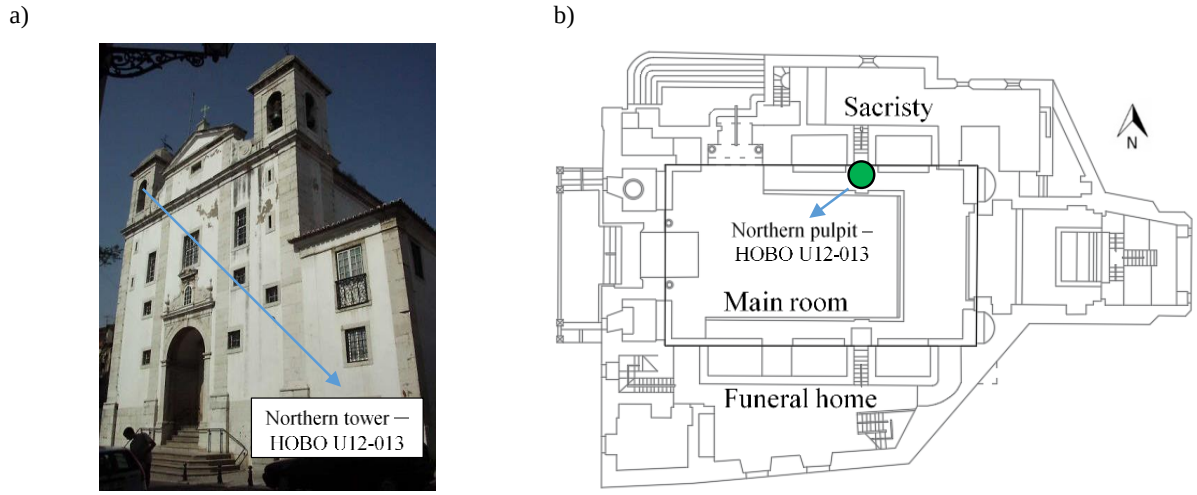

Figure 4.1 – Southern façade of St. Cristóvão church (a) and horizontal plan with reference sensor (b)

During the studied period, St. Cristóvão church was only open to the public for religious celebrations for six days, from 17:00 to 19:30 and mass was held in the last hour and a half, and on Sundays from 11:00 to 13:30 and mass was also held in the last hour and a half. It was considered that during the religious celebrations approximately 55 people were in the church and that during the hour before each mass approximately 5 people visited the church. The church was closed on Mondays.

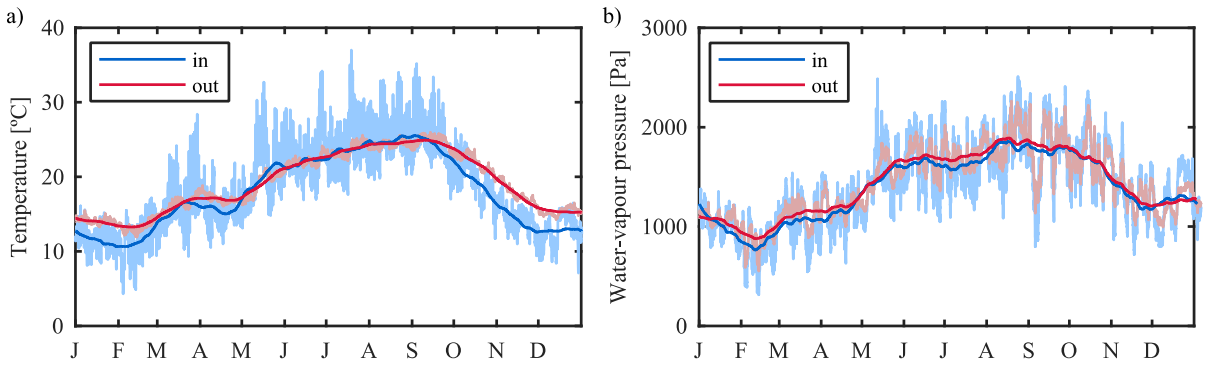

Figure 4.2 – Indoor and outdoor climate of St. Cristóvão church in 2012. The indoor data is recorded by the HOBO installed on the northern pulpit. The dashed lines correspond to the 10-minute recorded data and the bold lines to the seasonal cycle obtained from a 30-day running average. This data was recorded by the monitoring campaign described in [250,251]

4.2.2. Simulation settings

The hygrothermal model of St. Cristóvão church was developed in WUFI®Plus [292], a powerful hygrothermal simulation software based on the model developed by *Künzel* [163] that determines the indoor temperature and relative humidity for each zone of the model by taking into consideration the heat and moisture transfer that occurs through components, the gains/losses due to natural and/or mechanical ventilation and the gains/losses due to internal heat or moisture sources/sinks (people, lights

and equipment). WUFI®Plus has been validated over the years by many studies against experimental setups and other software [126,227,17] and has been used by many authors to build hygrothermal models of historic buildings (e.g. [18,39,125,87,152,162,217,111]).

4.2.2.1. Geometry and envelope

The geometry of the building was based on existing blueprints and, when needed, visits to the building to conduct *in-situ* surveys. The building geometry was designed in SketchUp and afterwards imported to WUFI®Plus using SketchUp-Import plugin. The geometry used in WUFI®Plus can be seen in Figure 4.3.

Figure 4.3 – WUFI®Plus developed model for St. Cristóvão church (Lisbon, Portugal)

The church has mortared limestone walls with a total thickness of 90 cm, rendered on both sides (1.5 cm each). Despite the impossibility of measuring the slab thickness accurately, a value of 0.2 m was adopted in accordance with the range usually found in other churches in Lisbon. The ceilings are made up of a doubled wood layer (2.0 cm thick each) with a 20 cm air gap in the middle, the roof is made with ceramic tiles and the doors are 5 cm thick oak. It was assumed that the church's windows had a thermal transmittance (U_w) of 5.1 W/m^{2}K, a frame factor (F_f) of 0.85 and an emissivity (E) of 0.80.

The adjacent buildings were also taken into account in the simulations. The ratio of window area per floor area is ca 11.6 %. The building's elements assemblies and U-value, as well as the corresponding basic and advanced properties of the materials can be seen in Table 4.1 and Figure 4.4. The building materials used to develop this model correspond to the WUFI®Plus database [292].

It is important to bear in mind that the church's eight compartments, one for each zone, were simulated with free-fluctuation indoor conditions and that the attic's climate was considered to be outdoor, due to the roof assembly.

Table 4.1 – Simulated building element assemblies and U-value, materials' thicknesses and basic hygrothermal proprieties.

Element	Assembly	Thick-ness (e, m)	Bulk density (ρ, kg/m^3)	Porosity (ε, kg/m^3)	Specific heat capacity, Dry (c_p, J/kg.K)	Thermal conductivity, Dry (λ_0, W/m.K)	Water vapour diffusion resistance factor (μ, -)	U-value (W/m^{2}K)
Walls	Lime mortar [292]	0.03	1600	0.30	850	0.70	7	1.36
	Mortared-limestone [292]	0.84	2122 [236]	0.13	850	1.76 [236]	140	
	Lime mortar [292]	0.03	1600	0.30	850	0.70	7	
Ceilings	Old oak [292]	0.02	740	0.35	1400	0.15	223	1.25
	Air gap [292]	0.20	1.3	-	1000	0.59	0.13	
	Old oak [292]	0.02	740	0.35	1400	0.15	223	
Roof	Ceramic tile [292]	0.02	1670	0.20	840	0.20	16	5.26
Doors	Old oak [292]	0.05	740	0.35	1400	0.15	223	2.01
Slab	Limestone [292]	0.20	2400 [235]	0.13	850	2.3 [235]	140	3.89
Clay (Soil) [292]		-	1500	-	880	1.50	-	-
Windows		Single-glazed window frames			U_w = 5.1 W/m^{2}K [235]		F_f = 0.85	E = 0.80

4.2.2.2. Internal loads

For human occupancy a metabolic rate of 1.3 met was considered in accordance with [262]. Since 1 met corresponds to 58.2 W/m^2 and allowing 1.8 m^2 for the surface corporal area of a male adult [4], a total heat gain of around 136 W was obtained. As the heat gain varies with gender, assuming an occupation equally divided between men and women and a reduction factor of 0.85 for the latter, an average heat gain of 126 W/person was obtained [6]. The total heat gain was divided into sensible and latent by applying a polynomial equation used by the software EnergyPlus [270], which uses total metabolic rate in W and temperature in ºC as inputs. From this equation 92 W of sensible heat (60 % by radiation and 40 % by convection in accordance to [6]) and 34 W of latent heat were obtained for a temperature of 19 ºC (the indoor annual average temperature). Since WUFI®Plus takes into account the latent heat as moisture generation, this parameter was obtained by dividing the latent heat in W by the water enthalpy evaporation (2257 J/g) in accordance with [156], thus obtaining a value of 54 g/h.

The church lighting is essentially guaranteed by halogen and tungsten lamps. According to [262] an illuminance of 200 lux was considered and it was assumed that 50% of the illumination is guaranteed

by halogen lamps with a luminous efficacy of 20 lm/W and the remaining 50% by tungsten lamps with a luminous efficacy of 15 lm/W [51]. The resulting lighting power density was obtained by dividing the illuminance by the luminous efficacy, which results in a value of 11.7 W/m^2 (30 % radiant + 70 % convective [262]).

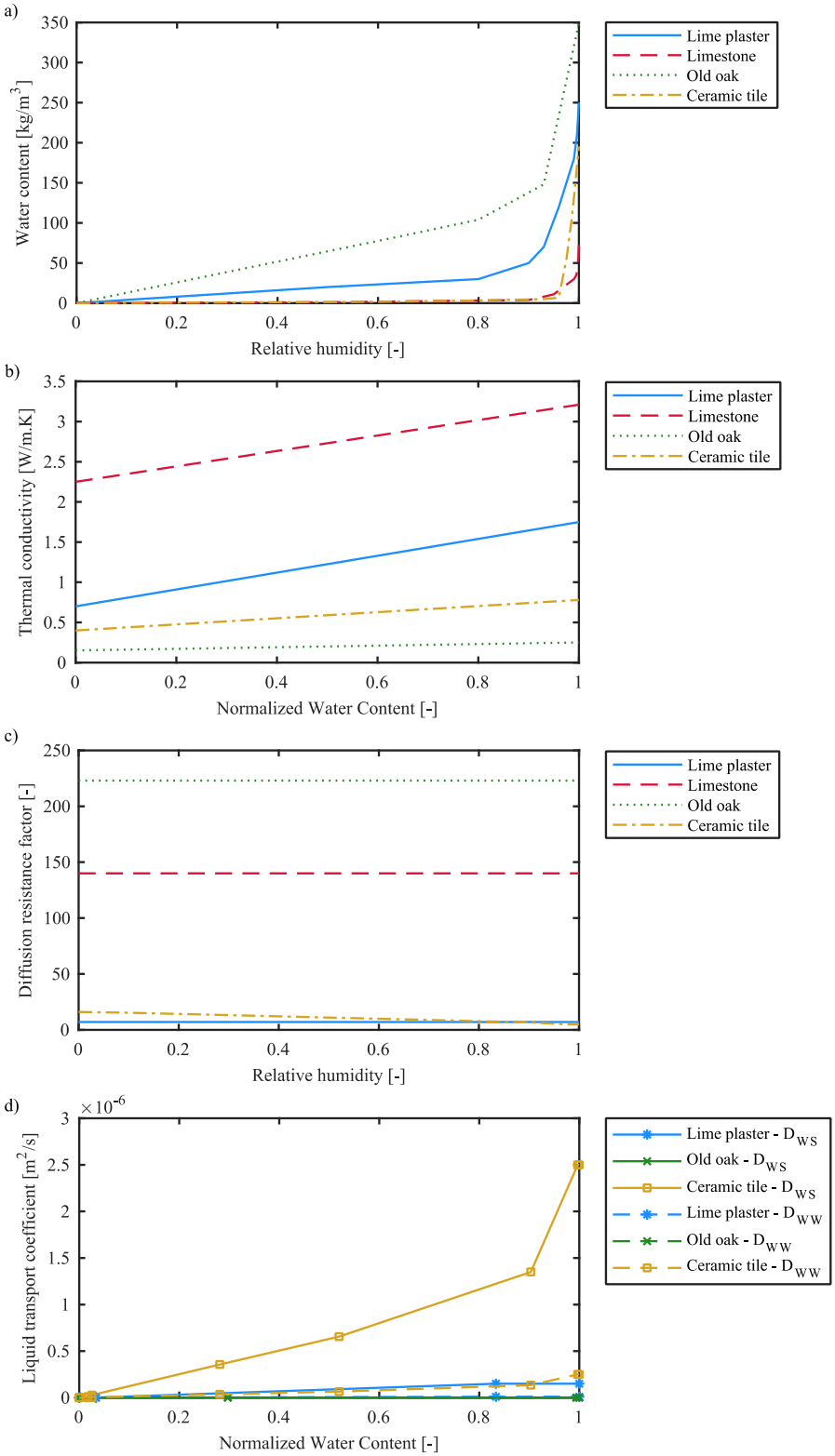

Figure 4.4 – Advanced hygrothermal proprieties of the simulated materials: a) moisture storage function; b) moisture-dependent thermal conductivity; c) moisture-dependent resistance factor; and d) liquid transport coefficient [292]

4.2.3. Model calibration

4.2.3.1. Outdoor climate

The weather files used in building simulation play a major role in its hygrothermal performance. The use of a generic local weather file to simulate a certain building and afterwards testing its accuracy against the indoor measured conditions may result in bad correlations. Even if the outdoor data is obtained for the same time period, if either different sensors are used or the datalogger is not installed in the vicinity of the building, the results may be unsatisfactory.

In order to obtain realistic results and to test the influence of weather files on the model accuracy, four weather files were used: the first two obtained from the EnergyPlus and WUFI®Plus weather databases, developed by the late National Institute of Engineering, Technology and Innovation (INETI) and Faculty of Engineering-University of Porto (FEUP) respectively; a third file was generated based on air temperature and water-vapour pressure, atmospheric pressure, wind direction and velocity, rain and global radiation data provided by the Portuguese Institute for Sea and Atmosphere (IPMA) for 2012 recorded by the Geofisico weather station (located 1.4 km from the church) and the fourth weather file was generated using the outdoor air temperature and water-vapour pressure recorded on the northern tower of the church, and using the remaining parameters from the Geofisico weather station.

The last two weather files were generated using the EnergyPlus Weather Converter (a complete description of this application and examples of application can be found in [271]), which is a useful tool that allows to generate weather files that may be used in some simulation software, namely WUFI®Plus. The annual temperature and water-vapour pressure variations for each of these four weather files are presented in Figure 4.5, showing the variability between the four weather files.

According to *Klöppen-Geiger* classification, Lisbon has a Mediterranean climate of class Csa, which stands for a temperate climate with rainy winters and hot summers [153]. This means that the outdoor temperature does not reach values below the freezing point, has a rather high annual temperature average (reaching highest values in summer) and it has a considerable precipitation, mainly during winter [65].

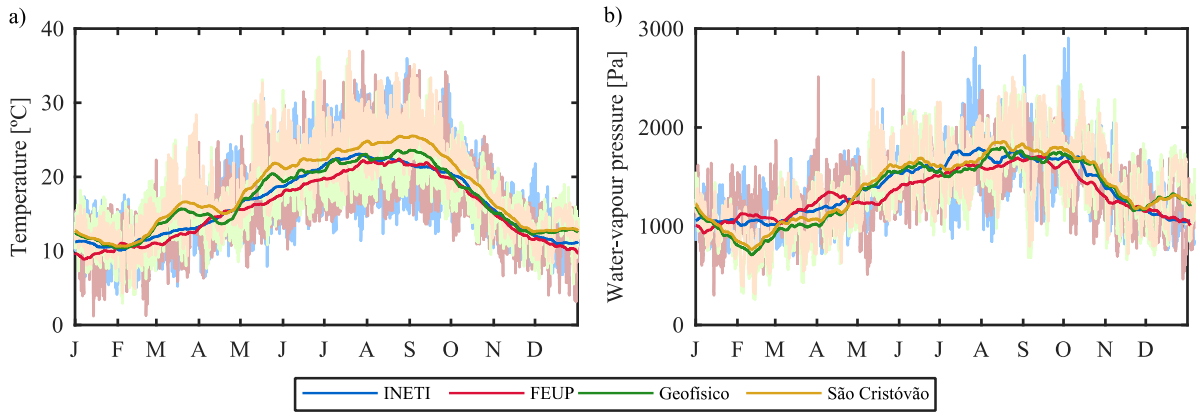

Figure 4.5 – Annual outdoor temperature (a) and water-vapour pressure (b) variation for the four weather files – INETI, FEUP, Geofísico and St. Cristóvão's. The seasonal cycles obtained from a 30-day running average for both variables is also shown in bold lines

4.2.3.2. Soil temperature

The soil/slab interface temperature is an important input for hygrothermal simulations since the soil behaves like a temperature buffer due to its properties. However, this interface temperature is not easily monitored due to its location, especially in historic buildings, and therefore it is necessary to find alternative ways to obtain it.

Although the soil/slab interface temperature is a key input in whole-building hygrothermal simulations, it is not very often mentioned in the models' description. WUFI®Plus cannot determine this interface temperature. Therefore, the model was also developed in EnergyPlus [81], which can determine the interface temperature by the *Slab pre-processor* (through *Detailed Ground Heat Transfer* field) or *Ground Domain* (through one of the three available models to determine the undisturbed ground temperature). The interface temperature can also be rudimentarily determined by subtracting 2 ºC from the indoor monthly average [267]. The interface temperature was determined by the *Slab pre-processor* of EnergyPlus using the *Detailed Ground Heat Transfer* field, and the *Ground Domain* of EnergyPlus, with the undisturbed ground temperature being calculated by the *Finite Difference*, *Kusuda-Achenbach* and *Xing* models. A fully description of these models can be found in Ref. [164,170,296,268,297,270].

The other option is to use a sine curve to simulate the soil/slab interface temperature by providing the mean annual temperature and its amplitude, as well as the day with the highest temperature. This option is better since the results can be fitted to the real case. However, since the model is tailored to these conditions it cannot be applied to other outdoor conditions, therefore it does not contribute to the general calibration. Additionally, the soil/slab interface temperature was also obtained using a sine curve and the simplification of subtracting 2 ºC from the indoor temperature. The output variables were the monthly average temperature, which is shown in Figure 4.6 for the four models of EnergyPlus, the sine curve with the annual average of 17.7 ºC (± 3.4 ºC) – highest temperature on September 15 – and the simplification of subtracting 2 ºC from the indoor temperature.

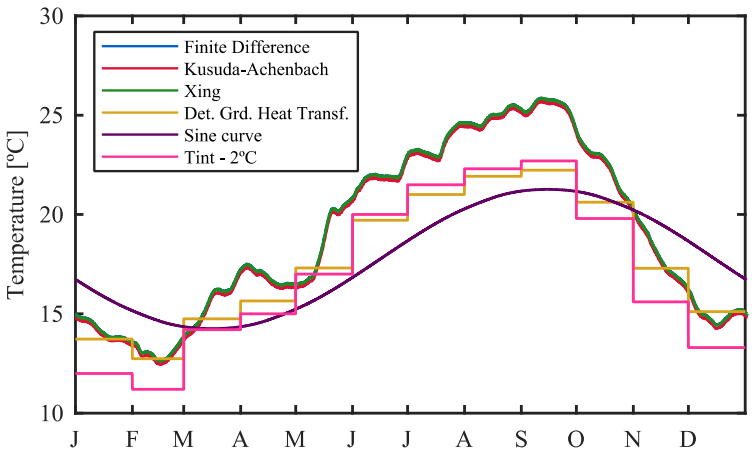

Figure 4.6 – Annual soil and slab interface temperature variation determined by the Finite Difference, Kusuda-Achenbach and Xing models, the Detailed Ground Heat Transfer in EnergyPlus, the sine curve and the simplification of subtracting 2 ºC from the indoor temperature

4.2.3.3. Input uncertainties

The construction of hygrothermal models of historic buildings has several gaps, and consequently various assumptions are needed. This problem increases when buildings are classified, since their preservation requirements and their opening to the public often makes it difficult to carry out destructive tests and the accurate determination of their characteristics. Some hygrothermal characteristics can be obtained locally or from literature, as presented in 4.2.2.1. However, sometimes doubts about the parameters that can influence the accuracy of the model cannot be clarified.

A sensitivity study can be a good solution to determine the parameters that best contribute to the quality of the model, thus allowing to optimize their numeric values. In this particular case, there were clear doubts about the church air change rate (ACH, h^{-1}), short-wave radiation absorption coefficient (α,-) of exterior walls and the solar heat gain coefficient of the windows (SHGC, -).

Ventilation

Some values of ACH for churches can be found in literature, namely: a mean ACH of 0.13 for a masonry basilica in Tarnow (Poland) [191,192]; an ACH between 0.08 and 0.12 for churches with stone vaults, and between 0.5 and 0.75 for churches with wooden vaults in the Netherlands [240]; an ACH of 0.17 for a brick structure church in Cracow [233]; and an ACH of 0.13 for a church with no heating system in Italy [35].

Although CO_2 measurements were not included in the church initial monitoring campaign, measurements for one week in September 2016 were carried out to determine the church's ACH. The ACH was estimated through the release and subsequent monitoring of the concentration values of the CO_2 generated by visitors, and fitting a decay curve to the gas concentration after the visitors leave, as reported in [240,191,192,156]. The CO_2 was measured by a low-cost and open-source data logger equipped with a SenseAir K-30 10,000 ppm sensor constructed for that purpose in accordance with the model presented and tested in Ref. [1]. The ACH was obtained by applying the equation [27]:

$$ACH = -ln\left(\frac{\left(c_{int,t} - c_{ext}\right)}{\left(c_{int,0} - c_{ext}\right)}\right) \times \frac{1}{t} \quad 4.1$$

where *ACH* is the air change per hour (h^{-1}), $c_{int,t}$ the internal gas concentration at the end of the slope (ppm), $c_{int,0}$ the internal gas concentration at the beginning of the slope (ppm), c_{ext} the external gas concentration (ppm) and *t* the time (s). Since only the indoor CO_2 concentration was monitored, the outdoor concentration was calculated from the indoor data, adopting the concentration measured when the indoor concentration reaches a steady state after people had left, with changes not higher than 1% for at least 1 h, following a similar approach used in [156].

The CO_2 concentration and the estimated ACH for the period immediately after the religious services and for a second period after the closing of doors and windows are provided in Figure 4.7. As expected,

higher values of ACH were obtained while the doors and windows were open, resulting in a mean value of 0.70. For the closed period, a mean ACH of 0.28 was obtained, resulting in a global weighted average of 0.32 by considering the period when the church was open and closed per week.

As well as the above estimated ACH, the authors also decided to carry out a sensitivity study to obtain the value that allowed the best calibration. The short-analysed period and the low differences of the CO_2 concentrations also contributed to this decision. Thus, it was decided to test the ACH ranging from 0.1 to 0.5, as shown in Figure 4.8.

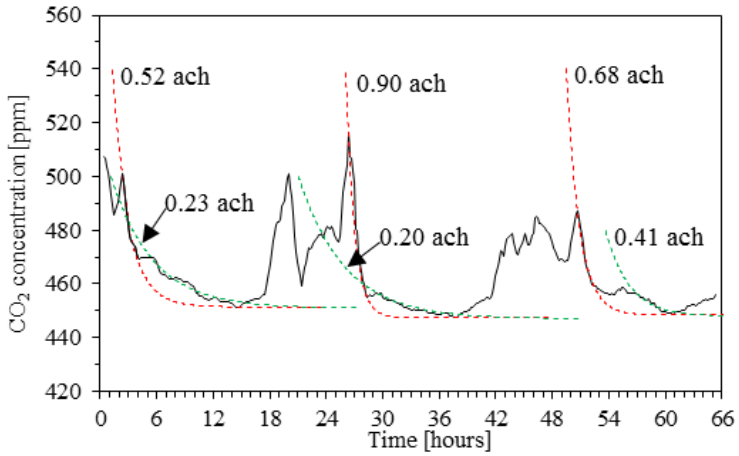

Figure 4.7 – CO_2 concentration and ACH estimation for St. Cristóvão church for 3 days in September 2016: red dashed lines correspond to the ACH when people leave the church but the doors and windows remain open; green dashed lines corresponds to the period after closing the doors and windows

Short-wave radiation absorption coefficient

The materials used in the building envelope absorb the incident solar radiation as a function of the short-wave radiation absorption coefficient that is directly related to the colour of the surfaces. This coefficient changes the way solar radiation is absorbed by the envelope and later propagated by conduction to the interior, having an influence on the interior hygrothermal balance [265].

Its choice may seem obvious as it is directly related to the colour, but old buildings sometimes have old paintings and plaster pathologies that make it difficult to choose an appropriate value. The church under study is mostly characterized by a light colour, but it presents various details in stone and defects in the plaster. Thus, the inclusion of this parameter in the sensitivity study was considered to obtain an average absorption coefficient that returns results closer to those measured, adopting a wide range from 0.2 (white paint) to 0.8 (dark stone) [204,36], as shown in Figure 4.8.

Solar heat gain coefficient

The solar heat gain coefficient is the quotient between the incident solar radiation and the solar radiation that actually crosses the window. This coefficient plays an important role in the control of the indoor climate of buildings, in the definition of their energy needs and can be estimated from tabulated values [6] or according to calculation methodologies [100,98,99].

The installed windows are single glazed and have wooden frames, usually characterised by SHGC of around 0.75. However, its definition is not always easy to obtain, given the difficulty of testing buildings in service, of getting access to all windows or because of the possible presence of randomly activated shading elements. Since in the present case it was not possible to obtain a reliable estimate for an average value, the authors decided to carry out a sensitivity study covering a range from 0.2 to 0.8 in order to obtain the most appropriate value through an equation of optimization.

Afterwards, a complete sensitivity study was performed to account for the most appropriate values of the three parameters in discussion, performing a total of 48 simulations, as can be seen in Figure 4.8.

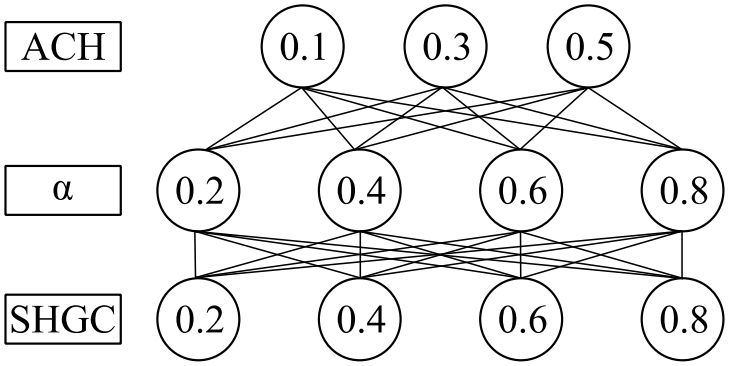

Figure 4.8 – Developed sensitivity analysis for St. Cristóvão church based on the ACH, α and SHGC

4.2.3.4. Accuracy assessment

The accuracy of the developed hygrothermal model was attested by using four statistical indices: *coefficient of determination (R^2), normalized mean bias error (NMBE), coefficient of variation of the root mean square error (CVRMSE)*, and *goodness-of-fit (fit)* – for two hygrothermal variables – temperature (T, ºC) and water-vapour pressure (P_v, Pa). The use of these four coefficients was based on the fact that calculating only one of them can produce an unreliable model. However, if the four parameters for the two variables are simultaneously considered, the obtained model will be much more robust. The R^2, which describes the correlation between the measured and simulated values, was calculated using the following equation:

$$R^2 = \left(\frac{\sum_{i=1}^{N} \left(X_{i,meas} - \overline{X_{meas}}\right) \cdot \left(X_{i,sim} - \overline{X_{sim}}\right)}{\sqrt{\sum_{i=1}^{N} \left(X_{i,meas} - \overline{X_{meas}}\right)^2 \cdot \sum_{i=1}^{N} \left(X_{i,sim} - \overline{X_{sim}}\right)^2}} \right)^2 \quad 4.2$$

The *NMBE* expresses the general normalized mean error and shows the influence of smaller errors [10]:

$$NMBE = 100 \cdot \frac{\sum_{i=1}^{N} \left(X_{i,meas} - X_{i,sim}\right)}{\overline{X_{meas}} \cdot (n-1)} \quad 4.3$$

The *CVRMSE* demonstrates how the model fits the measured data, overcoming possible compensation mistakes of the NMBE and it shows the influence of the higher errors [10]:

$$CVRMSE = 100 \cdot \frac{\sqrt{\frac{\sum_{i=1}^{N}\left(X_{i,meas} - X_{i,sim}\right)^2}{(n-1)}}}{\overline{X_{meas}}} \quad 4.4$$

The *fit*, which correlates the two data series and assesses their fluctuation, appears as a robust criterion to evaluate the level of fluctuation and, because it is presented in %, facilitates the comparison between the series [195]:

$$fit = \left(1 - \frac{\sqrt{\sum_{i=1}^{N}\left(X_{i,meas} - X_{i,sim}\right)^2}}{\sqrt{\sum_{i=1}^{N}\left(X_{i,sim} - \overline{X_{i,meas}}\right)^2}}\right) \cdot 100 \quad 4.5$$

where $X_{i,meas}$ is the measured value of the hygrothermal parameter at the time period *i*, $X_{i,sim}$ the simulated value of the hygrothermal parameter at the time period *i*, *n* the total number of points across the studied period of time (i.e. 8760 since it corresponds to one year worth of hourly values) and $\overline{X}_{meas}$ the average of the measured values of the hygrothermal parameter during the studied time period.

The model is more robust when the R^2 and *Fit* are higher, and *CVRMSE* and *NMBE* are lower. In this study, the model was considered validated if the R^2 is higher than 0.75 [80], the NMBE and CVRME are lower than 5 % and 20 %, respectively [80] and the fit is higher than 80% for each variable as considered in [160].

4.3. Results and discussion

In order to develop the first three studies (subchapter 4.3.1, 4.3.2 and 4.3.3) a start off-model was designed with a ACH of 0.20 h^{-1} (in all eight compartments), a short-wave radiation absorption coefficient for the exterior walls of 0.60 and a solar heat gain coefficient for the windows of 0.60. The soil/slab interface temperature was obtained using the simplification of subtracting 2 ºC to the indoor temperature [267]. The rest of the adopted parameters are described in 4.2.2.

4.3.1. Outdoor climate

Four different Lisbon weather files were simulated in order to demonstrate the importance of measuring the outdoor hygrothermal conditions as close as possible to the building in question. The obtained values for the accuracy coefficients demonstrate the importance of using the most appropriate outdoor weather file when validating a whole-building model.

The obtained values demonstrate that the use of Typical Meteorological Year (TMY) or Test Reference Year (TRY) weather files (such as INETI and FEUP) may not be suitable to validate whole-buildings models against measured conditions. For example, while comparing the temperature goodness of fit of the INETI and FEUP simulations (ca 56.5 % and 48.8 %, respectively) against St. Cristóvão simulation, the importance of the outdoor weather file becomes obvious, since St. Cristóvão attains a substantially higher goodness of fit than both simulations – 77.7 %, as can be seen in Figure 4.9c. This also occurs

for the water-vapour pressure (St. Cristóvão simulation attains a higher goodness of fit – while St. Cristóvão's attains 75.7 %, INETI attains 40.1 % and FEUP attains 33.5 %).

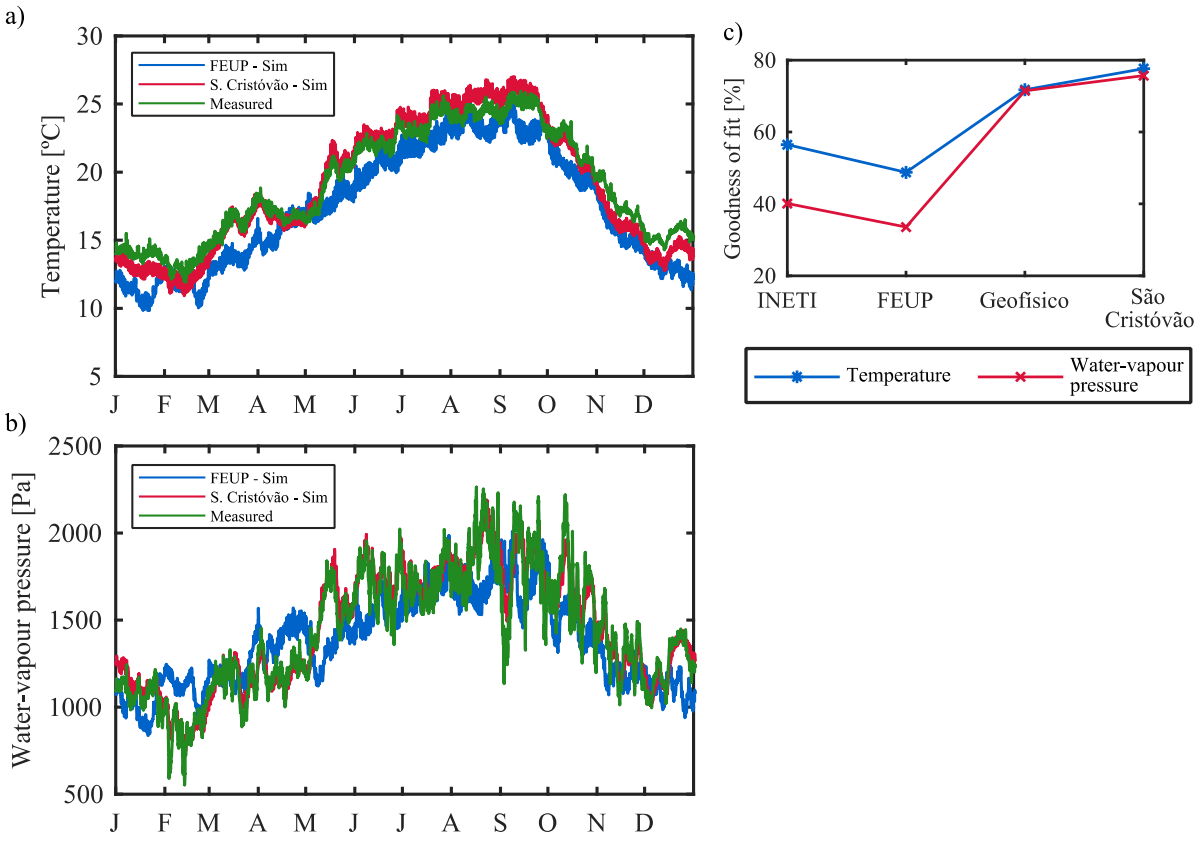

Figure 4.9 – Impact of the weather file on the model's accuracy: a) measured indoor temperature and model results for the FEUP and the St. Cristóvão's simulations; b) water-vapour pressure for the same conditions as a); and c) temperature and water-vapour pressure goodness of fit for the four weather files

What is even more interesting is the comparison between the simulation values of the Geofísico and the St. Cristóvão´s weather files since they correspond to the same year (both weather files data were registered in 2012) and also because the Geofísico station is only 1.4 km from the church. Although, the Geofísico simulation attains good values for both temperature and water-vapour pressure (ca 71.8 and 71.5 %, respectively), the St. Cristóvão's simulation attains higher goodness of fit for both the temperature and water-vapour pressure (77.7 and 75.7 %, respectively).

The St. Cristóvão's simulation attains lower CVRMSE and NMBE for both temperature and water-vapour pressure than the limits imposed by the ASHRAE guideline [10]. Even the more stringent values of the IPMVP [80] are assured by this simulation as summarized in Table 4.2. The attained coefficient of determination, for both temperature and water-vapour pressure are very near to the maximum. However, the validation process must be carried out since the goodness of fit still has not reached the same range of values as those obtained by Kramer *et al.* [160] for both variables. Henceforward, the St. Cristóvão's weather file is used as the outdoor weather file for the next steps. In Figure 4.9a) and b) the simulation results for the FEUP and the St. Cristóvão's simulations and the measured data were presented, both for temperature and for water-vapour pressure.

4.3.2. Soil/slab interface temperature

Although the model using the St. Cristóvão's weather file already has acceptable values, its calibration can be improved. The next step is to study the interface temperature between the soil and the slab's inferior surface. This was carried out by running the same model in WUFI®Plus for six different interface temperatures. The values obtained show the substantial importance of the soil/slab interface temperature on the indoor temperature and, consequently, the importance of obtaining this variable appropriately. On the other hand, the interface temperature does not cause a substantial variance in terms of indoor water-vapour pressure, therefore, this hygrothermal variable is disregarded in this subchapter.

Table 4.2 shows the accuracy parameters for the six simulated soil/slab interface temperatures. Figure 4.10 presents the measured indoor temperature, as well as the results for the interface temperature with the poorest model calibration (Finite Difference) and the best one (Detailed ground heat transfer) (a), and the temperature goodness of fit for the six soil/slab interface models (b). It can be seen that the first three EnergyPlus models worsen the accuracy values (e.g. the finite difference temperature causes the temperature goodness of fit to decrease from 77.5 to 72.6 %). However, it can also be seen that detailed ground heat transfer model achieves better accuracy values than the simplification of considering that the interface temperature is the indoor temperature minus 2 ºC (the CVRMSE decreases from 4.7 to 2.9 %, the NMBE decreases from 4.1 to 2.5 %, and the goodness of fit increases from 77.7 to 86.0 %).

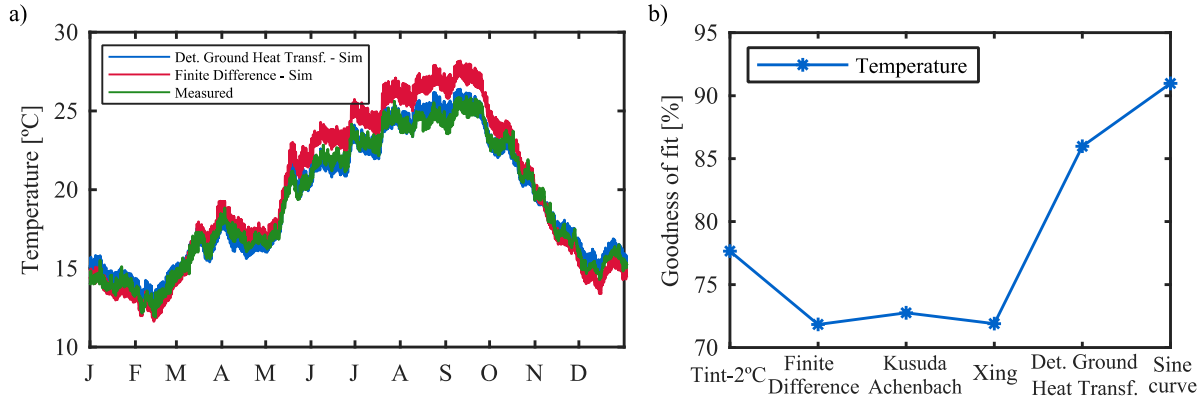

Figure 4.10 – Impact of the interface soil/slab temperature: a) measured indoor temperature and the simulated indoor temperature obtained using the detailed ground heat transfer and the finite differences, and b) temperature goodness of fit

Additionally, a fitted sine curve to the model with the St. Cristóvão's weather file was also simulated. It can be seen that accuracy values are even better than the detailed ground heat transfer simulation, the goodness of fit reaches ca 91 %. However, the use of these curves means that the model cannot be used in other locations, for example as developed by Kramer *et. al* in [155], since it is fitted to that climate file. Here, the interface temperature obtained by the detailed ground heat transfer model was adopted instead of the sine curve.

4.3.3. Sensitivity analysis

Although the range of values within which each parameter varies is known, its exact value is not. Hence,

a sensitivity analysis was carried out to optimize the model accuracy. The selected factors were the *ACH*, *α* and *SHGC*. The simulated values for each of these three parameters were chosen according to the type of building and include 48 simulations.

The goodness of fit coefficient was used for the model accuracy optimization since it proved to be the most demanding parameter. Figure 4.11 presents the temperature goodness of fit according to the ACH, α and SHGC, and Figure 4.12 presents the water-vapour pressure of goodness of fit according to the ACH. Based on this analysis it is possible to conclude that temperature is affected by the three parameters, while water-vapour pressure is only affected significantly by the ACH.

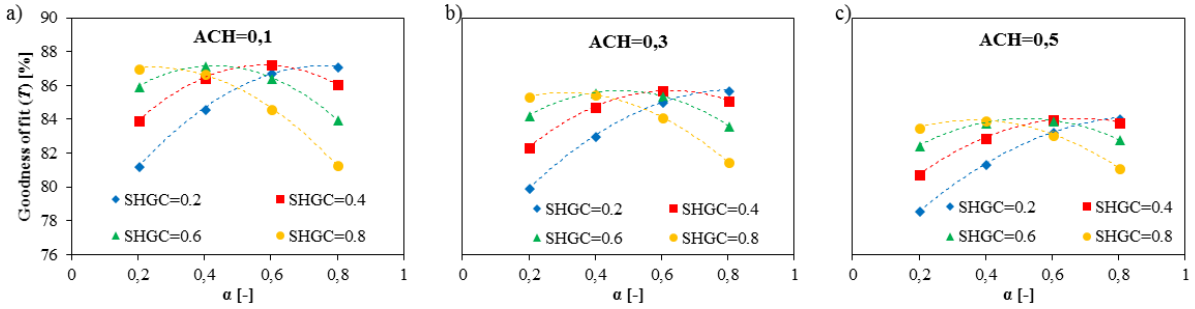

Figure 4.11 – Values of goodness of fit for temperature according to the ACH, α and SHGC

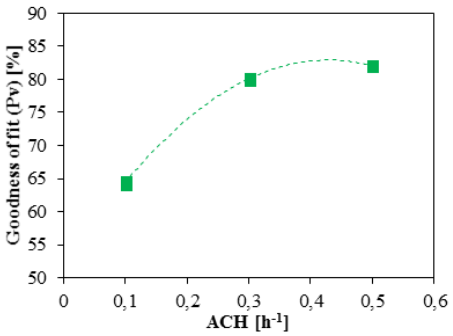

Figure 4.12 – Values of goodness of fit for the water-vapour pressure according to the ACH

Based on the sensitivity analysis results and with the aim of optimizing the model accuracy, the following equations were determined in order to estimate the temperature and water-vapour goodness of fit, respectively. The equations obtained adequately describe the temperature and water-vapour pressure goodness of fit, since the obtained R^2 is respectively 0.99 and 1.00.

$$fit(T) = [(-77.20 \cdot ACH + 58.85) \cdot SHGC^2 + (65.43 \cdot ACH - 58.06) \cdot SHGC + (-20.63 \cdot ACH^2 + 19.60 \cdot ACH - 12.54)] \cdot \alpha^2 + [(68.90 \cdot ACH - 58.23) \cdot SHGC^2 + (-64.88 \cdot ACH^2 + 8.45 \cdot ACH + 17.95) \cdot SHGC + (23.75 \cdot ACH^2 - 29.95 \cdot ACH + 30.14)] \cdot \alpha + (-10.93 \cdot ACH + 17.42) \cdot SHGC + 72.75 \quad R^2=0.99 \quad (4.6)$$

$$fit(P_v) = -171.17 \cdot ACH^2 + 146.71 \cdot ACH + 51.47 \quad R^2=1.00 \quad (4.7)$$

The average of the temperature and water-vapour pressure goodness of fit ($fit(T,P_v)$) was used as the optimization function, thus allowing us to determine the ACH, α and SHGC that correspond to the highest statistical values. In addition, the individual goodness of fit for the temperature and water-vapour pressure was limited to a minimum value of 80 %. Because the $fit(P_v)$ only depends on ACH values, a

range between 0.30 and 0.50 was directly obtained by imposing the 80 % limit to equation 4.7. The α-value was limited between 0.20 and 0.80 since equation 4.6 is only validated for this range, and the SHGC was limited between 0.20 and 0.75 (the presence of SHGC-values higher than 0.75 is not plausible). The optimization criteria that return the maximum f(x) can be seen in the following equation:

$$\begin{gathered} \int (x_1, x_2, x_3) \geq \int (x) \\ 0.30 \leq x_1 \leq 0.50 \\ 0.20 \leq x_2 \leq 0.80 \\ 0.20 \leq x_3 \leq 0.75 \end{gathered} \qquad 4.8$$

where x_1, x_2 and x_3 correspond to the ACH, α and SHGC, respectively and *f(x)* is the function *fit(T,P$_v$)*.

The solution of the optimization equation allows a value of 0.40 for the ACH, 0.40 for the α and 0.75 for the SHGC. The obtained parameters are physically admissible. An ACH of 0.40 does not differ significantly from the estimated value (0.32 h^{-1}) and from the values presented in literature (see 4.2.3.3). An α of 0.40 is acceptable for a light wall with some defects or some stone details and a SHGC of 0.75 is common in single-glazed window.

Figure 4.13 presents the annual variation of the indoor temperature and water-vapour pressure for both the simulated and measured values of the optimized model, where it can be seen that the simulated values acceptably overlay the measured ones.

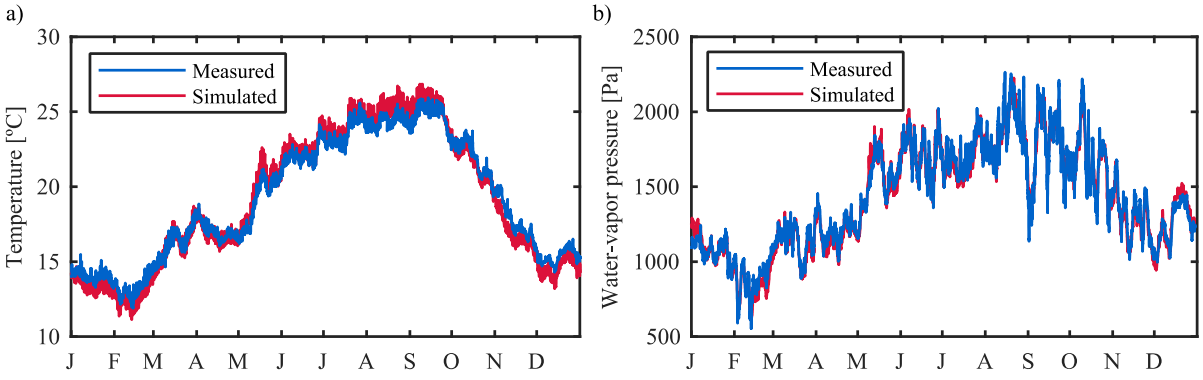

Figure 4.13 – Annual simulated and measured indoor temperature (a) and water-vapour pressure (b) variations for the optimized St. Cristóvão's model

In Table 4.2 the four statistic indices are summarized for the analysis of the impact of weather files (see subchapter 4.3.1), for the interface soil/slab temperature (see subchapter 4.3.2) and for the best accuracy model obtained from the sensitivity analysis (see subchapter 4.3.3).

Table 4.2 – Accuracy parameters for the four simulated weather files, the six simulated soil/slab interface temperature and the optimized St. Cristóvão model

Analysis		R^2 [-]		CV(RMSE) [%]		NMBE [%]		Goodness of fit [%]		
		T	P_v	T	P_v	T	P_v	T	P_v	T,P_v
Weather files	INETI	0.95	0.65	9.1	14.3	7.9	11.2	56.5	40.1	48.3
	FEUP	0.95	0.59	10.7	15.9	9.5	12.9	48.8	33.5	41.2
	Geofísico	0.98	0.93	5.9	6.8	5.1	5.3	71.8	71.5	71.6
	St. Cristóvão	0.99	0.94	4.7	5.8	4.1	4.3	77.7	75.7	76.7
Soil/slab Interface Temp.	Tint-2ºC	0.99	0.94	4.7	5.8	4.1	4.3	77.7	75.7	76.7
	Finite Difference	0.99	0.94	5.9	5.8	4.8	4.4	71.8	75.6	73.7
	Kusuda-Achenbach	0.99	0.94	5.7	5.8	4.7	4.4	72.8	75.5	74.1
	Xing	0.99	0.94	5.9	5.8	4.8	4.4	71.9	75.6	73.7
	Det. Ground Heat Transf.	0.99	0.94	2.9	5.7	2.5	4.2	86.0	76.1	81.0
	Sine curve	0.99	0.94	1.9	5.7	1.6	4.3	91.0	76.1	83.6
Optimized model		0.99	0.97	3.2	4.4	2.7	3.4	84.8	81.7	83.2

4.3.4. Model simplifications

A whole-building validated hygrothermal model is a powerful asset for the study of such a building since it allows a thorough analysis of most of the variables that influence the building's hygrothermal behaviour. However, the time that it takes to run a hygrothermal simulation is high and increases according to the complexity of the building geometry. Hence, the importance of studying model simplifications in hygrothermal simulation.

Nevertheless, the model's simplifications usually cause losses in the model's accuracy, which can be quite significant, and therefore these simplifications must be carefully chosen. The simplifications to the present model considered the time it took to complete each simulation and the losses of accuracy they caused. Secondly, a simplified model of the church was developed using only suitable simplifications, thus reducing the simulation time while maintaining the model's accuracy.

The following four simplifications were analysed while keeping the floor area, volume and height of the original model. These four simplifications are independently analysed, only the simplified model was subjected to the selected simplifications simultaneously.

Simplification 1 – Instead of considering two individual floors for the funeral home and sacristy (h_{1st}= 3.5 m and h_{2nd}= 3.0 m), only one floor with the same height was considered (h_{total} =6.5 m)

Simplification 2 – The windows were grouped together for each floor and according to their

orientation

Simplification 3 – The indoor walls that separate the balconies and the nave were discarded

Simplification 4 – The main door was moved forward so that it would coincide with the rest of the façade

Table 4.3 shows the time it takes to run the hygrothermal simulation and the goodness of fit for both the temperature and water-vapour pressure for the four simplifications and the final simplified model. The values of validated model subchapter 4.3.3 (i.e. optimized model) are also shown as a reference to see if a simplification is appropriate.

Table 4.3 – Simulation time (minutes), temperature and water-vapour pressure goodness of fit for optimized model, the four simplifications and the final simplified model

Simulation	Hygrothermal mode				
	Time [min]	*fit(T)* [%]	$\frac{fit}{Time}$	*fit(Pv)* [%]	$\frac{fit}{Time}$
Optimized model	60	84.8	1.4	81.7	1.4
Simpl. 1	51	83.5	1.6	81.9	1.6
Simpl. 2	61	83.4	1.4	81.9	1.3
Simpl. 3	66	82.3	1.3	81.9	1.2
Simpl. 4	60	85.1	1.4	81.8	1.4
Simplified model	44	81.2	1.9	81.7	1.9

This table shows that the first and the fourth simplifications are adequate for the St. Cristóvão's model. However, the other two simplifications are not suitable since their fit/time ratio is lower than those of the optimized model. Therefore, only the first and forth simplifications were adopted in the simplified model. In order to facilitate the replicability of the model, the compartments were transformed into rectangles while keeping the floor area, volume and height of the original model.

The adopted simplifications had both negative (the fit(T) and fit(P_v) decreased) and positive consequences (the simulation time decreased). However, it is the author belief that the positive consequences outweigh the negative ones (both fit/time ratios of the simplified model are higher than the optimized model ratios) and since the accuracy parameters are still in the same range of values as the other models validated in the literature (see 4.2.3.4), the developed simplified model is also viable to study the hygrothermal behaviour of St. Cristóvão church. For example, if the sensitivity analysis developed in 4.3.3 were to be repeated using the simplified model it would take almost 13 hours less than using the standard-case (the sensitivity analysis takes ca. 48 hours to be completed with the standard-case and ca. 35 hours with the simplified model).

Figure 4.14 presents the annual variation of the indoor temperature and water-vapour pressure measured in the church and the results obtained from the best accurate model (optimized model) and after the

simplifications (simplified model).

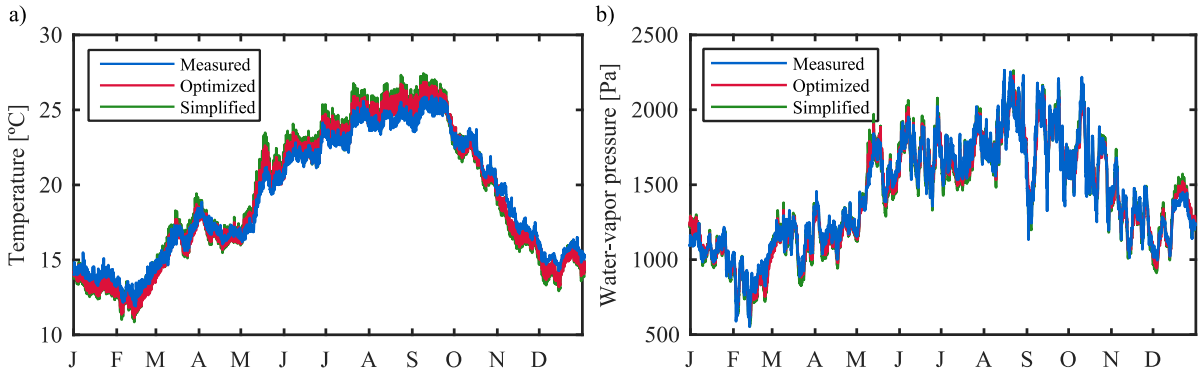

Figure 4.14 – Annual measured indoor climate and the results for the best accuracy model (optimized model) and after its simplification (simplified model): a) temperature; b) water-vapour pressure

4.4. Conclusions

A hygrothermal model of St. Cristóvão church was developed using WUFI®Plus and validated against measured data using four different statistic indices (R^2, *CVRMSE*, *NMBE* and *Goodness of fit*) for two hygrothermal variables (T and P_v) and its values were then compared with the limits present in literature and the existing standards/guidelines. The influence of weather files and the interface slab/soil temperature was analysed, and a sensitivity study was carried out to optimise the model accuracy for three undetermined variables – ACH, α and SHGC.

The developed analysis of the influence of the outdoor conditions in the accuracy of the model led to the conclusion that the use of weather files for the same city and even files of which the data was monitored during the same year may not lead to the best results. In the developed simulations the best fit was attained by the weather file developed with the temperature and water-vapour pressure obtained by the monitoring campaign (i.e. the St. Cristóvão's weather file, which attained a *fit(T)* of 77.7 % and *fit(P_v)* of 75.7 %). Using the weather file provided by IPMA for the same year and recorded by a meteorological station only 1.4 km from the church, a *fit(T)* of 71.8 % and *fit(P_v)* of 71.5 % were obtained, which, although they are lower values than St. Cristóvão's values, already allow the validation of the model. On the other hand, the use of the weather files for Lisbon obtained from the WUFI and EnergyPlus database attain much lower *fit(T)* and *fit(P_v)* than the St. Cristóvão's values: 48.8% and 33.5 %, and 56.5 % and 40.1 %, respectively.

The soil and slab interface temperature was also analysed although it is a parameter usually neglected or otherwise not mentioned in the description of many of the thermal and hygrothermal models found in literature. The simulations that were carried out showed the key influence that this parameter has on the hygrothermal behaviour of whole-building models, with the goodness of fit varying between 71.8 and 86.0 % depending on the adopted method. For the developed model the best goodness of fit was obtained for the Detailed Ground Heat Transfer. The sine curves were not considered for the final phase of the model development since this method cannot be adapted to new simulation conditions (e.g. to use

the same model for other outdoor conditions).

Another difficulty in a model validation is the uncertainties of the inputs. An optimization methodology for the model accuracy was developed based on three parameters, whose values could not be precisely determined: ACH, α and SHGC. The development of a sensitivity analysis which included 48 simulations allowed us to develop an accuracy optimization equation based on the goodness of fit, since it proved to be the most demanding parameter. The optimized values thus obtained were 0.4 for the ACH, 0.40 for the α and 0.75 for the SHGC, which resulted in the maximum values for both the *fit(T)* and the $fit(P_v)$. The optimized values are within the physical meaningful values of historic buildings.

Simplifications to hygrothermal models might reduce the simulation time considerably, but at the same time substantially reduce the model's accuracy. Hence, four different simplifications were analysed, but only two were found to be worthy of application, namely, considering a global floor for the funeral home and sacristy, and moving the main door forward. These simplifications allowed us to save 16 minutes per simulation while maintaining the model's accuracy. This saving is meaningful when developing a study that includes a large number of simulations. For example, if the sensitivity analysis were to be developed using the simplified model this would mean a saving of 13 hours.

5. IMPACT OF CLIMATE CHANGE ON ARTEFACTS KEPT IN CULTURAL HERITAGE BUILDINGS AND THE THERMAL COMFORT OF THE VISITORS

This chapter has been partly published in the following reference: Coelho, G. B. A., Silva, H. E., & Henriques, F. M. A. (2019). Impact of climate change on cultural heritage: a simulation study to assess the risks for conservation and thermal comfort. *International Journal of Global Warming*, *19*(4), 382–406. https://doi.org/10.1504/IJGW.2019.104268.

5.1. Introduction

The conservation of artefacts is highly dependent on the indoor conditions of the building in which they are kept, namely in terms of relative humidity and temperature [5]. The indoor relative humidity and temperature greatly influence the occurrence of chemical, biological and mechanical degradation [178]. On the other hand, it is also important to take into account the thermal comfort of the visitors [155], since they have a vital influence on the continuity of the stored artefacts collections and buildings.

Both indoor conditions can be significantly affected by climate changes, which are ultimately caused by the emission of greenhouse gas (GHG) into the atmosphere. Climate change will endanger even more the welfare of artefacts and may affect the visitors' thermal comfort. Hence, it is of key importance to perceive how the indoor climate of buildings without HVAC systems will react to changes, so that proper adaptive measures can be adopted.

Nowadays climate change is one of the key challenges that mankind faces since it greatly influences the environment, human health, global and local economy, as well as the maintenance of the building stock [284]. The changes of the outdoor climate will affect the durability of the buildings [18]. However, due to the variability of all the factors that affect the emission of GHG and, consequently, the outdoor climate, it was necessary to describe the different ways in which the outdoor climate might evolve.

For this purpose, the *Intergovernmental Panel on Climate Change* (IPCC) developed several scenarios that are based on different assumptions and, consequently, have different corresponding GHGs emissions of the several gases that contribute to the radiative forcing, e.g. CO_2, CH_4, N_2O [196]. These scenarios were used by IPCC in its Fourth Assessment Report [302].

The dominant anthropogenic contributor is carbon dioxide (CO_2), whose main sources of emission are the consumption of fossil fuel and the changes of land-use [196]. Furthermore, the building sector is also responsible for a large amount of CO_2 emissions [284]. For this latter reason and also because of the importance of maintaining heritage buildings, there has been a great emphasis in studying the impacts of climate change on this type of building (e.g. the *NOAH's Ark* project [229]).

Furthermore, UNESCO World Heritage Report 22 [288] defines several physical impacts of climate change in heritage buildings. Among all impacts mentioned in this report the following standout: physical changes of porous building materials and corrosion of metals (i.e. due to the *atmospheric moisture change*), deterioration of facades due to thermal stress and freeze-thaw/frost damage (i.e. due to the *temperature change*), penetrative moisture into porous building materials and deterioration of surface due to erosion (i.e. due to the *wind pattern changes*). This list of impacts shows the major negative effect that climate will have on heritage buildings.

More recently, and after the *NOAH's Ark* project, another European research project was developed that focused on the study of the effects of climate change on the decay process of artefacts housed in historic buildings, named *Climate for Culture* project [172]. A methodology based on computational models of

the buildings, future outdoor weather files and damage functions was used to assess the future risks for the collections. This methodology has been used in several other studies that analyse the future indoor conditions using computational models of historic buildings (e.g. [18,129,128,130,131,218,266]). For instance, Huijbregts et al. [128] developed a model of an unheated Dutch museum room and a Belgium museum room to assess the conservation quality of the future indoor conditions and concluded that an increase of both the indoor temperature and relative humidity is expected, which might affect the artefacts mainly in terms of biological decay. Additionally, Huijbregts et al. [129,130] developed and validated a model of a 19th century church to develop risk maps for Europe and determined that both the indoor temperature and the humidity ratio will increase in the future, more significantly in the far future, and that in terms of the conservation of artefacts there is no location in Europe that is safe from some sort of increased decay with each zone having its respective risks.

Recently, Rajčić et al. [218] developed and validated a model of the historic chapel named Barbara's chapel in Croatia and determined that for the simulated location there is an increase of both the risk of mechanical and biological decay, while Turhan et al. [266] used the model of a historic library named Necip Paşa Library in Turkey and determined that an increase of the risk of chemical decay and a decrease of the thermal comfort are expected due to the increase of the indoor temperature. Hence, it can be said that climate change will increase the risks of biological, chemical and mechanical decay to a different extent depending on the location.

The indoor climate can either be assessed from a conservation point-of-view; in terms of thermal comfort or even as a combination of both (e.g. [154,252,253,232]). In terms of the artefacts' conservation, one of the most used methodology is the one developed by Martens [178], which is based on damage functions that evaluate the risk of chemical, biological and mechanical damage occurrence depending on the indoor temperature and relative humidity. These damage functions, adapted from literature, were used to assess the degradation risk of four types of artefacts [181,244,186,44,144,45]: books, panel paintings, furniture and wood sculpture. Several applications of this methodology can be found in literature (e.g. [38,218]). More recently, this methodology was adapted by Silva et al. [253] to develop an indoor climate classification system for historic buildings.

In terms of thermal comfort, it is important that visitors have a pleasant experience while visiting the collection. Hence, it is necessary that the indoor temperature varies within an appropriated range of values, which can be assessed either using analytical models such as the Predicted Mean Vote [106], or an adaptive method such as the one developed in ASHRAE RP 884 (de Dear et al. [73]). In fact due to its simple approach to the thermal balance of the human body and also the fact that was updated by the authors through the years the Predicted Mean Vote was standardized in ASHRAE 55 [4] and ISO 7730 [137]. On the other hand, the method developed within ASHARE RP 884 was adopted with some modifications in ASHRAE 55 [4]. While the analytical models were based on climate controlled and steady-state laboratory experiments, the adaptive methods are based on field campaigns of in-use

buildings that admit that the occupants can adapt to the indoor condition up to a certain extent [180].

Normally, and due to high heritage value of many of the buildings that house these artefacts, the development of a computational model is based on a two-phase procedure: 1st) monitor the indoor conditions of the building (usually, temperature and relative humidity [250]), 2nd) develop and validate the computational model of the building against the measured indoor conditions (e.g. [66]). However, this procedure takes a considerable amount of time since both phases have several requirements. For example, the monitoring campaign must be long enough to record the indoor climate variability [51], whilst the validation of the model is based on the comparison of the annual simulated and the recorded indoor conditions [66].

The aim of this chapter is to determine how the quality of the indoor climate to preserve artefacts is going to change due to the climate change, which type of risks each selected climate will face in the future, as well as determining when it will be necessary to start implementing measures to counteract them. For this reason, a thoroughly validated whole hygrothermal model of a high thermal inertia church is used coupled to future weather files. The conservation quality of the indoor climate is assessed using a risk-based analysis that uses damage functions. Additionally, the thermal comfort of the visitors of the historic church is assessed by an adaptive thermal comfort method. The used methodology identifies not only the risks that each type of climate is more prone to, but also detects when these risks will occur more accurately, which allows a more adequate preparation.

This study is developed for three types of climate in Europe – Mediterranean, Humid continental and Oceanic – to determine how the climate change influences the indoor climate quality in terms of the artefacts' conservation and thermal comfort in each selected climate. The use of the validated model for different outdoor weather climates is possible due to the assumptions and the tools used in the model development. More precisely, in terms of the slab/soil interface temperature, which is neglected in most of the reviewed models in literature in spite of its key influence in the indoor climate [66].

The present chapter is subdivided in four subchapters, namely: 1)- Introduction, 2)- Methodology, 3)- Results and discussion and 4)-Conclusions. The first subchapter reviews the literature mainly dealing with the effects of climate change on the building heritage stock and artefacts conservation. The second subchapter addresses the hygrothermal model that is used coupled to the future outdoor weather files to obtain the future indoor climate. Additionally, the statistical indices, risk-based analysis and adaptive thermal comfort model used to analyse the simulated indoor climate are also addressed in this subchapter. The third subchapter presents and discusses the obtained results in terms of the variability of the simulated indoor climate, as well as the results of the risk-based analysis and the thermal comfort analysis. Finally, the main conclusions are presented in the last subchapter of this chapter.

5.2. Methodology

The following subchapter is organized in four subchapters in which the first summarizes the performed

study. The second briefly addresses the selected case-study, namely the performed monitoring campaign and the developed computational model. The third addresses the present and future outdoor conditions of the five selected climates. Finally, the fourth subchapter describes the methodologies used to analyse the indoor/outdoor climate.

5.2.1. General considerations

This subchapter studies the effect of climate change on artefacts based on the indoor conditions of the building. Hence, the future indoor conditions are obtained using an extensively validated hygrothermal model of a historic building (St. Cristóvão church in Lisbon) together with future weather files. Afterwards the indoor conditions are assessed in terms of chemical, biological and mechanical risks, as well as in terms of thermal comfort (using the optional model of standard ASHRAE 55 [4]). Additionally, the variability of the simulated indoor climate is also assessed using several statistical indices. This analysis was developed for three types of climate: Mediterranean (Lisbon, Portugal and Seville, Spain), Humid continental (Prague, Czech Republic and Oslo, Norway), and Oceanic (London, United Kingdom) [153]. The following subchapters briefly address the necessary tools to attain the proposed aims.

5.2.2. Model simulation

The selected case-study was a 13th century church located in Lisbon, Portugal, naturally ventilated and without any HVAC system (Figure 4.1 and Annex G). More precisely, the church is located in the slopes of St. Jorge's castle and is a good example of a high thermal inertia building due to its thick mortared limestone walls and limestone slabs. The church has a ceramic tile roof, single glazed windows and doubled layered wood ceilings. The window area/floor area ratio is approximately 0.12 and has a volume of approximately 5250 m^3. The church was recognized as a national monument in the 20th century [250].

In order to characterize the indoor climate of the church thoroughly, Silva and Henriques [250] installed adequately a multi-sensor temperature and relative humidity grid in the church [51]. The monitoring campaign lasted from November 2011 until August 2013 and had a recording frequency of 10 minutes. A detailed description of the monitoring campaign can be found elsewhere [250].

Based on this monitoring campaign, a whole-building hygrothermal model of the church was developed in WUFI®Plus [292] and EnergyPlus [81]. The model was developed using EnergyPlus so that the slab/soil interface temperature could be calculated in accordance with the outdoor climate both geographically and temporally. The adopted inputs of the developed model of St. Cristóvão church are presented in Table 4.1 and Table 5.1. The selected windows are single glazed with a window thermal transmittance (Uw) of 5.1 W/m^{2}K, a frame factor (F_f) of 0.85 and an emissivity (E) of 0.80.

Table 5.1 – Internal gains and ventilation for St. Cristóvão church model (adapted from Ref. [66])

Illumination	11.7 W/m^2 (30% radiant and 70 % convective)		
People	Metabolic rate – 1.3 met Heat – 126 W/person (92 W sensible heat and 34 W latent heat) Moisture – 54 g/h		
Occupation rate	Tuesday to Saturday	17h00–18h00	5 people (visits)
		18h00–19h30	55 people (mass)
	Sunday	11h00–12h00	5 people (visits)
		12h00–13h30	55 people (mass)
Ventilation	0.4 h^{-1}		

Water-vapour pressure was used to calibrate the hygric behaviour of the building instead of relative humidity [66]. Additionally to the graphical comparison between the simulated and monitored annual variations four statistical indices were used to obtain a robust hygrothermal model: the *coefficient of determination* (R^2, unitless), the *coefficient of variation of the root mean square error* (CV(RMSE), %), the *normalized mean bias error* (NMBE, %) and the *goodness of fit* (Fit, %). These indices were selected in accordance with literature, but also because they are either presented in percentage or are unitless, which allows the comparison between the performance of the thermal and hygric mode [160].

The model was calibrated by developing a sensitivity analysis for three pre-determined parameters: air change rate, the short-wave radiation absorption coefficient for the exterior walls and the solar heat gain coefficient of the windows [66]. The simulated indoor temperature and water-vapour pressure were compared against the monitored indoor conditions using the previously mentioned statistical indices – R^2, CV(RMSE), NMBE and Fit.

Based on the obtained results an optimization function was developed and the conjugation of the three parameters with the highest fit was obtained. The results of this calibration process can be consulted in Table 5.2. These values are very good considering other models in literature [66]. Hence, the annual variation of the simulated indoor conditions very closely overlays the measured conditions (Figure 4.13).

Table 5.2 – Statistical indices of St. Cristóvão church model after the validation process

Statistical indices	Temperature	Water-vapour pressure
CV(RMSE)	3.2 %	4.4 %
NMBE	2.7 %	3.4 %
Fit	84.8 %	81.7 %

5.2.3. Future outdoor climate assessment

The analysis performed in this subchapter was developed for three types of climates to identify how the artefacts' conservation and occupants' thermal comfort are going to change depending on the typology of climate. The chosen climate typologies according to Köppen classification were: Mediterranean

climate (Lisbon and Seville – Csa class); Humid continental climate (Prague and Oslo – Dfb class); and Oceanic climate (London – Cfb class) [153]. The Köppen classification was first introduced by Köppen [151], but it has suffered updates since then. In this subchapter an updated version of this classification is used, i.e. Kottek et al. [153].

Both Lisbon and Seville have mild and rainy winters, and hot and dry summers, but Lisbon has a higher annual precipitation and Seville reaches higher temperatures. On the other hand, Prague has cold winters with temperatures reaching values below the freezing point, hot summers, and low annual precipitation. Oslo also has warm summers and cold winters (reaching lower temperatures than Prague), but it has a higher annual precipitation than Prague. Finally, London has cold winters, warm summers and a moderate annual precipitation.

For each of these five climates, a set of climate change weather files was used – starting in 2020 and finishing in 2100, as well as a near-past weather file. This latter weather file was adopted as the standard-case for each selected climate (henceforth named 1990) to ease the comparison between different years of the same climate. These weather files were obtained from the widely used meteorological database Meteonorm [185]. This software is based on meteorological data from several international databases. Furthermore, the unavailable meteorological data is determined using literature validated methods [221].

Out of the several scenarios designed by IPCC in the way how the world is going to evolve for the Fourth Assessment Report (AR4) two scenarios were selected, namely A1B (mid-radiative forcing scenario) and A2 (high-radiative forcing scenario) [302]. It is expected that the amount of CO_2 emissions will depend on the total energy consumption and energy supply structure [196]. More recently, other scenarios named *Representative Concentration Pathway* (RCP) have been developed [303], in which scenario A1B of AR4 corresponds to RCP 6.0 and scenario A2 of AR4 corresponds to RCP 8.5 (Figure 2.18).

The A1B scenario is based on a rapid economic growth, an increase of the number of people until the mid-century and its decrease afterwards and a balanced development of both fossil and non-fossil energy source technologies [302]. These assumptions imply a substantial increase of the CO_2 emissions in the beginning of the 21st-century. However, after 2050 and until 2100, the CO_2 emissions will decrease steeply due to the structural changes of the energy sector [196]. On the other hand, the A2 scenario is based on heterogeneous world in which its population continuously increases and in the assumption that fossil fuels remain as the central source of energy [302]. These assumptions imply a significant increase of the CO_2 emissions from the beginning of the 21st-century until 2100 [196]. Both scenarios were already used in European projects that address cultural heritage, while the A1B scenario was used in *Climate for Culture* project [172], the A2 scenario was used in *Noah's Ark* project [229].

These two IPCC scenarios are based on certain scenarios drives that affect differently the outdoor conditions in Europe. In terms of temperature it is foreseen that the annual temperature will increase for

all Europe [302]. In contrast, the effect of climate change in precipitation will differ from region to region. For instance, both the annual precipitation and the number of precipitation days will decrease for the Mediterranean regions [302]. On the other hand, the precipitation will increase in winter and decrease in summer for central Europe [302]. However, the risk of drought in these two regions will increase in summer [302]. Distinctively, the annual precipitation and the extremes of daily precipitation will increase in the northern European regions [302]. The snow season is likely to shorten in all of Europe [302]. A detailed description of the effects of the climate change on the outdoor variables can be found in Ref. [302].

For the selected climates, there is a generalized and significant increase of the annual average outdoor temperature due to climate change, but at different rates depending on the type of climate (Figure 5.1). The highest values of the annual average temperature are reached in the Mediterranean climates, followed by London and Prague (which tend to a similar situation in terms of temperature), and then Oslo. The annual average outdoor temperature increases from 18.2 to 22.4 ºC in Seville (i.e. a total increase of 4.2 K for scenario A2), from 16.8 to 19.8 ºC in Lisbon (i.e. a total increase of 3.0 K for scenario A2), from 9.6 to 12.6 ºC in London (i.e. a total increase of 3.0 K for scenario A2), from 8.7 to 12.5 ºC in Prague (i.e. a total increase of 3.8 K for scenario A2) and from in 3.9 to 8.0 ºC in Oslo (i.e. a total increase of 4.1 K for scenario A2) for the selected period. The difference between the selected scenarios is only significant from 2070 onwards in which scenario A2 attains higher values (Figure 5.1).

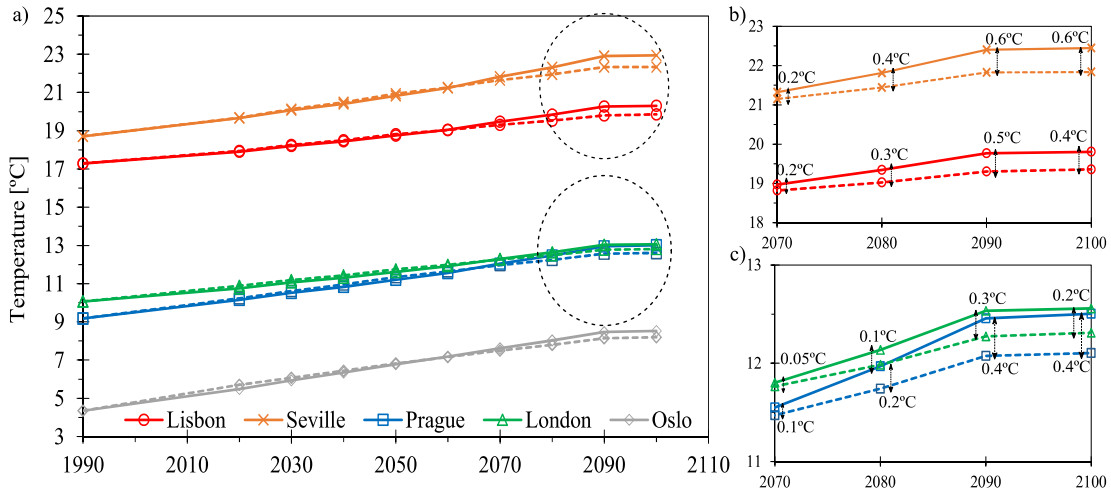

Figure 5.1 – Annual average of the outdoor temperature for Lisbon, Seville, Prague, London and Oslo for scenario A1B (dotted line) and A2 (solid line) between 1990 and 2100

The annual average of the outdoor water-vapour pressure follows the same tendency of the previously described variance of the outdoor temperature in which there is a generalized and significant increase of the values, but at a different rate depending on the climate (Figure 5.2). Once again, the highest values are reached in the Mediterranean climates (namely, Seville and Lisbon), followed by London and then by the humid continental climates (namely, Prague and Oslo). The annual average of the outdoor water-vapour pressure increases from 14.1 to 18.5 hPa in Seville (i.e. total increase of 4.3 hPa for scenario

A2), from 13.8 to 16.8 hPa in Lisbon (i.e. total increase of 3.0 hPa for scenario A2), from 9.5 to 11.6 hPa in London (i.e. a total increase of 2.1 hPa for scenario A2), from 8.2 to 10.6 hPa in Prague (i.e. a total increase of 2.4 hPa for scenario A2) and from 6.3 to 8.4 hPa in Oslo (i.e. a total increase of 2.1 hPa for scenario A2) for the selected period. The difference between the selected IPCC scenarios is more significant from 2070 onwards in which scenario A2 attains higher values, especially for the Mediterranean climates (Figure 5.2).

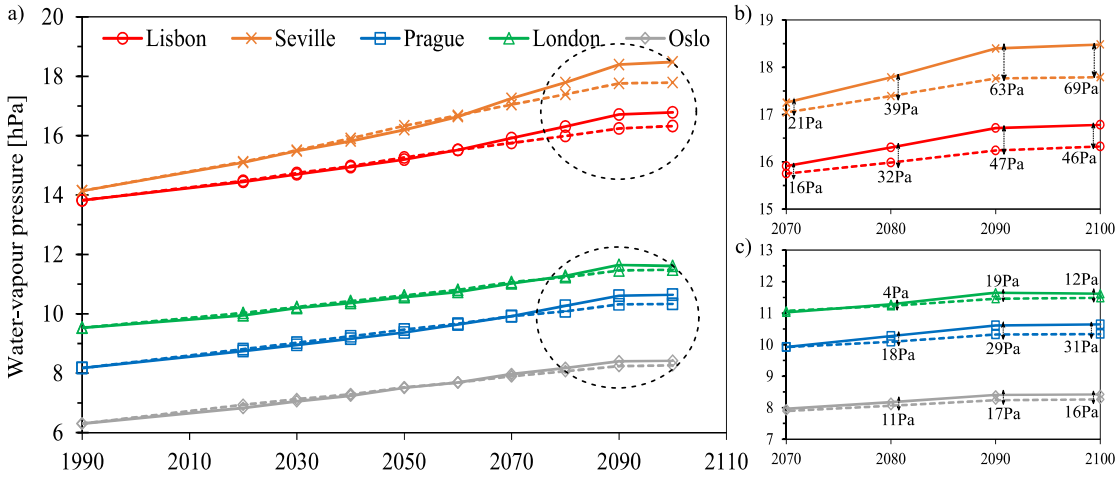

Figure 5.2 – Annual average of the outdoor water-vapour pressure for Lisbon, Seville, Prague, London and Oslo for scenario A1B (dotted line) and A2 (solid line) between 1990 and 2100

The annual precipitation tends to increase for Oslo from ca 860 to 1010 mm/year (i.e. a total increase of 150 mm for scenario A2) and for Prague from ca 521 to 551 mm/year (i.e. a total increase of 30 mm for scenario A1B) for the selected period (Figure 5.3). On the other hand, the annual precipitation decreases from ca 751 to 734 mm/year in London (i.e. a total decrease of ca 16 mm for scenario A1B), from ca 753 to 595 mm/year in Lisbon (i.e. a total decrease of ca 158 mm for scenario A2) and from ca 600 to 478 mm/year in Seville (i.e. a total decrease of ca 122 mm for scenario A2). Additionally, there is a significant difference between the two selected IPCC scenarios for Lisbon, Prague and Seville, which is more pronounced from 2050 onwards (Figure 5.3).

Finally, in terms of global radiation there is a generalized slight increase with occasional differences between the two IPCC selected scenarios (Figure 5.4). For instance, the annual global radiation increases from 2429 to 2448 kWh/m^2 in Seville (i.e. a total increase of ca 19 kWh/m^2 for scenario A2), from 2328 to 2364 kWh/m^2 in Lisbon (i.e. a total increase of ca 36 kWh/m^2 for scenario A1B), from 1595 to 1611 kWh/m^2 in Prague (i.e. a total increase of ca 16 kWh/m^2 for scenario A1B) and from 1571 to 1604 kWh/m^2 in London (i.e. a total increase of ca 33 kWh/m^2 for scenario A2). The only exception is Oslo in which the global sum decreases from 1379 to 1339 kWh/m^2 (i.e. a total decrease of ca 40 kWh/m^2 for both scenarios).

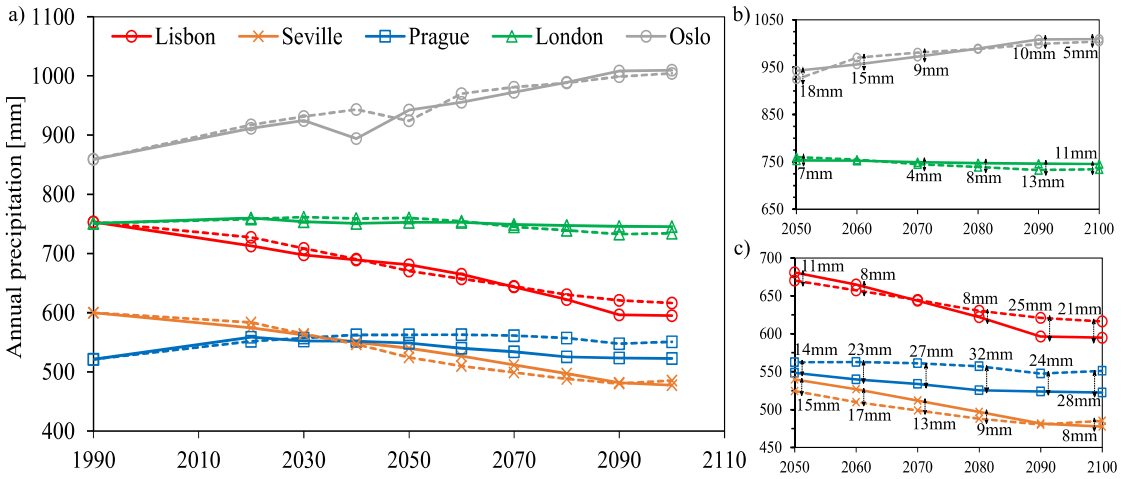

Figure 5.3 – Annual precipitation for Lisbon, Seville, Prague, London and Oslo for scenario A1B (dotted line) and A2 (solid line) between 1990 and 2100

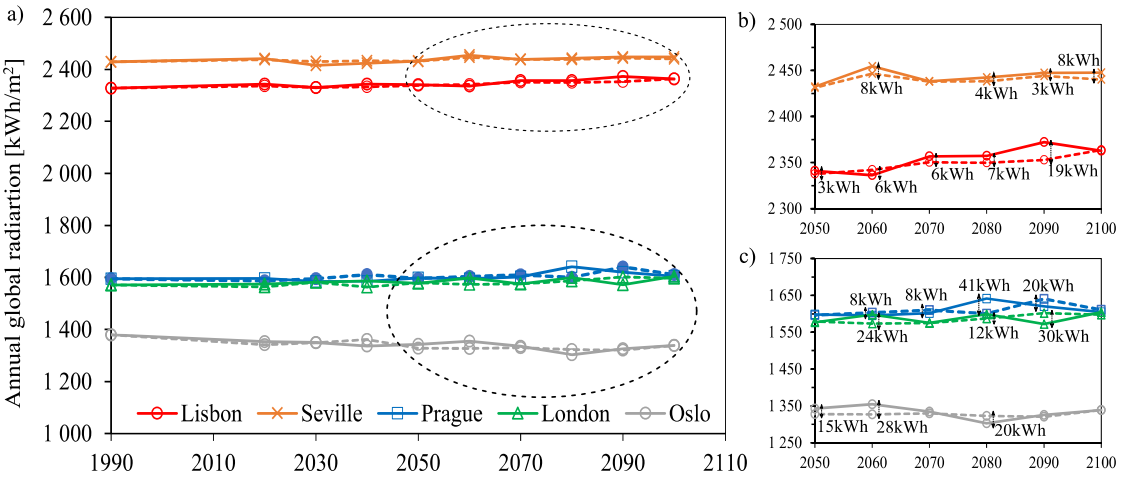

Figure 5.4 – Annual global radiation for Lisbon, Seville, Prague, London and Oslo for scenario A1B (dotted line) and A2 (solid line) between 1990 and 2100

5.2.4. Climate assessment tools

5.2.4.1. Statistical analysis

A methodology based on statistical indices was used to assess the future trend of the indoor conditions, namely in terms of temperature and relative humidity. This helps to perceive how the indoor climate is going to change throughout the years and to explain the results obtained from the risk-based analysis.

The statistical indices used to assess the variability of the indoor climate were the standard (average, maximum and minimum), the percentiles (5º, 25º, median, 75º, 95º), the short-term fluctuations and seasonal amplitudes. These last two statistical indices were calculated using the methodologies described in EN 15757 [90], in which the seasonal fluctuation is obtained using a 30-day moving average and the short-term fluctuations are obtained through the subtraction of the moving average to the instantaneous values.

5.2.4.2. Risk assessment

The risk-based analysis assesses the risk of occurring chemical decay using the lifetime multiplier [186],

biological decay using the isopleth method [244], and mechanical decay in which the applied methodology varies with the artefact based on the building's indoor conditions. Further information can be found in subchapter 2.2.2.2, but a detailed description of these methods is found in Ref. [178].

The isopleth method [244] is used for assessing the risk of biological decay, i.e. mould. The germination of mould occurs when the LIM – the *Lowest Isopleth for Mould* – is surpassed. This analysis is based on temperature and relative humidity, but also on the substrate since for mould to grow the substrate has to have nutrients [244]. The LIM curve is not constant and varies with temperature and relative humidity.

The chemical risk is assessed using the *lifetime multiplier* concept [186], which represents the amount of time that a material remains usable whilst compared to standard conditions (20 ºC and 50% RH), and is obtained using the following equation:

$$LM_x = \left(\frac{50\ \%}{RH_x}\right)^{1.3} \times e^{\frac{E_a}{R}\left(\frac{1}{T_X+273.15}-\frac{1}{293.15}\right)} \quad 5.1$$

where LM_x is the lifetime multiplier at point x (-), RH_x is the surface relative humidity at instant x (%), E_a is the material's activation energy (100 kJ/mol for paper and 70 kJ/mol for the other materials), R is the gas constant (8.314 J/Kmol) and T_x is the temperature at instant x (ºC). Moreover, to obtain a single value that represents the whole studied period, Silva and Henriques [251] established an *equivalent Lifetime Multiplier,* which is obtained using the following equation:

$$eLM = 1\Big/\left(\frac{1}{n}\cdot\sum_{x=1}^{n}\left(\frac{1}{LM_x}\right)\right) \quad 5.2$$

where *eLM* is the *equivalent Lifetime Multiplier* [-], *n* is the number of data points in considered period [-] and LM_x is the lifetime multiplier at instant x [-].

All hygroscopic materials are subjected to mechanical decay, since this process is governed by relative humidity, which is continuously varying indoors and subsequently inside the materials due to several factors [6]. The methodology to assess the mechanical decay varies with the artefact. For instance, while in wood sculptures the risk is assessed using an updated version of Jakiela et al. [144] method, in furniture it is assessed using an updated version of Bratasz et al. [45] method. The panel paintings are a particular case since the method used to assess the risk of mechanical decay in the wood substrate (Mecklenburg's et al. [181]) is different from the one used for the pictorial layer (Bratasz's et al. [44]). These methodologies determine if the limits of deterioration are surpassed, thus leading to mechanical decay (Figure 2.2), and are based on the material's response time (see subchapter 2.2.2.2).

5.2.4.3. Thermal comfort

Although the conservation requirements of artefacts are of the utmost importance while selecting the indoor conditions of the buildings, it is also necessary to consider the needs of the visitors, because without this source of income this type of buildings cannot exist. The thermal comfort was assessed

using the adaptive method of ASHRAE 55:2013 [4] for an 80 % acceptability limit. This method is valid for natural ventilated buildings without HVAC systems, in which occupants can adapt their clothing to the climate conditions, and the activity level is near-sedentary (varying between 1.0–1.3 met) [4]. Furthermore, this method accounts for local thermal discomfort effects, clothing adaptation and indoor air speed adaptation [4]. The outdoor air temperature is obtained using a 7-day exponential weighted running average of the daily averages of the outdoor temperature [4].

5.3. Results and discussion

5.3.1. Future indoor climate statistical analysis

As it was previously mentioned, the indoor climate was subjected to a statistical analysis using three types of indices to perceive how the indoor conditions are going to change in the future.

Based on Figure 5.5 it is visible that the indoor temperature is going to increase. This occurs for the five selected climates, but evidently at a different rate. For example, while the annual average indoor temperature in Seville increases from 19.1 ºC in 1990 to 21.8 ºC in 2100 (which means a total increase of 2.7 K for scenario A2), in Lisbon it increases from 18.3 to 20.2 ºC (i.e. a total increase of 1.9 K for scenario A2), in London it increases from 13.3 to 15.2 ºC (i.e. a total increase of 1.9 K for scenario A2), in Prague it increases from 12.7 to 15.1 ºC (i.e. a total increase of 2.4 K for scenario A2) and in Oslo it increases from 9.5 to 12.1 ºC (i.e. a total increase of 2.6 K for scenario A2). This generalized increase of indoor temperature is due to the increase of the outdoor temperature described by the IPCC scenarios (subchapter 5.2.3), and for the selected climates the indoor temperature of historic buildings increases around 2-3 K.

It is also interesting to observe that the variability of the indoor climate increases for all analysed climates, except for Oslo in which it decreases. The variability increases since the amplitude between the minimum and maximum temperature increases, with Seville showing the greatest increase.

Out of the selected climates, the indoor temperature is generally higher in the Mediterranean climates with Seville attaining the highest values. Both in terms of short-term fluctuations and of seasonal amplitude there is no significant variance during the study period – the seasonal amplitude average for Oslo is 17.6±0.4 ºC, 16.7±0.2 ºC for Prague, 15.1±0.4 ºC for Seville, 12.8±0.3 ºC for London, 11.8±0.2 ºC for Lisbon; and the short-term fluctuations vary between -4.2/3.1 ºC for Oslo, -3.3/+3.3 ºC for Prague, -2.5/2.9 ºC for Seville, -2.7/2.6 ºC for London and -2.1/+2.5 ºC for Lisbon.

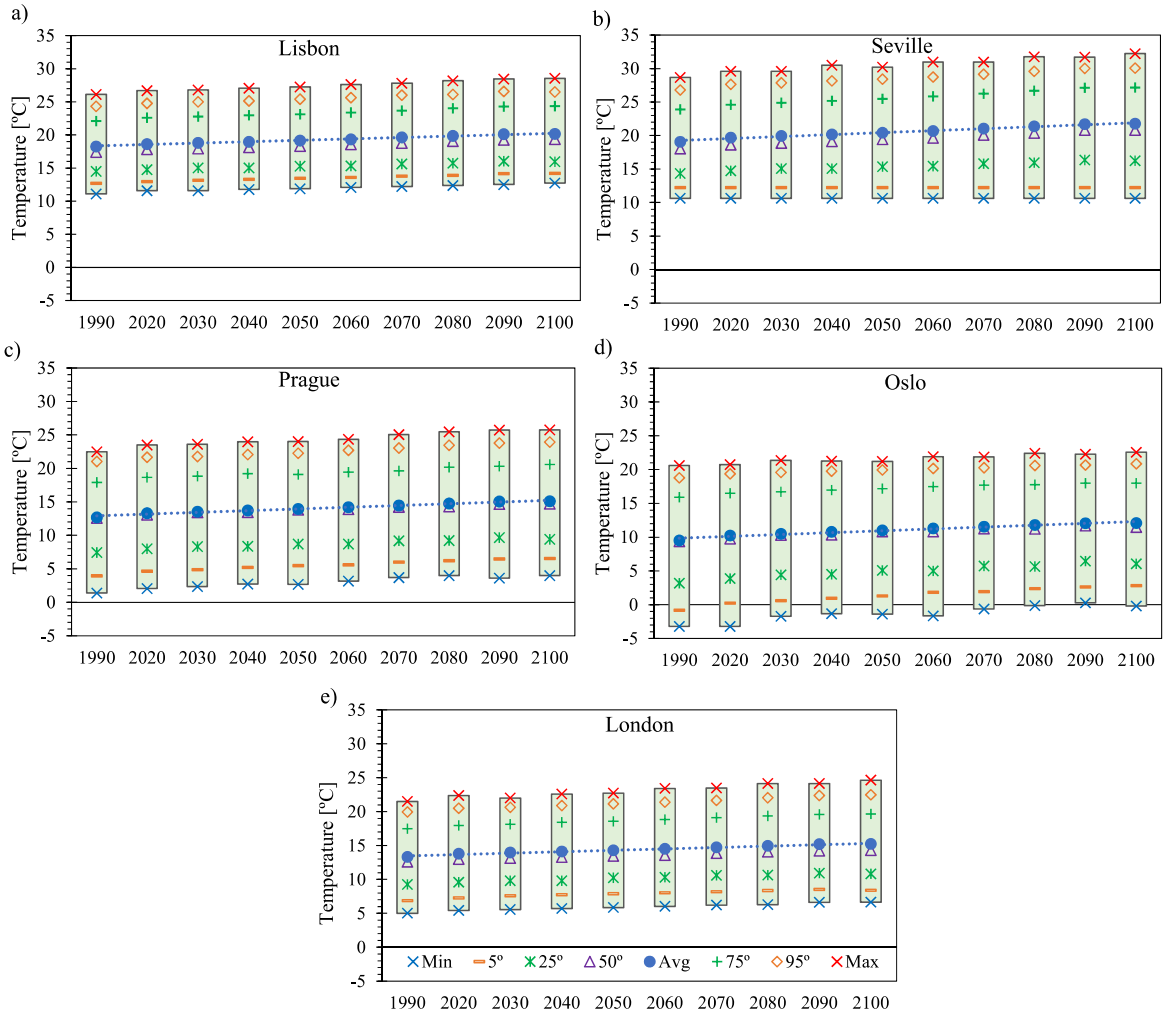

Figure 5.5 – Statistical analysis of the indoor temperature for Lisbon (a), Seville (b), Prague (c), Oslo (d) and London (e)

In terms of relative humidity, there is an increase of the annual average for the five climates (Figure 5.6). Lisbon has the highest values (the annual average increases from ca 66 to 71 %RH between 1990 and 2100 for scenario A2), followed by Seville (the annual average increases from ca 63 to 69 %RH for scenario A2), London (the annual average increases from ca 63 to 68 %RH for scenario A2), Prague (the annual average increases from ca 56 to 62 %RH for scenario A2) and Oslo (the annual average increases from ca 53 to 60 %RH for both scenarios).

On the other hand, there is a decrease of the variability of the indoor relative humidity for all select climates except for London. This occurs because both the maximum and minimum values of the indoor relative humidity increase, but the minimum indoor RH increases at a higher rate. For instance, the seasonal amplitude in Lisbon is 14.9 %RH in 1990 and it decreases to 12.7 %RH in 2100, whilst in Prague it decreases from 15.3 to 14.1 %RH, from 12.6 to 11.9 % in Seville, and from 12.3 to 7.8 %RH in Oslo during the same period. On the other hand, there is a slight increase of the variability for London since the seasonal amplitude increases from 6.5 to 8.2 %RH.

In addition, the short-term fluctuations do not change significantly for the five selected climates.

Nevertheless, the obtained values are included within the typical range of values for this type of building [250]. For instance, the highest short-term fluctuations in Lisbon is 14.1 %RH in 2100.

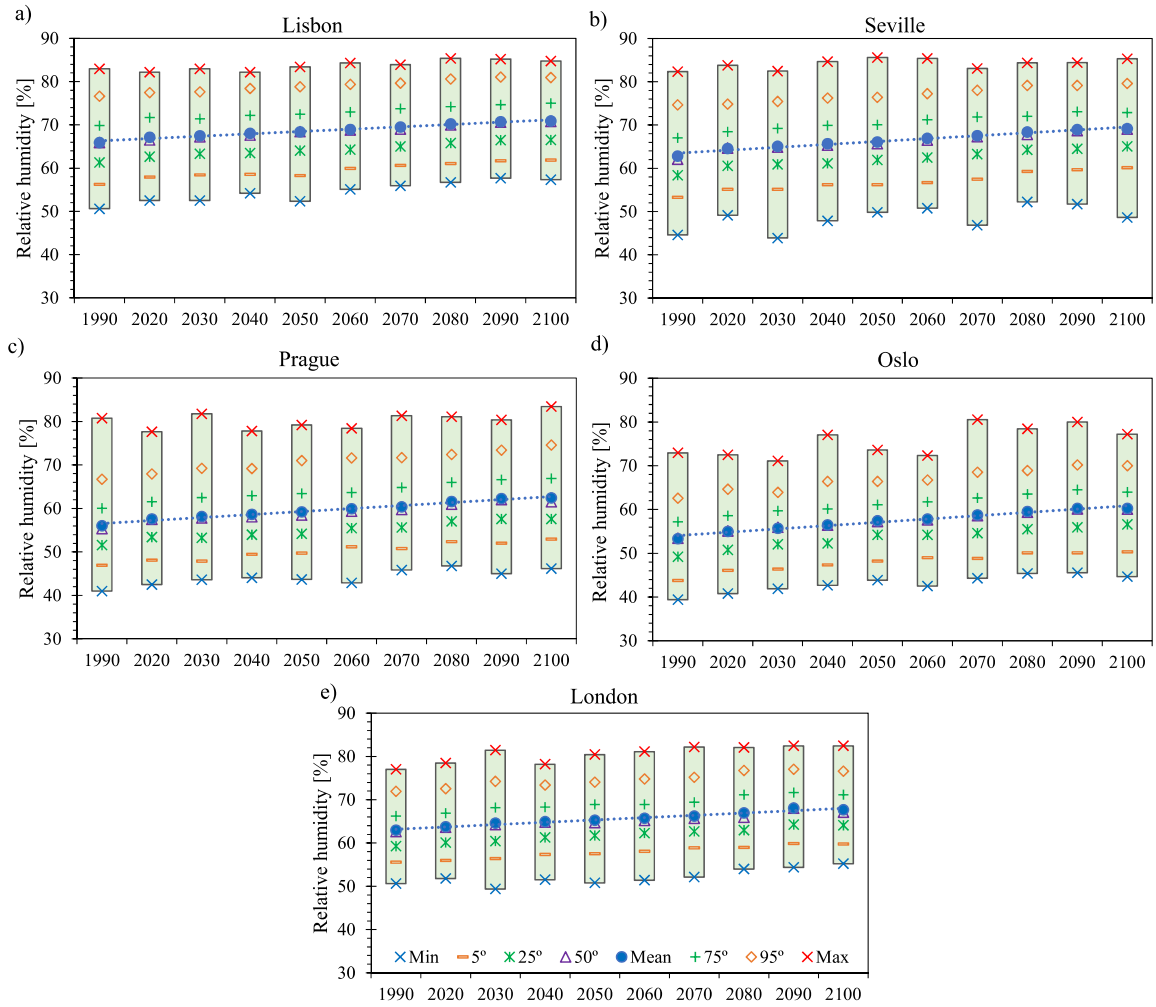

Figure 5.6 – Statistical analysis of the indoor relative humidity for Lisbon (a), Seville (b), Prague (c), Oslo (d) and London (e)

5.3.2. Risk and thermal comfort assessment

The quality of the indoor climate of historic buildings to preserve artefacts was assessed in terms of biological using the *isopleth method*, chemical using the *equivalent lifetime multiplier*, and mechanical using the four methods described in subchapter 5.2.4.2. The thermal comfort was analysed using the method described in subchapter 5.2.4.3. The weather files used correspond to the two previously addressed IPCC scenarios, i.e. A1B and A2.

The occupants' thermal comfort increases, more evidently for Oslo, London and Prague. This can be observed in Figure 5.7 which shows the percentage of time in a year where the limits of the adaptive model of ASHRAE 55:2013 [4] are guaranteed indoors for an acceptability limit of 80 %. This increase is due to the generalized increase of the indoor temperature (Figure 5.5), which is caused by the increase of outdoor temperature imposed by the IPCC scenarios. However, the attained values are low, for example for Lisbon the percentage of time that the indoor conditions can be classified as thermally

comfortable is 42 % in 1990 and reaches 46 % in 2100 (varying between 44–53% for Seville, 25–32 % for Prague, 20–29 % for London and 5–22 % for Oslo).

Furthermore, the thermal comfort increases because the selected case-study is non-heated. Hence, the indoor temperature will increase in the cold months, thus leading to higher indoor temperatures. But if the building were to be mechanically climatized this increase of the indoor temperature could lead to a higher energy consumption since it would have to balance out the indoor temperature to guarantee the building's indoor climate setpoints.

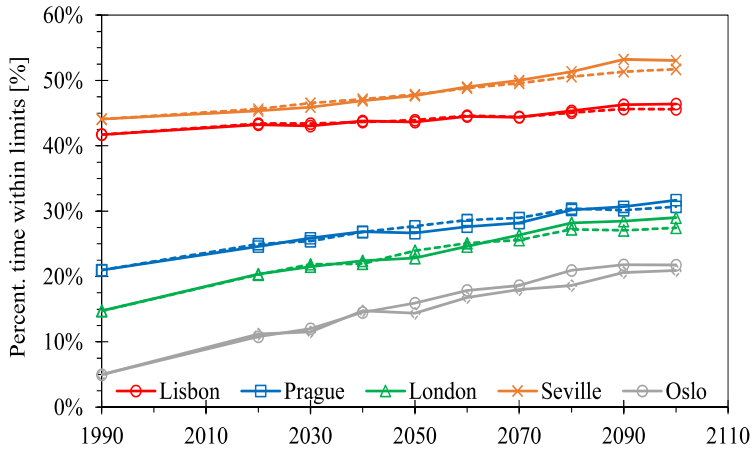

Figure 5.7 – Percentage of the time in a year that the imposed thermal comfort conditions are guaranteed for the adaptive model of ASHRAE 55 with a 80 % acceptability limit [4]

The performed analysis showed that the quality of the indoor climate to preserve artefacts worsens. In terms of biological decay there is a generalized increase of the amount of time the LIM is surpassed (Figure 5.8). As regard the chemical decay the equivalent lifetime multiplier greatly decreases (Figure 5.9). The sculptures and the base layer of the paintings panels significantly deteriorate (Figure 5.10). Evidently, the rates of these decay processes vary according to the climate and the IPCC scenario.

As regard the biological decay, it is visible that the quality of the indoor climate worsens since the amount of time that the indoor conditions surpass the LIM increases (Figure 5.8a). However, and contrary to the subsequent risk assessments, a considerable difference depending on the selected scenario is observable, especially for the Mediterranean climates (i.e. Lisbon and Seville). This means that a greater biological risk can be observed if the world evolves according to scenario A2, which in turn will lead to a more dangerous situation for the housed artefacts in this type of buildings.

For instance, in Lisbon the indoor conditions that exceed the LIM amounts to ca 3 % of the year in 1990 with this percentage increasing up to 18 % in 2100 (Figure 5.8b). The same magnitude of increase is visible in Seville (i.e. the number of hours in a year that the indoor conditions exceeds the LIM increases from 2 to 14 % between 1990-2100). Both these observations show that this type of climate is prone to mould germination and, consequently, it is necessary to take proper measures to mitigate this decay process. On the other hand, for the other three climates the biological decay is not a considerable risk,

especially for Oslo. The maximum amount of time that the LIM is exceeded in Prague is 3 % in 2100, whilst in London it is 4.6 % in 2090 and 0.6 % in Oslo in 2090.

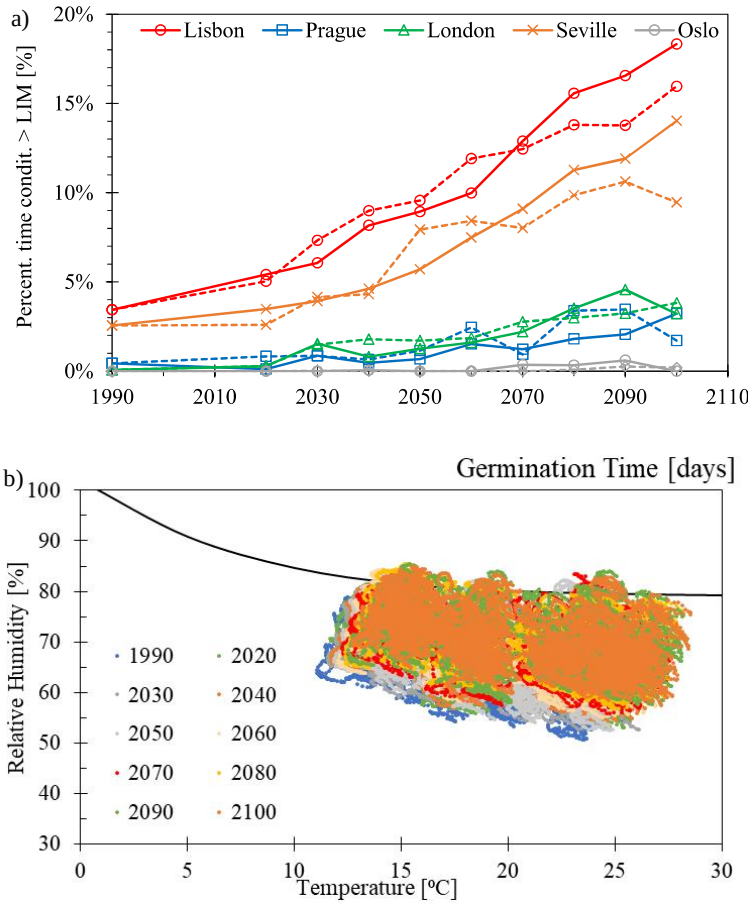

Figure 5.8 – Percentage of time that the indoor conditions overcome the LIM for the five selected climates and for the two IPCC scenarios A1B (dotted line) and A2 (solid line) (a) and spore germination for Lisbon and scenario A2 (b)

Regarding the chemical decay, the quality of the indoor climate decreases significantly for both cellulose and varnish materials (Figure 5.9). This decrease is more evident for Oslo (e.g. the eLM for cellulose decreases from 2.60 to 1.69 for the A2 scenario between 1990 and 2100, which represents a decrease of 91 %), but closely followed by Prague and London (e.g. the eLM for cellulose decreases respectively from 1.72 to 1.06 and from 1.59 to 1.07 for the A2 scenario between 2020 and 2100, which represents a decrease of 66 % and 52 %, respectively). On the other hand, and although Seville and Lisbon have the lowest decrease of quality, the obtained values for the present situation are critical for the preservation of artefacts and tend to aggravate (e.g. the eLM for cellulose in Seville is 0.69 in 1990, which is well below the ideal value – 1.0 [253], and decreases to 0.40 in 2100 for the A2 scenario, whilst in Lisbon it decreases from 0.80 to 0.54 for the same period), which shows that a special care has to be taken into account in this type of climate in terms of chemical decay.

In terms of varnish both Seville's, Lisbon's and London's climate are under the recommended limit in 2100 (i.e. eLM of 0.49, 0.59 and 0.97 for scenario A2, respectively), and closely followed by Prague (i.e. eLM of 1.01 for scenario A2 in 2100). On the other hand, the Oslo climate is very appropriate to

house varnish materials since the distance to the eLM limit is very substantial in 1990 and it remains considerable in 2100 (i.e. the eLM is 2.06 and 1.44 for scenario A2 in 1990 and 2100, respectively). This is understandable since the chemical decay is largely influenced by temperature and Oslo has the lower indoor temperature values (Figure 5.5). Furthermore, no significant difference between the results of the two scenarios was observed, which reinforces the idea of a decrease of quality in the future that will cause artefacts to be more prone to chemical decay.

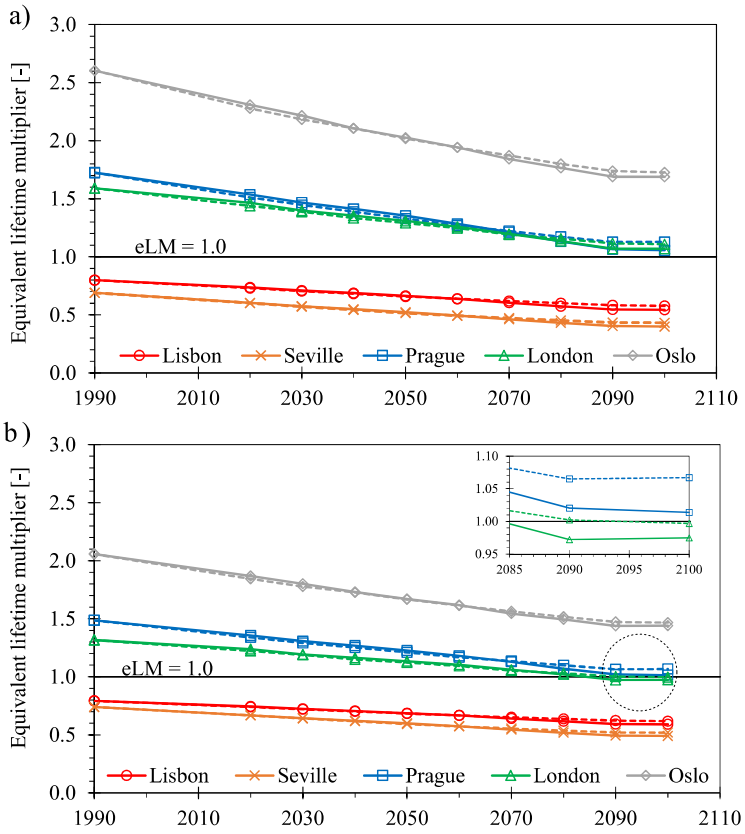

Figure 5.9 – Equivalent lifetime multiplier (eLM) for cellulose (a) and varnish (b) for the five selected climates and for the two IPCC scenarios A1B (dotted line) and A2 (solid line)

In terms of mechanical decay, three types of artefacts were evaluated using the respective method (subchapter 5.2.4.2): sculptures, furniture and panel paintings (in which the mechanical risk was assessed using a different method for the base and pictorial layer). For the carried-out simulations, furniture is not in danger of mechanical decay, either at the present, or in the future. This means that the yield strain is never crossed for this type of object and, therefore, its behaviour is solely elastic. Hence, this type of artefacts is not a limiting factor of the requirements of the indoor climate.

However, the case is different for the base layer of painted panels (Figure 5.10a). Based on the obtained data, the most dangerous climate for these materials is Lisbon, followed by Seville, London, Prague and lastly by Oslo (respectively, the percentage of time wood is under elastic behaviour decreases from ca. 86 to 68 %, 91 to 72%, 94 to 79 %, 99 to 91 % and 100 to 97 % of the year from 1990 to 2100). These ranges of values mean that the wood reaches plastic behaviour and, therefore, cannot revert to its original form. Seville is the one that has the most pronounced decrease of elastic behaviour with a decrease rate

of 0.20 %/year, followed by London with a decrease rate of 0.18 %/year and Lisbon with a decrease rate of 0.17 %/year and lastly by Prague with a decrease rate of 0.07 %/year. The decrease rate of Oslo is almost non-existent, only decreasing at the end of the century.

On the other hand, in terms of the pictorial layer the imposed limit of 14 % is never surpassed for five simulated climates. Hence, this component of the panels paintings is not in danger. The closest value to reach the limit was 12.5 % and it was reached in 2080 for Prague climate and scenario A1B. In addition, sculptures are also not completely safe from mechanical decay. However, the extent to which this type of artefact is in danger is very low for any of the selected type of climate.

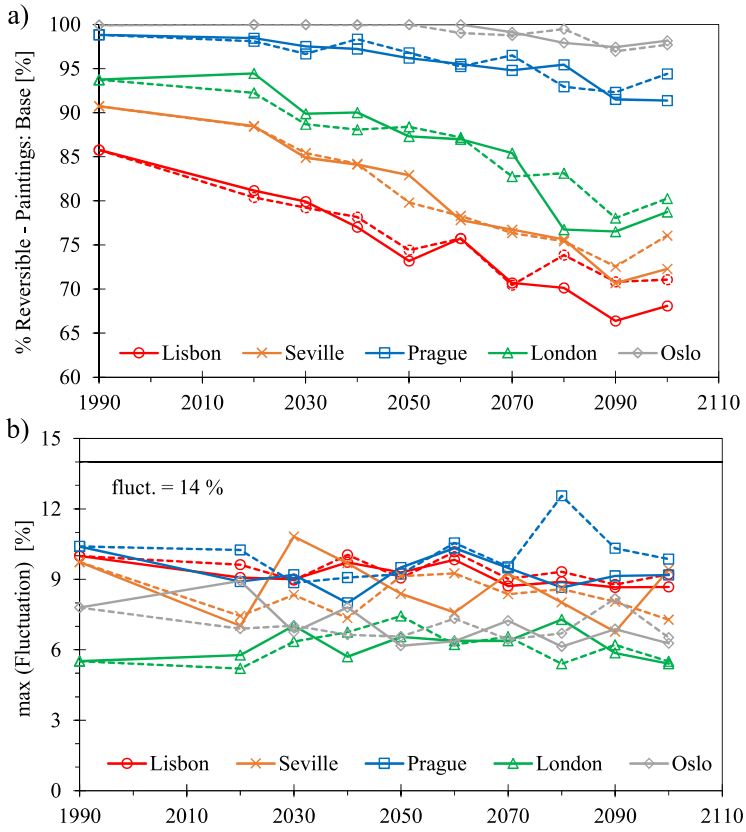

Figure 5.10 – Mechanical risk assessment in the paintings panels: base layer (a) and pictorial layer (b) for the five selected climates and for the two IPCC scenarios A1B (dotted line) and A2 (solid line)

5.4. Conclusions

This chapter aims to quantify how the indoor climate of high thermal inertia buildings is going to change in terms of artefacts' conservation and occupants' thermal comfort considering climate changes. Hence, a whole hygrothermal model of a historic building, which was extensively validate against measured indoor conditions, coupled to climate change weather files is used to obtain the future indoor conditions. Then, the indoor climate is assessed using a thermal comfort model and a risk-based analysis that assess the indoor climate in terms of chemical, biological and mechanical risk. These analyses allow to assess the quality of the future indoor climate. This study was carried out for Mediterranean (i.e. Lisbon and Seville), Humid continental (i.e. Prague and Oslo) and Oceanic climates (i.e. London).

Based on the performed analysis, both IPCC's selected scenarios point to a generalized increase of the indoor temperature as well as the indoor relative humidity, but at different rates depending on the type of climate. Their variability also increases at different rates, except for the indoor temperature of Oslo and the indoor relative humidity of London which decrease. In turn, these variances will lead to a change on the quality of the indoor climate of historic buildings to house artefacts and affect the thermal comfort of the building' occupants.

The use of risk-analysis led to the conclusion that the indoor climate quality to house artefacts worsens. The amount of time that the indoor climates conditions surpass the LIM curve increases in all tested climates. This behaviour is more significant for the Mediterranean climates – e.g. the LIM is surpassed ca 1/5 of the year in Lisbon in 2100. The equivalent lifetime multiplier significantly decreases for the three types of climate – e.g. the decrease varies between 0.3–0.9 for cellulose. In terms of mechanical decay, it was shown that the base layer of painting panels significantly deteriorates for the three types of climate. Sculptures will also be subjected to mechanical deterioration but to a lower extent. On the other hand, a slight increase of the thermal comfort conditions occurs, more evident for Oslo, London and Prague, since the indoor temperature also increases. These findings prove that there is an evident need to adopt appropriate changes in this type of buildings in order to safeguard the artefacts, but at the same time to take into account the requirements imposed by the building's visitors.

The use of a whole-building computational model has a lot of advantages in the study of the indoor climate. For instance, it allows to identify the influence that each parameter has on the building's indoor climate or to test several measures that can improve the quality of indoor climate in terms of, for example, artefacts conservation. However, the simulations take a lot more time than the ones performed in simplified models (e.g. [167]). This is a limitation if the study is to be reproduced for several locations. Additionally, it would also increase this study relevance if other case-studies, for example with a different volume or of different building typology, were included in the study to see if the same conclusions would prevail.

6. THE IMPACT OF CLIMATE CHANGE IN CULTURAL HERITAGE: FROM ENERGY CONSUMPTION TO ARTEFACTS' CONSERVATION AND BUILDING REHABILITATION

This chapter has been partly published in the following reference Coelho, G. B. A., Silva, H. E., & Henriques, F. M. A. Impact of climate change in cultural heritage: from energy consumption to artefacts' conservation and building rehabilitation. *Energy and Buildings*, 224 (2020) https://doi.org/10.1016/j.enbuild.2020.110250

6.1. Introduction

The main aim of buildings that house artefacts is to guarantee their safety, so that future generations may also have access to these objects. However, when addressing artefacts preservation it is necessary to analyse three types of decay, namely [178]: biological, chemical and mechanical, which can be accelerated by the existence of indoor air pollutants [5]. These three types of decay are governed, at different extents, by the indoor temperature and relative humidity, which vary due to several parameters, namely the building envelope, internal gains, climate control systems and outdoor meteorological conditions [5].

As in many other parts of society at the time, the industrial age brought a new beginning to climate control in cultural heritage buildings that house artefacts, such as museums, namely due to the development of air conditioning and humidity control systems. The major appeal of these systems was that they allowed to produce a uniform indoor climate or even a different indoor climate from the outdoor one. However, the setpoints to which many of the museums regulated their climate at the time were not based on concrete evidence that they really safeguarded the collections [171]. It is obvious that the awareness of this limitation led to the increase of studies focussed on the collections' needs on the coming years. In time, this resulted in the creation of standards/guidelines that limit the indoor climate in order to keep the collections safe (e.g. Thomson [264], ASHRAE [5], UNI 10829 [84], EN 15757 [90], among others).

Due to the importance of maintaining historical artefacts safe many standards and guidelines that aim to mitigate the risk of deterioration by limiting the variance of the indoor temperature and relative humidity have been developed over the years. Thomson [264] suggested a guideline that is less stringent than the "magic numbers" (i.e. setpoint of 20 ºC and 50 %RH), but it still based on the variance of the indoor conditions within fixed limits. The guideline divides buildings into two major classes – class 1, which aims to mitigate the deterioration risks with the indoor conditions varying within a more stringent range and it is recommended for major museums, and class 2 that aims to avoid major deterioration risks whilst keeping costs to a minimum [264].

Another important guideline was prepared by ASHRAE [5], which is centred in a five permissible class system in which the strictness in terms of indoor conditions lessens from the first class (class AA) to the last class (class D). In other words, the energy spent so that building complies with the setpoints preconized by the guideline decreases, but at the same time the risks of deterioration increase. In Europe, the standard that deals with the preservation of artefacts is EN 15757 [90]. This standard aims to reduce the mechanical risk induced by the indoor conditions to organic hygroscopic materials by maintaining the historical climate if the conditions are not harmful for the objects. If the climate is harmful, then it recommends the exclusion of the 14 % larger short-term fluctuations [51].

More recently, *Silva and Henriques* [250,252] developed a two-class guideline that aims to mitigate the

risk of deterioration of artefacts housed in historic buildings for temperate climates. This guideline limits the variance of the indoor temperature and relative humidity in terms of seasonal and short-term fluctuations with a more stringent class 1, and a more flexible class 2. This guideline was partially based on the ASHRAE guideline [5] and on standard EN 15757 [90].

In order to have the indoor climate varying within any of these ranges it is necessary that the buildings that house artefacts, such as, museums or galleries, are equipped with large mechanical systems. However, these systems can have a high energy consumption, which consequently leads to a high financial and environment costs. Additionally, due to climate change it is expected that the indoor climate of high inertia historic buildings is going to change in the future, which can result in higher energy consumptions. These changes will be translated in the increase of the free-floating indoor temperature and relative humidity in this type of buildings [128,67], but the magnitude of the changes will vary with the location [129,130,67]. Climate change is greatly due to the emission of large amounts of greenhouse gases into the atmosphere. These emissions are mainly due to anthropogenic activities, such as the use of fossil fuel and land-use changes [196].

Nowadays one of the main challenges for both the scientific community and society in general is to find ways to mitigate the effects of climate change and even mitigate the climate change itself, since it will negatively affect the environment, and consequently, both the human health and the world's economy [284]. Moreover, climate change will also have a negative effect on buildings [284]. According to UNESCO project 22 [288], which studied the effects of climate change in historic buildings, it is expected that the buildings' facades will deteriorate due to thermal stress and freeze-thaw/frost cycles, that the porous materials will suffer physical changes due to rising damp and that the superficial layers will suffer crack, among many other effects described in this document.

The high costs of energy associated with the stringent ranges of indoor temperature and relative humidity preconized by the mentioned standards and guidelines, and the changes that the indoor climate of high inertia historic buildings are going to suffer due to climate change will lead to an increase of the maintenance costs of these buildings, which might present a risk to their continuity. Hence, it is of great importance to study passive rehabilitation measures, active rehabilitation measures or combination of both types to decrease, as much as possible, the energy consumption of these buildings. For instance, Cornaro *et al.* [72] managed to achieve a 38 % reduction of the energy consumption for Villa Mondragone in Italy with the application of a high insulating plaster, while Muñoz-González *et al.* [193] managed to reduce the energy consumption of San Francisco de Asís church by 10–21 % combining active and passive measures.

Hence, this chapter starts by quantifying the energy consumption associated to each of the referred standards and guidelines, as well as the associated financial cost and their future trend. Secondly, four passive retrofit measures that aim to reduce the building's energy consumption are analysed. The retrofit

measures were a 10 cm interior calcium silicate board and an exterior 5 cm thermal plaster for the exterior walls, a 10 cm PUR-foam in-between the ceilings' wood slabs and the replacement of the existing windows with double-glazing windows. These measures have been used in other studies that concern historic buildings and were analysed separately.

A whole-building hygrothermal model of a historic building was used coupled to climate change weather files to obtain the future indoor conditions. This model was extensively validated against the measured indoor conditions [66,68], which were obtained through a long-term and multi-sensor campaign [250]. Since the outdoor climate plays a prominent role in the variance of the indoor climate, three different types of climate were simulated, namely: Mediterranean (Lisbon, Portugal and Seville, Spain), Humid continental (Prague, Czech Republic and Oslo, Norway) and Oceanic (London, United Kingdom).

Furthermore, the current and future indoor conditions were assessed using a risk-based analysis that assesses the risk of biological decay using the *isopleth method* [244], the chemical decay using the *lifetime multiplier* [186] and the mechanical decay in which the method used varies depending on the type of object [178]. This methodology has been used in several other studies since its development (e.g. [128,253,218]). In a word, this chapter aims to quantify how the energy consumption and, consequently, the energy costs will evolve in the future for buildings that house artefacts, but at the same time show that passive rehabilitation measures can be used to mitigate the effects of climate change in the artefacts' preservation. In order to develop this chapter more than 1400 hygrothermal simulations were run in WUFI®Plus [292], which corresponds to more than 1600 hours of simulations.

6.2. Methodology

This subchapter presents the tools that were used to achieve the chapter's aims. It is divided into five subchapters: 6.2.1) presents the selected case-study, the monitoring campaign performed to record the yearly variance of the indoor climate and the subsequent developed hygrothermal model; 6.2.2) presents the passive rehabilitation measures that will be tested; 6.2.3) briefly addresses the outdoor temperature and water-vapour pressure for the selected climates while taking climate change into account; 6.2.4) presents the temperature and relative humidity setpoints for the previously mentioned standards/guidelines; 6.2.5) addresses the past and future trend of the electricity price in some European countries; 6.2.6) presents the risk-based analysis used to assess the indoor conditions.

The term "artefact" refers to the movable cultural heritage definition specified by UNESCO [272], whilst the term "cultural heritage" encompasses both the architectural heritage buildings – i.e. the immovable cultural heritage [272] – and the historic collection – i.e. the movable cultural heritage [272].

6.2.1. Case-study

The case-study is the 13th-century church of St. Cristóvão, in Lisbon, Portugal (Figure 6.1 and Annex G). The church has a volume of ca 5250 m^3 and includes a nave, a sacristy and a mortuary, among other smaller compartments. The building has thick mortared-limestone walls and limestone slabs, which

makes it a good example of a high thermal inertia building and, consequently, representative of historic buildings that house artefacts. The church is not equipped with any climate control system, it is naturally ventilated, and has a ceramic tile roof and wooden frame windows.

The indoor climate of the church was monitored from November 2011 to August 2013 using a multi-sensor grid that included 17 thermocouples type T, a probe RHT2nl of Delta T and two HOBO U12-013 [250]. These sensors guarantee the accuracy limits imposed by the standards concerned with recording the indoor climate in historic buildings [91,92]. The monitoring campaign lasted for over a continuous year and had a recording frequency of 10 minutes, so that the indoor climate of the church was thoroughly characterized [51]. During the same period the outdoor temperature and relative humidity were monitored in the vicinity of the church. This allows to correlate the variance of the indoor climate with the respective variance of the outdoor conditions and, therefore, explain certain hygrothermal behaviours that occur indoors [248]. Further information can be consulted in Ref. [250].

Figure 6.1 – St. Cristóvão church in Lisbon, Portugal

Secondly, the recordings of the monitoring campaign were used to develop and extensively validate a whole-building hygrothermal model of the church in WUFI®Plus [292]. The model's calibration was performed using four statistical indices that compared the error between the simulated and monitoring values for both temperature and water-vapour pressure [66]: the coefficient of determination (R^2 - 0.99 for T and 0.97 for P_v), the coefficient of variation of the root mean square error (CV(RMSE) - 3.2 % for T and 4.4 % for P_v), the normalized mean bias error (NMBE - 2.7 % for T and 3.4 % for P_v) and the goodness of fit (*fit* - 84.8 % for T and 81.7 % for P_v). After the calibration process, the simulated values very accurately overlaid the campaign values [66].

The key parameters of the whole-building hygrothermal model of St. Cristóvão church are presented in Table 6.1 and Table 6.2. The church was only open to the public for mass services, i.e. between 18h00–19h30 from Tuesday to Saturday and between 12h00–13h30 on Sunday, and for one hour prior to each mass service. Further information can be consulted in Ref. [66].

Table 6.1 – Adopted internal gains and ventilation rate for the model of St. Cristóvão church (adapted from Ref. [66])

Lighting	11.7 W/m^2 (30% radiant and 70% convective heat gains)
Person – internal loads	Human activity – 1.3 met Heat load – 126 W (73% for sensible heat and 27% for latent heat) Moisture load – 54 g/h
Ventilation rate	0.4 h^{-1}

Table 6.2 – Hygrothermal properties of the building materials that compose the building envelopes of St. Cristóvão church (adapted from Ref. [66])

Building element	Thickness (m)	S_d-value (m)	U-value (W/m^{2}K)
Walls	0.90	118	1.36
Ceilings	0.24	8.9	1.25
Roof	0.02	0.3	5.26
Doors	0.05	11.2	2.01

6.2.2. Rehabilitation measures

The following four retrofit representative rehabilitation measures will be tested with the goal of decreasing the energy consumption in historic buildings that house artefacts ($U_{walls,\ ref}$ = 1.36 W/m^2.K, $U_{ceilings,\ ref}$ = 1.25 W/m^2.K and $U_{window,\ ref}$ = 5.1 W/m^2.K [66]):

Retrofit 1 – Application of a 10 cm interior insulation system of calcium silicate board to the exterior walls (λ = 0.050 W/m.K [292] and U_{walls} = 0.38 W/m^2.K)

Retrofit 2 – Application of exterior 5 cm thermal plaster to the exterior walls (λ = 0.045 W/m.K [292] and U_{walls} = 0.59 W/m^2.K)

Retrofit 3 – Application of a 10 cm PUR-foam layer in-between the ceilings' wood slabs (λ = 0.025 W/m.K [292] and $U_{ceilings}$ = 0.22 W/m^2.K)

Retrofit 4 – Replacement of the existing window for a double-glazing window with a low emissivity glass (U_w = 1.4 W/m^2.K [263])

These retrofit measures were selected since they have been used with positive outcomes in other studies that concern historic buildings [25,22,190,231,23,72,43,60,193,194] and each case is only representative of a type of retrofit, since the aim of this chapter is not to assess each retrofit measures, but to show the positive effect that their application has on the energy saving potential and in terms of improving the quality of the indoor climate to house historic artefacts. Hence, and though relevant, the materials' properties and respective thickness of the selected retrofit measures will not be further examined.

6.2.3. Outdoor climates

This subchapter is divided into two sections in which the first addresses the current outdoor conditions of the selected climates to perform the hygrothermal simulations using a 1990 weather file, which is henceforth known as reference climate for each climate. The second subchapter addresses how the outdoor conditions of these climates will evolve in the future in accordance with the IPCC scenarios: A1B and A2, from 2020 until 2100 using 10-year weather files.

6.2.3.1. Current weather

The outdoor climate has a very pronounced effect on the indoor climate of historic buildings [67], which means that if the same measure is applied in two different climates the result can be quite different. Hence, to determine how differently each of the selected standards/guidelines behaves in terms of energy consumption throughout Europe three types of climate were tested: Mediterranean (Lisbon and Seville), Humid continental (Prague and Oslo) and Oceanic (London).

Lisbon has mild and rainy winters, and warm and dry summers. For instance, for Lisbon's reference climate, the outdoor temperature varies between 4.5 and 19.4 ºC during winter, and between 12.4 and 37.2 ºC during summer. The annual outdoor temperature average is approximately 16.8 ºC and has an annual precipitation of 753 mm with the major precipitation occurring during winter. On the other hand, during summer Seville reaches higher temperatures than Lisbon (for Seville's reference climate the outdoor temperature varies between 11.6 and 40.1 ºC during summer), but it also has a mild winter like Lisbon's. In terms of precipitation the trend is similar to what was described for Lisbon, but the annual sum is approximately 150 mm smaller than Lisbon's (i.e. 600 mm).

Prague has cold winters and hot summers, and a moderate annual precipitation. For instance, for Prague's reference climate the outdoor temperature varies between -12.4 and 12.1 ºC during winter and between 4.1 and 32.9 ºC during summer. The annual average of the outdoor temperature is ca 8.7 ºC and has an annual precipitation of 521 mm with the major precipitation occurring during summer. On the other hand, Oslo attains lower temperatures than Prague both during winter (temperature varies between -21.9 and 5.5 ºC), as well as during summer (temperature varies between 2.6 and 25.2 ºC) with the annual average being 3.9 ºC. The major rainfalls in Oslo occur during summer in which the annual sum is approximately 338 mm higher than Prague's (i.e. 859 mm).

Finally, London also has a cold winter but not as severe as Prague's (temperature varies between -7.8 and 13.4 ºC), a warm summer between Prague's and Oslo's (the temperature varies between 3.6 and 27 ºC) and it rains moderately all year long with the annual sum being 751 mm. These values correspond to London's reference climate.

6.2.3.2. Climate change

The effects of climate change are multiple and will occur at several levels, namely in terms of the environment, the global economy, which in turn will affect the local economy, and the human health [284]. Additionally, it has been reported that if proper measures are not applied, climate change will also have a significant effect on the envelope of historic buildings [288,18], which in turn will affect the indoor climate and might accelerate the deterioration processes of the housed artefacts.

Hence, to ensure the continuity of artefacts it is of the utmost importance to study climate change. Over the years, the *Intergovernmental Panel on Climate Change* (IPCC) has developed several scenarios that translate how the climate might evolve in the future based on different assumptions which will mainly reflect on the amount of greenhouse gases (GHG) emitted into the atmosphere, namely CO_2 [196].

In this chapter, two IPCC scenarios from the Fourth Assessment Report (AR4) were used: scenario *A1B* (mid-radiative forcing scenario) and scenario *A2* (high-radiative forcing scenario), which are based on different assumptions in how the world will evolve [302]. Both scenarios have been used in European projects that deal with historic buildings, namely *Noah's Ark project* [229] used scenario A2 and *Climate for culture* [172] used scenario A1B.

Whilst scenario A1B rests on assumptions that will lead to an increase of the CO_2 emissions until 2050 but its steeply decrease until 2100, scenario A2 is based on a continuous increase of the CO_2 emissions throughout the 21st-century [196]. These assumptions will obviously cause the outdoor conditions to evolve differently. The outdoor temperature in Lisbon is expected to increase for both selected IPCC scenarios with the increase varying approximately 0.6–3.0 K for the annual average between 2020–2100 in relation to 1990 (Figure 6.2a). However, the difference between both scenarios is only substantial from 2060 onward in which the outdoor temperature in the A2 scenario is almost 0.5 K higher than for A1B scenario. The same can be said for Seville, however, it is also visible that the increase of outdoor temperature is higher than in Lisbon's, i.e. increase of 1.0–4.2 K from 2020-2100 (Figure 6.2a).

In both climates the water-vapour pressure increases with the A2 scenario reaching higher values from 2060 onward, but the increase is more significant for Seville than for Lisbon (Figure 6.2b). Whilst the water-vapour pressure increases between 103–460 Pa from 2020 to 2100 for Seville, it increases from 62–305 Pa for Lisbon. In conclusion, the outdoor temperature and water-vapour pressure increase in both Mediterranean climates, but Seville has a higher increase for both conditions.

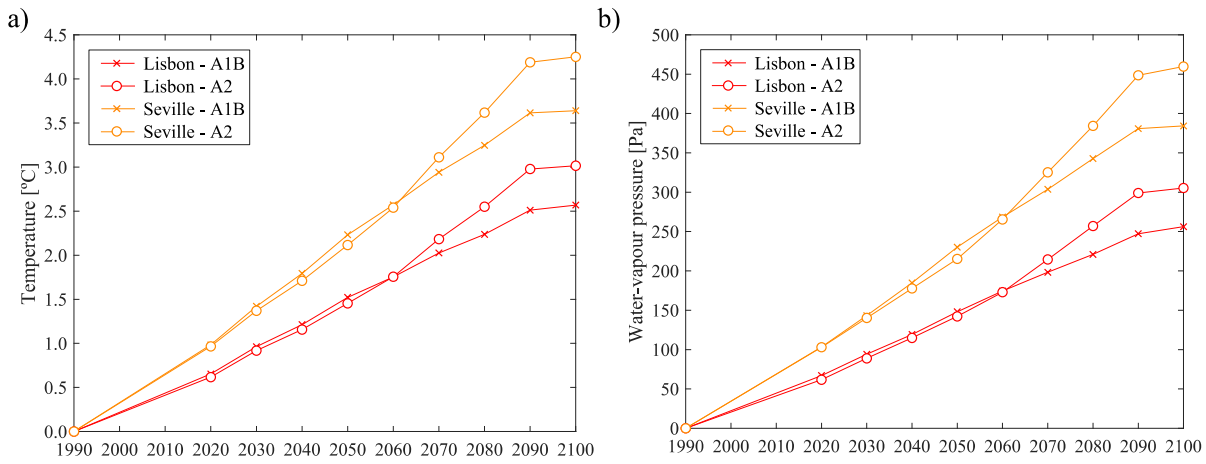

Figure 6.2 – Difference of the annual average of the outdoor temperature (a) and water-vapour pressure (b) for Lisbon (red) and Seville (orange) in relation to the 1990-value for scenario A1B and A2

The outdoor temperature in Prague increases substantially for both IPCC scenarios (Figure 6.3a). The increase of temperature varies between 1.0–3.8 K and the highest value is attained in 2100 for scenario A2, i.e. more 0.4 K than scenario A1B. In terms of water-vapour pressure it is also visible an increase trend, which ranges from 58–264 Pa with the highest value being achieved in 2100 for scenario A2, i.e. ca 40 Pa higher than scenario A1B (Figure 6.3b). A similar behaviour occurs in Oslo in terms of temperature but reaching higher values, since the temperature increases between 1.2–4.2 K (Figure 6.3a). In terms of water-vapour the increase is less substantial than Prague's, i.e. varies between 50–206 Pa (Figure 6.3b).

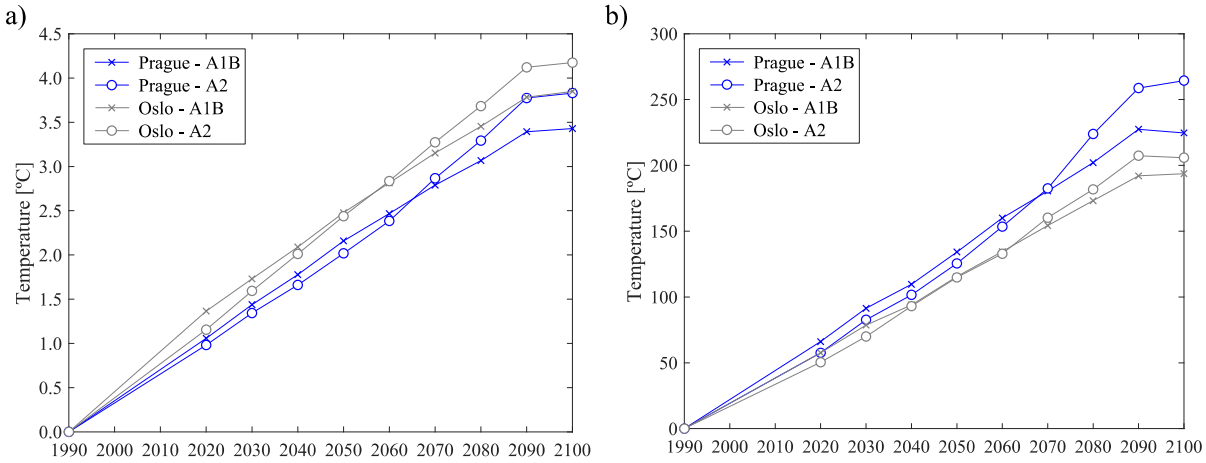

Figure 6.3 – Difference of the annual average of the outdoor temperature (a), and water-vapour pressure (b) for Prague (blue) and Oslo (grey) in relation to the 1990-value for scenario A1B and A2

Finally, both the outdoor temperature and the water-vapour pressure in London increase 0.7–3.0 K and 41–220 Pa until 2100, respectively (Figure 6.4). Overall, there is an increase trend in terms of outdoor temperature and water-vapour pressure for the five selected climates and for both IPCC scenarios, with the highest increase being reached in the end of the century by scenario A2. The difference between both IPCC scenarios is only substantial from 2070 onward.

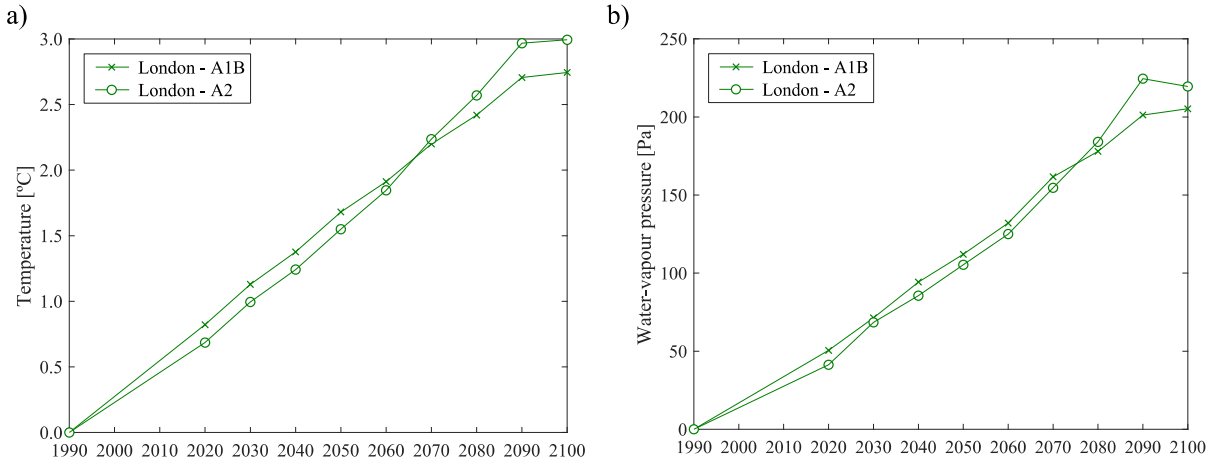

Figure 6.4 – Difference of the annual average of the outdoor temperature and water-vapour pressure for London (a and b, respectively) in relation to the 1990-value for scenario A1B and A2

6.2.4. Indoor climate control

The setpoints that the HVAC system must ensure depend on each standard/guideline (Table 6.3). Due to the large number of classes that some of these standards/guidelines have, it was decided to choose only one class for each, i.e. the most demanding in terms of indoor conditions. Since the case-study is a high thermal inertia building, ASHRAE's recommended class is either B, C or D, and since its classes are organized in decreasing order of strictness, B-class was chosen.

Table 6.3 – Temperature and relative humidity setpoints for each of the selected standard/guidelines

Standard Guideline	Temperature (ºC)	Relative humidity (%)	Comments
Thomson [264]	Winter: 19 ± 1ºC Summer: 24 ± 1ºC	Range: 50 or 55 ± 5 %	Class 1 – Major museums
ASHRAE [5]	Setpoint: 15–25 ºC Short fluctuations: ± 5 K Seasonal cycle: Up 10 K not above 30 ºC	Setpoint: 50 % or historic annual average Short fluctuations: ± 10 %RH Seasonal cycle: Up 10 %RH and down 10 %RH	Class B – Heavy masonry or composite walls with plaster
FCT-UNL [250]	Setpoint: historic annual average Short fluctuations: -5º/ +95º percentiles Seasonal cycle: -10º/ +90º percentiles Extra limits: $\lvert T - \bar{T} \rvert$ up to 10ºC not above 30ºC	Setpoint: historic annual average Short fluctuations: -5º/ +95º percentiles Seasonal cycle: -10º/ +90º percentiles Extra limits: $\lvert RH - \overline{RH} \rvert \leq 15\%$ and $RH_{max} \leq 75\%$	Class 1 – Low risk of mechanical damage and biological attack.

The range of values within which the indoor climate can vary according to ASHRAE class B and FCT-UNL class 1 were determined using the methodology presented by Kramer *et al.* [159] for each year,

namely: 1)- simulate a free-floating indoor climate, 2)- determine the respective temperature setpoints, 3)- simulate the indoor climate restrained by the temperature setpoints, 4)- determine the respective relative humidity setpoints, 5)- simulate the indoor climate restrained by temperature and relative humidity setpoints. Hence, the dynamic methodologies simulations were run three times. The analysed energy consumption for these cases correspond to the last simulation. This 5-step methodology allowed to account for the acclimatization behaviour of hygroscopic materials [84,90,51].

Since the aim of this chapter is to analyse the energy consumption associated to each of the standards and guidelines that limit the artefacts deterioration, rather than develop or optimize the HVAC system, the authors opted for an ideal HVAC system.

6.2.5. Energy price trend

The electricity prices in Europe have been increasing over the years. For example, the average electricity price for the European Union increased from 0.1805 €/kWh in 2007 to 0.2435 €/kWh in 2019 for band-IA [102]. This corresponds to an increase of approximately 0.063 €/kWh over a period of 13 years. Since the aim of this chapter is buildings that house artefacts, which evidently are non-household, they are subjected to industrial energy prices according to Ref. [103].

Hence, the price of energy varies according to the amount of energy consumed by the building. However, due to the liberalisation of the energy markets, the Eurostat energy price system was reorganized in 2007 from a 9 to a 7-level classification system that only takes the annual consumption of the building into account – *band-IA* (annual consumption below 20 MWh), *band-IB* (annual consumption between 20 and 500 MWh), *band-IC* (annual consumption between 500 and 2,000 MWh), *band ID* (annual consumption between 2,000 and 20,000 MWh), *band-IE* (annual consumption between 20,000 and 70,000 MWh), *band-IF* (annual consumption between 70,000 and 150,000 MWh) and *band-IG* (annual consumption higher than 150,000 MWh) [103].

This system was used to determine the overall cost of maintaining the indoor climate according to each of the selected standards/guidelines. Figure 6.5 presents the energy prices for all bands in each of the five selected climates between 2007-2019.

Additionally, it is expected that the electricity price will increase until 2030 and only after will it decrease (Table 6.4). From the selected countries only in Czech Republic will the electricity price not decrease after 2030. These annual changes for the electricity prices were taken from the "EU Reference Scenario 2016: Energy, transport and GHG emissions Trends to 2050" [79], which unfortunately does not include the annual changes for Norway. Hence, the electricity price between 2020-2100 was determined using a constant annual change for Norway depending on the annual consumption, which was based on the historical values of 2007 and 2019 [102] and varied between 0.1–0.2 % per year. Additionally, and since there is no annual change for the period 2050-2100, the same percentage as the one for the 2030-50 period was adopted for Czech republic, Portugal, Spain and the United Kingdom

(Table 6.4).

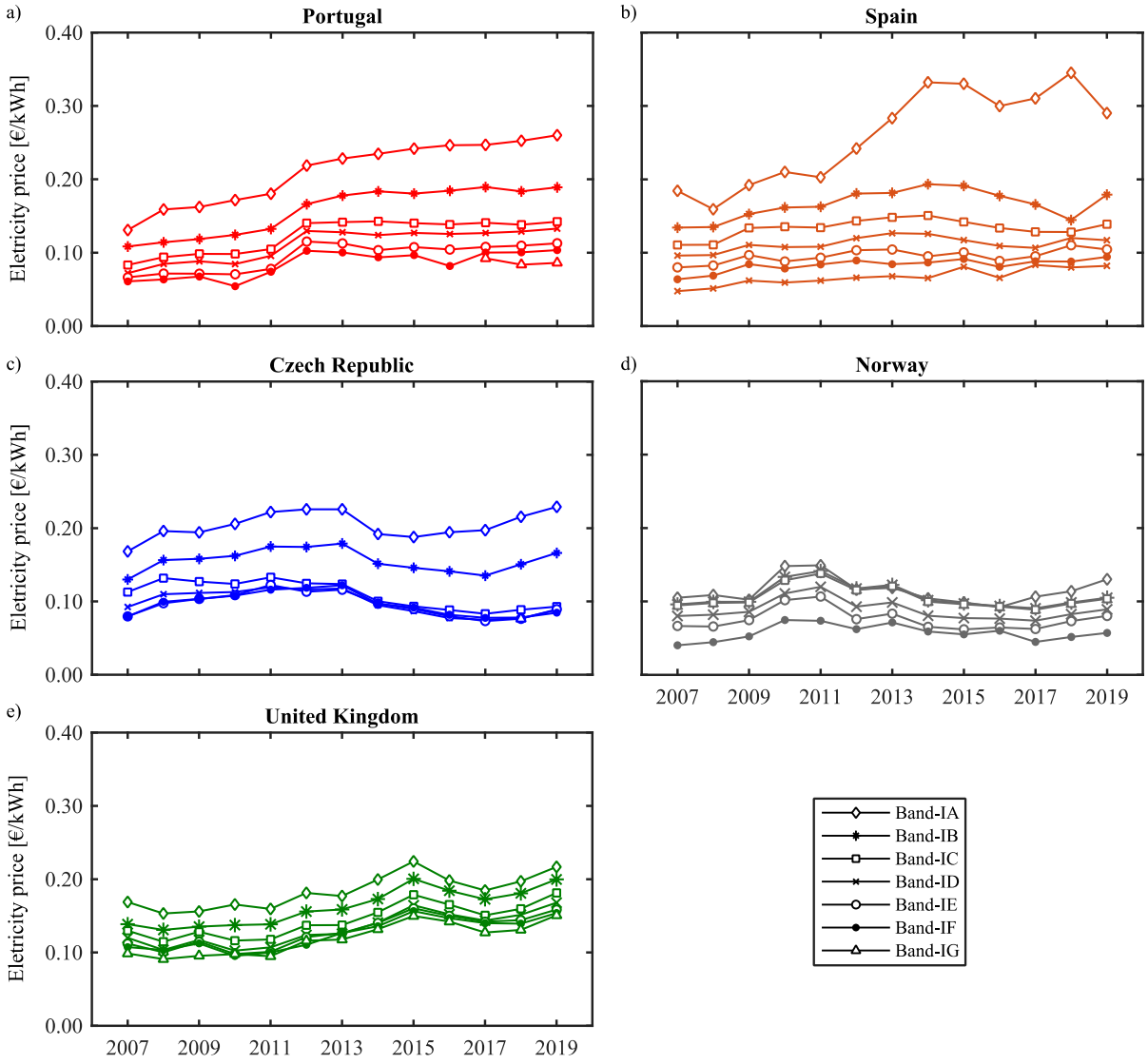

Figure 6.5 – Electricity price (€/kWh) for industrial users that includes all taxes and levies between 2007 and 2019 [102] for Portugal (red), Spain (orange), Czech Republic (blue), Norway (grey) and United Kingdom (green)

Table 6.4 – Annual change (%) of the electricity price for Czech Republic, Portugal, Spain and United Kingdom between 2010-2050 [79]

	Czech Republic	Portugal	Spain	United Kingdom
2010-20	-0.7	3.0	1.5	2.8
2020-30	0.2	0.6	-0.3	0.6
2030-50	0.1	-0.2	-0.2	-0.3

6.2.6. Risk-based analysis

A methodology that assesses the indoor conditions, namely the indoor temperature and relative humidity, in terms of artefacts conservation was developed by Martens [178], evaluating the risk of biological, chemical and mechanical decay using several methods. The risk of biological decay is

assessed using the *isopleth method* [244]. This method was developed by *Sedlbaeur* for his PhD thesis and determines the germination conditions depending on the temperature, the relative humidity and the substrate type. Mould grows if the *Lowest Isopleth for Mould* curve (LIM) is surpassed. The biological decay was analysed in terms of the amount of time the LIM curve is surpassed.

The risk of chemical decay is assessed using the *lifetime multiplier* concept [186]. This concept, which was developed by *Michalski* [186], basically determines the amount of time the material stays usable when compared to standard conditions – 20 ºC for temperature and 50 % for relative humidity. Usually, two different materials are analysed since their activation energy differ [178]: 70 kJ/mol for varnish, and 100 kJ/mol for cellulose. More recently, *Silva and Henriques* [251] introduced the *equivalent lifetime multiplier*, a concept which computes a representative value for the whole considered period.

$$eLM = 1 \Big/ \left(\frac{1}{n} \cdot \sum_{x=1}^{n} \left(\frac{1}{\left(\frac{50\%}{RH_x}\right)^{1.3} \cdot e^{\frac{E_a}{R}\left(\frac{1}{T_x+273.15}-\frac{1}{293.15}\right)}} \right) \right) \tag{6.1}$$

where *eLM* is the equivalent Lifetime Multiplier (-), *n* is the number of time steps within the considered period (-), RH_x is the surface relative humidity at instant x (%), E_a is the activation energy of the material (kJ/mol), *R* is the gas constant (8.314 J/Kmol) and T_x is the temperature at instant x (ºC).

Lastly, the method used to assess the risk of mechanical decay varies according to the type of object: a) wood sculpture – uses an updated version of the Jakiela et al. method [144], b) wood furniture – uses an updated version of the Bratasz *et al.* method [44], c) wood substrate of the panel paintings – uses an updated version of the Mechlenburg *et al.* method [181], and d) pictoral layer of the panel paintings – uses an updated version of the Bratasz *et al.* method [45]. These methods determine if the yield strain of the materials is surpassed (Figure 2.2). Since the performed analysis includes a great number of years, the mechanical decay was analysed in terms of the amount of time the objects are under reversible conditions in each year [67].

6.3. Results and discussion

This subchapter starts by addressing the amount of energy necessary to guarantee the indoor conditions established by the three selected standards/guidelines. Furthermore, future trends and the respective financial cost are also assessed. Lastly, the energy saving potential of a set of passive retrofit measures is assessed, as well as its effect on the artefacts' conservation metrics in historic buildings.

In colder climates it is usual that the indoor climate of historic buildings that house artefacts is heated to ensure the thermal comfort of visitors [108,109,155,230]. However, due to the fact that the minimum temperature limit varies considerably from case- to case it was decided to choose a minimum temperature of 13 ºC for the methodologies that do not preconize temperature limits to guarantee that there is no embrittlement of the artefacts [182].

In order to develop this chapter more than 1400 simulations were run in WUFI®Plus, which correspond to more than 1600 hours of simulation on a computer with an Intel(R) Core(TM) i5-8500 CPU @ 3.00 GHz, 16 GB of RAM and a 64-bit operating system. However, to make this study time reasonable, the simulations were subdivided into 20 computers equipped with an Intel(R) Core(TM) i5-650 CPU @ 3.20 GHz, 4 GB of RAM and a 64-bit operating system, which drastically reduced the overall time.

6.3.1. Energy expenditure and financial cost evolution

The energy spent to ensure a proper indoor climate for artefacts preservation will greatly depend on the adopted methodology (Figure 6.6). Furthermore, the effect of climate change on energy consumption will also depend on the climate, since it can either be responsible for its increase or decrease. The following subchapter first addresses the constant value methodology suggested by Gary Thomson (class 1) and then the dynamic methodologies – namely ASHRAE class B and FCT-UNL class 1. In addition, the calculated heating, cooling, humidification and dehumidification energy demands are presented in tables at the annex section (Annex I).

By limiting the indoor climate according to Thomson's methodology, it is visible that climate change is responsible for an energy saving for all selected climates except for Seville (Figure 6.6a). The decrease of energy consumption in Prague, Oslo and London is easily understood by the fact that in these climates the HVAC needs are mostly heating, which correspond to 93–96 % of the total consumed energy (Table I.1), since the free-floating indoor temperature will be very often below the 18 ºC limit. Moreover, since climate change is responsible for the increase of the free-floating indoor temperature, this will lead to energy saving. The greatest savings at the end of the century correspond to scenario A2 (Figure 6.6a), since the free-floating indoor temperature reaches higher values for this IPCC scenario [67].

On the other hand, Lisbon is an interesting case, because climate change is also responsible for an energy saving, but more substantially for scenario A1B. This occurs because the need to heat the room will decrease (Table I.1). For instance, the number of hours that the HVAC system is operating to guarantee the 18 ºC-limit decreases 25% between 1990–2100 for scenario A1B. However, the free-floating indoor temperature will increase more for scenario A2 than for scenario A1B [67], which means that the upper limit will be overcome for a larger period of time. For instance, the number of hours that the HVAC system has to guarantee the 25 ºC-limit when compared to the reference climate is 6 and 8 times higher for scenario A1B and A2, respectively. Hence, the HVAC system has to decrease the free-floating indoor temperature to comply with Thomson's methodology, thus increasing the cooling needs (Table I.1) and, consequently, increasing the total energy consumption. The cooling needs increase from 0.4 to 6.8 MWh between 1990 and 2100 for scenario A2 (Table I.1). The dehumidifying needs are also responsible for a substantial part of the total energy consumption (ranging between 7-25%) due to the increase of the indoor water-vapour pressure [67].

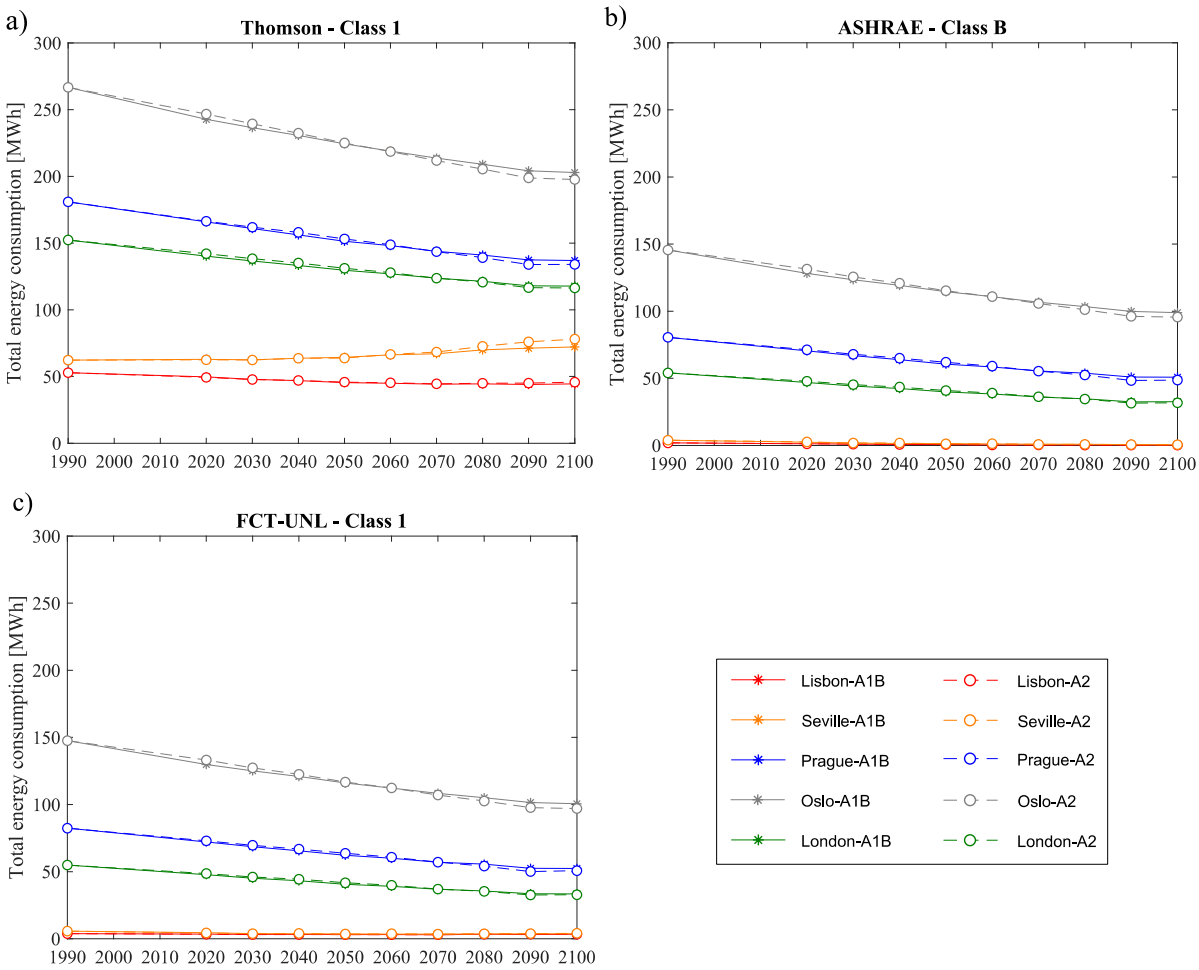

Figure 6.6 – Assessment of the energy consumption to guarantee the indoor conditions according to Thomson class 1 (a), ASHRAE class B (b) and FCT-UNL class 1 (c) for the five selected climate and the two IPCC scenarios (A1B and A2)

Finally, Seville is the only one of the selected climates in which the energy consumption increases with time (Figure 6.6a). Seville's indoor climate is similar to Lisbon's, however, since its free-floating indoor temperature is higher than Lisbon's and because climate change increases the free-floating indoor temperature, this will lead to the overcome of the 25 ºC-limit much more often than in Lisbon (Figure 6.7). Thus, increasing the cooling needs substantially (Table I.1), which goes from corresponding to 12 % of the total energy needs in 1990 to 43 % in 2100 for scenario A2, i.e. 10 % higher than heating needs for that year. This increase of the cooling needs will overshadow the decrease of heating needs (Table I.1), thus being responsible for the increase of the total energy consumption for Seville, while in the other climates the consumption decreases.

Nevertheless, the energy consumption associated to each of these climates is still very significant, and this will lead to great financial costs (Table 6.5). Prague has the highest overall cost to maintain the indoor conditions suggested by Thomson, although it does not correspond to the highest energy consumption (Figure 6.6a). This is due to the fact that currently energy costs more in Prague than in Oslo and it is expected to remain so. The overall cost of energy in Prague is closely followed by London's and Oslo's, but the selected Mediterranean climates (i.e. Seville and Lisbon) present a much

lower overall energy cost.

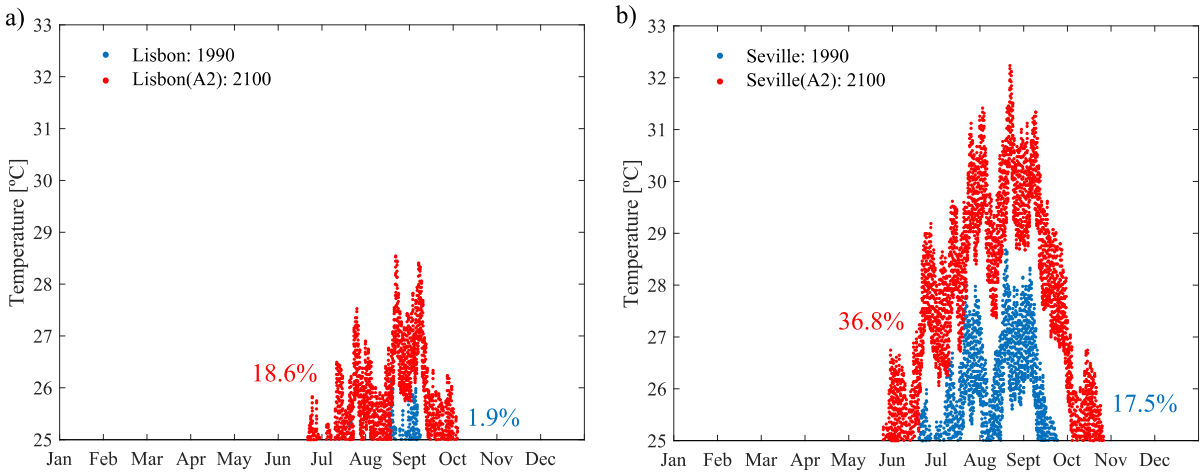

Figure 6.7 – Free-floating indoor temperature higher than the 25 ºC-limit for Lisbon (a) and Seville (b) in 1990 and 2100 (scenario A2), and respective percentage of the year that the 25 ºC-limit is surpassed

Both selected dynamic methodologies have a very similar energy consumption trend, i.e. the energy consumption decreases for all selected climates with the Mediterranean climates consuming a relatively smaller amount of energy (Figure 6.6b for ASHRAE and Figure 6.6c for FCT-UNT). Nonetheless, FCT-UNL methodology attains higher overall costs than ASHRAE's, which is more significantly for the Mediterranean climates (Table 6.5), since it preconizes a more stringent indoor climate range (Table 6.3).

The energy consumption necessary to limit the indoor climate according to these two methodologies is almost non-existent for the selected Mediterranean climates, i.e. Lisbon and Seville, due to their flexible ranges. For example, the annual consumption for Lisbon is 1.9 MWh in 1990 for the ASHRAE methodology, mainly heating needs, and tends to decrease with climate change (Table I.2), since the free-floating indoor temperature will increase. The same behaviour is observed for Seville although the energy spent to ensure an indoor climate according to ASHRAE class B guideline is slightly higher, e.g. the annual consumption for Seville in 1990 is 3.9 MWh (Table I.2). Whilst in terms of the FCT-UNL methodology the value for Lisbon in 1990 is 3.8 MWh and 5.7 MWh for Seville with the tendency to decrease on the subsequent years, but slightly increasing 2070-onwards until they reach respectively 3.4 MWh and 4.1 MWh for scenario A2 in 2100 (Table I.3).

On the other hand, it is also easily understandable that the energy consumption in Prague, Oslo and London decreases substantially, since the key factor for energy consumption in this type of climates is to guarantee the minimum indoor temperature. Since climate change will increase the indoor free-floating temperature, then it is evident that energy consumption will decrease. For example, the energy consumption for Oslo between 1990 and 2100 for scenario A2 decreases approximately 34 % for the ASHRAE methodology, i.e. from an energy consumption of ca 146 to 96 MWh (Table I.2), and 34 % for the FCT-UNL methodology, i.e. from a consumption of ca 148 to 97 MWh (Table I.3).

In terms of overall cost to guarantee the indoor climate according to ASHRAE Class B and FCT-UNL Class 1 it is obvious that for Mediterranean climates the cost is very small with climate change being responsible for its decrease, but for the other three climates the costs are much more substantial with Oslo having the highest cost, followed by Prague and then London (Table 6.5).

Table 6.5 – Overall energy cost per square meter between 2020-2100 for each of the five selected climates and the change induced by climate change in the overall energy cost (in percentage). ↓ green – means decrease of the overall energy consumption and ↑ red – means increase

	Lisbon		Seville		Prague		Oslo		London	
	A1B	A2	A1B	A2	A1B	A2	A1B	A2	A1B	A2
Thomson class 1	2768 €/m²	2791 €/m²	3503 €/m²	3579 €/m²	8039 €/m²	8022 €/m²	7491 €/m²	7462 €/m²	7872 €/m²	7905 €/m²
	↓ 13.4 %	↓ 12.7 %	↑ 6.8 %	↑ 9.1 %	↓ 17.8 %	↓ 18.0 %	↓ 17.5 %	↓ 17.8 %	↓ 16.2 %	↓ 15.8 %
ASHRAE class B	48 €/m²	46 €/m²	106 €/m²	112 €/m²	3180 €/m²	3169 €/m²	3795 €/m²	3785 €/m²	2389 €/m²	2411 €/m²
	↓ 69.5 %	↓ 71 %	↓ 68.3 %	↓ 66.7 %	↓ 26.9 %	↓ 27.2 %	↓ 23.4 %	↓ 23.6 %	↓ 28.3 %	↓ 27.6 %
FCT/UNL class 1	267 €/m²	268 €/m²	321 €/m²	329 €/m²	3266 €/m²	3264 €/m²	3850 €/m²	3838 €/m²	2440 €/m²	2463 €/m²
	↓ 16.7 %	↓ 16.5 %	↓ 34.3 %	↓ 32.7 %	↓ 26.7 %	↓ 26.7 %	↓ 23.3 %	↓ 23.6 %	↓ 27.9 %	↓ 27.2 %

6.3.2. Passive rehabilitation measures

Taking the previously obtained results for the tested standards/guidelines into account (Table 6.5), it is visible that there is a need to decrease the energy consumption if the aim is to substantially decrease the GHG emissions, which are directly related to energy consumption [196]. This behaviour is more substantial for the constant valued standards/guidelines, such as Thomson's. Obviously, if a dynamic methodology is chosen (e.g. FCT-UNL), the energy consumption decreases considerably (Figure 6.6). Moreover, this energy saving can be heightened if a less stringent indoor climate methodology is combined with a proper set of passive retrofit measures.

Hence, four retrofit measures were tested to determine their energy saving potential (see subchapter 6.2.2). The indoor climate was limited according to a constant and a dynamic methodology to determine to which extent the energy saving potential would differ. Additionally, the simulations were run for the two most demanding climates of each climate type: Seville and Oslo.

6.3.2.1. Energy saving potential

Table 6.6 presents the energy consumption of the four retrofit measures for Seville and Oslo, and the respective saving potential, which is calculated based on the correspondent reference case, i.e. the case-study that does not have any retrofit measure. Although the energy saving potential for the retrofit measures in the Mediterranean climates is in the same range of values as the ones described in Table 6.6, its overall energy saving is small (see subchapter 6.3.1). Therefore, it was discarded from the analysis performed in this subchapter.

Based on this table it is clear that the four selected retrofit measures are responsible for a reasonable energy saving. Furthermore, it is also clear that both indoor climate limiting methodologies attain close energy saving potentials, although evidently Thomson attains much higher consumptions in both climates, since it is a constant value methodology with a much stringent indoor temperature/relative humidity range than those obtained with the FCT-UNL methodology (subchapter 6.2.4).

The application of an interior insulation system (R1) reaches the highest energy saving potential – between ca 20 and 32 %, followed by the application of an exterior thermal plaster (R2) – between ca 16 and 20 %, and then by the application of an insulation foam in the ceilings of the case-study (R3) – between ca 13 and 20 %. The replacement of the windows (R4) has the lowest energy saving potential – i.e. between ca 4 and 6 % – due to the low window/wall ratio of the case-study [251].

Nonetheless, the obtained values demonstrate that a less stringent climate limiting methodology decreases the energy consumption considerably, but this effect can be heightened if an individual or a set of passive retrofit measures is applied to the building. However, the selected passive retrofit measures should take into account the special requirements of both historic buildings, since insufficient studied retrofit measures can lead to irrecuperable damages [224], and the artefacts housed on those buildings, which need that the indoor conditions vary within certain values for preservation purposes [5].

Table 6.6 – Total energy consumption (in MWh/m^2) and energy saving potential (in percentage) between 2020-2100 for Seville and Oslo for the four retrofit measures: ↓ green – means decrease and ↑ red – means increase of the energy consumption compared to the reference case

	Total energy consumption (MWh/m^2)					
	Seville – Thomson		Oslo –Thomson		Oslo – FCT-UNL	
	A1B	A2	A1B	A2	A1B	A2
Reference	21.0	21.5	69.3	69.1	35.7	35.5
Retrofit #1	16.8 (↓ 20.8%)	17.1 (↓ 20.2%)	51.4 (↓ 25.8%)	51.3 (↓ 25.8%)	24.2 (↓ 32.2%)	24.1 (↓ 32.2%)
Retrofit #2	18.1 (↓ 16.7%)	18.5 (↓ 16.7%)	58.3 (↓ 16.0%)	58.1 (↓ 16.0%)	28.7 (↓ 19.5%)	28.6 (↓ 19.6%)
Retrofit #3	18.2 (↓ 13.5%)	18.6 (↓ 13.3%)	58.3 (↓ 15.9%)	58.1 (↓ 15.9%)	28.7 (↓ 19.5%)	28.6 (↓ 19.5%)
Retrofit #4	20.1 (↓ 4.4%)	20.6 (↓ 4.4%)	66.1 (↓ 4.6%)	65.9 (↓ 4.6%)	33.6 (↓ 5.8%)	33.5 (↓ 5.8%)

6.3.2.2. Risk-based analysis

The effect of these retrofit measures in the artefacts' conservation metrics was also assessed using the risk-based analysis presented in subchapter 6.2.6. Note that all figures presented in this subchapter have, as reference, a case without any retrofit measure but with the indoor climate limited by the corresponding standard/guideline, which are either named Ref-A1B and Ref-A2 depending on the IPCC scenario. This

reference allows to determine the effect that applying a certain rehabilitation measure has on the indoor climate of the case-study.

It was observed that the risk of *biological decay* for Thomson is non-existent for both climates (Figure 6.8a), since the recommended temperature and relative humidity setpoints do not surpass the LIM curve. For the temperature range preconized by Thomson – i.e. 18 to 25 ºC, the LIM curve varies between 80.5 and 79.6 %RH. Since the highest allowed relative humidity in Thomson's methodology is 60 % (Table 6.3), then it is clear that for this methodology the LIM curve is never surpassed.

The risk of *biological decay* is also non-existent for the FCT-UNL methodology. Although the preconized temperature ranges vary with the historical climate, the first class of this methodology limits superiorly the relative humidity (Table 6.3). Since the maximum admissible value is 75 %, the LIM is never surpassed because its minimum value is approximately 79.2 %RH for 30 ºC. This is the reason why Oslo does not have nor will it ever have a risk of biological decay for the adopted climate control strategy, which was also shown for free-floating conditions [67]; and why Seville, which substantially and gradually surpassed the LIM curve for free-floating conditions [67], now that is limited by the FCT-UNL methodology, does not show risks of biological decay (Figure 6.8b).

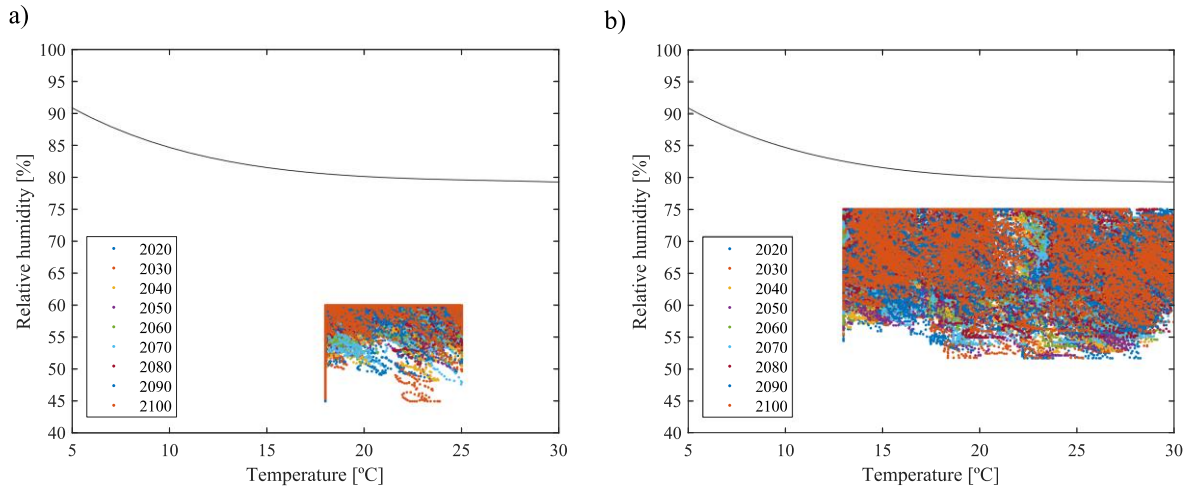

Figure 6.8 – Spore germination for the reference case of Seville between 2020 and 2100 for scenario A2 for Thomson's methodology (a) and for FCT-UNL methodology (b)

It is expected that the risk of chemical decay increases over the years for both IPCC scenarios [67], with the highest risks being reached at the end of the century by scenario A2. On the other hand, the application of retrofit measures to this kind of buildings can have two different effects, which are greatly dependent on the type of the outdoor climate. Whilst for Seville the application of the retrofit measures improves the quality of the indoor climate (Figure 6.9a and b), for Oslo it has the opposite effect, i.e. it decreases the quality of the indoor climate to preserve artefacts that are susceptible to chemical decay (Figure 6.10). In Seville, the application of the retrofit measures improves the quality of the indoor climate because they are able to reduce the increase of the free-floating temperature that occurs mainly

in summer significantly, which is the season that mainly limits the Mediterranean climates. This lowering of the indoor temperature is beneficial to avoid chemical decay, because chemical processes are slowed by lower temperatures [178]. On the other hand, in Oslo the retrofit measures are responsible for an overall increase of indoor free-floating temperature, but more significant during the spring and summer seasons. This higher temperature level will increase the risk of chemical decay [178].

In addition, the best performing retrofit measure for Seville is the application of the interior insulation system – R1 (Figure 6.9), followed by the application of the exterior thermal plaster – R2. The application of the PUR-foam layer in-between the ceilings' wood slabs (R3) or the replacement of the existing window (R4) lead to a small improvement of the indoor conditions in terms of chemical risk, although a slightly more significant for the FCT-UNL methodology (e.g. Figure 6.9a and c). These observations show that the performance of each retrofit in terms of decreasing the risk of chemical decay is slightly affected by the methodology chosen to control climate.

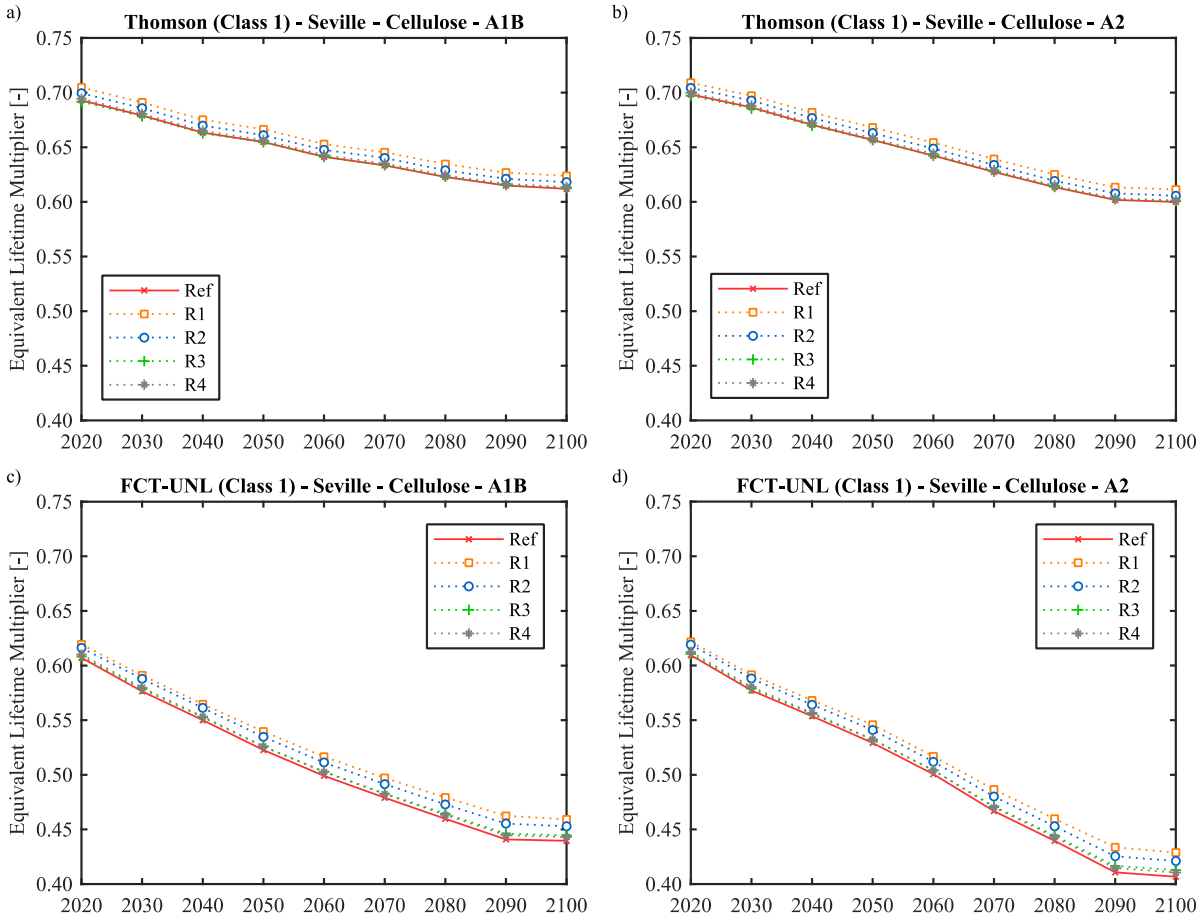

Figure 6.9 – Equivalent lifetime multiplier for the reference case and retrofits #1–4 following Thomson' methodology for IPCC scenario A1B (a) and A2 (b), and following FCT-UNL methodology for IPCC scenario A1B (c) and A2 (d) between 2020-2100 for cellulose in Seville climate

Furthermore, it is also observable that whilst the Thomson methodology is responsible for a significant increase of the risk of chemical decay, the FCT-UNT methodology manages to maintain the same level of risk if the indoor climate was already appropriate to preserve artefacts susceptible to chemical decay.

This occurs, for example, for Oslo (Figure 6.10), whose free-floating conditions were already deemed appropriate to preserve artefacts susceptible to chemical decay [67]. This particularity of the FCT-UNT methodology and other dynamic methodologies (such as, ASHRAE [5] and EN 15757 [90]) is due to the fact that they are based on the acclimatization concept, which allows to obtain an indoor climate adequate for the preservation of the artefacts based on the historical climate. Note that since the previously described behaviours also occur for varnish, it was decided to leave it out so as not to duplicate the same analysis.

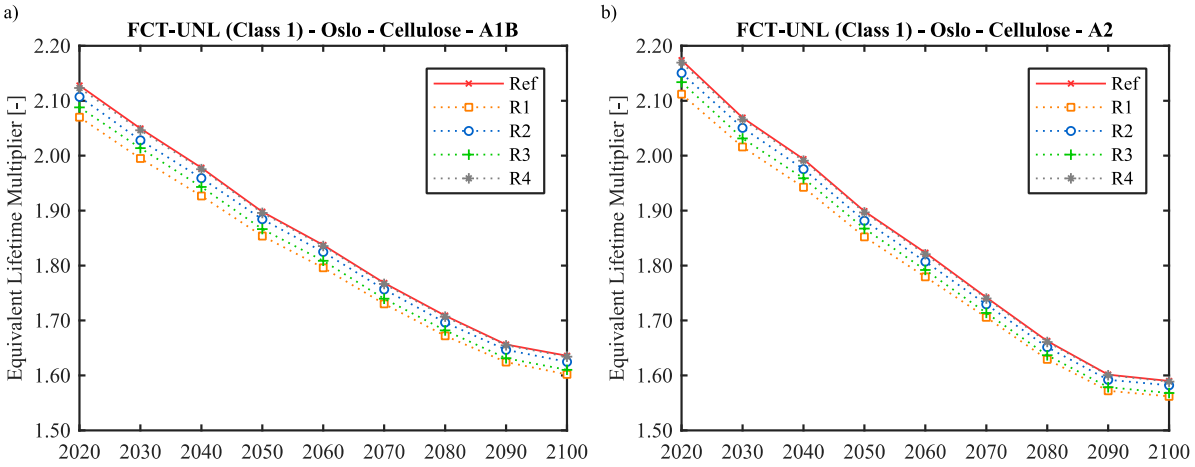

Figure 6.10 – Equivalent lifetime multiplier for the reference case and retrofits #1–4 for IPCC scenario A1B (a) and A2 (b) between 2020–2100 for cellulose in Oslo climate and following the FCT-UNL methodology

Thomson's methodology will not lead to the mechanical decay of furniture, sculptures pieces or panel paintings in nowadays conditions nor will it lead to mechanical decay in the future. These observations are valid for both selected climates. In addition, the application of any of the four selected retrofit measures will not decrease the quality of the indoor climate to safeguard these artefacts.

On the other hand, the FCT-UNL methodology can cause the mechanical decay of the base layer of panel paintings in Seville (Figure 6.11a and b) and the mechanical decay of the pictorial layer of panel paintings in Oslo (Figure 6.11c and d), since the 14%-limit is surpassed. Whilst the first observation worsens with time and it is heightened by the application of the retrofit measures, the second behaviour is attenuated by the application of these retrofit measures, since they manage to reduce the amplitude of the RH cycles.

Regarding Seville, the application of the retrofit measures decreases the free-floating indoor temperature mainly during the summer and spring, as was previously mentioned. This decrease will increase the relative humidity values since the water-vapour pressure does not change significantly due to the rather low moisture impregnability capacity of the selected measures. This will inevitably increase the amount of time that the yield strain is surpassed. These observations show that the performance of retrofit measures is dependent on the climate.

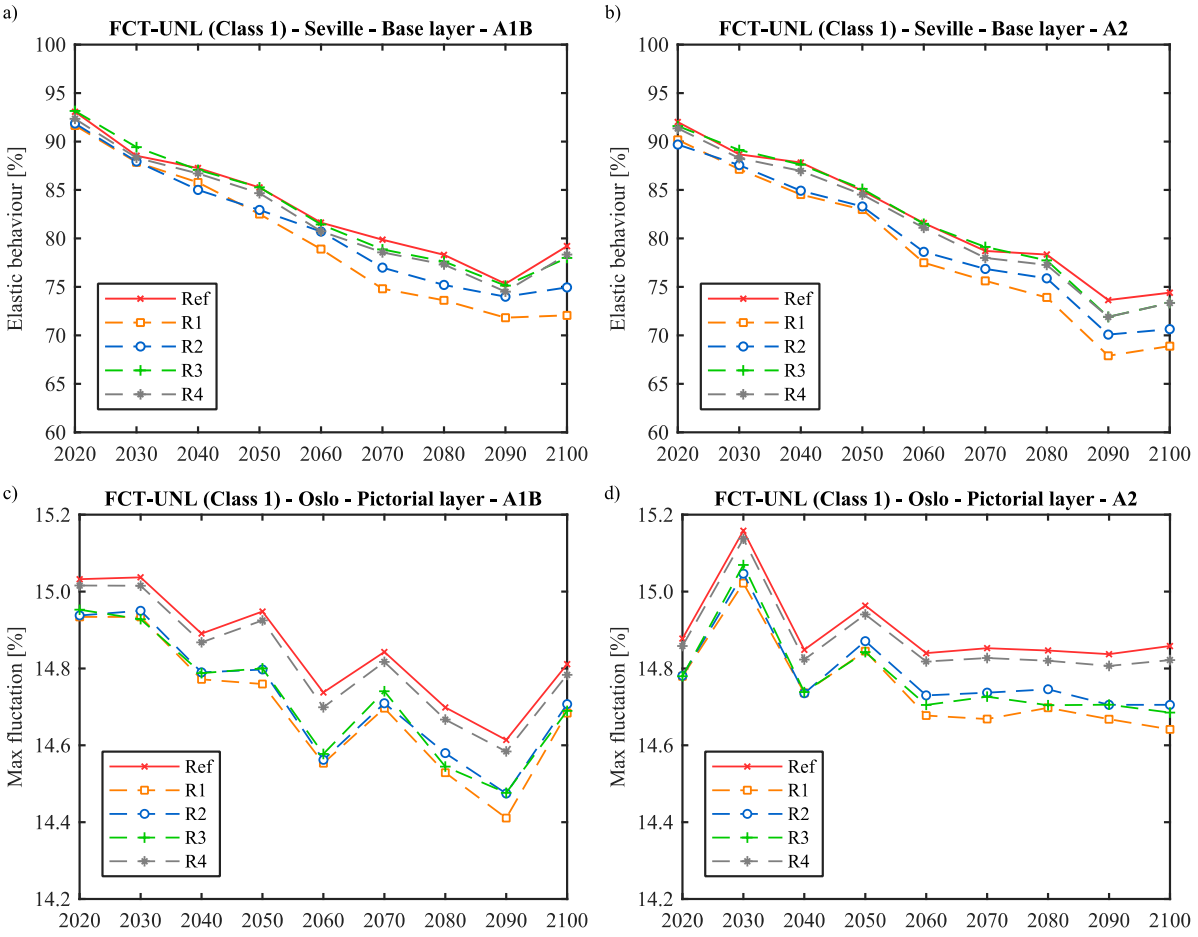

Figure 6.11 – Risk of mechanical decay in the base layer of panel paintings according to FCT-UNL methodology for Seville for scenario A1B (a) and A2 (b), and the risk of mechanical decay in the pictorial layer of panel paintings according to FCT-UNL methodology for Oslo for scenario A1B (c) and A2 (d)

6.4. Conclusions

The present chapter aimed to determine the energy consumption associated to three of the most used standards/guidelines to limit the indoor climate in buildings that house artefacts. It also aimed to determine how this consumption will evolve in the future due to climate change and how much it will cost to guarantee each standard/guideline for three types of climate in Europe. Additionally, four representative passive retrofit measures were tested to determine their energy saving potential.

In order to achieve these aims a validated whole-building hygrothermal model of a historic building (Church of St. Cristóvão in Lisbon, Portugal) was used coupled to future weather files based on two IPCC scenarios – A1B and A2 – for five climates, namely: Lisbon (Portugal), Seville (Spain), Prague (Czech Republic), Oslo (Norway) and London (United Kingdom). Lastly, the indoor climates were also assessed in terms of biological, chemical and mechanical decay using a methodology based on several validated methods.

This chapter intends to reinforce the idea that passive retrofit measures can be used to decrease the energy consumption of buildings that house artefacts considerably and, consequently, the financial and environmental costs, associated to guaranteeing the indoor climate adequate for artefacts in the future.

It was also shown, that if the passive retrofit measures are combined with a more adequate relative humidity and temperature setpoint strategy the energy savings are even higher. Hence, this chapter allowed to test the impact of a representative set of passive retrofit measures on conservation, which highlighted the potential of various rehabilitation strategies in the studied climates.

Based on the shown data it is clear that some of the existing methodologies that aim to preserve artefacts will lead to high energy consumption in the future, but there are other methodologies in which the opposite occurs. Evidently, the magnitude of these behaviours varies with the methodology and the climate. For instance, the highest energy consumptions were attained by Oslo using Thomson's methodology, ca 267 MWh in 1990, but it tends to decrease in the future. Whilst the lowest energy consumptions were attained by Lisbon and Seville using ASHRAE methodology, ca 0.2 and 0.5 MWh in 2100 for scenario A1B respectively, as well as the FCT-UNL methodology, ca 3.3 and 3.7 MWh in 2100 for scenario A1B, respectively.

It was also shown that for the constant valued methodologies the key factor for the colder climates is the minimum temperature limit, whilst for the Mediterranean climates is the maximum limit. However, this latter factor will gain even more importance in the future since it is expected that the indoor free-floating temperature is going to increase substantially. In contrast, the overall energy costs for the dynamic methodologies will be quite significant for climates like Oslo, Prague and London mostly due to the minimum temperature limit.

It was demonstrated the positive outcome of implementing retrofit measures in historic buildings for future conditions in terms of energy saving potential. The application of an interior insulation achieved the highest saving potential which varies between 20–32 %, followed by the application of an exterior thermal plaster which varies 16–20 %, application of a thermal insulation layer in the ceilings which varies 13–20 % and lastly by replacing the existing windows which varies 4–6 %.

The energy saving potential of the case-study could be even higher if these retrofit measures would be properly combined. However, this is a complex challenge due to the large variability of the input parameters. Nonetheless, it is important to bear in mind that the energy saving potentials can vary significantly from case to case, since they are dependent on a large number of variables, such as the building's volume, window/wall area ratio, among many others.

The risk-based analysis showed that, although retrofit measures are an interesting tool to significantly decrease the energy consumption in historic buildings that house artefact, their choice must be thoroughly studied prior to application, since their improvement potential can greatly differ according to the outdoor conditions. Hence, a more detailed analysis concerning these measures need to be performed.

In conclusion, it was shown that the standards/guidelines that buildings that house artefacts will lead to rather high financial costs for most of the tested cases, which shows the importance of studying ways to

counteract this trend. In addition, it was shown the positive potential that applying passive retrofit measures can have on the energy consumption of these buildings, but a risk-based analysis should be performed to assess if the indoor conditions in terms of artefacts conservation really improve.

7. PERFORMANCE OF PASSIVE RETROFIT MEASURES FOR HISTORIC BUILDINGS THAT HOUSE ARTEFACTS VIABLE FOR FUTURE CONDITIONS

This chapter has been partly published in the following reference: Coelho, G. B. A., & Henriques, F. M. A. (2021). Performance of passive retrofit measures for historic buildings that house artefacts viable for future conditions. Sustainable Cities and Society, 71, 102982. https://doi.org/10.1016/j.scs.2021.102982

7.1. Introduction

Nowadays, one of the most important problems of society is the major effects of climate change in the world [284], namely in the environment, human health and global economy, but also in our building stock due to the likely impacts of climate change on buildings [288]. A substantial amount of the greenhouse emissions, which are greatly responsible for climate change, is due to buildings (for instance, in the OECD countries, buildings are responsible for a 25–40 % portion of the greenhouse emissions [284]), which in turn is largely due to operational energy use [284]. Hence, the importance of optimizing the use of energy in buildings by adopting appropriate improvement measures. However, these measures differ according to the type and the use of the building since their indoor climate requirements will also differ.

This chapter addresses service buildings that house artefacts, such as museums and churches, since artefacts are the main source of conveying society's history through generations. The primary mission of these buildings is extending, as much as possible, the lifetime of their artefacts [136]. Hence, it is necessary to ensure certain indoor conditions. This endeavour can be quite difficult, since the requirements vary according to the type of collection [84] and sometimes even within the collection itself. Furthermore, many of the museums are installed in historic buildings, which typically have very thick walls [248] and were not initially built to house them, thus making it harder to guarantee the proper indoor conditions.

Due to their high heritage value, passive retrofit measures (such as, the application of a thermal insulation layer in the exterior walls) or the installation of mechanical systems always face a lot of adversities [203]. Hence, before application, these measures must be thoroughly studied, and their effects quantified. This is one of the reasons why the development of computational models is a very useful tool for historic buildings. In order to replicate reality accurately, these models have to be validated against the indoor conditions, which is a difficult task especially for historic buildings [66].

Furthermore, due to the difficulty to implement this type of measures it is predictable that historic buildings are more susceptible to the effects of climate change [129,167]. As pointed out by *Lucchi* [175], preventive conservation is the best course of action to reduce the energy demand in a sustainable way without jeopardizing the artefacts welfare and human comfort. However, to develop proficient preventive conservation methodologies, climate change must be taken into account.

The effects of climate change in cultural heritage have been studied throughout the years with two projects standing out: *Noah's ark* [229] and *Climate for Culture* [172]. The Noah's ark project mainly studied the several effects of climate change on the envelope of historic buildings throughout Europe [229]. On the other hand, the *Climate for Culture* project [172] focussed on assessing the effects of climate change on Europe's cultural heritage stock using A1B and RCP 4.5 scenarios. Computational models of historic buildings were developed and validated against their measured indoor conditions.

The effects of climate change in the artefacts were assessed using damage functions, and the results were used to develop risk-based maps for all Europe.

Several studies which take into account the effects of climate change in heritage have been developed using computational models of historic buildings to obtain the future indoor conditions [18,129,128,130,131,218]. Their common conclusion is that an increase of both the indoor temperature and humidity is expected in the future, but also the fact that each location in Europe will have some sort of conservation risk with a tendency to increase the more we go into the future. For instance, while Huijbregts *et al.* [129,128] identified that both the indoor temperature and relative humidity will increase, and determine that each location in Europe has its respective decay risks, and Rajčić *et al.* [218] showed that the risks of mechanical and biological decay in Croatia will worsen. These conclusions show that the adaptations this type of buildings must go through to mitigate the effects imposed by climate change will depend on their location.

The artefacts welfare is affected by several environmental variables, such as relative humidity and temperature [207,5]. Martens [178] developed a methodology, based on several methods presented in literature, to assess the risk of chemical (using the *Lifetime Multiplier* concept [186]), biological (using the *isopleth method* [244]) and mechanical deterioration of four types of artefacts induced by the indoor conditions. The mechanical degradation is assessed using one of four methods depending on the type of artefact since they answer differently to the RH solicitations [178]. This methodology has been used in several studies (e.g. [128,253]). Another aspect that must be assessed in buildings that house artefacts is the visitors' thermal comfort due to their importance in the building's revenues. This can either be evaluated using an adaptive thermal comfort model, which is based on the concept that the building's users can, up to a certain extent, adjust to the changes in the indoor climate (e.g. [4]), or an analytical thermal comfort model that recommends more narrow ranges for the indoor temperatures [137].

Sometimes, it is necessary to adopt passive or active measures or even a combination of both to achieve a proper indoor climate for the preservation of artefacts. For example, Muñoz-González *et at.* [194] studied several of these options to improve the indoor climate of a 17th-century church in Seville (Spain), and Sciurpi *et al.* [243] studied several windows replacing options and different solar shadings for "La Specola" Museum in Florence (Italy). Both these studies used computational models to assess the improvement measures performance. This type of analysis can be further developed if climate change and a risk assessment methodology are used to determine if the tested measures are adequate to preserve the artefacts in the future.

This chapter aims to assess the viability of today's retrofit measures in historic buildings while taking climate change into account. The future indoor conditions were obtained using a validated hygrothermal model and climate change weather files. The case-study selected for this chapter was St. Cristóvão church in Lisbon. Additionally, the hygrothermal model was artificially relocated using the outdoor

climates of different European cities to replicate this analysis throughout Europe, namely Seville (Spain), Prague (Czech Republic), Oslo (Norway) and London (United Kingdom). This relocation will allow to assess how differently the selected measures will perform in each climate. The indoor conditions were assessed using a risk-based analysis and an adaptative thermal comfort model.

7.2. Methodology

7.2.1. General considerations

To achieve the aim of this chapter, a validated hygrothermal model (St. Cristóvão church), which meant a long-term monitoring campaign, coupled to climate change weather files were used to obtain the future indoor conditions. These conditions were assessed using a risk-based analysis, which evaluates the risk of mechanical, chemical, and biological degradation in artefacts, and a thermal comfort model. The set of selected retrofit measures and their limitations are addressed. For the purpose of this study, a total of 1350 simulations were run in WUFI®Plus, which amounts to ca 1485 hours of simulation.

7.2.2. Case-study

St. Cristóvão church was built in the 13th-century and has approximately 5250 m^3 (Figure 7.1a and Annex G). The church is composed by several compartments, namely: a nave, a mortuary, a sacristy, an annex and two towers (Figure 7.1b). The church has very thick mortared limestone walls (U_{wall} = 1.36 W/m^{2}K), a limestone slab (U_{slab} = 3.89 W/m^{2}K), a ceiling composed by two wood slabs with a 20 cm air layer in-between ($U_{ceiling}$ = 1.25 W/m^{2}K), a ceramic tile roof (U_{roof} = 5.26 W/m^{2}K) and single-glazed windows (U_w = 5.1 W/m^{2}K). Detailed description of all parameters can be consulted in Ref. [66,68].

The indoor conditions of the church were monitored using several sensors from November 2011 to August 2013 with a recording frequency of 10 minutes. During the same period, the outdoor conditions were monitored using a data logger in the north tower. The church was open to the public all week, except on Mondays, during specific periods of time. A detailed description of the monitoring campaign can be found in Ref. [250,251].

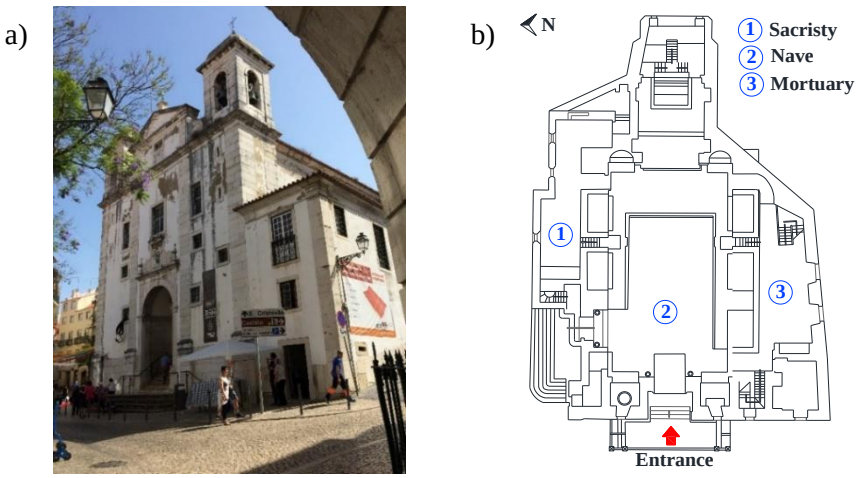

Figure 7.1 – St. Cristóvão church façade (a) and St. Cristóvão church plan (b)

A whole building hygrothermal model of St. Cristóvão church was developed using WUFI®Plus [292]. The adopted lighting power density was 11.7 W/m^2, and each occupant had a metabolic rate of 1.3 met and produced 126 W of heat and 54 g/h of moisture. The model's calibration was carried out using four statistic indices to compare the simulated indoor conditions against the measured conditions [66]: the *coefficient of determination* (R^2), the *coefficient of variation of the root mean square error* (CV(RMSE)), the *normalized mean bias error* (NMBE) and the *goodness of fit* (fit). The optimized model attained a CV(RMSE) of 3.2 % for T and 4.4 % for P_v, a NMBE of 2.7 % for T and 3.4 % for P_v and a fit of 84.8 % for T and 81.7 % for P_v. The simulated conditions accurately overlay the monitored conditions [66].

7.2.3. Outdoor climate

7.2.3.1. Weather files

The projections of the future outdoor conditions are based on the influence of several aspects on the environment, namely in terms of socio-economics, technological, energy use and land use, as well as the emissions of greenhouse gases (GHG) [278]. Due to the range of years considered in these projections and the variability of each of these aspects, there is a great number of scenarios that describe how the world's climate is going to evolve. These scenarios are organized in four distinctive groups, named the *Representative Concentration Pathways* (RCP): 2.6, 4.5, 6.0 and 8.5 W/m^2, whose value corresponds to their level of radiative forcing in 2100 [278].

In this chapter, the simulations will be run using outdoor weather files built with meteorological data that correspond to RCP 4.5 and RCP 8.5 scenarios. Whilst the RCP 4.5 corresponds to a medium stabilization scenario, the RCP 8.5 attains higher GHGs emissions because it does not encompass future climate policies [303]. Out of the four groups, the RCP 4.5 attains the lowest world population throughout all the period, and it starts to substantially decrease in the final part of the century. RCP 4.5 has the second highest *Gross Domestic Product* (GPD), only overcome by RCP 2.4 [278]. In terms of energy use, RCP 4.5 corresponds to a steady increase of primary energy consumption through the considered period with the non-fossil fuels gaining a great importance [278]. In terms of land use, which has a great influence on the GHG emissions, RCP 4.5 is based on a great change in the way how land is used, since the cropland area and grassland area greatly decrease through all considered period, whilst the vegetation area greatly increases [278]. Finally, in terms of CO_2 emissions, RCP 4.5 corresponds the second lowest, only overcome by RCP 2.6 [278]. Both RCP 4.5 and RCP 8.5 have been used in studies that deal with the effects of climate change in historic buildings, Climate for Culture [172] or Ref. [237].

The climate change weather files were constructed using the CORDEX database [71], which is an international coordinated framework that aims to comprehend the variability of the meteorological variables at a regional level by downscaling global climate model (GCM) into regional climate models (RCM). The data used in this chapter corresponds to model HadGEM2-SMHI-RCA4, which accurately

simulates the Portuguese climate and has been used in two projects SIAM 1 and 2 [306,307] and *ClimAdaPT* project, which develop strategies to adapt the country to climate change in several regions of Portugal [62].

In order to build the weather files that include the necessary meteorological data that allows WUFI®Plus to perform at its full capacity [293], the following meteorological variables were downloaded from the CORDEX database [70]: air temperature (ºC), relative humidity (%), atmospheric pressure (Pa), global radiation (W/m^2), global counter radiation (W/m^2), precipitation (mm/h), cloud index (%), wind speed (m/s) and direction (º).

The global radiation was divided in its direct and diffuse components using *Skartveit and Olseth* model that was firstly developed in 1986 [254] and then updated in 1998 [255] in order to obtain more reliable values. This model has been compared against the other models that exist in literature by *Lanini* [166] and achieved one of the best performances of all analysed models. Kim *et al.* [150] used this model to split the global radiation to build weather files using the procedure described in EN 15927-4 [89] for several locations in South Korea to perform hygrothermal simulations.

This building weather file procedure has been broadly used in hygrothermal simulations, e.g. Barreira *et al.* [32] used it to build weather files and run hygrothermal simulations for Oporto climate, Portugal. This chapter followed the same methodology to develop the future weather files. The code developed for *Skartveit and Olseth* model is validated by Figure J.1, which shows the same results that are presented in figure 2), and figure 3a) and 3b) of Ref. [255] for three specific cases.

7.2.3.2. Selected climates

7.2.3.2.1. Present conditions

Due to the key influence of the outdoor climate on a building's indoor climate, this study was developed for five European cities, namely Lisbon (Portugal) and Seville (Spain) – Mediterranean climates, Prague (Czech Republic) and Oslo (Norway) – Humid continental climate, and London (United Kingdom) – Oceanic climate.

Lisbon has a temperate climate with rainy winters and hot summers [153], the outdoor temperature does not reach values below the freezing point, it has a rather high annual temperature average and it is subject to a considerable amount of rain [121], mainly during winter [65]. Seville has a rather similar climate to Lisbon, but it reaches higher temperatures, mainly during summer, and has a lower annual precipitation than Lisbon.

Prague is classified as a humid continental climate with cold winters, temperatures that reach below the freezing point values, hot summers, and an annual low precipitation. Oslo has a similar climate to Prague, but its temperature is lower than Prague's all year round and it has a higher annual precipitation than Prague. Finally, London is classified as an oceanic climate with cold winters, warm summers, and

an annual moderate precipitation.

7.2.3.2.2. Future conditions

Climate change will significantly change the outdoor conditions. Its impact tends to worsen the further into the future we go, namely by the generalized increase of the outdoor air temperature and the water-vapour pressure. Precipitation will decrease in the Mediterranean zone and increase in central and northern Europe. In terms of global radiation there is an increase in the Mediterranean zone and a decrease in the other zones of Europe.

These changes occur to a different extent depending on the location and the scenario considered: Figure 7.2 for RCP 4.5 and Figure 7.3 for RCP 8.5. The differences mentioned in this subchapter are relative to near-past values. The annual thirty-year normal and the water-vapour pressure were calculated using the methodology described in Ref. [289] and Ref. [92], respectively.

In terms of temperature, the trend is similar in all selected climates for both scenarios, i.e. there is a substantial increase of the temperature across the 21st-century, but RCP 8.5 attains higher values in the far-future. The thirty-yearly average in Lisbon increases 1.4 ºC in the near-future and 2.5 ºC in the far-future for RCP 4.5 relative to the near-past values, while for RCP 8.5 it increases 1.7 and 4.1 ºC. In Seville, it increases 1.7 and 3.0 ºC for RCP 4.5, and 2.0 and 5.0 ºC for RCP 8.5, respectively. In Prague, it increases 1.9 and 2.8 ºC for RCP 4.5, and 2.0 and 4.8 ºC for RCP 8.5, respectively. In Oslo, it increases 2.3 ºC and 3.4 ºC for RCP 4.5, and 2.3 and 5.2 ºC for RCP 8.5, respectively. In London, it increases 1.5 and 2.5 ºC for RCP 4.5, and 1.6 and 4.0 ºC for RCP 8.5, respectively.

In terms of water-vapour pressure, the trend is similar in all selected climates for both scenarios, i.e. there is a substantial increase of the water-vapour pressure across the 21st-century. Although differences between both scenarios are detected in the near-future, the substantial differences occur in the far-future, with RCP 8.5 attaining higher values. The thirty-yearly average in Lisbon increases 100 Pa in the near-future and 186 Pa in the far-future for RCP 4.5 relative to the near-past values, while it increases 123 Pa and 306 Pa for RCP 8.5. In Seville, it increases 97 and 168 Pa for RCP 4.5, and 115 and 281 Pa for RCP 8.5, respectively. In Prague, it increases 102 Pa and 172 Pa for RCP 4.5, and 111 and 282 Pa for RCP 8.5, respectively. In Oslo, it increases 107 Pa and 169 Pa for RCP 4.5, and 109 and 276 Pa for RCP 8.5. In London, it increases 92 Pa and 170 Pa for RCP 4.5, and 105 and 275 Pa for RCP 8.5, respectively.

In terms of precipitation, two opposite behaviours occur which depend on the location, i.e. precipitation decreases for the Mediterranean climates, whilst it increases for the three remaining climates. The highest differences relative to the near-past values are reached in the far-future for scenario RCP 8.5. The precipitation decreases in Lisbon in the near-future – i.e. -69 mm for RCP 4.5 and -36 mm for RCP 8.5, and in the far-future – i.e. -99 mm for RCP 4.5 and -235 mm for RCP 8.5 in relation to the near-past values. The same behaviour occurs for Seville in both the near-future – i.e. -41 mm for RCP 4.5 and -56 mm for RCP 8.5, and the far-future – i.e. -122 mm for RCP 4.5 and -202 mm for RCP 8.5. On

the other hand, it increases for Prague, Oslo and London for both the near-future – i.e. 119, 220 and 98 mm for RCP 4.5, and 124, 162 and 89 mm for RCP 8.5, and the far-future – i.e. 124, 218 and 150 mm for RCP 4.5, and 160, 314 and 142 mm for RCP 8.5 in relation to the near-past values.

In terms of global radiation, two behaviours of opposite nature also occur, i.e. the global radiation increases for the Mediterranean climates, whilst it decreases for the three remaining climates. The most substantial differences relative to the near-past values are obtained in the far-future. The global radiation increases for Lisbon – i.e. 21W/m^2 in the near-future and 38 W/m^2 in the far-future for RCP 4.5, and 21 in the near-future and 61W/m^2 in the near-future for RCP 8.5, and for Seville – i.e. 20 and 40 W/m^2 respectively for RCP 4.5, and 11 and 45 W/m^2 respectively for RCP 8.5 in relation to the near-past values. On the other hand, it decrease for Prague – i.e. -27 and -44 W/m^2 respectively for RCP 4.5, and -22 and -44 W/m^2 respectively for RCP 8.5, for Oslo – i.e. -55 and -71 W/m^2 respectively for RCP 4.5, and -46 and -95 W/m^2 respectively for RCP 8.5, and for London – i.e. -2 and -33 W/m^2 respectively for RCP 4.5, and -14 and -11 W/m^2 respectively for RCP 8.5 in relation to the near-past values.

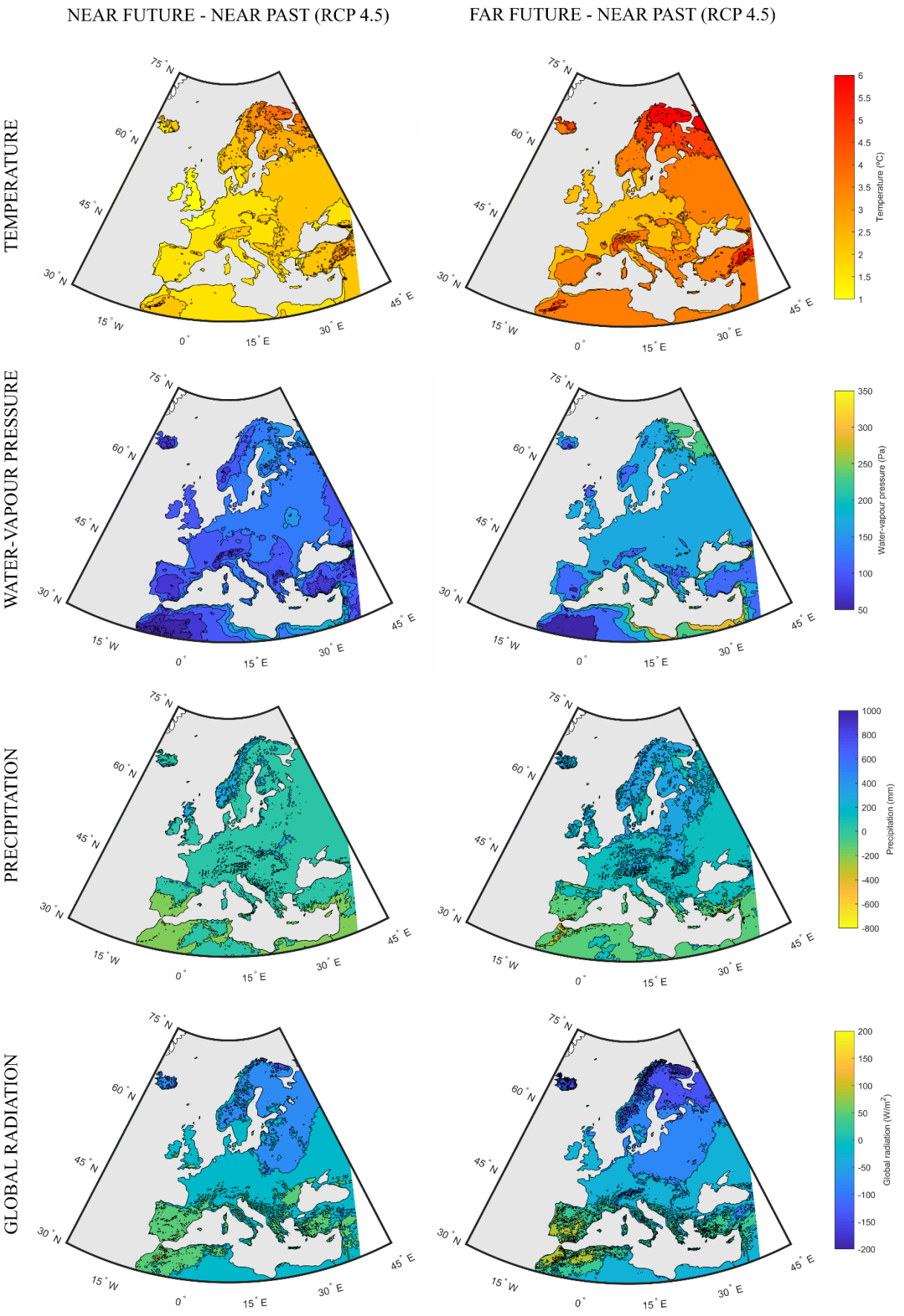

Figure 7.2 – Difference between the annual thirty-year normals of the outdoor temperature, water-vapour pressure, precipitation and global radiation between the near-future and near-past (2nd column), as well as the far-future and the near-past (3rd column) in Europe for RCP 4.5

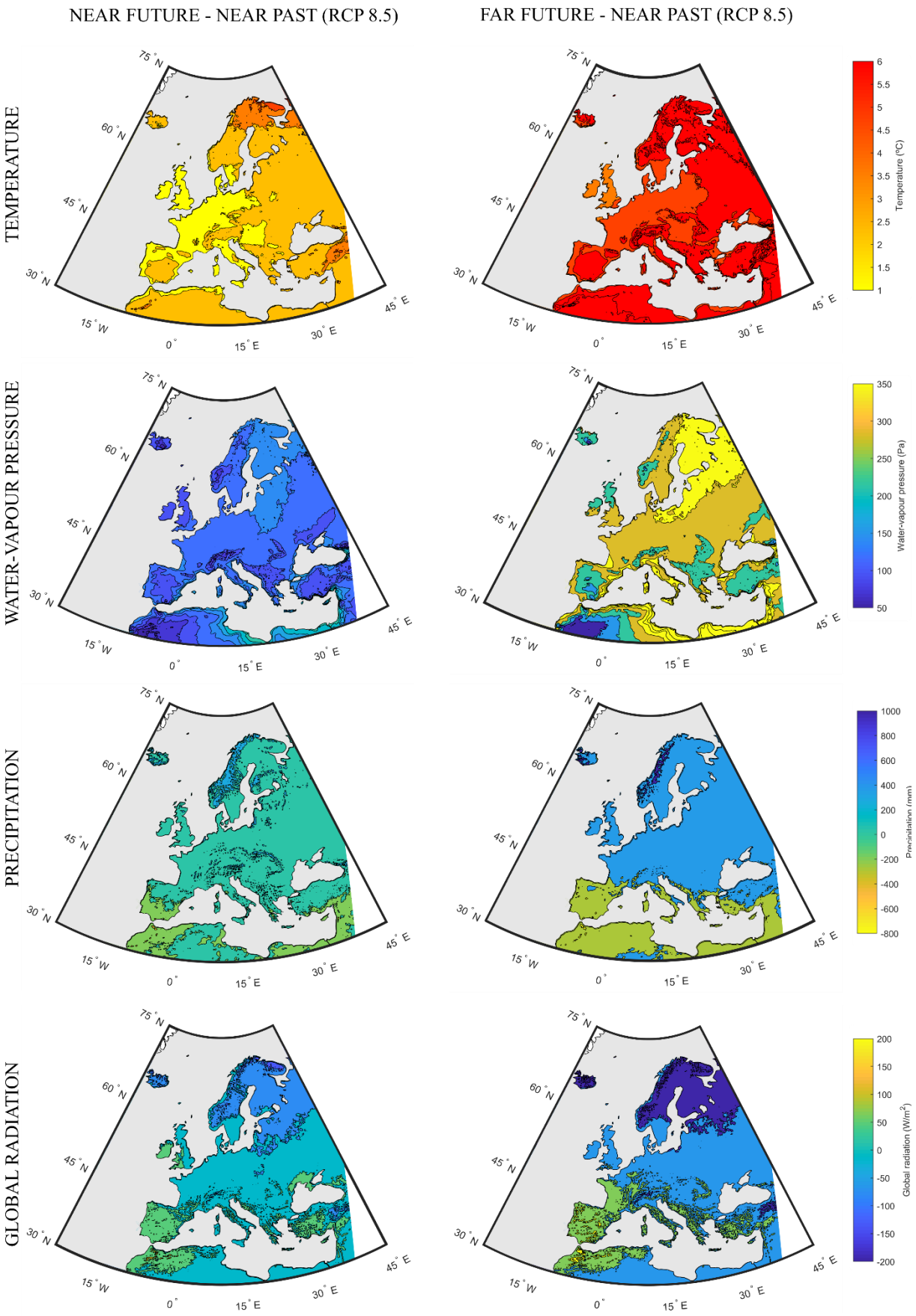

Figure 7.3 – Difference between the annual thirty-year normals of the outdoor temperature, water-vapour pressure, precipitation and global radiation between the near-future and near-past (2nd column), as well as the far-future and the near-past (3rd column) in Europe for RCP 8.5

7.2.4. Risk assessment and thermal comfort

As previously mentioned, this subchapter includes three distinctive materials risk assessments: chemical, biological, and mechanical for four different artefacts: paper, panel paintings, furniture, and wooden sculpture. The thermal comfort was assessed using an adaptive thermal comfort model developed for buildings without climate control systems. To assess the materials' behaviour according to the variation of the indoor conditions it is necessary to calculate its *response time*. This parameter was developed by *Martens* [178] and it consists in the amount of time that an object takes to get to 95% of the end value in case of a RH step change, i.e. it reflects how fast a material reacts to the variation of the indoor climate.

7.2.4.1. Chemical risk

Although chemical decay is a slow process, all organic materials are vulnerable to it, especially paper. Its speed is proportional to temperature and relative humidity, i.e. the higher the temperature and relative humidity, the faster chemical decay will occur. The damage of the material is caused by chemical reactions, namely hydrolysis and oxidation, which take place within the material and depend primarily on the temperature and secondly on its moisture content. Michalski [186] states that for each 5 K drop, the chemical lifetime of most chemical sensitivity materials doubles. The life expectancy for the several types of chemical sensitivity materials can be consulted elsewhere [188,187].

The chemical decay can be assessed using the *lifetime multiplier* concept, which was developed by Michalski based on the Arrhenius equation [186], and reflects for how much time the object remains usable by comparison to standard conditions, i.e. 20 ºC and 50% RH. The activation energy necessary for the reactions to start occurring is 100 kJ/mol for paper (i.e. cellulose) and 70 kJ/mol for the other materials (i.e. varnish) [178]. The *equivalent Lifetime Multiplier* can be used to quantify the chemical risk under a single value [253]:

$$eLM = 1 \Big/ \left(\frac{1}{n} \cdot \sum_{x=1}^{n} \left(\frac{1}{\left(\frac{50\ \%}{RH_x}\right)^{1.3} \cdot e^{\frac{E_a}{R}\left(\frac{1}{T_x+273.15}-\frac{1}{293.15}\right)}} \right) \right) \tag{7.1}$$

Where *eLM* is the *equivalent Lifetime Multiplier* [-], *n* is the number of data points in the considered period [-], RH_x is the surface relative humidity at instant x [%], E_a is the activation energy [J/mol], *R* is the gas constant [8.314 J/Kmol] and T_x is the temperature at instant x [ºC]. The use of this concept is beneficial for this type of research because it enables to assess the risk of chemical decay throughout a large period much more easily.

7.2.4.2. Biological risk

Many of the artefacts that are housed in buildings, such as museums, are vulnerable to fungal growth, especially those that are composed by at least one organic material, but also inorganic materials with

organic films [197]. For fungal to grow it is necessary to attain certain values of relative humidity and temperature, but it is also necessary that the substrate has nutrients [244]. These three conditions must be met simultaneously and endure for a specific period of time for mould growth to occur. Due to the risk that mould presents to artefacts conservation it is of key importance to cease this process. This can be achieved by first knowing the conditions under which mould growth occurs and secondly by acting appropriately.

Sedlbauer [244] developed a two phase method, known as *isopleth model*, that allows to study the mould growth based on relative humidity, temperature and substrate, firstly, by determining the time needed for the spores to became active and secondly, by determining the rate of the mould growth once they are active. For the first phase the *Spore germination* graph is used, in which spores became active fungi when the *Lowest Isopleth for Mould* (LIM) is surpassed. The germination time decreases as temperature and relative humidity increase. In the second phase, the speed of the fungi growth is determined using the *Mycelium growth rate* graph. If the active fungi die, the germination process has to start all over again. It is also important to bear in mind that the maximum RH in which there is no mould growth varies according to the type of climate, while in temperate regions the RH should remain below 70 %, higher values maybe acceptable in cold regions [51].

The *mould risk factor* (MRF) was used in this chapter to quantify the biological risk under a single value. The MRF is the sum of the time contributions to spore germination of each set of temperature and relative humidity that overcomes the respective LIM. This is performed by adding the reciprocal of the corresponding germination time. The spores become active fungi when the MRF reaches 1.0. According to IPI metrics [197], if the MRF is lower than 0.5 there is little or no risk of mould growth. It is important to bear in mind that due to MRF restrictions (namely, the possibility of the active fungi dying), the MRF value can vary through the considered period. Hence, this assessment should be focussed on the maximum values and not necessarily in the final value. A key advantage of this factor is that it manages to reflect the risk of mould growth occurrence throughout a large period under a single value, which is vital for this specific research.

7.2.4.3. Mechanical risk

All hygroscopic organic materials are susceptible to mechanical decay, which is a process that is mainly governed by relative humidity. The variation of relative humidity will lead to the variation of the moisture content of these materials, which will cause the material to shrink if relative humidity decreases or to swell if it increases. Additionally, and if the material has internal or external restraints, it will cause stresses within itself, which may eventually result in its cracking.

This chapter follows a validated methodology of mechanical decay assessment [178], and analyses the dimensional change of furniture, sculptures and panel paintings, whose constituents have to be analysed individually – i.e. wood substrate and pictorial layer (Figure 7.4). For furniture, the mechanical decay is

assessed using an adapted version of Bratasz *et al.* graph [44], in which the x-axis corresponds to the annual average of relative humidity and the y-axis corresponds to the surface response to relative humidity. For sculptures, the mechanical decay is assessed using an adapted version of Jakiela *et al.* graph [144], in which the x-axis corresponds to the sub surface response to relative humidity and the y-axis corresponds to the surface response to relative humidity.

The mechanical decay in the wood substrate and the pictorial layer of painted panels must be assessed using two different methods. The mechanical decay of the wood substrate is assessed using an adapted version of Mecklenburg's *et al.* graph [181] in which the x-axis corresponds to the object full response to relative humidity and the y-axis corresponds to the surface response to relative humidity. On the other hand, the mechanical decay of the pictorial layer is assessed using Bratasz's *et al.* graph [45]. A more detailed explanation of these methods can be found elsewhere [178].

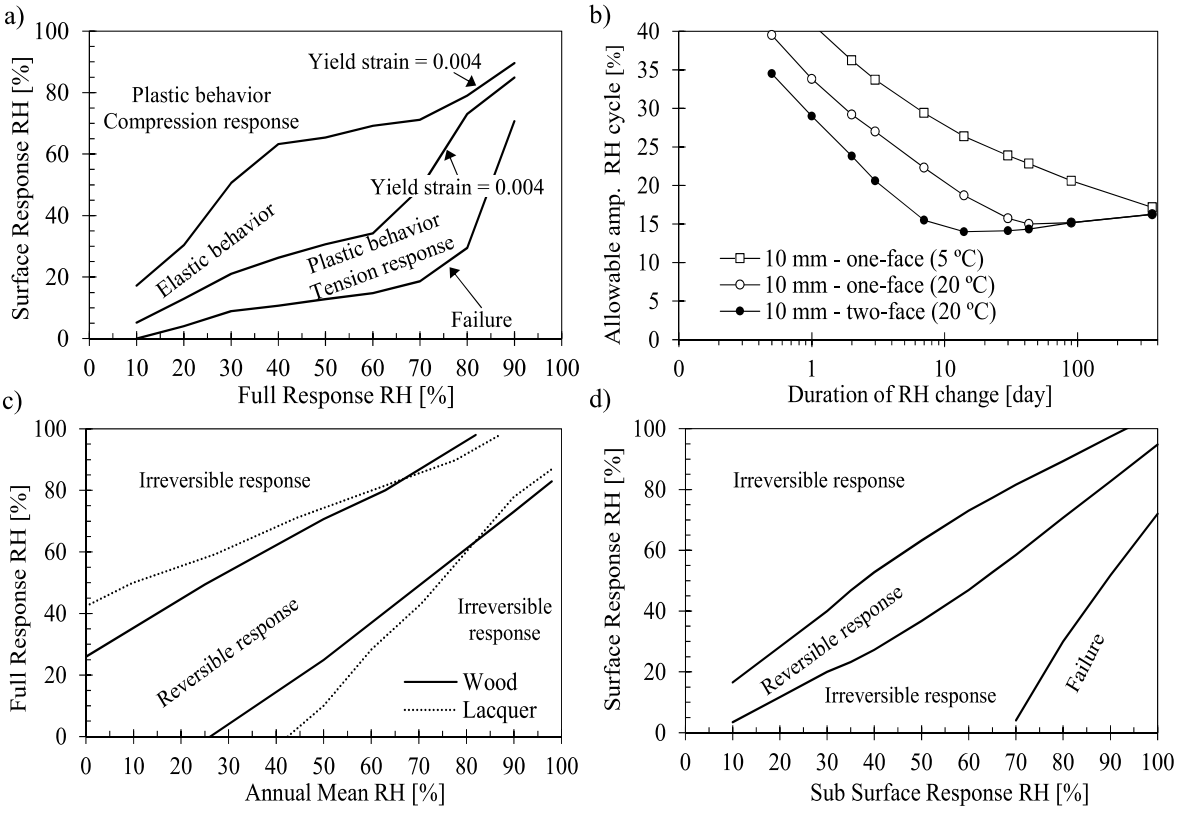

Figure 7.4 – Mechanical decay assessment for: a) wood substrate of the panel painting [181], b) pictorial layer of the panel painting [45], c) wood furniture [44] and d) wood sculptures [144]

7.2.4.4. Thermal comfort

Due to the importance of visitors in maintaining this type of buildings, it is important to guarantee that the indoor climate is thermally comfortable for them, as well as to preserve the artefacts welfare. Hence, the indoor conditions obtained from the run simulations were assessed using the adaptive method of ASHRAE 55:2013 [4] for an acceptability limit of 80 %. This method is valid for buildings that are naturally ventilated that do not have any mechanical systems [4]. Further information about this method can be consulted in Ref. [4]. It was assumed that the building would be open from 10h00–18h00 with a

visitor frequency of six people per hour [249]. The artificial illumination was also taken into account during this period due to the preference for type of illumination in terms of artefacts preservation concerns [264].

7.2.5. Retrofit measures

In the past few years, retrofit measures have been subject to a significant number of studies that test them in historic buildings due to today's sustainability concerns (e.g. [25,22,190,231,72,193,225,194]), but also because they are a protective measure that ensures that these buildings are used in the future [282]. However, their viability is greatly dependent on the outdoor climate [205], which means that a thorough study of the effects of each measure has to be developed in each specific case to ensure that they lead to an improvement of the indoor climate quality and not the opposite.

This type of study is even more important for historic buildings that house collections due to these buildings' specific characteristics and the fact that most of them were not initially built to house artefacts. An inadequate retrofit measure might even threaten the collection welfare and might lead to irreparable damages in the building itself [224].

A set of retrofit measures were selected with the aim of improving the indoor climate in terms of conservation and thermal comfort (Table 7.1). These measures were chosen due to their applicability in heritage buildings. Each one was applied individually to the model to study the corresponding effect. Three types of building elements were subjected to retrofit measures: a) walls, b) ceilings/roof and c) windows. To make this analysis as comprehensive as possible, the validated model of St. Cristóvão church was used without taking any type of constraint into account, such as high value interior wall surfaces that would not allow the application of an interior thermal insulation system.

Based on literature, two types of retrofit were selected for walls: external thermal mortar and interior thermal insulation systems, despite the disadvantages usually associated to applying the thermal insulation internally [59]. The selected insulations were vapour-open insulation materials [42]: PUR-boards, mineral wool, perlite boards and calcium silicate boards. The thermal mortar was also assessed, since this retrofit measure has recently been tested in several Refs. [25,22,72,176], despite the fact that this layer has to be rather thick to ensure a significant increase of the wall's thermal resistance, which might lead to compatibility problems with the building's exterior elements (such as the windows' sills).

In terms of windows, the single-glazed windows were replaced by double-glazed with clear float with or without low emissivity glass. Lastly, the insulation of the roof and insulation of the ceilings were individually tested. Each insulation system has the same orientation as the building element to which it corresponds. An expanded polystyrene (EPS) and extruded polystyrene (XPS) insulation systems were tested on the roofs. A mineral wool insulation system and polyurethane projected foam (PUR) were tested on the ceilings. Retrofitting the roof/ceilings is the less intrusive measure in historic buildings with heritage value [231], which is why it is favoured for this type of building.

Table 7.1 – Selected retrofit measures and corresponding thickness, thermal conductivity (λ-value) and water-vapour diffusion resistance factor (μ-value). Data taken from WUFI®Plus database [292] and LG10:1999 [263]

Element	Retrofit measure	Material	Thickness [cm]	λ-value [W/m.K]	μ-value [-]	Code
Walls A_{wall} – 1146 m^2	Interior thermal insulation system	PUR boards	2–10 & 20	0.031	69	W1
		Mineral wool		0.035	1.3	W2
		Perlite board		0.042	3.1	W3
		Calcium silicate boards		0.050	3.2	W4
	Exterior thermal insulation mortar		1.5/3/5	0.045	4.0	W5
Roof/Ceiling A_{roof} – 543 m^2 $A_{ceiling}$ – 466 m^2	Thermal insulation system beneath the ceramic tiles	XPS	2–10	0.030	100	R1
		EPS		0.040	30	R2
	Thermal insulation system between wood slabs (air layer)	PUR foam	2–10	0.025	50	C1
		Mineral wool		0.035	1.3	C2
Windows $A_{windows}$ – 56 m^2	Double glazing with clear float		U_w = 2.8 W/m^2K			Wd1
	Double glazing with low E glass		U_w = 1.4 W/m^2K			

7.3. Results and discussion

7.3.1. General considerations

The viability of retrofit measures for historic buildings in terms of artefacts conservation – biological, chemical, and mechanical decay –, and visitors' thermal comfort was assessed for three different types of climate whilst considering climate change by means of scenario RCP 4.5 and 8.5, namely: mediterranean (Lisbon and Seville), humid continental (Prague and Oslo) and oceanic (London).

This option is due to the fact that the performance of the selected retrofit measures can greatly differ with the location, and also because climate change will affect each region of Europe differently [305], which can also lead to different performances. The key results of the performed simulations are presented below, and all retrofit measures were tested individually. The MRF and eLM figures follow the colour code presented in table 2.3 of Ref. [247].

In addition to the specified thicknesses in Table 7.1 for the walls' interior insulations systems, an extra equivalent thickness, named lm*, that corresponds to a 30 cm layer was included in the walls' figures to show the results for each performed assessment for thicknesses higher than 20 cm, which will show their tendency. This extra thickness was determined by running a simulation with a 50 cm insulation layer for each retrofit measure. Then, the respective value for the 30 cm layer was determined through

linear interpolation.

7.3.2. Viability of retrofit measures for historic buildings for future conditions: Mediterranean climates

Biological decay

The results show that the selected retrofit measures can have a key effect in decreasing the damaging effects caused by climate change in Mediterranean climates, which are more pronounced for RCP 8.5 in the far-future. A reduction of the risk of biological decay in Lisbon was detected for both selected climate change scenarios, as well as for both selected periods of time – i.e. near- and far-future, with the installation of the selected walls retrofits. However, the thickness from which it is worth performing the wall retrofit measures will differ according to the type of retrofit, the outdoor climate and the way in which the world will evolve (Table L.1). This topic will be further discussed at the end of this subchapter.

While mineral wool, calcium silicate board and the thermal mortar have a positive effect right from the beginning, the PUR-boards and perlite boards are only worth applying from a certain thickness onwards (Table L.1). This last behaviour is more noticeable in the far-future, which means that retrofit measures that nowadays have a positive performance may not do so in the future. Figure 7.5a shows the performance of PUR-boards for Lisbon. For instance, for RCP 8.5 in the far-future, the PUR-boards only overcome the case without retrofit measures (WR) at 15 cm and never reach ideal conditions.

In Seville, the effects of the retrofit measures are similar to what was reported for Lisbon. Nonetheless, the risk of occurring biology decay in this climate is lower than in Lisbon (Figure 7.5b), the only case that poses a real risk is RCP 8.5 in the far-future (i.e. MRF is above 1.0 [197]), but this risk is mitigated by the application of the retrofit measures. On the other hand, the WR occurs at a larger thickness in Seville than in Lisbon, for example, the WR for RCP 4.5 is 7 cm for Lisbon and 18 cm for Seville for PUR-boards (Table L.1). The thermal mortar has an interesting effect for both climates, but mostly for Lisbon, since for example, a 5 cm layer has the same effect as 8 cm of calcium silicate boards for RCP 8.5 in the far-future, but due to the thickness restrictions this solution should be accompanied by other retrofit measures.

The roofs' retrofit also has a very positive outcome for both Lisbon and Seville, i.e. it considerably decreases the risk of biological decay (Figure L.1 and Figure L.2, a and b). However, this reduction is only substantial for the first tested thickness, which means that this reduction is mainly due to the air tightening of the roof that results from applying the insulation system. On the other hand, the insulation of the ceilings leads to a smaller decrease of the risk of biological decay for the first tested thickness, but thereafter there is a gradual decrease of the risk, which leads to believe that higher thicknesses could be tested (Figure L.1 and Figure L.2, c and d). As it was reported for the walls, only the RCP 8.5 in the far-future is within the risk zone (i.e. MRF > 1.0 [197]) for both climates, with a higher extent for Lisbon, but the application of any of the four retrofit measures mitigates this situation. The only exception is

mineral wool that is only worth installing from a certain thickness onwards (Table L.1).

Lastly, the replacement of the windows leads to a slight improvement for both climates, which is more substantial in the far-future. However, if the windows are to be replaced, other retrofit measures must accompany their replacement if the indoor climate is to improve significantly. This near neglectable effect of windows is transversal to the other assessments.

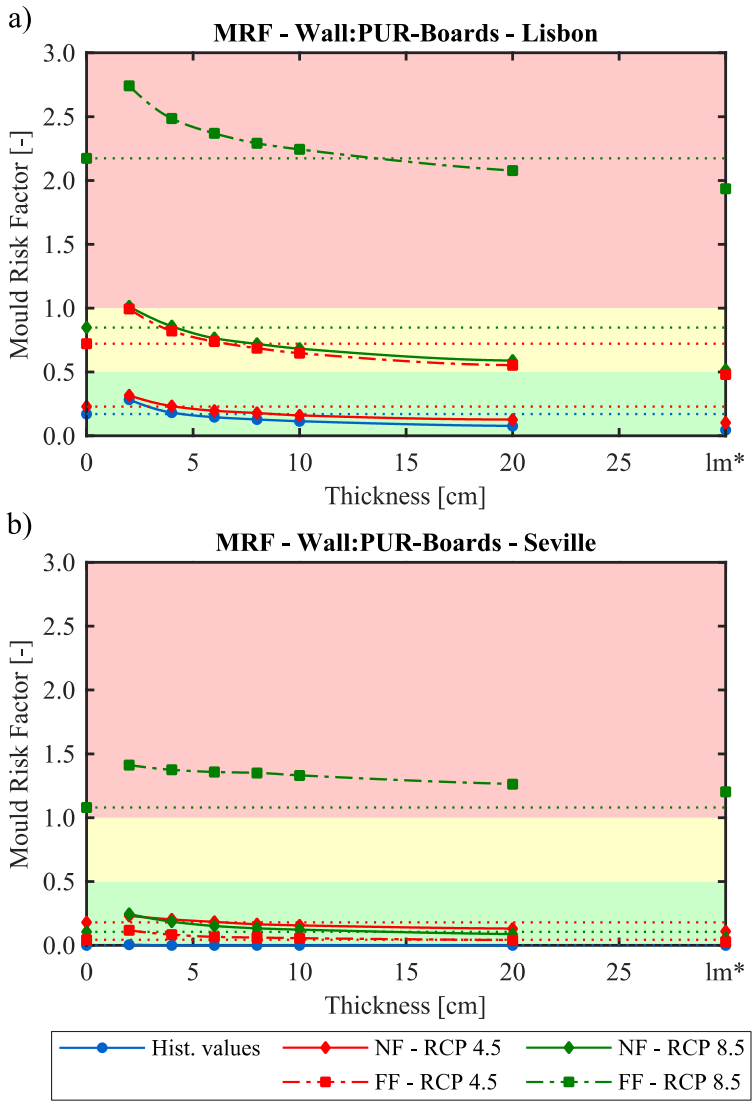

Figure 7.5 – Biological decay assessment using MRF for historical values, near-future and far-future for Lisbon and Seville for the case-study with PUR-boards ranging from 2 to 20 cm (W1), and for the case without any retrofit (dotted lines)

Chemical decay

Climate change also increases the odds of occurring chemical decay in both climates, more significantly in the far-future. However, the two mediterranean climates respond differently to the application of the retrofit measures in the walls. While in Lisbon the walls' retrofit measures increase the risk of occurring chemical decay since eLM decreases [251], although less substantially in the far-future (Figure 7.6a), in Seville the walls' retrofit measures decrease the risk of occurring chemical decay since eLM increases [251] and more substantially in the far-future (Figure 7.6b).

In Lisbon, the applications of the retrofit measures lead to the increase of the indoor temperature and the decrease of the relative humidity all year around except for summer, which will result in the decrease of the lifetime multiplier (LM). This behaviour will decrease with climate change. As pointed out by Silva et al. [251], the lifetime multiplier response in mediterranean climates is mainly governed by winter, since it is when the lifetime multiplier reaches its highest values.

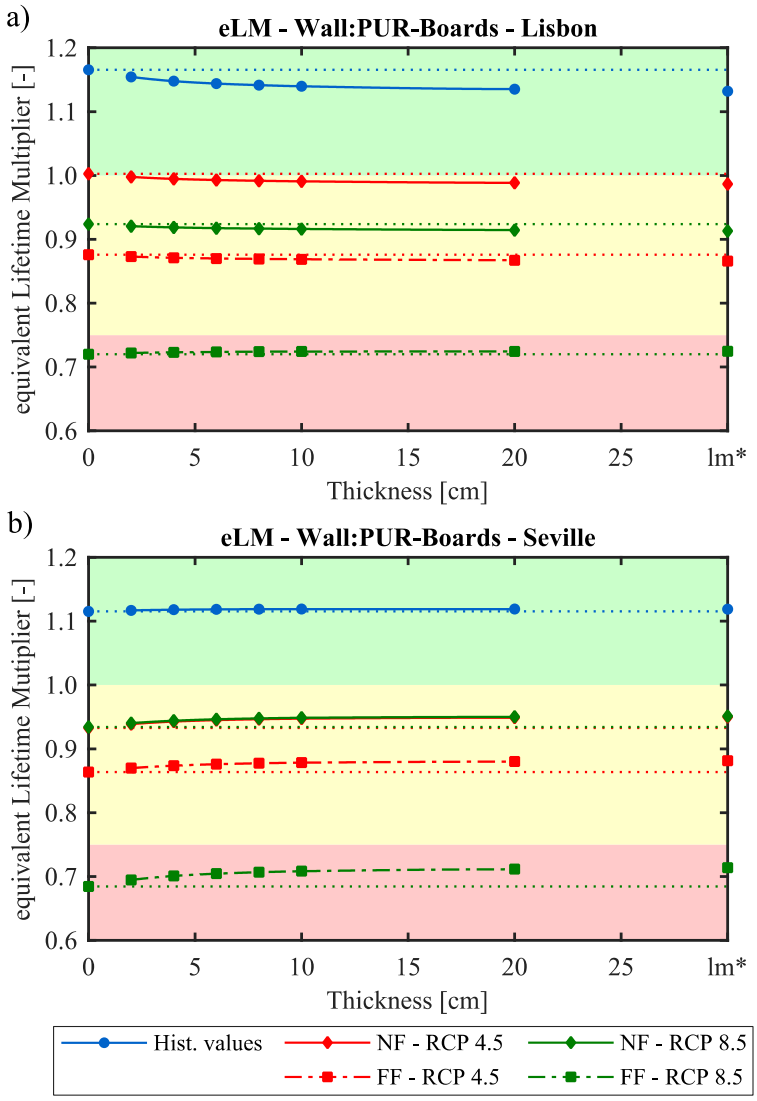

Figure 7.6 – Chemical decay assessment using the eLM for historical values, near-future and far-future for Lisbon and Seville for the case-study with PUR-boards ranging from 2 to 20 cm (W1), and for the case without any retrofit (dotted lines)

On the other hand, the application of the retrofit measures in Seville will lead to the increase of the indoor temperature and relative humidity during winter and autumn, and the decrease of the indoor temperature during summer and spring. While the first behaviour will result in the decrease of the LM, the second behaviour will increase the LM. This behaviour gains importance with climate change, since the decrease of temperature during these two seasons is more prominent, which will lead to superseding the first behaviour impact, thus leading to the increase of the eLM.

The replacement of the windows does not reduce the risk of occurring chemical decay, whilst the other

tested retrofits, i.e. the application of insulation layer in the ceilings and in the roofs, even worsens it (Table 7.2). These observations show that these measures are not very proficient in counteracting the increase of the probability of occurring chemical risk in historic buildings associated with climate change for Mediterranean climates.

Mechanical decay

Since furniture is not endangered of mechanical decay, nor will it be in the future, it will not be further addressed in this subchapter. In addition, sculptures are also only slightly affected by climate change, i.e. the maximum time that sculptures are not under elastic behaviour is only 2.3 % lower than the maximum limit for the worst-case scenario for Lisbon, i.e. RCP 8.5 in the far-future. However, these decreases are compensated, at a different extent, by the application of the wall's retrofit measures in both climates (e.g. Figure 7.7 for PUR-boards). The remaining retrofits do not significantly decrease the risk of mechanical decay in sculptures and, in some cases, they even worsen it (Table 7.2).

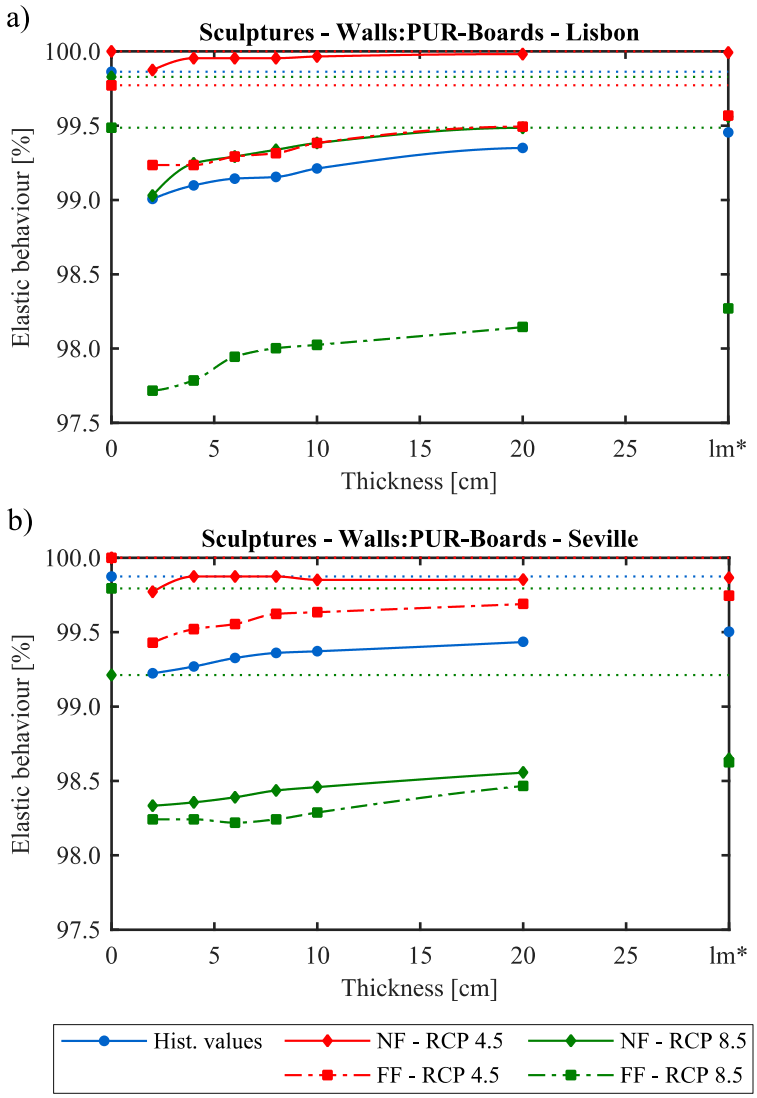

Figure 7.7 – Mechanical risk assessment of sculptures for historical values, near-future and far-future for Lisbon and Seville for the case-study with PUR-boards ranging from 2 to 20 cm (W1) and for the case without any retrofit (dotted lines)

The application of the retrofit measures decreases the risk of mechanical decay for the base layer of the panel paintings in both climates substantially – up to 3.5 % for Lisbon for calcium silicate boards in the near-future for RCP 4.5 and 4.6 % for Seville in the far-future for RCP 4.5, managing to counteract the negative effects of climate change to a certain extent.

The risk of occurring this type of decay is greater in Lisbon than in Seville. In Lisbon, the time the indoor climate is within the elastic behaviour zone can range between 81–90 % for the case without retrofits (dotted lines in Figure 7.8a), while in Seville it varies between 92–95 % (dotted lines in Figure 7.8b), depending on how the world will evolve in the future, i.e. either following the path described in scenario RCP 4.5 or in scenario RCP 8.5.

The walls' retrofits lead to the most prominent improvements with calcium silicate boards performing the best for both climates at the higher thicknesses (Figure 7.8). In fact, the application of the walls' retrofit even enables the indoor climate to eventually reach the 100%-value for historical values in Seville (e.g. Figure 7.8b). Another interesting observation is the fact that whilst for Lisbon the two worst-case scenarios correspond to the far-future (both dash dotted lines in Figure 7.8a), for Seville the two worst-case scenarios correspond to RCP 8.5 in the far-future and in the near-future (both green lines in Figure 7.8b). This shows that scenario RCP 8.5 is more strongly felt in Seville than in Lisbon throughout the whole studied period.

The thermal mortar has an interesting performance, since it is responsible for increasing the time that the indoor conditions are under elastic behaviour, i.e. 2.4 % for Lisbon and 2.7 % for Seville for historical values (Table 7.2), despite its thickness restrictions.

The roof retrofits are interesting only due to the roof's air tightening, since the time that the indoor climate is under elastic behaviour increases with the initial installation of the retrofit measures (i.e. 2 cm thick) but stagnates thereafter. On the other hand, the ceilings retrofit gradually increase the amount of time that the indoor climate is under elastic behaviour, thus leading to the belief that greater thicknesses could be tested. Finally, the windows replacement does not improve the indoor climate in terms of decreasing the risk of occurring mechanical decay in the base layer of panel paintings, but at the same time it does not exclude its application for other purposes.

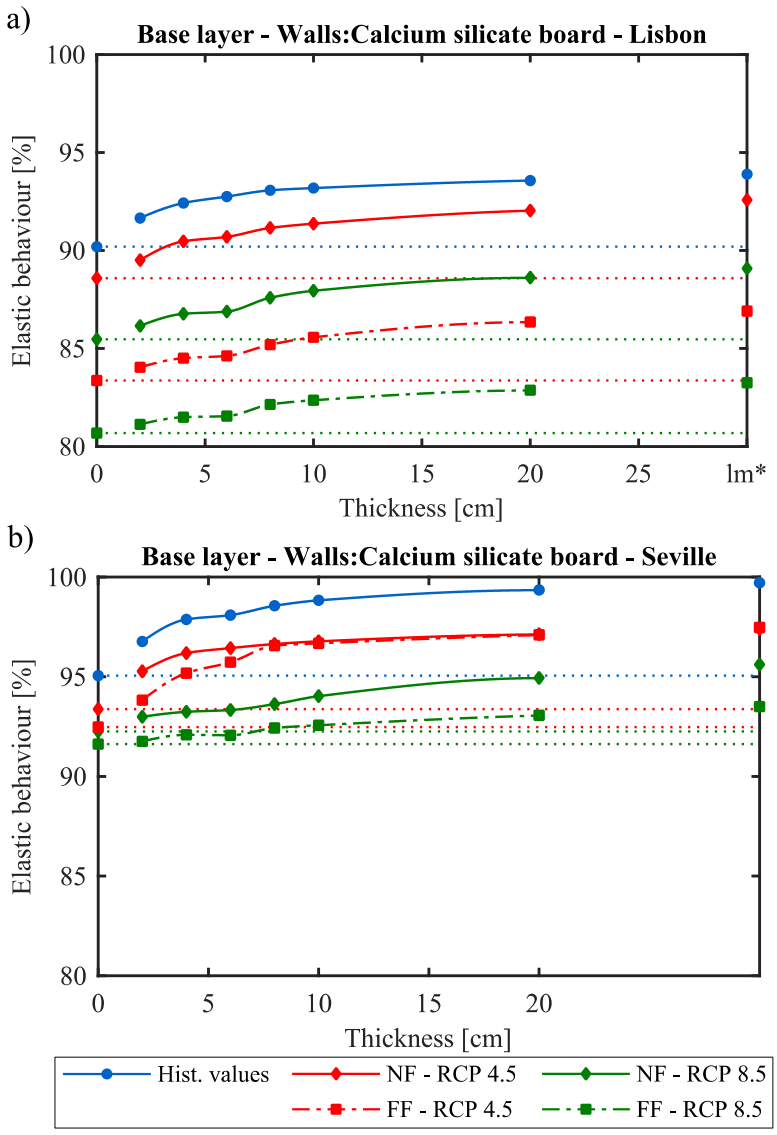

Figure 7.8 – Mechanical risk assessment of base layer (panel paintings) for historical values, near-future and far-future for Lisbon and Seville for the case-study with calcium silicate boards ranging from 2 to 20 cm (W4), and for the case without any retrofits (dotted lines)

The application of the retrofit measures has the effect of decreasing the indoor fluctuations in both climates (Figure 7.9). However, whilst in Lisbon the values are always below the 14%-limit (e.g. Figure 7.9a), in Seville they are over this limit (e.g. Figure 7.9b), which is problematic for the preservation of the pictorial layer of panel paintings. It is also evident that climate change is responsible for decreasing the indoor fluctuations for both climates. The only exception occurs for Seville in the far-future for RCP 8.5 in which there is an increase of the indoor fluctuations in relation to the historical values. Nonetheless, and like the other cases, this behaviour is mitigated by the application of the retrofit measures (e.g. Figure 7.9b).

The ceilings' retrofits have positive outcomes in both climates, but more substantially in Seville (Table 7.2), and whilst the roof retrofit is not advisable for Lisbon, it has positive outcomes in Seville (Table 7.2). Once again, the windows replacement does not improve the indoor climate in terms of decreasing the risk of occurring mechanical decay in the pictorial layer of panel paintings, but at the same time it

does not exclude its application if other purposes are pursued.

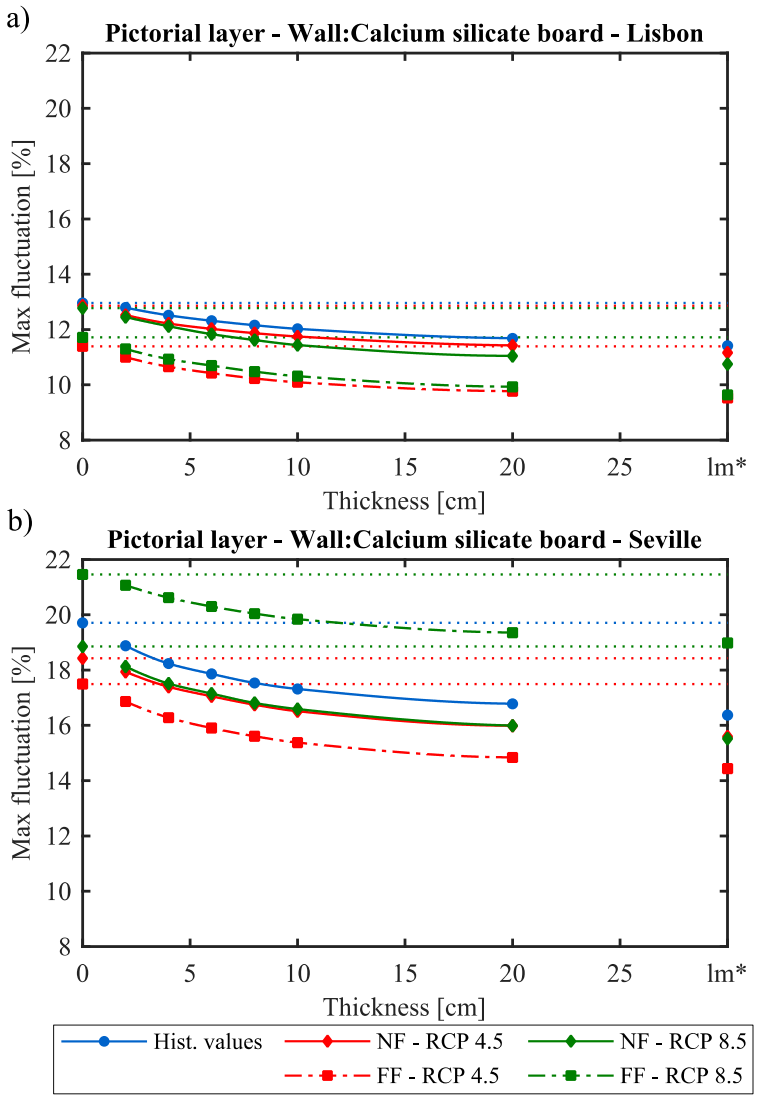

Figure 7.9 – Mechanical risk assessment of the pictorial layer (panel paintings) for historic values, near-future and far-future for Lisbon and Seville for the case-study with calcium silicate board ranging from 2 to 20 cm (W4), and for the case without any retrofit (dotted lines)

Thermal comfort

In terms of thermal comfort, the application of the retrofit measures leads to the improvement of the indoors conditions for both climates (Figure 7.10), with the walls' retrofits having the most prominent performance, followed by the roofs' retrofits and then by the ceilings' retrofits (Table 7.2). This is expected, since they will be responsible for the increase of the indoor temperature during the cold months and its decrease during the warm months, which evidently will increase the amount of time the indoor conditions are within the limits imposed by ASHRAE 55 [4]. However, there are some exceptions, namely for the walls' retrofits in Seville for scenario RCP 8.5 in the far-future (Figure 7.10b), in which the retrofits are responsible for decreasing the number of hours during which the indoor climate is within the imposed limits.

The application of the thermal insulation system has the impact of decreasing the variation of the indoor

temperature, i.e. it increases the minimal temperatures in winter and decreases the maximal temperature in summer. For example, the seasonal fluctuations for the historical values in Seville is 17.2 ºC for the case-study without retrofit measures and 15.9 ºC if it is equipped with a 10 cm PUR-board layer.

The difference for the RCP 8.5 is that since the outdoor climate will reach higher temperatures (subchapter 7.2.3.2.2), then the most distinctive effect will be the reduction of the maximum temperatures. This will also affect the in-between seasons – i.e. spring and autumn – causing the decrease of the indoor temperature, which will result in having more hours that fail the inferior limit of ASHRAE 55 [4], and consequently, the number of hours that the indoor climate is within the imposed limits will decrease. The limits imposed by ASHRAE 55 [4] for RCP 8.5 in the far-future are rather high because the outdoor temperatures are also the highest (subchapter 7.2.3.2.2).

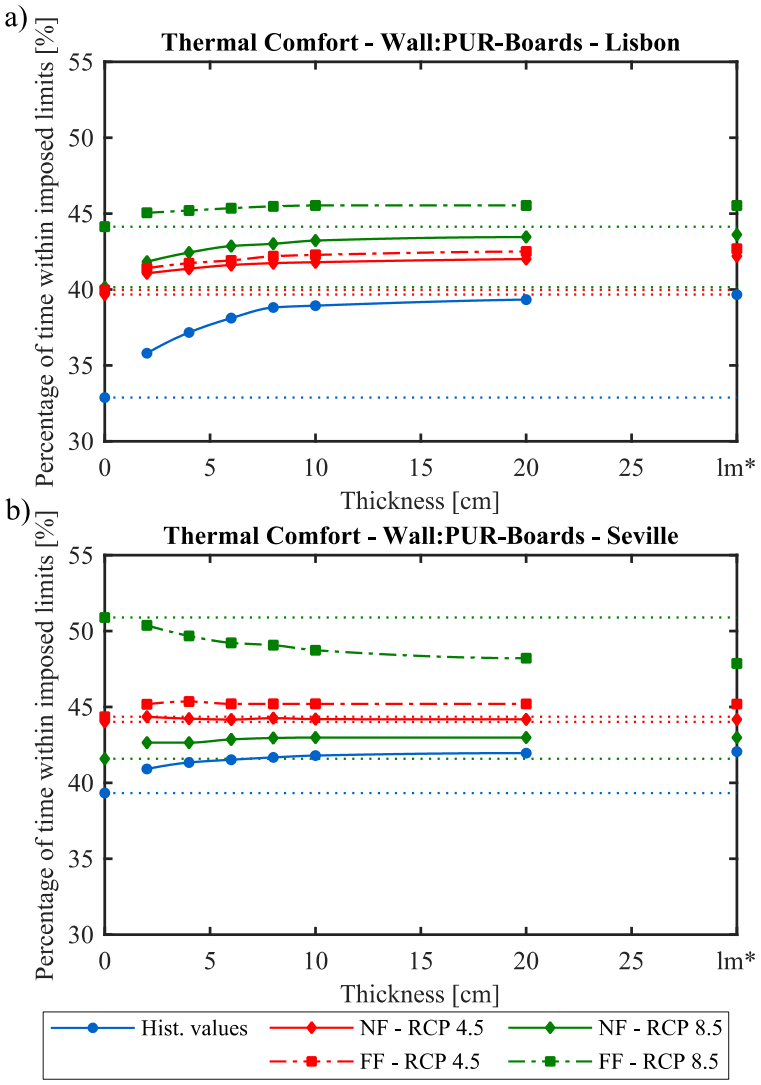

Figure 7.10 – Thermal comfort assessment for historical values, near-future and far-future for Lisbon and Seville for the case-study with PUR-boards ranging from 2 to 20 cm (W4), and for the case-study without any retrofit (dotted lines)

Retrofit performance comparison

Table 7.2 compares the performance of each selected retrofit measures to the case-study without

retrofits. The tested retrofits have two different aims, namely: 1) the reduction of both the MRF and the maximum indoor fluctuations (i.e. pictorial layer), and 2) the increase of the eLM, the amount of time that the indoor climate is under elastic conditions (i.e. sculpture and base layer), and the amount of time that the indoor climate is defined as thermal comfortable. These two aims will introduce some differences. Whilst for MRF and the pictorial layer, the negative values, which are presented in green, mean the improvement of the indoor climate; for eLM, sculptures, the base layer and thermal comfort, the positive values, which are presented in green, mean the improvement of the indoor climate.

The walls retrofit measures lead to the most important improvements of the indoor climate in terms of artefacts conservation and thermal comfort. Among them, the most beneficial in terms of artefacts' conservation is the calcium silicate boards (W4), and the mineral wool retrofit (W2). The W2 is the one that decreases the most the risk of mechanical decay for base layers (i.e. 4.0 %) and the risk of mechanical decay for the pictorial layer (i.e. -2.7 %) for Seville and W4 is the one that decreases the most the risk of mechanical decay for pictorial layer for Lisbon (i.e. -0.94), despite they have a slightly lesser performance in terms of thermal comfort than, for example, PUR-boards. The remaining retrofits also lead to improvements, although less substantial. The tested retrofits do not decrease the risk of chemical decay substantially, and they do not decrease the risk of biological decay for Seville because it is already zero or close to zero for the historical values, but they will in the future (Figure 7.8b).

Table 7.2 – Performance of 10 cm of W1-4, 10 cm of R1-2 and C1-2, and 5 cm of W5 in relation to the case without retrofit for the historical climate Lisbon and Seville

Climate	Assessment	**W1**	**W2**	**W3**	**W4**	**W5**	**R1**	**R2**	**C1**	**C2**	**Wd1**
Lisbon	MRF	-0.06	-0.14	-0.11	-0.15	-0.12	-0.12	-0.12	-0.11	-0.11	-0.03
	eLM	-0.03	-0.03	-0.02	-0.02	-0.01	-0.03	-0.03	-0.02	-0.02	0.00
	Sculpture	-0.65	-0.26	-0.50	-0.08	0.06	-0.03	-0.02	-0.09	-0.08	-0.05
	Base layer	3.14	3.32	3.07	2.99	2.39	2.29	2.28	2.09	2.02	0.79
	Pictorial layer	-0.52	-0.84	-0.69	-0.94	-0.55	0.11	0.14	-0.12	-0.12	-0.13
	Thermal comfort	6.06	5.57	4.69	5.18	1.74	3.99	4.26	2.56	2.25	0.03
Seville	MRF	0.00	0.00	0.00	0.00	0.00	0.00	0.00	0.00	0.00	0.00
	eLM	0.00	0.00	0.01	0.00	0.01	-0.02	-0.02	-0.01	-0.01	0.00
	Sculpture	-0.50	-0.19	-0.35	-0.19	0.00	0.02	0.02	0.02	0.01	0.00
	Base layer	3.08	4.00	3.23	3.78	2.72	2.76	2.76	2.68	2.65	0.86
	Pictorial layer	-2.27	-2.67	-2.36	-2.39	-1.73	-1.20	-1.15	-1.24	-1.17	-0.39
	Thermal comfort	2.47	1.92	1.61	1.89	0.49	2.65	2.71	1.80	1.52	-0.43

Thickness range recommendations

Another aspect that is very important in building retrofit is to guarantee that the applied retrofit measures really improve the indoor climate. Hence, the effects of the selected retrofits on the indoor climate were assessed in terms of the artefacts' conservation and the visitors' thermal comfort requirements for future conditions relative to the case-study without retrofits.

Annex L tables reflect this analysis in terms of recommending ranges of thicknesses that improve the indoor climate whilst compared with the case without retrofits. For example, Table L.1 presents the ranges of thicknesses that guarantee that retrofit measures have a positive effect on the indoor climate in terms of either artefacts' conservation or thermal comfort for the mediterranean climates in the future. A zero value means that it is not worth performing the retrofit for that aim, and if the superior limit is equal to the inferior limit, then there is only one recommended thickness for that retrofit measure.

Table L.1 shows that the furniture assessment does not narrow the thickness range. Based on this table it is also visible that the highest radiative forcing of RCP 8.5 reflects on the thickness ranges, since more narrow ranges than RCP 4.5 are recommended in most cases.

In addition, it is possible to perform the intersection of two or more of these ranges if the aim of the retrofit project is to protect more than one type of artefact, or if the thermal comfort requirements are also to be accounted for in the project. The limits imposed by the sculpture analysis should be considered carefully if they are to be taken into account when choosing the thickness for the retrofit measures, because for the worst-case scenario there is only a 2.3 % drop from the 100%-value, which is even compensated by the application of the retrofits (Figure 7.7).

7.3.3. Viability of retrofit measures for historic buildings for future conditions: Humid continental climates

Biological decay

In general, this type of climate is not prone to biological decay due to the lower indoor temperature and relative humidity when compared to the mediterranean climates. The only exception to this behaviour is if the world evolves according to scenario RCP 8.5, namely in the far-future, in which the MRF amounts to values above 1.0. From the two analysed climates, Oslo presents the greater risk of biological decay in the far-future for scenario RCP 8.5 (Figure 7.11).

Fortunately, the application of most of the selected retrofit measures mitigate this risk, but the extent of the mitigation will depend on the measure's properties (Table 7.3). The more substantial impacts are observed for the walls' retrofits, but the insulation of the roofs or the ceilings also lead to the reduction of the risk of biological decay, which is more substantial for Oslo. The fact that only scenario RCP 8.5 has a MRF above 0.5 in the far-future, whilst all the other cases have a MRF below this limit, will reflect on the thickness range that each retrofit measures will have within ideal conditions (Table L.4).

The thermal mortar and the windows replacement do not reduce the risk of biological decay, in fact they even increase it (Table 7.3). This happens for the thermal mortar because its application decreases the temperature during the critical season for biological decay, i.e. spring, since the water-vapour pressure will not change significantly, the relative humidity increases. This RH rise will increase the time contributions, which in turn will increase the MRF. The windows' replacement impact is not substantial, which enables its replacement if other aims are pursued, e.g. acoustic improvement.

The thickness from which it is worth implementing each select measure varies according to its properties, the outdoor climate and the IPCC scenario (Table L.2). For example, whereas the mineral wool can be applied from 2 cm onwards in Prague if the world evolves as described in scenario RCP 4.5, the perlite boards must be at least 6 cm thick to overcome the behaviour of the case without retrofits. This table limits the thicknesses ranges that can be applied, but on the other hand, it ensures that the applied retrofit measures really improve the indoor climate quality.

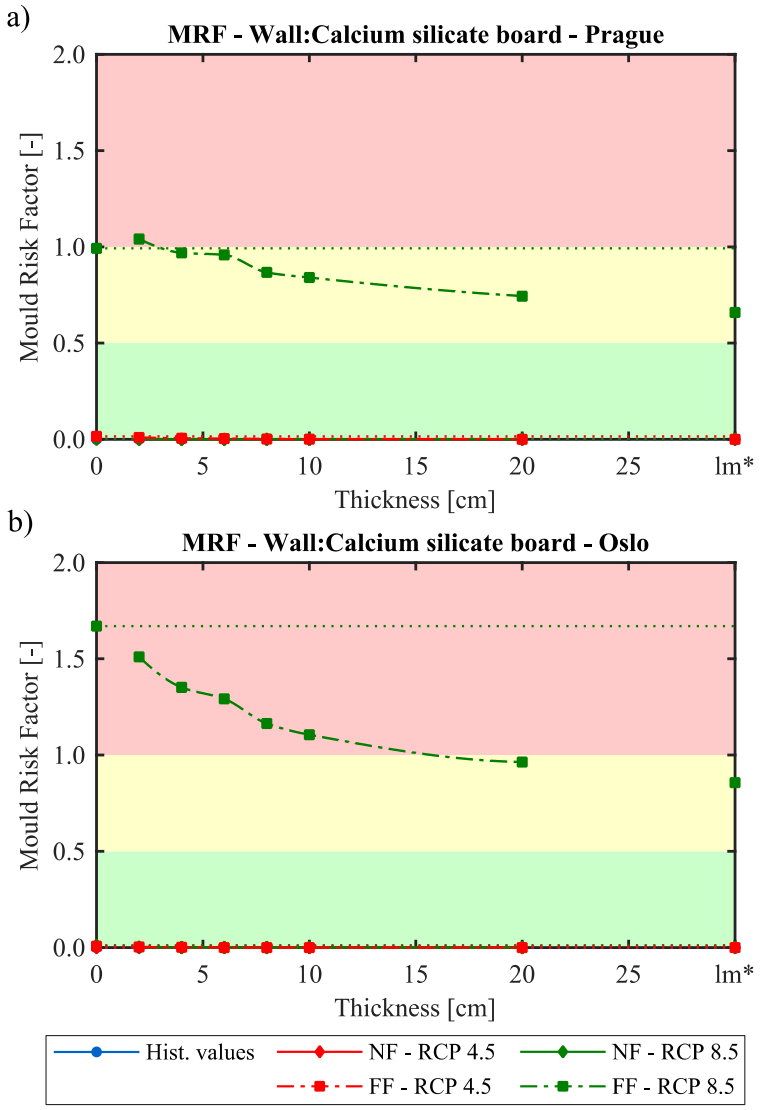

Figure 7.11 – Biological decay assessment using MRF for historical values, near-future and far-future for Prague and Oslo for the case-study with calcium silicate boards ranging from 2 to 20 cm (W4), and for the case without any retrofit (dotted lines)

Chemical decay

In terms of chemical risk, both climates are within ideal conditions (i.e. eLM above 1.0). The application of the retrofit measures and the impact of climate change will worsen the situation, since they will be responsible for decreasing the eLM, but both climates will remain within ideal conditions (Figure 7.12). Ultimately, this means that although the retrofit measures cannot be applied with the purpose of decreasing chemical risk, they can be applied with other purposes, e.g. to improve the thermal comfort,

and still keep the indoor climate within ideal conditions in terms of chemical decay (Table L.4).

The performance of each type of retrofit is rather similar (Table 7.3), with Oslo attaining the most substantial decreases. Nonetheless, Oslo is also the climate in which the eLM can decrease more without compromising the welfare of the artefacts (Figure 7.12). This occurrence will reflect on the thicknesses recommended in Table L.2 in which almost no retrofit is recommended to decrease the risk of chemical decay, but it does not limit its application if other purposes are pursued.

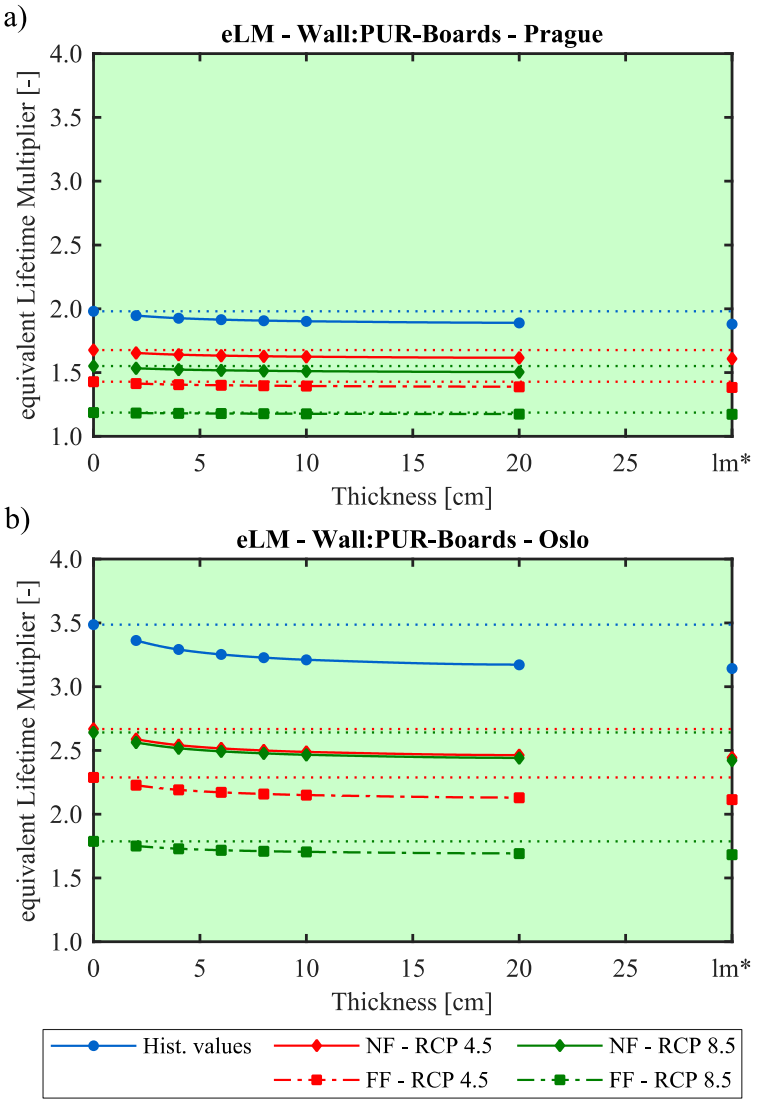

Figure 7.12 – Chemical decay assessment using eLM for historical values, near-future and far-future for Prague and Oslo for the case-study with PUR-boards ranging from 2 to 20 cm (W1), and for the case without any retrofit (dotted lines)

Mechanical decay

The furniture mechanical risk assessment does not limit the thickness ranges for Prague and Oslo now, nor will it limit them in the future (Table L.2). On the other hand, climate change slightly reduces the amount of time that the indoor climate is under elastic behaviour for sculptures. The minimum value is 98.3 %, which is attained for Prague in the far-future if the world evolves as described in scenario RCP 4.5 (Figure 7.13a). However, this occurrence is mitigated by the application of the walls' retrofit to a

certain extent, which will vary according to the properties of the retrofit measures (Table 7.3). Consequently, this variance will limit the range of recommended thicknesses differently (Table L.2).

Contrary to what was reported for the walls, in the case of the roofs' and ceilings' retrofits, and the windows' replacement, their application does not increase the number of hours that the indoor climate is under elastic behaviour conditions for sculptures. They are even responsible for worsening them. However, since it only worsens the indoor climate slightly (Figure 7.13b), it does not limit the application of these measures for other purposes. Nonetheless, this occurrence will have consequences on the recommended thicknesses in Table L.2 for the roofs' and ceilings' retrofits. The recommended limits of thicknesses based on the mechanical risk assessment for sculptures should be considered carefully, and they should not condition the retrofitting of this type of buildings for other purposes, since they correspond to small decreases that can be endured.

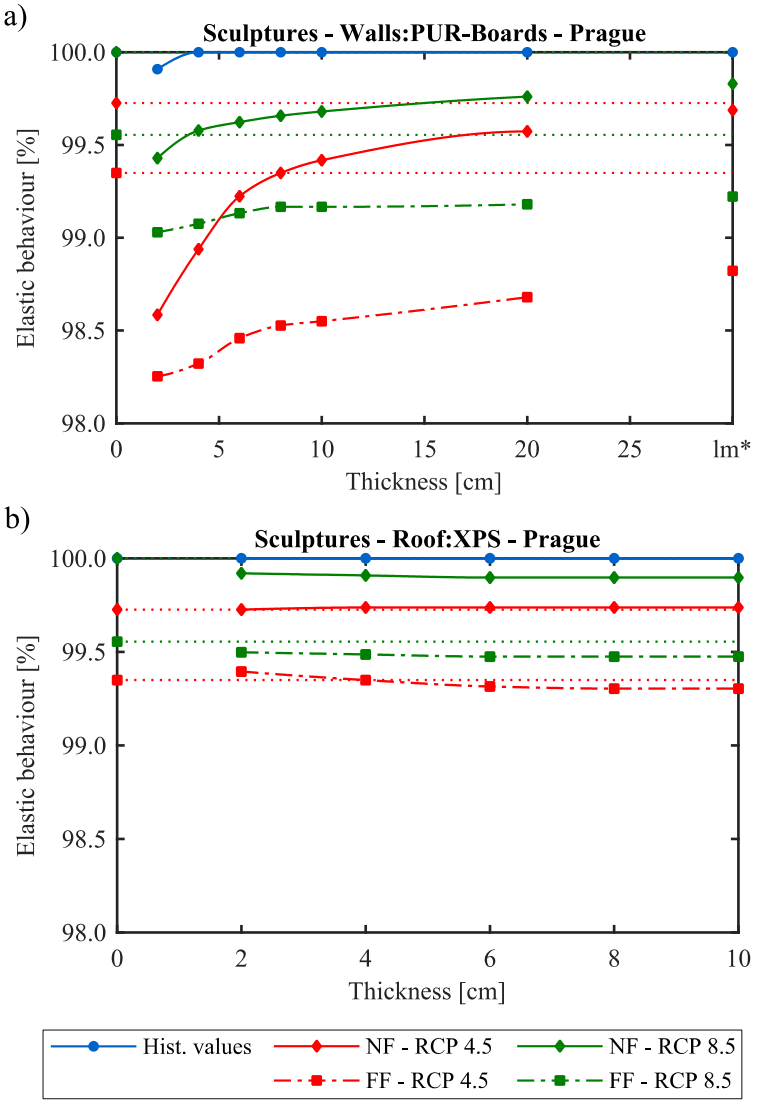

Figure 7.13 – Mechanical risk assessment of sculptures for historical values, near-future and far-future for Prague for the case-study with PUR-boards ranging from 2 to 20 cm (W1) and XPS ranging from 2 to 10 cm (R1), and for the case without any retrofit (dotted lines)

One of the most important impacts of the retrofit measures concerns the mechanical risk assessment of

the base layers of panel paintings (Figure 7.14). The retrofits manage to counter the negative effect of climate change for both climates substantially, which decreases the number of hours in which the indoor climate in under elastic conditions for base layers. There are even cases in which the application of the retrofit measures manages to make the indoor climate within elastic behaviour conditions all-year round (e.g. Figure 7.14b for RCP 4.5 in the near-future, 8 cm onward).

The most substantial impacts were detected for the walls' retrofits, with mineral wool having the best performance, then followed by the roof and ceilings retrofits (Table 7.3). The windows' replacement slightly increases the number of hours that the indoor climate is under elastic conditions for base layers. However, to improve the indoor climate in terms of decreasing the risk of mechanical decay for the base layers of panel paintings proficiently other measures will also have to be applied (Table 7.3). The recommended thickness ranges are only occasional narrowed (Table L.2). This is due to the positive impact that the retrofit measures have in the conservation metrics of the base layers.

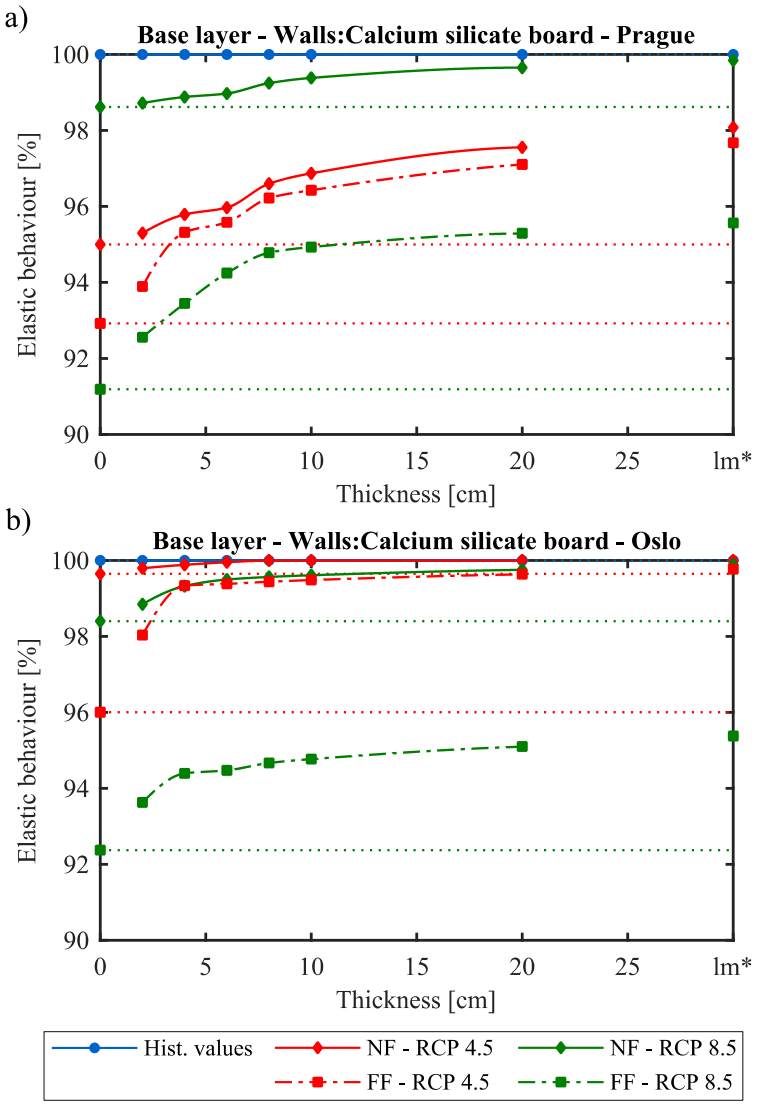

Figure 7.14 – Mechanical risk assessment of base layer (panel paintings) for historical values, near-future and far-future for Prague and Oslo for the case-study with calcium silicate board ranging from 2 to 20 cm (W4), and for the case without any retrofits (dotted lines)

For most analysed cases in the two climates, the application of the retrofit measures leads to the increase of the maximum indoor fluctuations, but on the other hand the 14%-limit value is not reached (e.g. Figure 7.15 for PUR boards). This fact leads to the conclusion that the retrofit measures can be applied if other purposes are pursued. Their performance will vary according to the properties of each retrofit type (Table 7.3).

The exceptions that were detected for the walls' retrofit are RCP 8.5 in the far-future for both climates and scenario RCP 4.5 in the near-future for Prague. In fact, the most worrying cases are RCP 4.5 in the near-future for Prague (Figure 7.15a) and RCP 8.5 in the far-future for Oslo (Figure 7.15b) because the application of the retrofit measures leads to the increase of the indoor fluctuations, whereas for Prague in far-future of RCP 8.5, the application of the retrofit measures will eventually lead to the decrease of the indoor fluctuation (Figure 7.15a), which is due to the specificities of each analysed time frame and scenario.

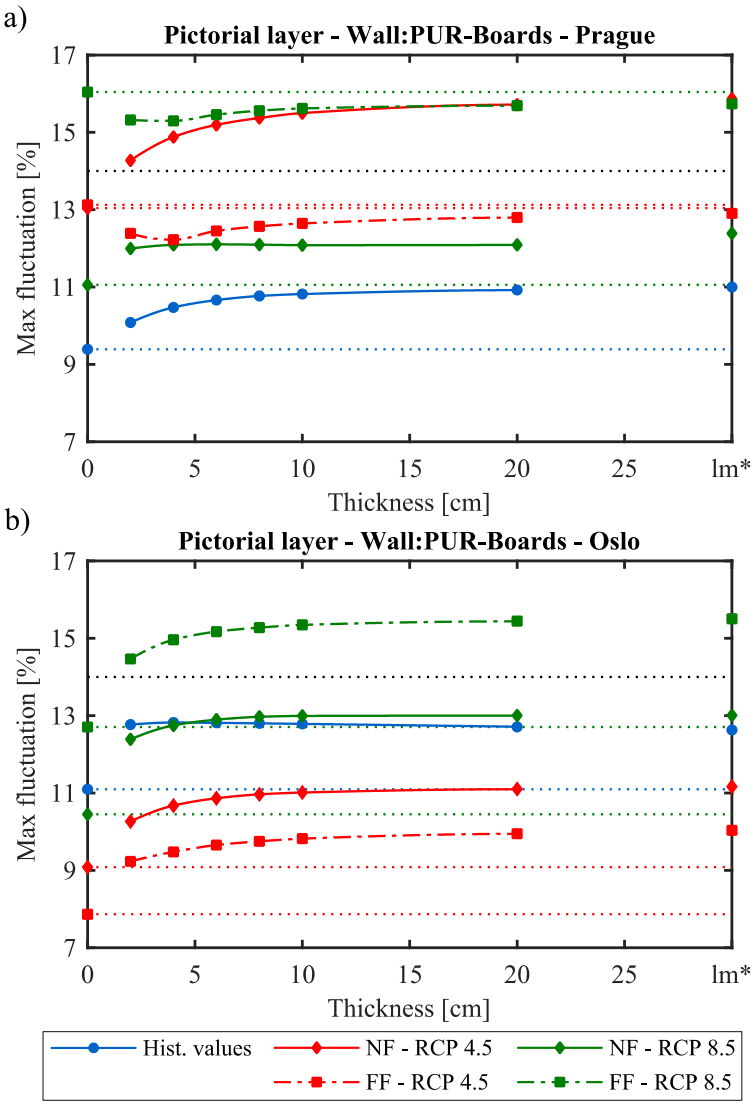

Figure 7.15 – Mechanical risk assessment of the pictorial layer (panel paintings) for historical values, near-future and far-future for Prague and Oslo for the case-study with PUR-boards ranging from 2 to 20 cm (W4), and for the case without any retrofit (dotted lines)

Note that these exceptions and respective observations are also true for the roofs' and ceilings' retrofits, i.e. the worrying cases are RCP 4.5 in the near-future for Prague and RCP 8.5 in the far-future for Oslo, since the application of the retrofit measures will lead to the increase of the indoor fluctuations, which will eventually overcome the 14%-limit value. This means that special attention must be paid to these climates if the world evolves as described in the respective scenario. The application of the thermal mortar is not very advisable for reducing the indoor fluctuations in the studied cases. Considering all these observations it is obvious that the recommended thicknesses ranges are almost non-existent (Table L.2), but this should not limit the application of these retrofit measures in most cases.

Thermal comfort

The application of the retrofit measures has a very positive effect on the thermal comfort for both climates, but more substantially for Oslo (e.g. Table 7.3 shows the results for scenario RCP 8.5 in the far-future). With the application of the retrofit measures, the thermal resistance of the building will increase, which will lead to higher indoor temperatures during the in-between seasons. Consequently, the number of hours that the indoor climate is within the limits imposed by the ASHRAE standard [4] will also increase. PUR-boards have the best performance, which is understandable since it has the lowest thermal conductivity (Table 7.1). This positive effect reflects on the recommended thicknesses measures ranges, which are almost full range (Table L.2).

Table 7.3 – Performance of 10 cm of W1-4, 10 cm of R1-2 and C1-2, and 5 cm of W5 in relation to the case without retrofit for scenario RCP 8.5 in the far-future for Prague and Oslo

Climate	Assessment	W1	W2	W3	W4	W5	R1	R2	C1	C2	Wd1
Prague	MRF	0.09	-0.01	0.12	-0.15	0.28	-0.18	-0.22	-0.04	-0.05	0.06
	eLM	-0.01	-0.01	0.00	-0.01	0.00	-0.02	-0.02	-0.01	-0.01	0.00
	Sculpture	-0.39	-0.02	-0.23	0.15	0.11	-0.08	-0.08	-0.09	-0.09	-0.01
	Base layer	3.76	3.85	3.61	3.74	1.00	1.76	1.78	1.51	1.45	0.30
	Pictorial layer	-0.42	-0.54	-0.44	-0.98	-0.65	-0.86	-0.83	-0.93	-0.87	-0.29
	Thermal comfort	3.04	2.68	2.37	2.71	1.31	1.98	2.07	1.58	1.40	0.06
Oslo	MRF	-0.27	-0.45	-0.20	-0.56	0.22	-0.37	-0.39	-0.20	-0.19	0.01
	eLM	-0.08	-0.08	-0.07	-0.07	-0.03	-0.06	-0.06	-0.05	-0.05	-0.01
	Sculpture	-0.66	-0.21	-0.53	-0.05	-0.06	-0.07	-0.07	-0.15	-0.11	0.00
	Base layer	2.48	2.47	2.25	2.40	1.59	2.02	2.01	1.86	1.80	0.56
	Pictorial layer	2.64	2.41	2.48	1.79	2.27	1.15	1.06	1.38	1.27	0.53
	Thermal comfort	10.59	10.08	8.83	9.32	3.14	8.01	8.07	6.30	5.88	0.21

7.3.4. Viability of retrofit measures for historic buildings for future conditions: Oceanic climates

Biological decay

In London, the risk of biological decay is non-existent since the MRF is below 0.5 for every analysed case, i.e. RCP 4.5 and RCP 8.5 in the near- and far-future. The MRF will increase in the future since both the indoor temperature and relative humidity will increase [67], consequently, the LIM curve will be more easily overcome [244], but due to the climate characteristics, this increase is not sufficient to

make the indoor climate leave the ideal conditions zone (Table L.4).

In addition, the application of the retrofit measures has a positive impact since they are responsible for decreasing the MRF (Figure 7.16). As the values of MRF are rather low, it can be difficult to ascertain the differences of performance in-between each typology measure (Table 7.4). Nonetheless, their differences will be more substantial for lower thicknesses, since there is a minor limitation in the range of thickness for PUR-boards (W1), Perlite boards (W3) and mineral wool (C1) retrofits in both IPCC scenarios and the thermal mortar for scenario 8.5 (Table L.3).

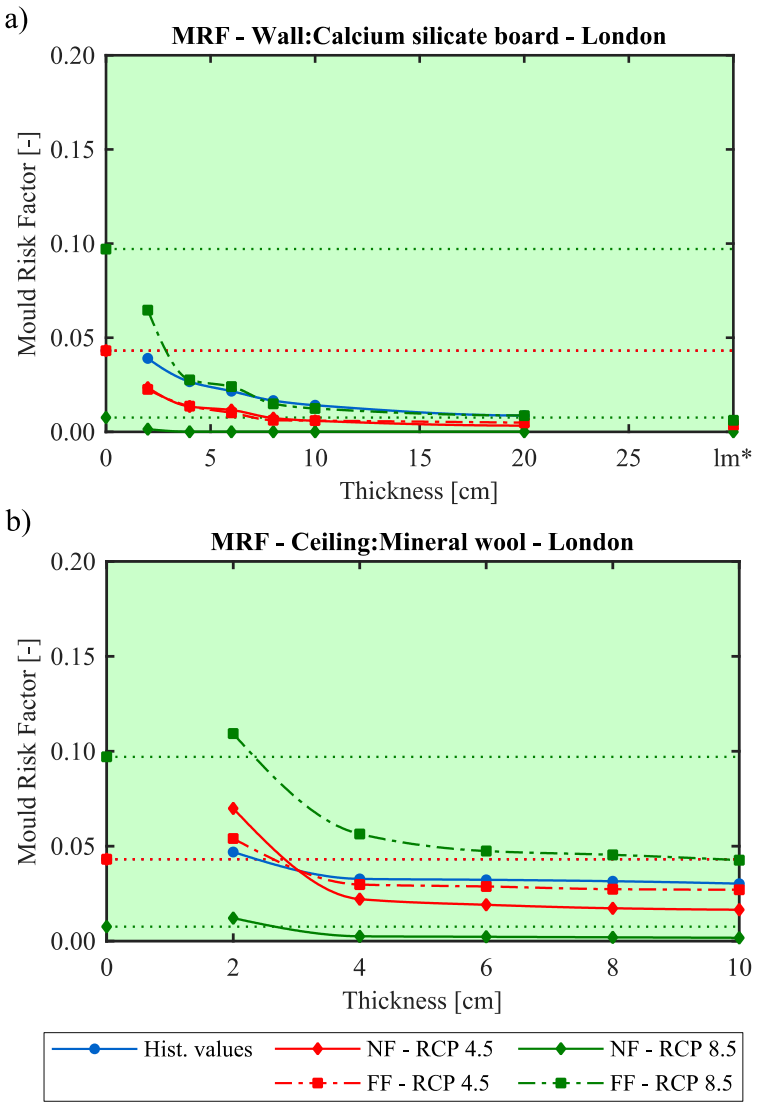

Figure 7.16 – Biological decay assessment using MRF for historical values, near-future and far-future for London for the case-study with calcium silicate boards ranging from 2 to 20 cm (W4) and mineral wool ranging from 2 to 10 cm (C2), and for the case without any retrofit (dotted lines)

Chemical decay

Climate change has the negative impact of decreasing the eLM, this happens mainly due to the increase of the indoor temperature associated to climate change. In fact, the application of any of the selected retrofit measures will intensify this occurrence. However, neither behaviours manage to decrease the eLM enough so that the indoor climate leaves the ideal conditions (e.g. Figure 7.17a for PUR-boards).

This means that although the retrofit measures will not improve the indoor climate in terms of reducing the risk of chemical decay, they can be applied nonetheless, if other aims are pursued, such as increasing the thermal comfort, without endangering chemical susceptible artefacts.

The only detected exception to the decrease of eLM corresponds to the application of mineral wool at lower thicknesses (Figure 7.17b, with the limit ranging from 2.3 to 2.8 cm depending on the analysed IPCC scenarios and time periods). This is belief to be because the insulation layer is still not thick enough to lead to the substantial increase of the indoor temperature, and the decrease of the eLM.

The previously described behaviour will reflect on the recommended thickness in Table L.3, since most cases will not overcome the case without retrofits. Nonetheless, since climate change and the application of the retrofit measures are not sufficient to take out the indoor climate from the ideal condition zone, Table L.4 recommends the full range thicknesses for all cases.

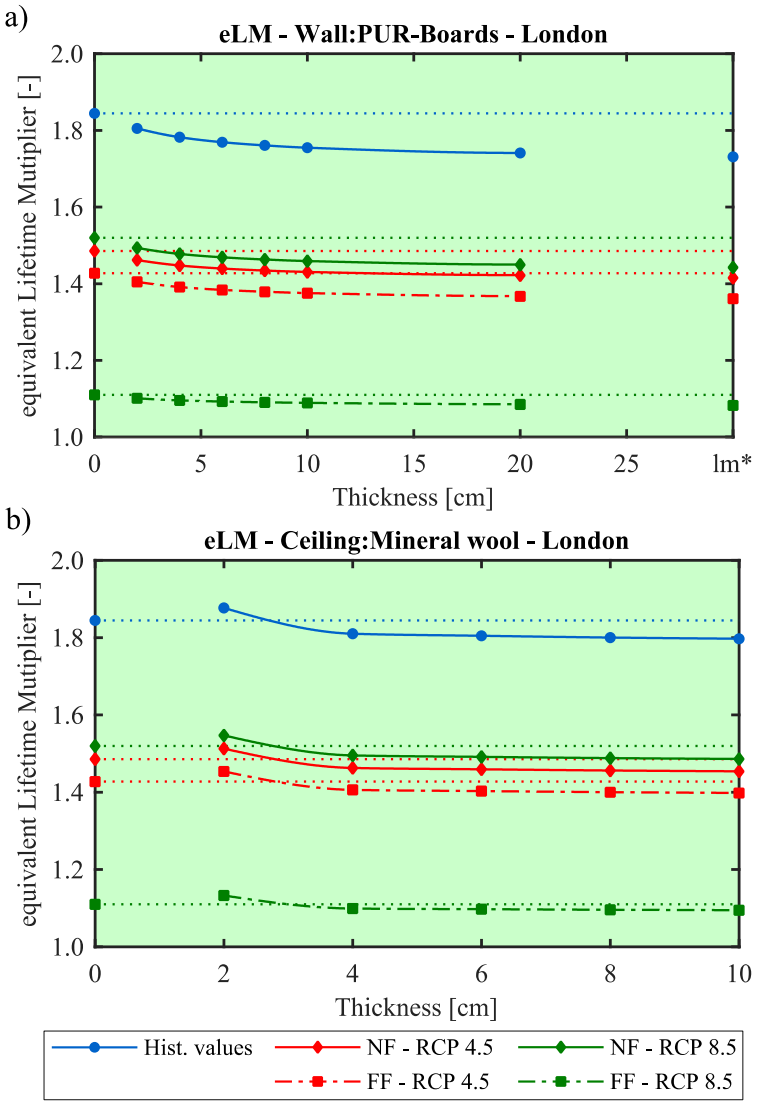

Figure 7.17 – Chemical decay assessment using eLM for historical values, near-future and far-future for London for the case-study with PUR-boards ranging from 2 to 20 cm (W1) and with mineral wool ranging from 2 to 10 cm (C2), and for the case without any retrofit (dotted lines)

Mechanical decay

As it was mentioned for the other types of climate, the furniture assessment does not reveal any risk of mechanical decay neither for present nor for future conditions, thus it will not be further discussed. In addition, climate change has a rather small negative impact on the risk of mechanical decay for sculptures, i.e. under 0.5% for all analysed cases, which is almost neglectable and should not limit the choice of thickness in case of installing any of the studied retrofit measures.

Nonetheless, this impact is mitigated by the application of the selected wall retrofit measures (e.g. Figure 7.18a for PUR-boards), except the thermal mortar that does not manage to increase the number of hours that the indoor climate is in elastic behaviour for RCP 4.5 in the far-future and RCP 8.5 in the near-future (Figure 7.18b). The remaining measures, i.e. roof, ceilings, and windows retrofits, are also not appropriate to reduce this risk (Table 7.4). These occurrences will be reflected on the recommended thicknesses (Table L.3), which are non-existent for RCP 8.5 since this is the most severe scenario.

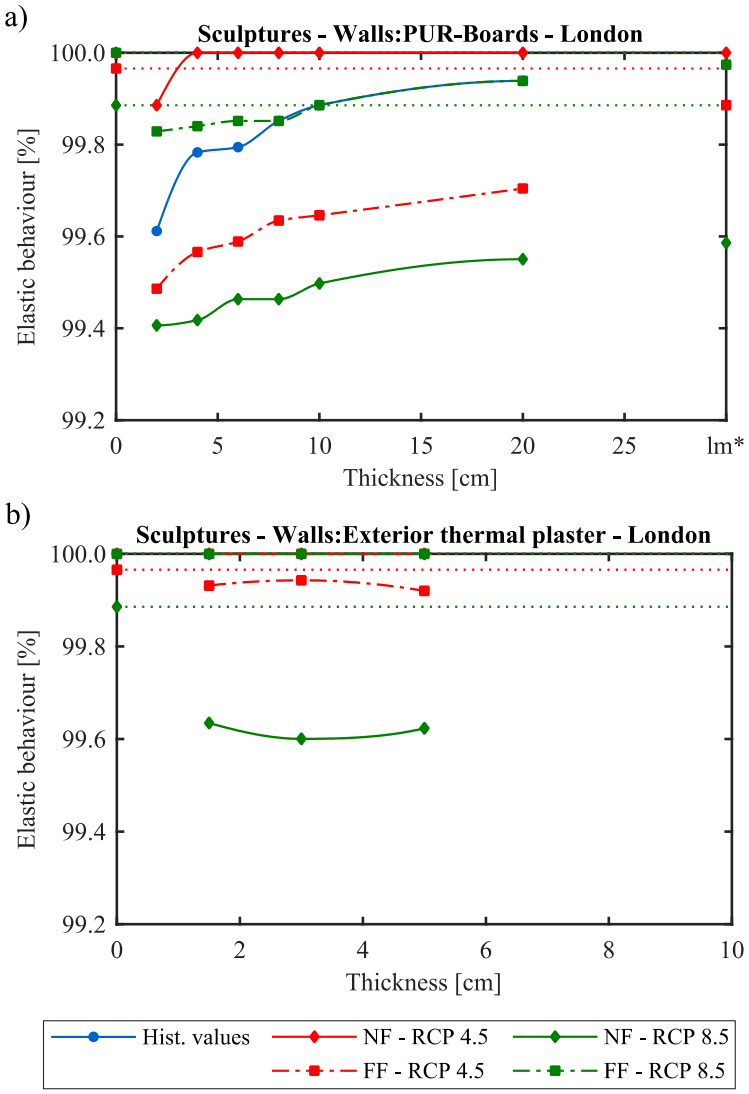

Figure 7.18 – Mechanical risk assessment of sculptures for historical values, near-future and far-future for London for the case-study with PUR-boards ranging from 2 to 20 cm (W1), and with thermal mortar ranging from 1.5 to 5 cm (W5) and for the case without any retrofit (dotted lines)

Climate change also has a substantial negative impact on the welfare of the base layer of panel paintings, since it reduces quite substantially the amount of time that the indoor climate corresponds to elastic behaviour, e.g. the time that the indoor climate corresponds to elastic behaviour for RCP 8.5 in the far-future drops 15 % in relation to the historical values. Fortunately, this effect is also counteracted by the application of the selected retrofit measures (Figure 7.19).

The performance of the selected retrofit measure will vary according to their characteristics. The walls' retrofits have the highest mitigation impact, followed by the roofs' and then the ceilings' retrofits (Table 7.4). The thermal mortar has an interesting mitigation impact since it corresponds to a rather slender layer when compared to the other wall retrofits. Table L.3 recommended the full thickness range for both IPCC scenarios due to the positive outcome of applying the selected retrofits measures in terms of reducing the risk of mechanical decay in the base layer of panel paintings. The only exception is the thermal mortar that has its range of thickness slightly reduced in the near-future.

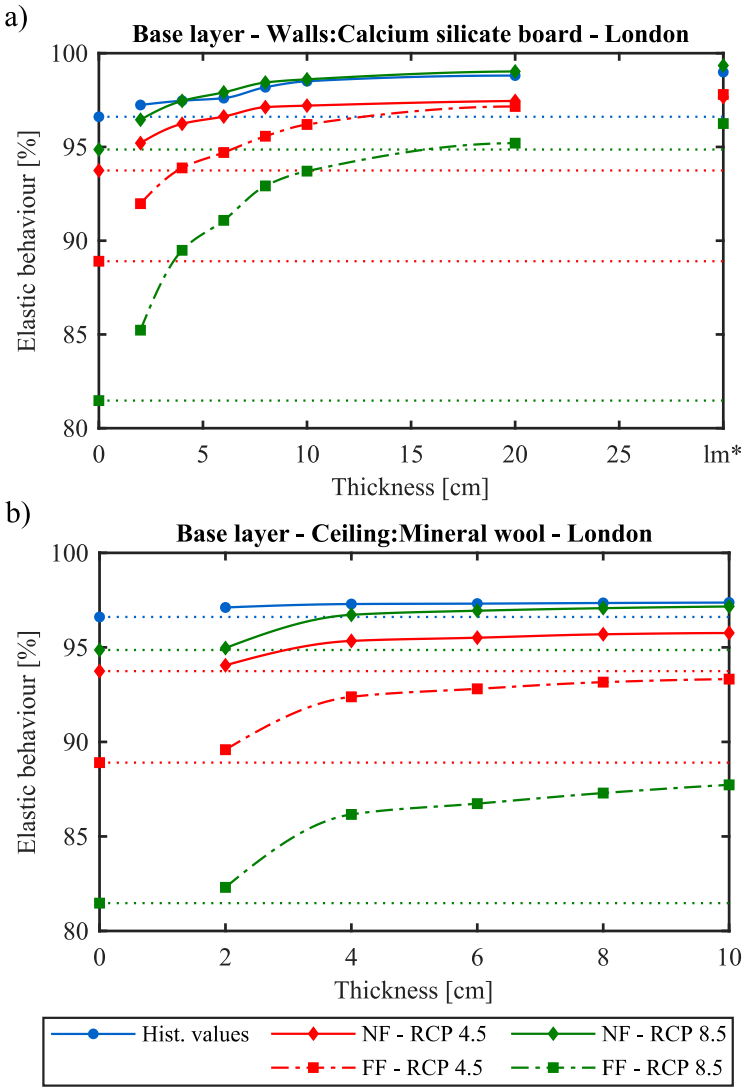

Figure 7.19 – Mechanical risk assessment of base layer (panel paintings) for historic values, near-future and far-future for London for the case-study with calcium silicate board ranging from 2 to 20 cm (W4) and with mineral wool ranging from 2 to 10 cm (C2), and for the case without retrofits (dotted lines)

Climate change also has the effect of increasing the indoor fluctuations in relation to the historical values. This occurs because climate change widens the amplitude between the minimum and maximum indoor temperature [67]. Yet, the application of the selected retrofit measures has the effect of decreasing the fluctuations for most analysed cases (Figure 7.20), which is reasonable since the application of these measures will make the indoor climate less dependent on the variations of the outdoor conditions. In addition, all the analysed cases are below the 14%-limit value, which enables the application of the retrofit measures even if they were responsible for increasing the indoor fluctuations.

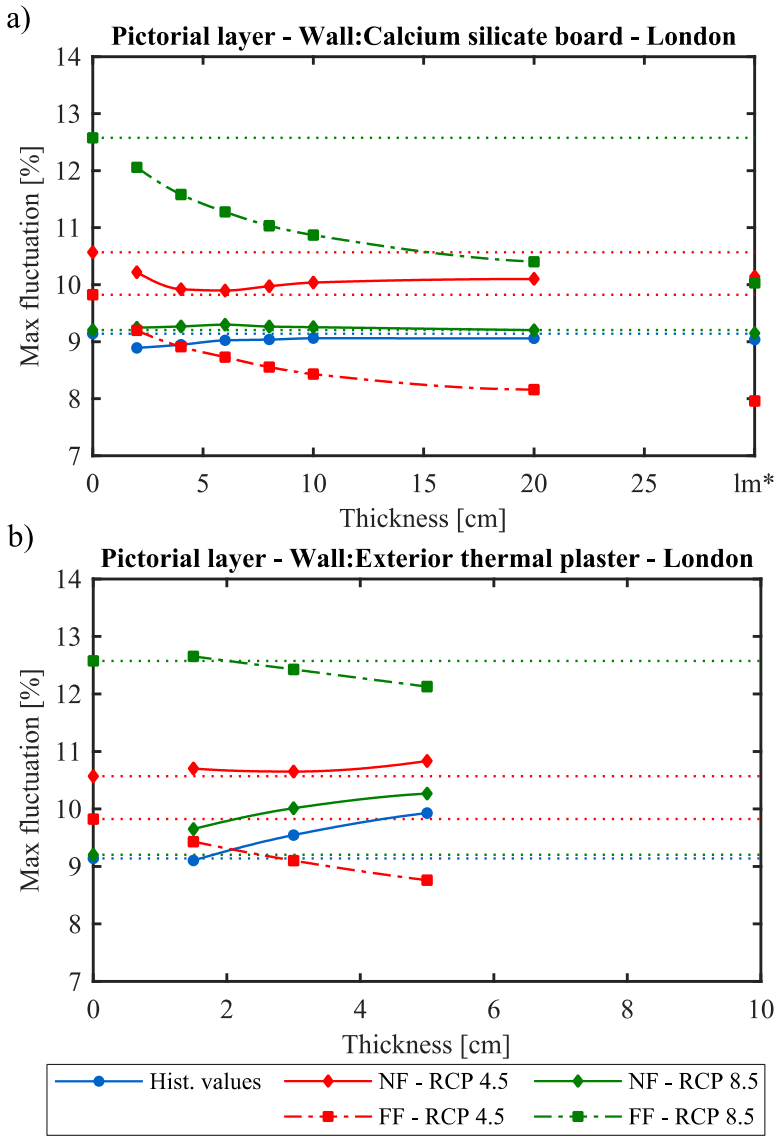

Figure 7.20 – Mechanical risk assessment of the pictorial layer (panel paintings) for historical values, near-future and far-future for London for the case-study with calcium silicate board ranging from 2 to 20 cm (W4) and thermal mortar ranging from 1.5 to 5 cm (W5), and the case without any retrofit (dotted lines)

The performance of each retrofit measure typology will be different. The highest decreases of the indoor fluctuations were obtained by the walls' retrofits, with mineral wool achieving the best results, followed by the ceilings' and then the roofs' retrofits (Table 7.4). The performance of all retrofit measures at near-future for scenario RCP 8.5 is rather worrying since the indoor fluctuations are higher than the case

without retrofits. However, this behaviour is overcome by the walls' retrofits for the thicker layers. This does not occur for the other retrofits (e.g. Figure 7.20b for thermal mortar). This will have consequences in the recommended thicknesses presented in Table L.3, more noticeably for RCP 8.5.

Thermal comfort

The application of the retrofit measures has the expected result in terms of thermal comfort, i.e. it considerably increases the time that the indoor climate is within the limits imposed by ASHRAE 55 (Table 7.4). Consequently, this will reflect on the recommendation of the full range of analysed thicknesses (Table L.3). The only two exceptions are the thermal mortar (W5) and the mineral wool (C2), which are only worth applying from a certain thickness onwards (Table L.3).

The application of the retrofit measures will decrease the variation of the indoor temperature, i.e. it will reduce the maximum temperatures, and increase the minimum temperatures. However, the application of a 2 cm mineral wool layer is not sufficient to compensate the temperature reductions in spring and autumn, which will increase the number of hours that the indoor climate fails to overcome the inferior limit. This does not occur for the PUR-foam since it has a higher thermal conductivity value than mineral wool (Table 7.1). For example, 10 cm of PUR foam has more 43 % thermal resistance than 10 cm of mineral wool.

Table 7.4 – Performance of 10 cm of W1-4, 10 cm of R1-2 and C1-2, and 5 cm of W5 in relation to the case without retrofit for scenario RCP 4.5 in the far-future for London

Climate	Assessment	W1	W2	W3	W4	W5	R1	R2	C1	C2	Wd1
London	MRF	-0.02	-0.03	-0.02	-0.04	0.01	-0.03	-0.03	-0.02	-0.02	0.00
	eLM	-0.05	-0.05	-0.04	-0.04	-0.02	-0.04	-0.04	-0.03	-0.03	0.00
	Sculpture	-0.32	-0.07	-0.23	0.03	-0.05	-0.17	-0.16	-0.18	-0.16	-0.03
	Base layer	7.09	7.63	6.66	7.29	3.66	5.45	5.49	4.53	4.42	1.12
	Pictorial layer	-1.05	-1.55	-1.18	-1.39	-1.06	-0.25	-0.22	-0.46	-0.47	-0.37
	Thermal comfort	6.51	6.12	4.81	5.48	1.77	5.42	5.57	4.32	3.99	0.15

7.4. Conclusions

The aim of this chapter was to test a set of retrofit measures adequate for historic buildings that aimed to improve the indoor climate in terms of conservation metrics whilst considering climate change. A validated whole-building hygrothermal model of a high thermal building was used coupled with outdoor weather files that take climate change into account. The obtained indoor conditions were assessed using a risk-based analysis. The thermal comfort of the visitors was also considered by means of an adaptive model. This study was performed for several climates, namely: Lisbon (Portugal) and Seville (Spain), Prague (Czech Republic) and Oslo (Norway), and London (United Kingdom). Ultimately, it was shown that measures that nowadays have a positive performance may not have one in the future.

The outdoor weather files used in this chapter were created using the methodology recommended by standard EN 15927-4. Since WUFI®Plus needs the global radiation and its diffuse fraction to run

properly, the updated *Skartveit and Olseth* model was used to obtain the diffuse fraction. Lastly, the WAC weather files, i.e. the type of weather files typically used by WUFI®Plus, were created. All these processes were performed using MATLAB, which greatly reduced the amount of time it took to perform each individual activity and, at the same time, guaranteed the quality of the created weather files.

For Mediterranean climates, the application of the selected retrofits measures manages to mitigate, to a certain extent, the negative effects imposed by climate change in terms of artefacts' conservation requirements in historic buildings. The extent of these mitigations varies according to the retrofit measure. The application of calcium silicate board and mineral wool in walls achieved the most impressive results in terms of reducing the risk of biological decay, and mechanical decay in panel paintings – both in terms of the base layer and the pictorial layer. These retrofit measures also improved the thermal comfort. In addition, it was shown that furniture does not limit the building's retrofit in any way, and that sculptures should not condition the building's retrofit, since their drop from the maximum value is only minimal. Lastly, it was observed that the selected retrofit measures are not effective in decreasing the risk of chemical decay.

For Humid continental climates, the main observation based on the several developed assessments was the fact that although the retrofits do not always improve the indoor climate in terms of artefacts conservation, there is a considerable margin for their application in contrast to the Mediterranean climates due to their colder climate. This margin enables the application of the retrofit measures even though they sometimes may reduce the conservation metrics. These retrofit measures will increase the indoor thermal comfort substantially, but they will also improve some of the artefacts' conservation metrics. They will reduce the risk of biological decay, and mechanical decay in sculptures and in the base layer of panel paintings. On the other hand, the retrofit measures will be responsible for the decrease of the equivalent lifetime multiplier (i.e. they will increase the risk of chemical decay). However, this decrease is not sufficient to make the indoor climate leave the ideal conditions zone. In addition, the retrofit measures are also responsible for increasing the indoor fluctuations in most analysed cases.

The oceanic climates also have a margin to implement the retrofits, even if these do not improve the indoor climate in terms of artefacts conservation. In fact, this margin in terms of chemical decay is even bigger than for the humid continental climates since they are not conditioned by the RCP 8.5 scenario in the far-future. The retrofit measures positive impacts will be the increase of the thermal comfort conditions, the reduction of the biological decay risk, the increase of time that the indoor climate corresponds to elastic behaviour for the base layers (panel paintings) and sculptures (for some cases), and the reduction of the indoor fluctuations in some cases. On the other hand, the retrofit measures will be responsible for the decrease of the eLM, but this will not be enough for the indoor climate to leave the ideal conditions zone. Some of these measures will be responsible for decreasing the amount of time that the indoor climate corresponds to elastic behaviour for sculptures, as well as the increase of the indoor fluctuations.

The exterior thermal mortar can be an interesting measure for historic buildings, since it works as a protection layer that limits the variation of the indoor climate. Due to its position it is also responsible for the storage of heat inside the wall, which will decrease the occurrence of interstitial condensation. However, due to the thickness limitation typical of this type of measure, it cannot be applied without additional retrofit measures if they are to reach the same level of proficiency as the other wall retrofit measures. To test the effects of replacing the windows more effectively, another case-study with a higher window/wall ratio should also be used.

8. CONCLUSIONS

The present work consists in the analysis of the use of passive retrofit measures in historic buildings that house artefacts with the aim of mitigating the effects of climate change. The main conclusions of this thesis are presented in subchapter 8.1.The research topics that the author believes are also worth pursuing in the future are presented in subchapter 8.2.

8.1. Final remarks

Literature review

Monitoring campaigns are of great importance since they enable the characterization of a building's indoor climate by means of using sensors and dataloggers. Normally, the used sensors only monitor the indoor conditions (e.g. temperature, relative humidity, indoor pollutants), hence they are based on a non-destructive assessment, which is vital for historic buildings due to their heritage value.

The campaign should last at least one complete year, more if possible, and have a recording frequency of 10/15 minutes so that the indoor climate variability is thoroughly recorded. In addition to the minimum of 12 months recordings, it is advisable to monitor one extra month in order to calculate the seasonal fluctuations, which is based on the concept of the monthly moving average.

A thorough monitoring campaign should use several sensors installed throughout the case-study in locations that are important for the specific study. A preliminary assessment based on a short-term monitorization can be performed to help deciding the locations of the sensors for the long-term monitoring campaign. The sensors should be installed in locations where recordings are not influenced by unwanted sources (e.g. a T&RH sensor should not be installed in the vicinity of a window or else it can be heated due to the radiation that comes through the window). The sensors have to guarantee certain minimum accuracies in accordance with the condition that they measure, so that their results are reliable enough. In addition, the sensors should go through a thorough calibration process prior to installation.

The recorded indoor conditions can be assessed at several levels, namely in terms of thermal comfort (either using an analytical or an adaptive thermal comfort model), in terms of conservation metrics (through a risk-based analysis), or in terms of indoor pollutants, among others.

Due to the key importance that preserving artefacts has in buildings such as museums, the use of a risk-based analysis is of the utmost importance to assess the indoor climate. Usually, this type of analysis is based on damage functions that use the recorded indoor temperature and relative humidity values to determine if the indoor climate is adequate or not to safeguard artefacts. This analysis usually includes the assessment of the risk of biological, chemical and mechanical decay. At a second level of importance, it is also common to assess the indoor climate in terms of thermal comfort, due to the importance that visitors have on the revenues and, therefore, on the continuity of this type of buildings.

The indoor climate of buildings can be largely influenced by the outdoor climate, which is expected to change considerably due to climate change. The overall increase of the air temperature, the decrease of precipitation in the southern region and its increase in the northern region of Europe, the increase of droughts events and extreme precipitation events will significantly affect several regions of Europe.

There is uncertainty on how the world's climate will in fact evolve until the end of the century due to the variability of all parameters that are considered. To mitigate this situation, several scenarios have been developed to encompass the possible ways in which the world's climate can evolve in the future.

It is only natural that these changes will change the indoor climate of buildings, which might put the welfare of the artefacts in danger. Hence, it is necessary to find ways to counteract the negative effects that climate change might have inside buildings. A very useful tool, which allows a thorough analysis of the effects of the selected measures without compromising the building's welfare, is to the develop a computational model based on the monitoring campaign data. As previously mentioned, this procedure is based on a non-destructive methodology, which is of the utmost importance for buildings of great heritage value, as the buildings where museums are usually installed.

The computational model has to go through an extensive validation procedure, so that its results are reliable. Normally, this procedure is based on the comparison between the recorded conditions and the simulated conditions either solely by means of visual comparison, i.e. graphs, or also using several statistical parameters (e.g. coefficient of determination, coefficient of variation of the root mean square error, normalized mean bias error and goodness of fit). The use of several statistical parameters for more than one indoor condition will lead to a more robust validation of the computational model.

In order to counteract the negative effects that climate change can have inside historic buildings that house artefacts several measures, such as the application of passive retrofit measures, can have a positive impact. Moreover, the application of this type of measures also has a very key impact in terms of energy saving potential, more substantial for constant climate control strategies, but also for dynamic strategies. Their effects have to be thoroughly examined prior to application, since untested measures can lead to irrecuperable damages, this being one of the key reasons for developing of computational models.

Whole-building hygrothermal modelling using WUFI

WUFI®Plus is a powerful hygrothermal simulation software that determines the indoor temperature and relative humidity for each zone of the model by taking into consideration the heat and moisture transfer that occurs through components, which is induced by the boundary conditions; the gains/losses due to natural and/or mechanical ventilation and the gains/losses due to internal heat or moisture sources/sinks.

It is one of the most known software where studies concerning the hygrothermal behaviour of buildings have been developed. It has been extensively validated over the years, it is continuously subjected to updates and it accounts for several of the behaviours that affect the thermal and moisture behaviour of

buildings. In order to run a simulation to its fullest, WUFI®Plus needs: basic materials' properties, as well as advanced materials' properties; a complete outdoor weather file; as well as a detailed schedule for the internal sources. Nonetheless, it has same disadvantages, such as the fact that the temperature and relative humidity are constant in each zone or that the hysteresis in the moisture storage function is disregarded.

Developing thorough and accurate hygrothermal studies in WUFI®Plus can be highly time consuming. Hence, several strategies that aim to reduce the amount of time needed to perform large-sized hygrothermal simulation studies were presented. Ultimately, all those strategies were organised in a methodology that makes this type of studies more time-efficient. This allows the use of powerful tools, such as simulation software, to optimize buildings more frequently and straightforwardly.

The used methodology lead to substantial time savings at the several steps that incorporate the typical building simulation studies. By using MATLAB in the simulation setup, a task that would take between 11 to 23 h to perform manually, only takes between 1-3 minutes, i.e. a time saving of almost 100 %. Secondly, dividing the simulations by 20 PCs, the overall simulation time decreased between 34-62 %. This decrease is of key importance since it corresponds to the task that conditions this type of studies, because it is the one that takes longer to complete. Lastly, the data processing using MATLAB also has a substantial time reduction that ranged from ca 51 to almost 100 %, transforming a task that would take hours to complete into a task that can be performed in a matter of seconds. This task duration is greatly dependent on the complexity of the performed analysis. However, since it performs independently from the user, the drawback of its longer duration associated to more complex analysis is somehow lessened.

In addition, the automatic insertion of inputs in WUFI®Plus has a key advantage in simulation studies, i.e. it enables the algorithm to learn with the outputs of WUFI®Plus, and according to the outlined goals, it changes the inputs of the model and then runs more simulations until it overcomes the termination criteria selected by its authors. This procedure can have numerous applications in literature.

Finally, it is the author's belief that the development of hygrothermal simulation studies that include a great number of simulations, should be accompanied by a software that deals with numerical calculation. This is due to the ease that this type of software has in analysing large amounts of data, but also because this type of software can assist on the simulations' setup stage proficiently.

Validation of hygrothermal models of historic buildings

A hygrothermal model of St. Cristóvão church was developed using WUFI®Plus and validated against measured data using four different statistic indices for temperature and water-vapour pressure. The obtained values were then compared with the limits presented in literature and the existing standards/guidelines. The influence of weather files and the interface slab/soil temperature was analysed, and a sensitivity study was carried out to optimise the model accuracy for three undetermined variables – ACH, α and SHGC.

- The developed analysis of the influence of the outdoor conditions in the accuracy of the model showed that the use of weather files for the same city and even files of which the data was monitored during the same year may not lead to the best results. In the developed simulations, the best fit was attained by the weather file that used the temperature and water-vapour pressure obtained by the monitoring campaign.
- The soil and slab interface temperature was also analysed although it is a parameter usually neglected or otherwise not mentioned in the description of many of the thermal and hygrothermal models found in literature. The simulations that were carried out showed the key influence that this parameter has on the hygrothermal behaviour of whole-building models.
- Another difficulty in a model validation is the uncertainties of the inputs. An optimization methodology for the model's accuracy was developed based on three parameters, whose values could not be precisely determined: ACH, α and SHGC. The development of a sensitivity analysis which included 48 simulations allowed to develop an accuracy optimization equation based on the goodness of fit, since it proved to be the most demanding parameter.

In addition, a set of simplifications to hygrothermal models, which might reduce the simulation time considerably, were tested. However, these simplifications can substantially reduce the model's accuracy. Four different simplifications were analysed, but only two were found to be worthy of application, namely, considering a global floor for the funeral home and sacristy, and moving the main door forward. These simplifications allowed to save 16 minutes per simulation while maintaining the level of the model's accuracy, which is quite meaningful when developing a study that includes a large number of simulations.

Impact of climate change on artefacts kept in cultural heritage buildings and the thermal comfort of the visitors

A whole hygrothermal model of a historic building, which was extensively validated against its measured indoor conditions, coupled to climate change weather files is used to quantify how the indoor climate of high thermal inertia buildings is going to change in terms of artefacts' conservation and occupants' thermal comfort due to climate change. The indoor climate was assessed using a thermal comfort model and a risk-based analysis for several types of climate in Europe, namely: Mediterranean, Continental and Oceanic climates.

Based on the performed analysis, both IPCC's selected scenarios (A1B and A2) point to a generalized increase of the indoor temperature, as well as the indoor relative humidity, but at different rates depending on the type of climate. Their variability also increases at different rates, except for the indoor temperature of Oslo and the indoor relative humidity of London which decrease. In turn, these variances will lead to a change in the quality of the indoor climate of historic buildings to house artefacts and they

will also affect the thermal comfort of the building' occupants. The use of the risk based-analysis led to the conclusion that the indoor climate quality to house artefacts worsens:

- The amount of time that the indoor climates conditions surpasses the LIM curve increases in all tested climates. This behaviour is more significant for the Mediterranean climates.
- The equivalent lifetime multiplier significantly decreases for the three types of climate.
- In terms of mechanical decay, it was shown that the base layer of painting panels significantly deteriorates for the three types of climate. Sculptures will also be subjected to mechanical deterioration but to a lower extent.

On the other hand, a slight increase of the thermal comfort conditions occurs, more evident for Oslo, London and Prague, since the indoor temperature also increases. These findings prove that there is an urgent need to adopt appropriate changes in this type of buildings in order to safeguard artefacts, and at the same time to take into account the requirements imposed by the building's visitors.

The impact of climate change in cultural heritage: from energy consumption to artefacts' conservation and building rehabilitation

The energy consumption associated to three of the most used standards/guidelines to limit the indoor climate in buildings that house artefacts was calculated. It was also determined how this consumption will evolve in the future due to climate change and how much it will cost to guarantee each standard/guideline for three types of climate in Europe.

Additionally, four representative passive retrofit measures were tested to determine their energy saving potential. A validated whole-building hygrothermal model of a historic building was used coupled to future weather files based on two IPCC scenarios (A1B and A2). Lastly, the indoor climates were also assessed using a risk-based analysis to assess the risk of artefacts' decay.

- Based on the shown data it is clear that some of the existing methodologies that aim to preserve artefacts will lead to high energy consumption in the future, but there are others in which the opposite occurs. The magnitude of these behaviours varies with the methodology and climate.
- It was shown that for the constant valued methodologies, the key factor for the colder climates is the minimum temperature limit, whilst for the Mediterranean climates is the maximum limit. However, this latter factor will gain even more importance in the future since it is expected that the indoor temperature is going to increase substantially. In contrast, the overall energy costs for the dynamic methodologies will be quite significant for climates like Oslo, Prague and London, mostly due to the minimum temperature limit.
- It was shown that there is a positive outcome of implementing retrofit measures in historic buildings for future conditions in terms of energy saving potential. The application of an interior

insulation achieved the highest saving potential, followed by the exterior thermal plaster, the thermal insulation layer in the ceilings and lastly by replacing the existing windows.

- It was shown, that if passive retrofit measures are combined with a more adequate relative humidity and temperature setpoint strategy the energy savings are even higher.
- The risk-based analysis showed that the retrofit must be thoroughly studied prior to application, since their improvement potential can greatly differ according to the outdoor conditions.

Performance of passive retrofit measures for historic buildings that house artefacts viable for future conditions

A set of retrofit measures adequate for historic buildings that aimed to improve the indoor climate in terms of conservation metrics whilst considering climate change were tested. A validated whole-building hygrothermal model of a high thermal building was used coupled with outdoor weather files that take climate change into account to obtain the future indoor conditions, which were assessed using a risk-based analysis. The thermal comfort was also assessed by means of an adaptive model.

The used outdoor weather files used were created using standard EN 15927-4 methodology. Since WUFI®Plus needs the global radiation and its diffuse fraction to run properly, the updated *Skartveit and Olseth* model was used to obtain the diffuse fraction. This study was performed for several climates, namely: Lisbon and Seville (Mediterranean climates), Prague and Oslo (Humid continental climates), and London (Oceanic climate).

Ultimately, it was shown that measures that nowadays have a positive performance may not have one in the future and that the future risks that historic buildings are going to face in the future will differ in accordance with the climate typology:

- For Mediterranean climates, the retrofits measures manage to mitigate, to a certain extent, the negative effects imposed by climate change in terms of artefacts' conservation requirements. The application of calcium silicate board and mineral wool in walls achieved the most impressive results in terms of reducing the risk of biological decay, and mechanical decay in panel paintings. These retrofit measures also improved the thermal comfort. Furniture does not limit the building's retrofit in any way, and that sculptures should not condition the building's retrofit. The selected retrofit measures are not effective in decreasing the risk of chemical decay.
- For Humid continental climates, the main observation was the fact that although the retrofits do not always improve the indoor climate in terms of artefacts conservation, there is a considerable margin for their application in contrast to the Mediterranean climates. This margin enables the application of the retrofit measures even though they sometimes may reduce the conservation metrics. These retrofit measures will increase the indoor thermal comfort substantially and reduce the risk of biological decay, and mechanical decay in sculptures and in the base layer of

panel paintings. On the other hand, the retrofit measures will be responsible for the decrease of the equivalent lifetime multiplier, but it is not sufficient to make the indoor climate leave the ideal conditions zone, and they will increase the indoor fluctuations in most cases.

- The oceanic climates also have a margin to implement the retrofits. In fact, this margin in terms of chemical decay is even bigger than for the humid continental climates since they are not conditioned by the RCP 8.5 scenario in the far-future. The retrofit measures will increase the thermal comfort conditions, reduce the biological decay risk, increase the time that the indoor climate corresponds to elastic behaviour for the base layers (panel paintings) and sculptures (for some cases), and reduce the indoor fluctuations in some cases. In contrast, the retrofit measures will the decrease the eLM. Some measures will decrease the amount of time that the indoor climate corresponds to elastic behaviour for sculptures and increase the indoor fluctuations.

Exterior thermal mortars can be an interesting measure for historic buildings, since it works as a protection layer that limits the variation of the indoor climate. Due to its position it is also responsible for the storage of heat inside the wall, which will decrease the occurrence of interstitial condensation. However, due to the thickness limitation typical of this type of measure, it cannot be applied without additional retrofit measures if they are to reach the same level of proficiency as the other wall measures.

8.2. Future work

Throughout this thesis there were topics that, due to time constraints, could not be fully addressed. Nonetheless, these topics have scientific relevance and it is the author's belief that they are worthy being developed. The following list highlights some of these topics:

- Multi-objective passive retrofit optimization of historic buildings considering the building's energy consumption, artefacts' conservation, and visitors' thermal comfort requirements
- The study of the influence of artificial lighting and daylight in historic buildings, which house artefacts, by installing a monitoring campaign, and the subsequent development and validation of computational models that account for their influence
- The analysis of the effect of the outdoor pollutants in the indoor climate of historic buildings by installing a multi-sensor monitoring campaign, and the subsequent development and validation of computational models that account for their influence
- The development of a thermal comfort model that include buildings that house artefacts, such as museums and galleries
- The development of maps that present the geographical variance of the following variables:
    - Variance of the conservation metrics (chemical, biological and mechanical risk) of the indoor climate of historic buildings that house artefacts for future conditions

- Variance of the thermal comfort conditions in historic buildings that house artefacts for future conditions
- Energy consumption of historic buildings to guarantee that the indoor climate is adequate for the conservation of artefacts in future conditions
- Improvement potential of retrofit measures appropriate for historic buildings that house artefacts whilst considering climate change

The work developed in this thesis would gain even more validation if this research included other historic buildings with different characteristics, namely size, occupation rates, among other. Hence, in the future additional case-studies should be included, so that this research can become more comprehensive.

REFERENCES

[1] Ali, A.S., Zanzinger, Z., Debose, D., Stephens, B., Open Source Building Science Sensors (OSBSS): A low-cost Arduino-based platform for long-term indoor environmental data collection, Building and Environment. 100 (2016) 114–126. https://doi.org/10.1016/j.buildenv.2016.02.010.

[2] Alliance for Sustainable Energy LLC, OpenStudio - Version 2.3.0, (2017).

[3] Almeida, R.M.S.F., Barreira, E., Moreira, P., Assessing the variability of the air change rate through tracer gas measurements, in: NSB 2017, 2017.

[4] American Society of Heating Refrigerating and Air-Conditioning Engineers, ASHRAE 55:2013, Thermal environmental conditions for human occupancy, (2013).

[5] American Society of Heating Refrigerating and Air-Conditioning Engineers (ASHRAE), ASHRAE Handbook-HVAC Applications, Atlanta, USA, 2015.

[6] American Society of Heating Refrigerating and Air-Conditioning Engineers (ASHRAE), ASHRAE Handbook - Fundamentals, Atlanta, USA, 2013.

[7] American Society of Heating Refrigerating and Air-Conditioning Engineers (ASHRAE), Chapter 9 - Thermal comfort, in: ASHRAE Handbook - Fundamentals, 2013: pp. 173–204.

[8] American Society of Heating Refrigerating and Air-Conditioning Engineers (ASHRAE), ASHRAE Standard 90.1:2010, Energy Standard for Buildings Except Low-Rise Residential Buildings, (2010).

[9] American Society of Heating Refrigerating and Air-Conditioning Engineers (ASHRAE), ANSI/ASHRAE 140-2007. Standard Method of Test for the Evaluation of Building Energy Analysis Computer Programs., (2007).

[10] American Society of Heating Refrigerating and Air-Conditioning Engineers (ASHRAE), ASHRAE Guideline 14:2002, Measurement of Energy and Demand Savings, (2002).

[11] Andarini, R., The Role of Building Thermal Simulation for Energy Efficient Building Design, Energy Procedia. 47 (2014) 217–226. https://doi.org/10.1016/j.egypro.2014.01.217.

[12] Andretta, M., Coppola, F., Seccia, L., Investigation on the interaction between the outdoor environment and the indoor microclimate of a historical library, Journal of Cultural Heritage. 17 (2016) 75–86. https://doi.org/10.1016/j.culher.2015.07.002.

[13] Antretter, F., Kosmann, S., Kilian, R., Holm, A., Ritter, F., Wehle, B., Controlled Ventilation of Historic Buildings: Assessment of Impact on the Indoor Environment via Hygrothermal Building Simulation, in: Springer, Berlin, Heidelberg, 2013: pp. 93–111. https://doi.org/10.1007/978-3-642-31158-1_5.

[14] Antretter, F., Künzel, H., Winkler, M., Pazold, M., Radon, J., Kokolsky, C., Stadler, S., WUFI®Plus – Fundamentals, (2017).

[15] Antretter, F., Mitterer, C., Young, S.M., Use of moisture-buffering tiles for indoor climate stability under different climatic requirements, in: 7th International Conference on Indoor, 2010. https://doi.org/10.1080/10789669.2012.645399.

[16] Antretter, F., Randon, J., Pazold, M., Coupling of Dynamic Thermal Bridge and Whole-Building Simulation, in: Thermal Performance of the Exterior Envelopes of Whole Buildings XII International Conference, 2013.

[17] Antretter, F., Sauer, F., Schöpfer, T., Holm, A., Validation of a hygrothermal whole building simulation software, in: 12th Conference of International Building Performance Simulation Association, Sydney, Australia, 2011: pp. 1694–1701.

[18] Antretter, F., Schöpfer, T., Kilian, R., An approach to assess future climate change effects on indoor climate of a historic stone church, in: 9th Nordic Symposium on Building Physics, 2011.

[19] Antretter, F., Winkler, M., Radon, J., Sadlowska, A., Assessment of a historic church, in: Built Cultural Heritage in Times of Climate Change, 2014: pp. 17–19.

[20] Aries, M., Aarts, M., van Hoof, J., Daylight and health: A review of the evidence and consequences for the built environment, Lighting Research & Technology. 47 (2015) 6–27. https://doi.org/10.1177/1477153513509258.

[21] Ascione, F., Bellia, L., Capozzoli, A., Minichiello, F., Energy saving strategies in air-conditioning for museums, Applied Thermal Engineering. 29 (2009) 676–686. https://doi.org/10.1016/j.applthermaleng.2008.03.040.

[22] Ascione, F., Bianco, N., De Masi, R.F., De'Rossi, F., Vanoli, G.P., Energy retrofit of an educational building in the ancient center of Benevento. Feasibility study of energy savings and respect of the historical value, Energy and Buildings. 95 (2015) 172–183. https://doi.org/10.1016/j.enbuild.2014.10.072.

[23] Ascione, F., Cheche, N., Masi, R.F. De, Minichiello, F., Vanoli, G.P., Design the refurbishment of historic buildings with the cost-optimal methodology: The case study of a XV century Italian building, Energy and Buildings. 99 (2015) 162–176. https://doi.org/10.1016/j.enbuild.2015.04.027.

[24] Ascione, F., Minichiello, F., Microclimatic control in the museum environment: Air diffusion performance, International Journal of Refrigeration. 33 (2010) 806–814. https://doi.org/10.1016/j.ijrefrig.2009.12.017.

[25] Ascione, F., De Rossi, F., Vanoli, G.P., Energy retrofit of historical buildings: Theoretical and experimental investigations for the modelling of reliable performance scenarios, Energy and Buildings. 43 (2011) 1925–1936. https://doi.org/10.1016/j.enbuild.2011.03.040.

[26] Aste, N., Torre, S. Della, Adhikari, R.S., Buzzetti, M., Del Pero, C., Leonforte, F., Manfren, M., Sustainable church heating: The Basilica di Collemaggio case-study, Energy and Buildings. 116 (2016) 218–231. https://doi.org/10.1016/j.enbuild.2016.01.008.

[27] Awbi, H.B., Ventilation of buildings, 2nd ed., Taylor & Francis, 2003.

[28] De Backer, L., Janssens, A., Steeman, M., De Paepe, M., Evaluation of display conditions of the Ghent altarpiece at St. Bavo Cathedral, Journal of Cultural Heritage. 29 (2018) 168–172. https://doi.org/10.1016/j.culher.2017.08.002.

[29] Balocco, C., Calzolari, R., Natural light design for an ancient building: A case study, Journal of Cultural Heritage. 9 (2008) 172–178. https://doi.org/10.1016/j.culher.2007.07.007.

[30] Balocco, C., Marmonti, E., Energy and Sustainability in Museums. The Plant Refurbishment of the Medieval Building of Palagio di Parte Guelfa in Florence, Open Journal of Energy Efficiency. 01 (2012) 31–47. https://doi.org/10.4236/ojee.2012.13004.

[31] Barclay, M., Holcroft, N., Shea, A.D., Methods to determine whole building hygrothermal performance of hemp–lime buildings, Building and Environment. 80 (2014) 204–212. https://doi.org/10.1016/j.buildenv.2014.06.003.

[32] Barreira, E., Simões, M.L., Delgado, J.M.P.Q., Sousa, I., Procedures in the construction of a test reference year for Porto-Portugal and implications for hygrothermal simulation, Sustainable Cities and Society. 32 (2017) 397–410. https://doi.org/10.1016/j.scs.2017.04.013.

[33] Basto, C., Pelà, L., Chacón, R., Open-source digital technologies for low-cost monitoring of historical constructions, Journal of Cultural Heritage. 25 (2017) 31–40. https://doi.org/10.1016/j.culher.2016.12.003.

[34] Bellia, L., Capozzoli, A., Mazzei, P., Minichiello, F., A comparison of HVAC systems for artwork conservation, International Journal of Refrigeration. 30 (2007) 1439–1451. https://doi.org/10.1016/j.ijrefrig.2007.03.005.

[35] Bencs, L., Spolnik, Z., Limpens-Neilen, D., Schellen, H.L., Jütte, B.A.H.G., Van Grieken, R., Comparison of hot-air and low-radiant pew heating systems on the distribution and transport of gaseous air pollutants in the mountain church of Rocca Pietore from artwork conservation points of view, Journal of Cultural Heritage. 8 (2007) 264–271. https://doi.org/10.1016/j.culher.2007.05.001.

[36] Bergman, T.L., Incropera, F.P., Introduction to heat transfer, John Wiley & Sons, 2011.

[37] Bertolin, C., Camuffo, D., Bighignoli, I., Past reconstruction and future forecast of domains of

indoor relative humidity fluctuations calculated according to EN 15757:2010, Energy and Buildings. 102 (2015) 197–206. https://doi.org/10.1016/j.enbuild.2015.05.028.

[38] Bertolin, C., Luciani, A., Valisi, L., Camuffo, D., Landi, A., Del Curto, D., Laboratory tests for the evaluation of the heat distribution efficiency of the Friendly-Heating heaters, Energy and Buildings. 107 (2015) 319–328. https://doi.org/10.1016/j.enbuild.2015.08.003.

[39] Bichlmair, S., Kilian, R., Room climate in Linderhof Palace: impact of ambient climate and visitors on room climate with a special focus on the bedchamber of King Ludwig II, in: Developments in Climate Control of Historic Buildings, 2011: pp. 49–55.

[40] Bichlmair, S., Kilian, R., Krus, M., Sedlbauer, K., Building simulation modelling of the historic building Linderhof Palace taking account visitors, in: Proceedings of ESim 2012: The Canadian Conference on Building Simulation, 2012: pp. 296–309.

[41] Big Ladder - Engineering Reference - EnergyPlus 8.3, https://bigladdersoftware.com/ (accessed December 2020), (n.d.).

[42] Bishara, A., Plagge, R., Chapter 5 - Energy efficiency solutions, in: Energy Efficiency Solutions for Historic Buildings, 2015: pp. 120–195.

[43] Blecich, P., Franković, M., Kristl, Ž., Energy retrofit of the Krsan Castle: From sustainable to responsible design—A case study, Energy and Buildings. 122 (2016) 23–33. https://doi.org/10.1016/j.enbuild.2016.04.011.

[44] Bratasz, L., Kozlowski, R., Kozlowska, A., Rivers, S., Conservation of the Mazarin Chest: structural response of Japanese lacquer to variations in relative humidity, 15th Triennial Conference, New Delhi, 22-26 September 2008: Preprints/ICOM Committee for Conservation NV - 8 Figs. (2 Color), Refs. II (2008) 1086–1093.

[45] Bratasz, Ł., Kozłowski, R., Lasyk, Ł., Allowable microclimatic variations for painted wood: numerical modelling and direct tracing of the fatigue damage, ICOM CC 16th. (2011).

[46] Bratasz, Ł., Camuffo, D., KozŁowski, R., Target microclimate for preservation derived from past indoor conditions, in: Museum Microclimates, T. Padfield & K. Borchersen (Eds.), National Museum of Denmark, 2007: pp. 129–134.

[47] Bratasz, Ł., Kozłowski, R., Camuffo, D., Pagan, E., Impact of Indoor Heating on Painted Wood - Monitoring the Altarpiece in the Church of Santa Maria Maddalena in Rocca Pietore, Italy, Studies in Conservation. 52 (2007) 199–210. https://doi.org/10.1179/sic.2007.52.3.199.

[48] British Standards Institution (BSi), Pas 198:2012, Specification for Managing Environmental Conditions for Cultural Collections, (2012).

[49] Burhenne, S., Radon, J., Pazold, M., Herkel, S., Antretter, F., Integration of HVAC models into a hygrothermal whole building simulation tool, in: 12th Conference of International Building Performance Simulation Association, 2011: pp. 1777–1783.

[50] Calheiros, T., Dias, L., Marreiros, S., Lourenço, T.C., Santos, F.D., Carvalho, S., Climate synthesis - Lisbon (in Portuguese), in: Manual Para a Avaliação de Vulnerabilidades Futuras, 2016: p. 4.

[51] Camuffo, D., Microclimate for Cultural Heritage: Conservation, Restoration, and Maintenance of Indoor and Outdoor Monuments, 2nd Ed., Elsevier, New York, USA, 2014.

[52] Camuffo, D., Bertolin, C., Bonazzi, A., Campana, F., Merlo, C., Past, present and future effects of climate change on a wooden inlay bookcase cabinet: A new methodology inspired by the novel European Standard EN 15757:2010, Journal of Cultural Heritage. 15 (2014) 26–35. https://doi.org/10.1016/j.culher.2012.12.005.

[53] Camuffo, D., Brimblecombe, P., Van Grieken, R., Busse, H.-J., Sturaro, G., Valentino, A., Bernardi, A., Blades, N., Shooter, D., De Bock, L., Gysels, K., Wieser, M., Kim, O., Indoor air quality at the Correr Museum, Venice, Italy, Science of The Total Environment. 236 (1999) 135–152. https://doi.org/10.1016/S0048-9697(99)00262-4.

[54] Camuffo, D., Pagan, E., Rissanen, S., Bratasz, Ł., Kozłowski, R., Camuffo, M., della Valle, A., An advanced church heating system favourable to artworks: A contribution to European standardisation, Journal of Cultural Heritage. 11 (2010) 205–219.

https://doi.org/10.1016/j.culher.2009.02.008.

[55] Camuffo, D., Sturaro, G., Valentino, A., Thermodynamic exchanges between the external boundary layer and the indoor microclimate at the Basilica of Santa Maria Maggiore, Rome, Italy: The problem of conservation of ancient works of art, Boundary-Layer Meteorology. 92 (1999) 243–262. https://doi.org/10.1023/A:1002026711404.

[56] Carrier Air Conditioning Company, Handbook of Air Conditioning System Design, McGraw-Hill, New York, USA, 1965.

[57] Chaudhary, G., New, J., Sanyal, J., Im, P., O'Neill, Z., Garg, V., Evaluation of "Autotune" calibration against manual calibration of building energy models, Applied Energy. 182 (2016) 115–134. https://doi.org/10.1016/j.apenergy.2016.08.073.

[58] Christensen, J.E., Kollias, C.G., Hygrothermal evaluation of a museum storage building based on actual measurements and simulations, Energy Procedia. 78 (2015) 651–656. https://doi.org/10.1016/j.egypro.2015.11.051.

[59] Cirami, S., Evola, G., Gagliano, A., Margani, G., Thermal and Economic Analysis of Renovation Strategies for a Historic Building in Mediterranean Area, Buildings. 7 (2017) 60. https://doi.org/10.3390/buildings7030060.

[60] Ciulla, G., Galatioto, A., Ricciu, R., Energy and economic analysis and feasibility of retrofit actions in Italian residential historical buildings, Energy and Buildings. 128 (2016) 649–659. https://doi.org/10.1016/j.enbuild.2016.07.044.

[61] Clarke, L., Edmonds, J., Jacoby, H., Pitcher, H., Reilly, J., Richels, R., Scenarios of Greenhouse Gas Emissions and Atmospheric Concentrations. Sub-Report 2.1a of Synthesis and Assessment Product 2.1 by the U.S. Climate Change Science Program and the Subcommittee on Global Change Research, Department of Energy, Office of Biolog, (2007).

[62] ClimAdapPT Project, http://climadapt-local.pt/(accessed January 2019), (n.d.).

[63] Climate Change - SPM, Synthesis Report - Summary for Policymakers (SPM). Contribution of Working Groups I, II and III to the Fifth Assessment Report of the Intergovernmental Panel on Climate Change [Core Writing Team, R.K. Pachauri and L.A. Meyer (eds.)], (2014). https://doi.org/10.1017/CBO9781107415324.

[64] Coelho, G.B.A., Optimization of historic buildings that house artefacts for future conditions (Research Proposal), FCT-UNL, 2020.

[65] Coelho, G.B.A., Henriques, F.M.A., Influence of driving rain on the hygrothermal behavior of solid brick walls, Journal of Building Engineering. (2016). https://doi.org/10.1016/j.jobe.2016.06.002.

[66] Coelho, G.B.A., Silva, H.E., Henriques, F.M.A., Calibrated hygrothermal simulation models for historical buildings, Building and Environment. 142 (2018) 439–450. https://doi.org/10.1016/j.buildenv.2018.06.034.

[67] Coelho, G.B.A., Silva, H.E., Henriques, F.M.A., Impact of climate change on cultural heritage: a simulation study to assess the risks for conservation and thermal comfort, International Journal of Global Warming. 19 (2019) 382. https://doi.org/10.1504/IJGW.2019.104268.

[68] Coelho, G.B.A., Silva, H.E., Henriques, F.M.A., Development of a hygrothermal model of a historic building in WUFI®Plus vs EnergyPlus, in: 4th Central European Symposium on Building Physics (CESBP 2019), Prague, Czech Republic, 2019. https://doi.org/10.1051/matecconf/201928202079.

[69] Coelho, G.B.A., Silva, H.E., Henriques, F.M.A., Impact of climate change in cultural heritage: from energy consumption to artefacts' conservation and building rehabilitation, Energy and Buildings. (2020) 110250. https://doi.org/10.1016/j.enbuild.2020.110250.

[70] Coordinated Regional Climate Downscaling Experiment (CORDEX), https://esgf-data.dkrz.de/search/cordex-dkrz/ (accessed January 2019), (n.d.).

[71] Coordinated Regional Climate Downscalling Experiment (CORDEX), http://www.cordex.org/ (accessed January 2019), (n.d.).

[72] Cornaro, C., Puggioni, V.A., Strollo, R.M., Dynamic simulation and on-site measurements for

energy retrofit of complex historic buildings: Villa Mondragone case study, Journal of Building Engineering. 6 (2016) 17–28. https://doi.org/10.1016/j.jobe.2016.02.001.

[73] de Dear, R., Brager, G.S., Cooper, D., Developing an adaptive model of thermal comfort and preference - Final Report on RP-884, 1997.

[74] Delgado, J.M.P.Q., Ramos, N.M.M., Barreira, E., de Freitas, V.P., A critical review of hygrothermal models used in porous building materials, Journal of Porous Media. 13 (2010) 221–234. https://doi.org/10.1615/jpormedia.v13.i3.30.

[75] Delgado, J.M.P.Q., Barreira, E., Ramos, N.M.M., de Freitas, V.P., Hygrothermal Numerical Simulation Tools Applied to Building Physics, Springer Berlin Heidelberg, Berlin, Heidelberg, 2013. https://doi.org/10.1007/978-3-642-35003-0.

[76] Design Building - Software, https://designbuilder.co.uk/software/product-overview (accessed December 2020), (n.d.).

[77] Druzik, J.R., Michalski, S.W., Guidelines for Selecting Solid-State Lighting for Museums, (2012) 59.

[78] Duffie, J.A., Beckman, W.A., Solar Engineering of Thermal Processes, 4th ed., John Wiley & Sons, Inc., 2013.

[79] E3M-Lab, EU Reference Scenario 2016: Energy, transport and GHG emissions Trends to 2050, Directorate-General for Energy, (2016) 1–221. https://doi.org/10.2833/9127.

[80] Efficiency Valuation Organization, International Performance Measurement and Verification Protocol: Concepts and Options for Determing Energy and Water Savings Vol 1, (2002).

[81] EnergyPlus, EnergyPlus - Version 8.8.0, U.S. Department of Energy's (DOE) - Building Technologies Office (BTO), (2017).

[82] EnergyPlus - Documentation, https://energyplus.net/documentation (accessed December 2020), (n.d.).

[83] EnergyPlus - Weather Data, EnergyPlus - Weather Data, https://energyplus.net/weather (accessed January 2020), (n.d.).

[84] Ente Nazionale Italiano di Unificazione (UNI), UNI 10829:1999, Beni di interesse storico e artistico - Condizioni ambientali di conservazione - Misurazione ed analisi, (1999).

[85] Ente Nazionale Italiano di Unificazione (UNI), UNI 10586:1997, Condizioni climatiche per ambienti di conservazione di documenti grafici e caratteristiche degli alloggiamenti, (1997).

[86] Erhardt, D., Antretter, F., Applicability of regional model climate data for hygrothermal building simulation and climate change impact on the indoor enviroment of a generic church in Europe, in: EWCHP, 2011.

[87] Erhardt, D., Antretter, F., Kilian, R., Measured and Modeled Influence of the Moisture Buffer Effect in a Historic Stone Church and its Influence on Possible HVAC Measures, in: Clima 2013, 2013.

[88] European Commission, Climate strategies & targets, https://ec.europa.eu/clima/policies/strategies/2020_en (accessed February 2020), (n.d.).

[89] European Commitee for Standardization (CEN), EN ISO 15927-4:2005, Hygrothermal performance of buildings - Calculation and presentation of climatic data - Part 4: Hourly data for assessing the annual energy use for heating and cooling, (2005) 16.

[90] European Committee for Standardization (CEN), EN 15757:2010, Conservation of Cultural Property - Specifications for temperature and relative humidity to limit climate-induced mechanical damage in organic hygroscopic materials, (2010).

[91] European Committee for Standardization (CEN), EN 15758:2010, Conservation of cultural property. Procedures and instruments for measuring temperatures of the air and the surfaces of objects, European Committee for Standardization (CEN), (2010) 19.

[92] European Committee for Standardization (CEN), EN 16242:2012, Conservation of cultural heritage - Procedures and instruments for measuring humidity in the air and moisture exchanges between air and cultural property, (2012).

[93] European Committee for Standardization (CEN), EN ISO 13788:2012 Hygrothermal performance of building components and building elements - Internal surface temperature to avoid critical surface humidity and interstitial condensation Calculation methods, European Committee for Standardization (CEN), (2012).

[94] European Committee for Standardization (CEN), EN ISO 13370:2007, Thermal performance of buildings - Heat transfer via the ground - Calculation methods, (2007).

[95] European Committee for Standardization (CEN), EN 13779:2007, Ventilation for non-residential buildings - Performance requirements for ventilation and room-conditioning systems, (2007).

[96] European Committee for Standardization (CEN), CEN/TS 16163:2014, Conservation of Cultural Heritage - Guidelines and procedures for choosing appropriate lighting for indoor exhibitions, (2014).

[97] European Committee for Standardization (CEN), EN 12464-1:2011, Light and lighting - Lighting of work places - Part 1: Indoor work places, (2011).

[98] European Committee for Standardization (CEN), EN 14501:2005, Blinds and shutters - Thermal and visual comfort - Performance characteristics and classification, (2005).

[99] European Committee for Standardization (CEN), EN 13363-1:2003+A1, Solar protection devices combined with glazing - Calculation of solar and light transmittance - Part 1: Simplified method, (2007).

[100] European Committee for Standardization (CEN), EN 13363-2:2005, Solar protection devices combined with glazing - Calculation of solar and light transmittance - Part 2: Detailed calculation method, (2005).

[101] Eurostat, Emissions of greenhouse gases and air pollutants from final use of CPA08 products - input-output analysis, https://appsso.eurostat.ec.europa.eu/nui/show.do?dataset=env_ac_io10&lang=en (accessed in September 2019), (n.d.).

[102] Eurostat - Electricity prices for non-household consumers - bi-annual data (from 2007 onwards), https://ec.europa.eu/eurostat/web/energy/data/database?p_p_id=NavTreeportletprod_WAR_NavTreeportletprod_INSTANCE_QAMy7Pe6HwI1&p_p_lifecycle=0&p_p_state=normal&p_p_mode=view&p_p_col_id=column-2&p_p_col_count=1 (accessed November 2019), (n.d.).

[103] Eurostat - Energy statistics - electricity prices for domestic and industrial consumers, price components, https://ec.europa.eu/eurostat/cache/metadata/en/nrg_pc_204_esms.htm (accessed November 2019), (n.d.). https://ec.europa.eu/eurostat/cache/metadata/en/nrg_pc_204_esms.htm.

[104] Evola, G., Marletta, L., Natarajan, S., Maria Patanè, E., Thermal inertia of heavyweight traditional buildings: experimental measurements and simulated scenarios, Energy Procedia. 133 (2017) 42–52. https://doi.org/10.1016/j.egypro.2017.09.369.

[105] Fabbri, K., Pretelli, M., Heritage buildings and historic microclimate without HVAC technology: Malatestiana Library in Cesena, Italy, UNESCO Memory of the World, Energy and Buildings. 76 (2014) 15–31. https://doi.org/10.1016/j.enbuild.2014.02.051.

[106] Fanger, P.O., Thermal comfort. Analysis and applications in environmental engineering., Danish Technical Press, Copenhagen, Denmark, 1970.

[107] Federal Energy Management Program (FEMP), M&V Guidelines: Measurement and Verification for Performance-Based Contracts - Version 4.0, (2015) 1–108.

[108] Ferdyn-Grygierek, J., Indoor environment quality in the museum building and its effect on heating and cooling demand, Energy and Buildings. 85 (2014) 32–44. https://doi.org/10.1016/j.enbuild.2014.09.014.

[109] Ferdyn-Grygierek, J., Monitoring of indoor air parameters in large museum exhibition halls with and without air-conditioning systems, Building and Environment. 107 (2016) 113–126. https://doi.org/10.1016/j.buildenv.2016.07.024.

[110] Ferdyn-Grygierek, J., Baranowski, A., Internal environment in the museum building—

Assessment and improvement of air exchange and its impact on energy demand for heating, Energy and Buildings. 92 (2015) 45–54. https://doi.org/10.1016/j.enbuild.2015.01.033.

[111] Ferreira, C., de Freitas, V.P., Ramos, N.M.M., Quantifying the Influence of Hygroscopic Materials in the Fluctuation of Relative Humidity in Museums Housed in Old Buildings, in: 10th Nordic Symposium on Building Physics, 2014: pp. 600–607.

[112] Frasca, F., Siani, A.M., Casale, G.R., Pedone, M., Bratasz, Strojecki, M., Mleczkowska, A., Assessment of indoor climate of Mogiła Abbey in Kraków (Poland) and the application of the analogues method to predict microclimate indoor conditions, Environmental Science and Pollution Research. 24 (2017) 13895–13907. https://doi.org/10.1007/s11356-016-6504-9.

[113] Fraunhofer Institue for Building Physics, WUFI 4.2 - PRO, (2008).

[114] de Freitas, V.P., Abrantes, V., Crausse, P., Moisture Migration in Building Walls - Analysis of the Interface Phenomena, Building and Environment. 31 (1996) 99–108. https://doi.org/10.1016/0360-1323(95)00027-5.

[115] de Freitas, V.P., Torres, M.I., Guimarães, A.S., Rising damp (in Portuguese), 1st ed., FEUP, Porto, 2008.

[116] Fujino, J., Nair, R., Kainuma, M., Masui, T., Matsuoka, Y., Multi-gas Mitigation Analysis on Stabilization Scenarios Using Aim Global Model Author (s): Junichi Fujino , Rajesh Nair , Mikiko Kainuma , Toshihiko Masui and Yuzuru Matsuoka Source : The Energy Journal , Vol . 27 , Special Issue : Multi-Greenhouse Gas, The Energy Journal. 27 (2006) 343–353.

[117] García-Diego, F.-J., Fernández-Navajas, Á., Beltrán, P., Merello, P., Study of the Effect of the Strategy of Heating on the Mudejar Church of Santa Maria in Ateca (Spain) for Preventive Conservation of the Altarpiece Surroundings, Sensors. 13 (2013) 11407–11423. https://doi.org/10.3390/s130911407.

[118] García-Diego, F.J., Zarzo, M., Microclimate monitoring by multivariate statistical control: The renaissance frescoes of the Cathedral of Valencia (Spain), Journal of Cultural Heritage. 11 (2010) 339–344. https://doi.org/10.1016/j.culher.2009.06.002.

[119] Giuseppe, E. Di, D'Orazio, M., Favi, C., Rossi, M., Lasvaux, S., Padey, P., Favre, D., Wittchen, K., Du, G., Nielsen, A., Blumberga, A., Kamendere, E., Report and tool: Probability based Life Cycle Impact Assessment, Robust Internal Thermal Insulation of Historic Buildings (RIBuild project) - Project nr 637268, 2019.

[120] Grondzik, W.T., Kwok, A.G., Mechanical and Electrical Equipment for Buildings, 12th ed., John Wiley & Sons, Inc., 2014.

[121] Henriques, F.M.A., Quantification of wind driven rain. An experimental approach, Building Research & Information. 20 (1992) 295–297. https://doi.org/10.1080/09613219208727227.

[122] Henriques, F.M.A., O Clima de Portugal, in: Comportamento Higrotérmico de Edifícios, FCT-UNL, Monte de Caparica, 2013: pp. 285–312.

[123] Henriques, F.M.A., Comportamento Higrotérmico de Edifícios, Monte de Caparica, 2016.

[124] Hijioka, Y., Matsuoka, Y., Nishimoto, H., Masui, T., Kainuma, M., Global GHG emission scenarios under GHG concentration stabilization targets, Journal of Global Environmental Engineering. 13 (2008) 97–108.

[125] Holm, A.H., Antretter, F., Kilian, R., Ritter, F., Wehle, B., Controlled Ventilation of Historic Buildings - Assessment of Impact on the Indoor Environment via Hygrothermal Building Simulation, in: 12th International Conference on Durability of Building Materials and Components, Porto, Portugal, 2011: pp. 923–930.

[126] Holm, A., Kuenzel, H.M., Sedlbauer, K., The Hygrothermal Behaviour of Rooms : Combining Thermal Building Simulation and Hygrothermal Envelope Calculation, in: Eighth International IBPSA Conference, Eindhoven, Netherlands, 2003: pp. 499–506.

[127] Houghton, J.T., Filho, L.G.M., Callander, B.A., Harris, N., Kattenberg, A., Maskell, K., Climate Change 1995: The Science of Climate Change, Contribution of WGI to the Second Assessment Report of the Intergovernmental Panel on Climate Change, Press Syndicate of the University of Cambridge, New York, USA, and University Press, Cambridge, UK, 1995.

[128] Huijbregts, Z., Kramer, R.P., Martens, M.H.J., van Schijndel, A.W.M., Schellen, H.L., A proposed method to assess the damage risk of future climate change to museum objects in historic buildings, Building and Environment. 55 (2012) 43–56. https://doi.org/10.1016/j.buildenv.2012.01.008.

[129] Huijbregts, Z., Martens, M.H.J., Conen, C.M.H., Nugteren, I.M., van Schijndel, A.W.M., Schellen, H.L., Damage risk assessment of museum objects in historic buildings due to shifting climate zones in Europe, in: Proceedings of the 5th International Building Physics Conference, Kyoto, 28-31 May 2012, 2012: pp. 1271–1278.

[130] Huijbregts, Z., Martens, M.H.J., van Schijndel, A.W.M., Schellen, H.L., The use of computer simulation models to evaluate the risks on damage to objects exposed to varying indoor climate conditions in the past, present, and future, in: Proceedings of the 2nd Central European Symposium on Building Physics, 2013: pp. 335–342.

[131] Huijbregts, Z., Schellen, H., van Schijndel, J., Ankersmit, B., Modelling of heat and moisture induced strain to assess the impact of present and historical indoor climate conditions on mechanical degradation of a wooden cabinet, Journal of Cultural Heritage. 16 (2015) 419–427. https://doi.org/10.1016/j.culher.2014.11.001.

[132] Intergovernmental Panel on Climate Change (IPCC), IPCC, 2007: Climate Change 2007: Synthesis Report. Contribution of Working Groups I, II and III to the Fourth Assessment Report of the Intergovernmental Panel on Climate Change [Core Writing Team, Pachauri, R.K and Reisinger, A. (eds.)], (2007) 104. https://doi.org/10.1256/004316502320517344.

[133] Intergovernmental Panel on Climate Change (IPCC), IPCC, 2014, Climate Change 2014: Synthesis Report. Contribution of Working Groups I, II and III to the Fifth Assessment Report of the Intergovernmental Panel on Climate Change [Core Writing Team, R.K. Pachauri and L.A. Meyer (eds.)]., (2014) 151. https://doi.org/10.1017/CBO9781107415324.

[134] Intergovernmental Panel on Climate Change (IPCC), Emissions Scenarios - Summary for Policymakers, (2000) 1–27.

[135] Intergovernmental Panel on Climate Change (IPCC), IPCC, 2001: Climate Change 2001: The Scientific Basis. Contribution of Working Group I to the Third Assessment Report of the Intergovernmental Panel on Climate Change [Houghton, J.T., Y. Ding, D.J. Griggs, M. Noguer, P.J. van der Linden, X. Dai, K. Maskel, (2001) 881. https://doi.org/10.1016/S1058-2746(02)86826-4.

[136] International Commission on Illumination (CIE), CIE 157:2004, Control of damage to museum objects by optical radiation, (2004) 35.

[137] International Organization for Standardization (ISO), ISO 7730:2005, Ergonomics of the thermal environment - Analytical determination and interpretation of thermal comfort using calculation of the PMV and PPD indices and local thermal comfort criteria, (2005).

[138] International Organization for Standardization (ISO), ISO 15927-3:2009 - Hygrothermal performance of buildings - Calculation and presentation of climatic data -- Part 3: Calculation of a driving rain index for vertical surfaces from hourly wind and rain data, (2009) 17.

[139] International Organization for Standardization (ISO), ISO 12571:2013 (E) - Hygrothermal performance of building materials and products - Determination of hygroscopic sorption properties, 2013.

[140] International Organization for Standardization (ISO), ISO 8996:2004, Ergonomics of the thermal environment — Determination of metabolic rate, (2004).

[141] IPCC website - Reports, IPCC website - Reports, https://www.ipcc.ch/reports/(accessed March 2020), (n.d.).

[142] IPMA - Climate normals - 1971-2000 for Geofisico station in Lisbon, https://www.ipma.pt/en/oclima/normais.clima/1971-2000/#535 (accessed February 2020), (n.d.).

[143] Iqbal, M., An Introduction to Solar Radiation, Academic Press, 1983.

[144] Jakieła, S., Bratasz, Kozłowski, R., Numerical modelling of moisture movement and related

stress field in lime wood subjected to changing climate conditions, Wood Science and Technology. 42 (2008) 21–37. https://doi.org/10.1007/s00226-007-0138-5.

[145] Janssen, H., Christensen, J.E., Hygrothermal optimisation of museum storage spaces, Energy and Buildings. 56 (2013) 169–178. https://doi.org/10.1016/j.enbuild.2012.08.043.

[146] Jones, F.E., Harris, G.L., ITS-90 density of water formulation for volumetric standards calibration, Journal of Research of the National Institute of Standards and Technology. 97 (1992) 335. https://doi.org/10.6028/jres.097.013.

[147] Karami, M., McMorrow, G.V., Wang, L., Continuous monitoring of indoor environmental quality using an Arduino-based data acquisition system, Journal of Building Engineering. 19 (2018) 412–419. https://doi.org/10.1016/j.jobe.2018.05.014.

[148] Karyono, T., Sri, E., Sulistiawan, J., Triswanti, Y., Thermal Comfort Studies in Naturally Ventilated Buildings in Jakarta, Indonesia, Buildings. 5 (2015) 917–932. https://doi.org/10.3390/buildings5030917.

[149] Kilian, R., Broström, T., Ashley-Smith, J., Schellen, H., Martens, M., Antretter, F., Winkler, M., Bertolin, C., Camuffo, D., Leissner, J., Holl, K., Maas-Diegeler, G., Wittstadt, K., Tornari, V., The Climate for Culture method for assessing future risks resulting from indoor climate in historic buildings, in: 3rd Cultural Heritage PreservationCultural Heritage Preservation, 2013.

[150] Kim, S., Zirkelbach, D., Künzel, H.M., Lee, J.H., Choi, J., Development of test reference year using ISO 15927-4 and the influence of climatic parameters on building energy performance, Building and Environment. 114 (2017) 374–386. https://doi.org/10.1016/j.buildenv.2016.12.037.

[151] Köppen, W., Klassifikation der Klimate nach Temperatur, Niederschlag und Jahresablauf (Classification of climates according to temperature, precipitation and seasonal cycle), Petermanns Geogr. Mitt. 64 (1918) 193–203.

[152] Kosmann, S., Antretter, F., Kilian, R., The Gate Hall of Lorsch – Comprehensive Assessment Methods to calibrate Simulation Models and adapt Conservation Strategies, in: Clima, 2013.

[153] Kottek, M., Grieser, J., Beck, C., Rudolf, B., Rubel, F., World Map of the Köppen-Geiger climate classification updated, Meteorologische Zeitschrift. 15 (2006) 259–263. https://doi.org/10.1127/0941-2948/2006/0130.

[154] Kramer, R.P., Maas, M.P.E., Martens, M.H.J., van Schijndel, A.W.M., Schellen, H.L., Energy conservation in museums using different setpoint strategies: A case study for a state-of-the-art museum using building simulations, Applied Energy. 158 (2015) 446–458. https://doi.org/10.1016/j.apenergy.2015.08.044.

[155] Kramer, R.P., van Schijndel, J., Schellen, H., Dynamic setpoint control for museum indoor climate conditioning integrating collection and comfort requirements: Development and energy impact for Europe, Building and Environment. 118 (2017) 14–31. https://doi.org/10.1016/j.buildenv.2017.03.028.

[156] Kramer, R.P., van Schijndel, A.W.M., Schellen, H.L., The importance of integrally simulating the building, HVAC and control systems, and occupants' impact for energy predictions of buildings including temperature and humidity control: validated case study museum Hermitage Amsterdam, Journal of Building Performance Simulation. 10 (2017) 272–293. https://doi.org/10.1080/19401493.2016.1221996.

[157] Kramer, R.P., van Schijndel, J., Schellen, H., Dynamic setpoint control for museum indoor climate conditioning integrating collection and comfort requirements: Development and energy impact for Europe, Energy Procedia. 118 (2017) 14–31. https://doi.org/10.1016/j.buildenv.2017.03.028.

[158] Kramer, R.P., Schellen, H.L., van Schijndel, J.W., Towards Adaptive Temperature Limits for museums: a building simulation study for four fictive museum zones with different quality of building envelopes, in: Proceedings Healthy Buildings Europe, Eindhoven, Netherlands, 2015.

[159] Kramer, R., Schellen, H., van Schijndel, J., Energy Impact of ASHRAE's Museum Climate Classes: A Simulation Study on Four Museums with Different Quality of Envelopes, Energy

Procedia. 78 (2015) 1317–1322. https://doi.org/10.1016/j.egypro.2015.11.147.

[160] Kramer, R., van Schijndel, J., Schellen, H., Inverse modeling of simplified hygrothermal building models to predict and characterize indoor climates, Building and Environment. 68 (2013) 87–99. https://doi.org/10.1016/j.buildenv.2013.06.001.

[161] Krus, M., Moisture transport and storage coefficients of porous mineral building materials: Theoretical principles and new test methods (PhD thesis), Fraunhofer IRB Verlag, Stuttgart, 1996.

[162] Krus, M., Rösler, D., Klemm, L., Hygrothermal Simulations of Energy-saving Measures to Stabilize the Internal Environment of an Archive Depot, in: Clima, 2013.

[163] Künzel, H.M., Simultaneous Heat and Moisture Transport in Building Components One- and two-dimensional calculation using simple parameters (PhD thesis), University of Stuttgart, 1995.

[164] Kusuda, T., Achenbach, P.R., Earth Temperatures and Thermal Diffusivity at Selected Stations in the United States, in: ASHRAE Transactions, 1965: pp. 61–74.

[165] labEEE - Laboratório de Eficiência Energética em Edificações, https://labeee.ufsc.br/ (accessed December 2020), (n.d.).

[166] Lanini, F., Division of Global Radiation into Direct Radiation and Diffuse Radiation (MSc dissertation), Faculty of Science, University of Bern, 2010.

[167] Lankester, P., Brimblecombe, P., The impact of future climate on historic interiors, Science of The Total Environment. 417–418 (2012) 248–254. https://doi.org/10.1016/j.scitotenv.2011.12.026.

[168] Lara, R.A., Naboni, E., Pernigotto, G., Cappelletti, F., Zhang, Y., Barzon, F., Gasparella, A., Romagnoni, P., Optimization Tools for Building Energy Model Calibration, Energy Procedia. 111 (2017) 1060–1069. https://doi.org/10.1016/j.egypro.2017.03.269.

[169] Leccese, F., Cagnetti, M., Calogero, A., Trinca, D., Pasquale, S., Giarnetti, S., Cozzella, L., A New Acquisition and Imaging System for Environmental Measurements: An Experience on the Italian Cultural Heritage, Sensors. 14 (2014) 9290–9312. https://doi.org/10.3390/s140509290.

[170] Lee, E.S., An Improved Hydronic Loop System Solution Algorithm with a Zone-Coupled Horizontal Ground Heat Exchanger Model for Whole Building Energy Simulation (PhD thesis), Oklahoma State University, Stillwater, United States, 2013.

[171] legnér, M., On the Early History of Museum Environment Control - Nationalmuseum and Gripsholm Castle in Sweden, c.1866-1932, Studies in Conservation. 56 (2011) 125–137. https://doi.org/10.1179/sic.2011.56.2.125.

[172] Leissner, J., Kilian, R., Kotova, L., Jacob, D., Mikolajewicz, U., Broström, T., Smith, J.A., Schellen, H.L., Martens, M., Schijndel, J. Van, Antretter, F., Winkler, M., Bertolin, C., Camuffo, D., Simeunovic, G., Vyhlídal, T., Climate for Culture : assessing the impact of climate change on the future indoor climate in historic buildings using simulations, Heritage Science. (2015) 1–15. https://doi.org/10.1186/s40494-015-0067-9.

[173] Liu, G., Liu, M., A rapid calibration procedure and case study for simplified simulation models of commonly used HVAC systems, Building and Environment. 46 (2011) 409–420. https://doi.org/10.1016/j.buildenv.2010.08.002.

[174] LNEG - Climates-SCE - Climatic data for the Portuguese Building Certification System, https://www.lneg.pt/servicos/328/2263/ (accessed January 2020), (n.d.).

[175] Lucchi, E., Review of preventive conservation in museum buildings, Journal of Cultural Heritage. 29 (2018) 180–193. https://doi.org/10.1016/j.culher.2017.09.003.

[176] Maia, J., Ramos, N.M.M., Veiga, R., Evaluation of the hygrothermal properties of thermal rendering systems, Building and Environment. 144 (2018) 437–449. https://doi.org/10.1016/j.buildenv.2018.08.055.

[177] Markopoulos, A., Conservation of cultural heritage in the UK, in: Built Cultural Heritage in Times of Climate Change, 2014: pp. 24–26.

[178] Martens, M., Climate risk assessment in museums: degradation risks determined from

temperature and relative humidity data (PhD thesis), Technische Universiteit Eindhoven, Eindhoven, 2012. https://doi.org/10.6100/IR729797.

[179] Martínez-Molina, A., Tort-Ausina, I., Cho, S., Vivancos, J.-L., Energy efficiency and thermal comfort in historic buildings: A review, Renewable and Sustainable Energy Reviews. 61 (2016) 70–85. https://doi.org/10.1016/j.rser.2016.03.018.

[180] Matias, L.M.C., Development of an adaptive model for defining the thermal comfort conditions in Portugal (PhD thesis in Portuguese), Instituto Superior Técnico, Universidade Técnica de Lisboa (IST-UL), 2010.

[181] Mecklenburg, M.F., Tumosa, C.S., Erhardt, D., Structural response of painted wood surfaces to changes in ambient relative humidity, Painted Wood: History and Conservation. (1998) 464–483.

[182] Mecklenburg, M.F., Determining the acceptable ranges of relative humidity and temperature in museums and galleries. Part 2, Structural Response to Relative Humidity, Smithsonian Institute. (2007) 1–29. https://doi.org/10.1103/PhysRevB.90.165140.

[183] MediaWorkstations, a-X – AMD Threadripper Workstation for CPU and GPU Rendering, https://www.mediaworkstations.net/systems/amd-workstations/a-x/ (accessed September 2020), (n.d.).

[184] Mesas-Carrascosa, F., Verdú Santano, D., Meroño de Larriva, J., Ortíz Cordero, R., Hidalgo Fernández, R., García-Ferrer, A., Monitoring Heritage Buildings with Open Source Hardware Sensors: A Case Study of the Mosque-Cathedral of Córdoba, Sensors. 16 (2016) 1620. https://doi.org/10.3390/s16101620.

[185] Meteonorm, Version 7, Meteotest Genossenschaft, (2014).

[186] Michalski, S., Double the life for each five-degree drop, more than double the life for each halving of relative humidity, in: Thirteenth Triennial Meeting ICOM-CC, Rio de Janeiro, 22-27 September 2002, 2002: pp. 66–72.

[187] Michalski, S., Agent of Deterioration: Incorrect Temperature (accessed in October 2018), (n.d.). https://www.canada.ca/en/conservation-institute/services/agents-deterioration/temperature.html.

[188] Michalski, S., Agent of Deterioration: Incorrect Relative Humidity (accessed in October 2018), (n.d.). https://www.canada.ca/en/conservation-institute/services/agents-deterioration/humidity.html.

[189] Mikofski, M., Solar Position Calculator, https://www.mathworks.com/matlabcentral/fileexchange/58405-solar-position-calculator?s_tid=prof_contriblnk (accessed June 2019), (n.d.).

[190] Milone, D., Peri, G., Pitruzzella, S., Rizzo, G., Are the Best Available Technologies the only viable for energy interventions in historical buildings?, Energy and Buildings. 95 (2015) 39–46. https://doi.org/10.1016/j.enbuild.2014.11.004.

[191] Mleczkowska, A., Strojecki, M., Bratasz, Ł., Kozłowski, R., Particle penetration and deposition inside historical churches, Building and Environment. 95 (2016) 291–298. https://doi.org/10.1016/j.buildenv.2015.09.017.

[192] Mleczkowska, A., Strojecki, M., Bratasz, Ł., Kozłowski, R., The effect of ventilation on soiling by particles of outdoor and indoor origin in historical churches, Building Simulation. 10 (2017) 383–393. https://doi.org/10.1007/s12273-016-0335-y.

[193] Muñoz-González, C.M., León-Rodríguez, A.L., Navarro-Casas, J., Air conditioning and passive environmental techniques in historic churches in Mediterranean climate. A proposed method to assess damage risk and thermal comfort pre-intervention, simulation-based, Energy and Buildings. 130 (2016) 567–577. https://doi.org/10.1016/j.enbuild.2016.08.078.

[194] Muñoz-González, C.M., León-Rodríguez, A.L., Campano-Laborda, M., Teeling, C., Baglioni, R., The assessment of environmental conditioning techniques and their energy performance in historic churches located in Mediterranean climate, Journal of Cultural Heritage. (2018). https://doi.org/10.1016/j.culher.2018.02.012.

[195] Mustafaraj, G., Chen, J., Lowry, G., Development of room temperature and relative humidity linear parametric models for an open office using BMS data, Energy and Buildings. 42 (2010) 348–356. https://doi.org/10.1016/j.enbuild.2009.10.001.

[196] Nakicenovic, N., Alcamo, J., Davis, G., Vries, B. de, Fenhann, J., Gaffin, S., Gregory, K., Griibler, A., Jung, T.Y., Kram, T., Rovere, E.L. La, Michaelis, L., Mori, S., Morita, T., Pepper, W., Pitcher, H., Price, L., Riahi, K., Roehrl, A., Rogner, H.-H., Sankovski, A., Schlesinger, M., Shukla, P., Smith, S., Swart, R., Rooijen, S. van, Victor, N., Dadi, Z., Special Report on Emissions Scenarios - A Special Report of Working Group III of the Intergovernmental Panel on Climate Change, Cambridge University Press, 2000.

[197] Nishimura, D.W., Understanding Preservation Metrics, Image Permanence Institute (IPI). (2007) 11.

[198] NOAA ESRL - Solar Calculator Glossary (Azimuth/Elevation/Zenith figure), https://www.esrl.noaa.gov/gmd/grad/solcalc/azelzen.gif (accessed June 2019), (n.d.).

[199] NOAA ESRL - Solar Geometry Calculator, https://www.esrl.noaa.gov/gmd/grad/antuv/SolarCalc.jsp (accessed June 2019), (n.d.).

[200] NORDTEST, NT BUILD 481 - Building materials: retention curve and pore size distribution, 1997.

[201] OECD stat, Greenhouse gas emissions, https://stats.oecd.org/Index.aspx?DataSetCode=AIR_GHG# (accessed February 2020), (n.d.).

[202] Official Journal of the European Union, Directive 2008/50/EC of the European Parliament and of the Council of 21 May 2008 on ambient air quality and cleaner air for Europe, (2008).

[203] Ornelas, C., Guedes, J.M., Breda-Vázquez, I., Cultural built heritage and intervention criteria: A systematic analysis of building codes and legislation of Southern European countries, Journal of Cultural Heritage. 20 (2016) 725–732. https://doi.org/10.1016/j.culher.2016.02.013.

[204] Özisik, M., Heat transfer: a basic apporach, McGraw-Hill, 1990.

[205] Padfield, T., Exploring the limits for passive indoor climate control, Contribution to the Experts' Roundtable on Sustainable Climate Management Strategies, Held in April 2007, in Tenerife, Spain. (2008) 1–12.

[206] Paris Agreement, https://unfccc.int/process-and-meetings/the-paris-agreement/the-paris-agreement (accessed August 2020), (n.d.).

[207] Pavlogeorgatos, G., Environmental parameters in museums, Building and Environment. 38 (2003) 1457–1462. https://doi.org/10.1016/S0360-1323(03)00113-6.

[208] Pazold, M., Antretter, F., Radon, J., HVAC Models coupled with hygrothermal building simulation software, in: 10th Nordic Symposium on Building, 2014: pp. 854–863. https://doi.org/10.1002/bapi.200710011.

[209] Pereira, P.F., Ramos, N.M.M., Almeida, R.M.S.F., Lurdes, M., Barreira, E., Occupant influence on residential ventilation patterns in mild climate conditions, in: NSB 2017, n.d.

[210] Pérez-Lombard, L., Ortiz, J., Pout, C., A review on buildings energy consumption information, Energy and Buildings. 40 (2008) 394–398. https://doi.org/10.1016/j.enbuild.2007.03.007.

[211] Perez, R., Ineichen, P., Seals, R., Michalsky, J., Stewart, R., Modeling daylight availability and irradiance components from direct and global irradiance, Solar Energy. 44 (1990) 271–289. https://doi.org/10.1016/0038-092X(90)90055-H.

[212] Pernetti, R., Prada, A., Baggio, P., On the influence of several parameters in energy model calibration: the case of a historical building, IBPSA Italy. (2013) 263–272.

[213] Pisello, A.L., Castaldo, V.L., Pignatta, G., Cotana, F., Integrated numerical and experimental methodology for thermal-energy analysis and optimization of heritage museum buildings, Building Services Engineering Research and Technology. 37 (2016) 334–354. https://doi.org/10.1177/0143624415609910.

[214] PORDATA - Resident population: total and by large age groups (in Portuguese), https://www.pordata.pt/Municipios/Popula%C3%A7%C3%A3o+residente+total+e+por+grand

es+grupos+et%C3%A1rios-390 (accessed February 2020), (n.d.).

[215] QualAR - More about the project (in Portuguese), https://qualar.apambiente.pt/node/acerca-do-projeto (accessed February 2020), (n.d.).

[216] QualAR - Online database on air quality (in Portuguese), https://qualar1.apambiente.pt/qualar/index.php?page=5 (accessed February 2020), (n.d.).

[217] Radon, J., Antretter, F., Sadlowska, A., Lukomski, M., Bratasz, L., Simulation of energy consumption for dehumidification with cooling in National Museum in Krakow, in: 3rd European Workshop on Cultural Heritage Preservation (EWCHP), 2013: pp. 227–233.

[218] Rajčić, V., Skender, A., Damjanović, D., An innovative methodology of assessing the climate change impact on cultural heritage, International Journal of Architectural Heritage. 12 (2017) 1–15. https://doi.org/10.1080/15583058.2017.1354094.

[219] RCP Databse - version 2.0.5, https://www.iiasa.ac.at/web-apps/tnt/RcpDb/dsd?Action=htmlpage&page=compare# (accessed March 2020), (n.d.).

[220] Rea, M.S., The IESNA Lighting Handbook: Reference & Application, Illuminating Engineering Society of North America (IESNA), 2000.

[221] Remund, J., Müller, S., Kunz, S., Huguenin-Landl, B., Studer, C., Klauser, D., Schilter, C., Meteonorm - Global meteorological database - Handbook Part I: Software, (2014) 1–58.

[222] Riahi, K., and Nakicenovic, N. (eds), Greenhouse Gases - Integrated Assessment, Technological Forecasting and Social Change, Special Issue, (2007) 234. https://doi.org/0040-1625.

[223] Ridley, B., Boland, J., Lauret, P., Modelling of diffuse solar fraction with multiple predictors, Renewable Energy. 35 (2010) 478–483. https://doi.org/10.1016/j.renene.2009.07.018.

[224] Roberti, F., Oberegger, U.F., Gasparella, A., Calibrating historic building energy models to hourly indoor air and surface temperatures: Methodology and case study, Energy and Buildings. 108 (2015) 236–243. https://doi.org/10.1016/j.enbuild.2015.09.010.

[225] Roberti, F., Oberegger, U.F., Lucchi, E., Troi, A., Energy retrofit and conservation of a historic building using multi-objective optimization and an analytic hierarchy process, Energy and Buildings. 138 (2017) 1–10. https://doi.org/10.1016/j.enbuild.2016.12.028.

[226] Rocha, B., Influence of climate control strategies and the impact of visitors on the conservation of cultural heritage (MSc dissertation), FCT-UNL, 2017.

[227] Rode, C., Woloszyn, M., Whole-Building Hygrothermal Modeling in IEA Annex 41, in: Thermal Performance of the Exterior Envelopes of Whole Buildings: Buildings X, American Society of Heating, Refrigerating and Air-Conditioning Engineers (ASHRAE), 2007.

[228] Ryhl-Svendsen, M., Indoor air pollution in museums: prediction models and control strategies, Studies in Conservation. 51 (2006) 27–41. https://doi.org/10.1179/sic.2006.51.Supplement-1.27.

[229] Sabbioni, C., Brimblecombe, P., Cassar, M., The Atlas of Climate Change Impact on European Cultural Heritage: Scientific Analysis and Management Strategies, Anthem Press, 2012.

[230] Sadłowska-Sałęga, A., Radoń, J., Sobczyk, J., Wąs, K., Influence of microclimate control scenarios on energy consumption in the Gallery of the 19th-Century Polish Art in the Sukiennice (the former Cloth Hall) of The National Museum in Krakow, IOP Conference Series: Materials Science and Engineering. 415 (2018) 012026. https://doi.org/10.1088/1757-899X/415/1/012026.

[231] Şahin, C.D., Arsan, Z.D., Tunçoku, S.S., Broström, T., Akkurt, G.G., A transdisciplinary approach on the energy efficient retrofitting of a historic building in the Aegean Region of Turkey, Energy and Buildings. 96 (2015) 128–139. https://doi.org/10.1016/j.enbuild.2015.03.018.

[232] Sahin, C.D., Coşkun, T., Arsan, Z.D., Gökçen Akkurt, G., Investigation of indoor microclimate of historic libraries for preventive conservation of manuscripts. Case Study: Tire Necip Paşa Library, İzmir-Turkey, Sustainable Cities and Society. 30 (2017) 66–78. https://doi.org/10.1016/j.scs.2016.11.002.

[233] Samek, L., De Maeyer-Worobiec, A., Spolnik, Z., Bencs, L., Kontozova, V., Bratasz, Ł., Kozłowski, R., Van Grieken, R., The impact of electric overhead radiant heating on the indoor

environment of historic churches, Journal of Cultural Heritage. 8 (2007) 361–369. https://doi.org/10.1016/j.culher.2007.03.006.

[234] Samuel, D.G.L., Nagendra, S.M.S., Maiya, M.P., Passive alternatives to mechanical air conditioning of building: A review, Building and Environment. 66 (2013) 54–64. https://doi.org/10.1016/j.buildenv.2013.04.016.

[235] Santos, C.A.P. dos, Matias, L., U-value of building envelope elements (in Portuguese) - ITE 50, 20th ed., LNEC, Lisbon, Portugal, 2014.

[236] Santos, C.A.P. dos, Rodrigues, R., Thermal transmittance of building envelope opaque elements. Construction solutions for old buildings. Construction solutions adopted in the Autonomous Regions of Portugal (in Portuguese) – ITE 54, 6th ed., LNEC, Lisbon, Portugal, 2012.

[237] Sardella, A., Palazzi, E., von Hardenberg, J., Del Grande, C., De Nuntiis, P.D., Sabbioni, C., Bonazza, A., Risk mapping for the sustainable protection of cultural heritage in extreme changing environments, Atmosphere. 11 (2020) 1–11. https://doi.org/10.3390/atmos11070700.

[238] Scenario process for AR5 - Purpose and audiance, D.D.C., https://sedac.ciesin.columbia.edu/ddc/ar5_scenario_process/index.html (accessed March 2020), (n.d.).

[239] Scenario process for AR5 - Scenario process overview, D.D.C., https://sedac.ciesin.columbia.edu/ddc/ar5_scenario_process/scenario_overview.html (accessed March 2020), (n.d.).

[240] Schellen, H., Heating Monumental Churches Indoor Climate and Preservation of Cultural Heritage (PhD thesis), Technische Universiteit Eindhoven, 2002. https://doi.org/10.6100/IR561673.

[241] Schito, E., Testi, D., Integrated maps of risk assessment and minimization of multiple risks for artworks in museum environments based on microclimate control, Building and Environment. 123 (2017) 585–600. https://doi.org/10.1016/j.buildenv.2017.07.039.

[242] Schmidt, S., Lindauer, M., Hoppe, M., Comparing TRNSYS and WUFI®Plus simulation models-illustrated on models validated on measurements at Schack-Gallery Munich, in: 5th IBPC, Kyoto, Japan, 2012.

[243] Sciurpi, F., Carletti, C., Cellai, G., Pierangioli, L., Environmental monitoring and microclimatic control strategies in “La Specola” museum of Florence, Energy and Buildings. 95 (2015) 190–201. https://doi.org/10.1016/j.enbuild.2014.10.061.

[244] Sedlbauer, K., Prediction of mould fungus formation on the surface of and inside building components (PhD thesis), Fraunhofer Institute for Building Physics, 2001.

[245] Semprini, G., Galli, C., Farina, S., Reuse of an ancient church: thermal aspect for integrated solutions, Energy Procedia. 133 (2017) 327–335. https://doi.org/10.1016/J.EGYPRO.2017.09.395.

[246] Sileo, M., Gizzi, F.T., Masini, N., Low cost monitoring approach for the conservation of frescoes: The crypt of St. Francesco d’Assisi in Irsina (Basilicata, Southern Italy), Journal of Cultural Heritage. 23 (2017) 89–99. https://doi.org/10.1016/j.culher.2016.11.011.

[247] Silva, H.E., Indoor climate management on cultural heritage buildings: Climate control strategies, cultural heritage management and hygrothermal rehabilitation (PhD thesis), Faculdade de Ciências e Tecnologia, Universidade NOVA de Lisboa (FCT-UNL), 2019.

[248] Silva, H.E., Coelho, G.B.A., Henriques, F.M.A., Climate monitoring in World Heritage List buildings with low-cost data loggers: The case of the Jerónimos Monastery in Lisbon (Portugal), Journal of Building Engineering. 28 (2020) 101029. https://doi.org/10.1016/j.jobe.2019.101029.

[249] Silva, H.E., Coelho, G.B.A., Rocha, B., Henriques, F.M.A., Impacto dos visitantes na conservação do património cultural em Portugal, in: Construção 2018 - Reabilitar e Construir de Forma Sustentável, Porto, Portugal, 2018: pp. 1432–1441.

[250] Silva, H.E., Henriques, F.M.A., Microclimatic analysis of historic buildings: A new methodology for temperate climates, Building and Environment. 82 (2014) 381–387. https://doi.org/10.1016/j.buildenv.2014.09.005.

[251] Silva, H.E., Henriques, F.M.A., Preventive conservation of historic buildings in temperate climates. The importance of a risk-based analysis on the decision-making process, Energy and Buildings. 107 (2015) 26–36. https://doi.org/10.1016/j.enbuild.2015.07.067.

[252] Silva, H.E., Henriques, F.M.A., Hygrothermal analysis of historic buildings, Structural Survey. 34 (2016) 12–23. https://doi.org/10.1108/SS-07-2015-0030.

[253] Silva, H.E., Henriques, F.M.A., Henriques, T.A.S., Coelho, G., A sequential process to assess and optimize the indoor climate in museums, Building and Environment. 104 (2016) 21–34. https://doi.org/10.1016/j.buildenv.2016.04.023.

[254] Skartveit, A., Olseth, J.A., A model for the diffuse fraction of hourly global radiation, Solar Energy. 38 (1987) 271–274. https://doi.org/10.1016/0038-092X(87)90049-1.

[255] Skartveit, A., Olseth, J.A., Tuft, M.E., An hourly diffuse fraction model with correction for variability and surface albedo, Solar Energy. 63 (1998) 173–183. https://doi.org/10.1016/S0038-092X(98)00067-X.

[256] Smith, S.J., Wigley, T.M.L., Multi-Gas Forcing Stabilization with Minicam, The Energy Journal. SI2006 (2006). https://doi.org/10.5547/ISSN0195-6574-EJ-VolSI2006-NoSI3-19.

[257] Spencer, J.W., Fourier series representation of the position of the Sun, Search. 2 (1971).

[258] SRES Final Data - Online database, SRES Final Data - Online database, http://sres.ciesin.org/final_data.html (accessed March 2020), (n.d.).

[259] Stocker, T.F., D. Qin, G.-K. Plattner, M. Tignor, S.K. Allen, J. Boschung, A. Nauels, Y. Xia, V.B. and P.M.M. (eds. ., Summary for Policymakers, in: Climate Change 2013: The Physical Science Basis. Contribution of Working Group I to the Fifth Assessment Report of the Intergovernmental Panel on Climate Change [Stocker, T.F., D. Qin, G.-K. Plattner, M. Tignor, S.K. Allen, J. Boschung, A. Nauels, Y. Xia, Cambridge University Press, Cambridge, United Kingdom and New York, NY, USA., 2013. https://doi.org/10.1017/CBO9781107415324.004.

[260] Tétreault, J., Agent of Deterioration: Pollutants, (n.d.). https://www.canada.ca/en/conservation-institute/services/agents-deterioration/pollutants.html (accessed February 2020).

[261] Tétreault, J., Airborne Pollutants in Museums, Galleries and Archives: Risk Assessment, Control Strategies and Preservation Management, Canadian Conservation Institute, Ottawa, Canada, 2003.

[262] The Chartered Institution of Building Services Engineers (CIBSE), Environment Design: CIBSE Guide A, (2006).

[263] The Chartered Institution of Building Services Engineers (CIBSE), Daylighting and window design - Lighting Guide LG10: 1999, (1999).

[264] Thomson, G., The Museum Environment, Butterworth-Heinemann, 1986.

[265] Tombazis, A.N., Blomsterberg, A., Fisch, M.. N., Krainer, A., Maldonado, E., Mingozzi, A., Nordstrom, C., Museums - Energy Efficiency and Sustainability in Retrofitted and New Museum Buildings Handbook, Vivienne Brophy & John Goulding, University College Dublin, Dublin, Ireland, 2004.

[266] Turhan, C., Arsan, Z.D., Akkurt, G.G., Impact of climate change on indoor environment of historic libraries in Mediterranean climate zone, International Journal of Global Warming. 18 (2019) 206. https://doi.org/10.1504/IJGW.2019.101083.

[267] U.S. Department of Energy, Input Output Reference (version 8.8.0), (2017) 1–2657.

[268] U.S. Department of Energy, Auxiliary Programs (version 8.8.0), (2017) 1–258.

[269] U.S. Department of Energy, Engineering Reference (version 8.8.0), (2017) 1–1704.

[270] U.S. Department of Energy, EnergyPlus Version 8.9.0 Documentation - Engineering Reference, 2018.

[271] U.S. Department of Energy, Weather Converter Program. EnergyPlus TM Version 8.8.0 Documentation – Auxiliary Programs., (2017).

[272] UNESCO - What is meant by “cultural heritage”?, http://www.unesco.org/new/en/culture/themes/illicit-trafficking-of-cultural-property/unesco-

database-of-national-cultural-heritage-laws/frequently-asked-questions/definition-of-the-cultural-heritage/ (accessed November 2019), (n.d.).

[273] Unmet Hours - Question-and-Answer Resource for the Building Energy Modeling Community, https://unmethours.com/questions/ (accessed December 2020), (n.d.).

[274] Varas-Muriel, M.J., Fort, R., Microclimatic monitoring in an historic church fitted with modern heating: Implications for the preventive conservation of its cultural heritage, Building and Environment. 145 (2018) 290–307. https://doi.org/10.1016/j.buildenv.2018.08.060.

[275] Varas-Muriel, M.J., Martínez-Garrido, M.I., Fort, R., Monitoring the thermal-hygrometric conditions induced by traditional heating systems in a historic Spanish church (12th-16th C), Energy and Buildings. 75 (2014) 119–132. https://doi.org/10.1016/j.enbuild.2014.01.049.

[276] Varas-Muriel, M.J., Fort, R., Martínez-Garrido, M.I., Zornoza-Indart, A., López-Arce, P., Fluctuations in the indoor environment in Spanish rural churches and their effects on heritage conservation: Hygro-thermal and CO2 conditions monitoring, Building and Environment. 82 (2014) 97–109. https://doi.org/10.1016/j.buildenv.2014.08.010.

[277] Verein Deutscher Ingenieure (VDI), VDI Guideline 6020, Requirements on methods of calculation to thermal and energy simulation of buildings and plants buildings, (2001).

[278] van Vuuren, D.P., Edmonds, J., Kainuma, M., Riahi, K., Thomson, A., Hibbard, K., Hurtt, G.C., Kram, T., Krey, V., Lamarque, J.F., Masui, T., Meinshausen, M., Nakicenovic, N., Smith, S.J., Rose, S.K., The representative concentration pathways: An overview, Climatic Change. 109 (2011) 5–31. https://doi.org/10.1007/s10584-011-0148-z.

[279] van Vuuren, D.P., Eickhout, B., Lucas, P.L., Elzen, M.G.J. den, Long-Term Multi-Gas Scenarios to Stabilise Radiative Forcing — Exploring Costs and Benefits Within an Integrated Assessment Framework, The Energy Journal. 27 (2006) 201–233.

[280] van Vuuren, D.P., Den Elzen, M.G.J., Lucas, P.L., Eickhout, B., Strengers, B.J., Van Ruijven, B., Wonink, S., Van Houdt, R., Stabilizing greenhouse gas concentrations at low levels: An assessment of reduction strategies and costs, Climatic Change. 81 (2007) 119–159. https://doi.org/10.1007/s10584-006-9172-9.

[281] Wang, F., Pichetwattana, K., Hendry, R., Galbraith, R., Thermal performance of a gallery and refurbishment solutions, Energy and Buildings. 71 (2014) 38–52. https://doi.org/10.1016/j.enbuild.2013.11.059.

[282] Webb, A.L., Energy retrofits in historic and traditional buildings: A review of problems and methods, Renewable and Sustainable Energy Reviews. 77 (2017) 748–759. https://doi.org/10.1016/j.rser.2017.01.145.

[283] Weintraub, S., Using Risk Assessment Tools to Evaluate the Use of LEDs for the Illumination of Light-Sensitive Collections, American Institute of Conservation News. (2010) 14–17.

[284] de Wilde, P., Coley, D., The implications of a changing climate for buildings, Building and Environment. 55 (2012) 1–7. https://doi.org/10.1016/j.buildenv.2012.03.014.

[285] Wise, M., Calvin, K., Thomson, A., Clarke, L., Bond-Lamberty, B., Sands, R., Smith, S.J., Janetos, A., Edmonds, J., Implications of Limiting CO2 Concentrations for Land Use and Energy, Science. 324 (2009) 1183–1186. https://doi.org/10.1126/science.1168475.

[286] Woloszyn, M., Rode, C., Subtask 1 – Modelling Principles and Common Exercises, in: IEA Annex 41, MOIST-ENG, 2007: pp. 1–161.

[287] World Health Organization Regional Office for Europe, Air quality guidelines for Europe, 2nd Editio, 2000. http://link.springer.com/10.1007/BF02986808.

[288] World Heritage report 22, Climate Change and World Heritage: Report on predicting and managing the impacts of climate change on World Heritage and Strategy to assist States Parties to implement appropriate management responses, (2007) 1–55.

[289] World Meteorological Organization (WMO), Calculation of monthly and annual 30-year standard normals. WCDP 10 and WMOTD 341, Meeting of Experts. (1989) 14.

[290] WUFI-Pro - Performanceand Limitations, https://www.wufi-wiki.com/mediawiki/index.php/Discussion:WUFI-Pro_PerformanceandLimitations (accessed

in November 2017), (n.d.).

[291] WUFI-Wiki, Physical background for WUFI® PRO, 2D & Plus, https://www.wufi-wiki.com/mediawiki/index.php/Details:Physics (accessed September 2020), (n.d.).

[292] WUFI®Plus, Version 3.1.1.0, Fraunhofer Institute for Building Physics, (2017).

[293] WUFI - Creating weather files, https://wufi.de/en/service/downloads/creating-weather-files/ (accessed January 2019), (n.d.).

[294] WUFI software, WUFI®Plus, https://wufi.de/en/software/wufi-plus/ (accessed September 2020), (n.d.).

[295] WUFI updates, WUFI® Plus / WUFI® Passive, https://wufi.de/en/software/wufi-plus/wufi-plus-wufi-passive-updates/(accessed January 2020), (n.d.).

[296] Xing, L., Estimations of Undisturbed Ground Temperatures using Numerical and Analytical Modeling (PhD thesis), Oklahoma State University, Stillwater, United States, 2014.

[297] Xing, L., Spitler, J.D., Prediction of undisturbed ground temperature using analytical and numerical modeling. Part I: Model development and experimental validation, Science and Technology for the Built Environment. 23 (2017) 787–808. https://doi.org/10.1080/23744731.2016.1258371.

[298] Yang, Z., Becerik-Gerber, B., A model calibration framework for simultaneous multi-level building energy simulation, Applied Energy. 149 (2015) 415–431. https://doi.org/10.1016/j.apenergy.2015.03.048.

[299] Zarzo, M., Fernández-Navajas, A., García-Diego, F.J., Long-term monitoring of fresco paintings in the cathedral of Valencia (Spain) through humidity and temperature sensors in various locations for preventive conservation, Sensors. 11 (2011) 8685–8710. https://doi.org/10.3390/s110908685.

[300] Health Aspects of Air Pollution with Particulate Matter, Ozone and Nitrogen Dioxide Report, Report on a WHO working group, Boon, Germany, (2003).

[301] Climate change - The Intergovernmental Panel on Climate Change (IPCC) Scientific Assessment, Edited by J.T.Houghton, G.J.Jenkins and J.J.Ephraums, Press Syndicate of the Univversity of Cambridge, New York, USA, and University Press, Cambridge, UK, 1990.

[302] Solomon, S., Qin, D., Manning, M., Chen, Z., Marquis, M., Averyt, K.B., Tignor, M., Miller, H.L., eds., Climate Change 2007: The Physical Science Basis. Contribution of Working Group I to the Fourth Assessment Report of the Intergovernmental Panel on Climate Change (IPCC), Cambridge University Press, Cambridge, United Kingdom and New York, NY, USA, 2007.

[303] Stocker, T.F., Qin, D., Plattner, G.-K., Tignor, M., Allen, S.K., Boschung, J., Nauels, A., Xia, Y., Bex, V., Midgley, P.M., eds., Climate Change 2013: The Physical Science Basis. Contribution of Working Group I to the Fifth Assessment Report of the Intergovernmental Panel on Climate Change (IPCC), Cambridge University Press, Cambridge, United Kingdom and New York, NY, USA, 2013. https://doi.org/10.1017/CBO9781107415324.

[304] Solomon, S., Qin, D., Manning, M., Chen, Z., Marquis, M., Averyt, K.B., Tignor, M., Miller, H.L., eds., A report of Working Group I of the Intergovernmental Panel on Climate Change - Summary for Policymakers, in: Climate Change 2007: The Physical Science Basis. Contribution of Working Group I to the Fourth Assessment Report of the Intergovernmental Panel on Climate Change, Cambridge University Press, Cambridge, United Kingdom and New York, NY, USA, 2007.

[305] Climate change 2014: Impacts, adaptation, and vulnerability Part B: Regional aspects: Working group II contribution to the fifth assessment report of the intergovernmental panel on climate change [Barros, V.R., C.B. Field, D.J. Dokken, M.D. Mastrandrea, K, (2014) 688.

[306] Santos, F.D., Forbes, K., Moita, R., eds., Climate Change in Portugal. Scenarios, Impacts and Adaptation Measures - SIAM Project, Gradiva, Lisbon, Portugal, 2002.

[307] Santos, F.D., Miranda, P., eds., Climate Change in Portugal. Scenarios, Impacts and Adaptation Measures - SIAM Project II (in Portuguese), Gradiva, Lisboa, Portugal, 2006.

ANNEXES

Annex A. Academic Curriculum Vitae

International journal:

- **G. B. A. Coelho**, F. M. A. Henriques (2021). Performance of passive retrofit measures for historic buildings that house artefacts viable for future conditions. Sustainable Cities and Society, 71, 102982. https://doi.org/10.1016/j.scs.2021.102982
- A.D. Trindade, **G.B.A. Coelho**, F.M.A. Henriques, *Influence of the climatic conditions on the hygrothermal performance of autoclaved aerated concrete masonry walls*, Journal of Building Engineering, 33 (2021). doi:10.1016/j.jobe.2020.101578
- **G. B. A. Coelho**, H. E. Silva, F. M. A. Henriques. *Impact of climate change in cultural heritage: from energy consumption to artefacts' conservation and building rehabilitation*. Energy and Buildings, 224 (2020), doi: 10.1016/j.enbuild.2020.110250
- H.E. Silva, **G.B.A. Coelho**, F.M.A. Henriques, *Climate monitoring in World Heritage List buildings with low-cost data loggers: the case of the Jerónimos Monastery in Lisbon (Portugal)*, Journal of Building Engineering, 28 (2020). doi: 10.1016/j.jobe.2019.101029
- **G.B.A. Coelho**, H.E. Silva, F.M.A. Henriques, *Impact of climate change on cultural heritage: a simulation study to assess the risks for conservation and thermal comfort*, International Journal of Global Warming, 19 (2019) 382–406. doi: 10.1504/IJGW.2019.104268
- **G.B.A. Coelho**, H.E. Silva, F.M.A. Henriques, *Calibrated hygrothermal simulation models for historical buildings*, Building and Environment. 142 (2018) 439–450. doi:10.1016/j.buildenv.2018.06.034.
- H.E. Silva, F.M.A. Henriques, T.A.S Henriques, **G.B.A. Coelho**. *A sequential process to assess and optimize the indoor climate in museums*. Building and Environment. 104 (2016) 21–34. doi:10.1016/j.buildenv.2016.04.023.
- **G.B.A. Coelho**, F.M.A. Henriques. *Influence of driving rain on the hygrothermal behavior of solid brick walls*. Journal of Building Engineering (2016) doi:10.1016/j.jobe.2016.06.002.

International conference:

- **G.B.A. Coelho**, H.E. Silva, F.M.A. Henriques, *Development of a hygrothermal model of a historic building in WUFI®Plus vs EnergyPlus*, in: 4th Central European Symposium on Building Physics (CESBP 2019), Prague, Czech Republic, 2019. doi:10.1051/matecconf/201928202079.

National journal:

- **G.B.A. Coelho**, F.M.A. Henriques. *A influência da chuva incidente no desempenho térmico de*

paredes exteriores. Construção Magazine. 2017.

- H.E. Silva, F.M.A. Henriques, T.A.S Henriques, **G.B.A. Coelho**. *A análise climática na conservação e optimização energética de edifícios históricos: o caso do Museu Nacional de Arte Antiga*. Construção Magazine. 2017.

National conference:

- H.E. Silva, **G.B.A. Coelho**, B. Rocha, F.M.A. Henriques, *Impacto dos visitantes na conservação do património cultural em Portugal*, in: Construção 2018 – Reabilitar e Construir de Forma Sustentável, Porto, Portugal, 2018: pp. 1432–1441.

Reviews in Journals & Conferences:

- *Building and Environment* – 10 reviews (2017 – 1; 2019 – 2; 2020 – 7)
- *Journal of Building Engineering* – 4 reviews (2017 – 2; 2020 – 2)
- *Sustainable Cities and Society* – 3 reviews in 2019
- *Journal of Building Pathology and Rehabilitation* – 2 reviews in 2019
- *Journal of Cultural Heritage* – 1 review in 2020
- *4th Central European Symposium on Building Physics* – 1 review in 2019

Attended RILEM courses:

- *Computational Methods for Building Physics and Construction Materials*, RILEM EAC and TUDa course (via Zoom), Technical University Darmstadt, 6-10 July 2020, addressed topics: steady state problems – discretization and implementation in Excel; transient problems – explicit & implicit heat and moisture flow – implementation in Octave/Matlab/FEM; coupled systems – heat and moisture flow, discretization and implementation in Octave/Matlab/FEM; particle structure formation and hydration kinetics of cementitious systems
- *Materials, Systems and Structures in Civil Engineering: Moisture in Materials and Structures*, RILEM EAC course, Technical University of Denmark (DTU) in Lyngby, Denmark, 15-29 August 2016, addressed topics: thermodynamics of moisture; moisture fixation in materials; moisture transport in materials and structures; experimental methods; moisture measuring methods; prediction methods; field applications and coupled transport phenomena

Annex B. Standards/guideline climate limits

Table B.1 – Thomson's temperature (ºC) and relative humidity (%) ranges for class I - Major museums, and class II - remaining buildings (data taken from Ref. [264])

Class	Temperature [ºC]	Relative humidity [%]
I	18–25 ºC	45–60 %
II	≈ const.	40–70 %

Table B.2 – ASHRAE's temperature (ºC) and relative humidity (%) ranges for class AA, As, Ad, B, C and D for general museums, art galleries, libraries and archives (table adapted from Ref. [5])

Setpoint or Annual Average	Class	Short-term fluctuations	Seasonal fluctuations	Collection risks and benefits
50 %RH (or historic annual average for permanent collections	AA	± 5 %RH, ±2 K	RH no change ± 5 K	No risk of mechanical damage to most artefacts and paintings. Some metals and minerals may degrade if the 50 %RH exceeds a critical RH. Chemically unstable objects unusable within decades
	A – As	± 5 %RH, ±2 K	± 10 %RH up 5 K; down 10 K	Small risk of mechanical decay to highly vulnerable artefacts. No mechanical risk to most artefacts. Chemically unstable objects unusable within decades.
	A – Ad	± 10 %RH, ±2 K	RH no change up 5 K; down 10 K	
	B	± 10 %RH, ±2 K	± 10 %RH up 10, but not above 30 ºC K	Moderate risk of mechanical decay to highly vulnerable artefacts. Small risk to most paintings and photographs. No risk to most books. Chemically unstable objects unusable within decades, less if routinely at 30 ºC, but cold winter periods double life
Temperature set between 15-25 ºC	C	RH within 25-75 % year-round Temperature rarely over 30 ºC, usually below 25 ºC		High risk of mechanical decay to highly vulnerable artefacts. Moderate risk to most paintings and photographs. Small risk to most books. Chemically unstable objects unusable within decades, less if routinely at 30 ºC, but cold winter periods double life
	D	Reliably below 75 %RH		High risk or cumulative mechanical damage to most artefacts and paintings due to low-humidity fracture but avoids high-humidity delamination and deformations. Mold growth and rapid corrosion avoided. Chemically unstable objects unusable within decades, less if routinely at 30 ºC, but cold winter periods double life

Table B.3 – FCT-UNL's temperature (T, ºC) and relative humidity (RH, %) ranges for class I and II (table adapted from Ref. [250])

Reference value	Daily cycles[a]	Seasonal fluctuations[b]	Short-term fluctuations[c]	Extra limits	Collection risks and benefits
T and RH: Historic yearly average	90º percentile ($\Delta T \cap \Delta RH$) ≥ UNI 10829 limits	T & RH: -10º/+90º percentiles	T & RH: -5º/+95º percentiles	$\lvert RH - \overline{RH}\rvert \leq 15\%$ and $RH_{max} \leq 75\%$ $\lvert T - \bar{T}\rvert$ up to 10ºC not above 30ºC	Class I – Low risk of mechanical and biological decay. Applicable to buildings that house materials that require tight indoor climate control. Example: museums
				-	Class II – Moderate risk of mechanical decay. The biological risk is not a major factor and there is no need for an indoor climate constant as for class I. Example: churches

[a] The values defined by the 90th percentile of the recorded daily cycles if higher than the UNI 10829 limits.

[b] A seasonal cycle is determined by calculating a monthly moving average (equation 2.1). Then, subtracting to the maximum value of the annual moving average, the minimum value of the annual moving average (equations 2.2 and 2.3).

[c] The short-term fluctuations are calculated as the difference between the current value and the monthly moving average value (equations 2.4 and 2.5). Then, the short-term fluctuations are limited at the bottom and at the top by its 5th and 95th percentiles, respectively.

Annex C. Greenhouse emissions

Table C.1 – Air pollutants footprints for each product and service performed in the European Union in 2017 (data taken from Ref. [101])

Activities	2017
Products of agriculture, hunting and related services	66 483 843
Products of forestry, logging and related services	2 727 643
Fish and other fishing products; aquaculture products; support services to fishing	6 660 384
Mining and quarrying	29 518 939
Food, beverages and tobacco products	233 725 635
Textiles, wearing apparel, leather and related products	55 767 718
Wood and of products of wood and cork, except furniture; articles of straw and plaiting materials	8 783 188
Paper and paper products	27 114 272
Printing and recording services	1 776 360
Coke and refined petroleum products	238 168 257
Chemicals and chemical products	140 538 740
Basic pharmaceutical products and pharmaceutical preparations	39 690 072
Rubber and plastic products	24 517 674
Other non-metallic mineral products	54 729 417
Basic metals	81 493 096
Fabricated metal products, except machinery and equipment	45 844 281
Computer, electronic and optical products	47 356 337
Electrical equipment	43 821 244
Machinery and equipment n.e.c.	116 366 875
Motor vehicles, trailers and semi-trailers	133 787 393
Other transport equipment	44 176 170
Furniture and other manufactured goods	49 244 666
Repair and installation services of machinery and equipment	20 005 677
Electricity, gas, steam and air conditioning	403 439 549
Natural water; water treatment and supply services	14 308 377
Sewerage services; sewage sludge; waste collection, treatment and disposal services; materials recovery services; remediation services and other waste management services	28 439 435
Constructions and construction works	332 679 454
Wholesale and retail trade and repair services of motor vehicles and motorcycles	40 881 286
Wholesale trade services, except of motor vehicles and motorcycles	115 829 813
Retail trade services, except of motor vehicles and motorcycles	102 489 389
Land transport services and transport services via pipelines	117 372 041
Water transport services	109 796 969
Air transport services	136 357 771
Warehousing and support services for transportation	24 745 819
Postal and courier services	2 684 447
Accommodation and food services	107 461 657

Publishing services	13 849 417
Motion picture, video and television programme production services, sound recording and music publishing; programming and broadcasting services	10 790 641
Telecommunications services	18 681 504
Computer programming, consultancy and related services; Information services	30 017 321
Financial services, except insurance and pension funding	15 188 436
Insurance, reinsurance and pension funding services, except compulsory social security	18 933 270
Services auxiliary to financial services and insurance services	3 462 438
Real estate services	90 268 992
Legal and accounting services; services of head offices; management consultancy services	10 688 129
Architectural and engineering services; technical testing and analysis services	16 362 107
Scientific research and development services	56 886 231
Advertising and market research services	1 964 869
Other professional, scientific and technical services and veterinary services	5 271 327
Rental and leasing services	15 875 806
Employment services	542 787
Travel agency, tour operator and other reservation services and related services	13 760 698
Security and investigation services; services to buildings and landscape; office administrative, office support and other business support services	10 846 494
Public administration and defence services; compulsory social security services	103 846 698
Education services	51 343 205
Human health services	88 416 860
Residential care services; social work services without accommodation	36 812 012
Creative, arts, entertainment, library, archive, museum, other cultural services; gambling and betting services	17 295 841
Sporting services and amusement and recreation services	15 713 007
Services furnished by membership organisations	11 338 163
Repair services of computers and personal and household goods	2 749 842
Other personal services	19 506 865
Services of households as employers; undifferentiated goods and services produced by households for own use	385 627
Services provided by extraterritorial organisations and bodies	22
Direct emissions by private households	877 300 298

Annex D. Outdoor and indoor anthropogenic sources of the artefacts' key damaging pollutants, and their negative effects

Table D.1 – Outdoor and indoor anthropogenic sources of the artefacts' key damaging pollutants, and their respective negative effects (table adapted from Ref. [5] and [260])

Pollutants	Anthropogenic sources		Potential damage
Acetic acid (CH_3COOH)	Outside	• Results from atmospheric reactions with industrial and vehicle pollutants • Gases concentrated in fog, rain and snow	• Corrodes non-noble metals (e.g. leaded-bronzes and copper alloys) and base metals (e.g. lead, copper and silver) • Attacks calcareous materials and low-fire ceramics • Reacts with enamel and glass • Corrodes lead joints in stained glass
	Inside	• Gas-phase reactions • Floor materials (e.g. carpets) and other materials (e.g. furniture, varnishes, paper, among others)	
Hydrogen sulphide (H_2S)	Outside	• Fuel and coal combustion • Pulp-and-paper industry • Petroleum refineries	• Destroys immature plant tissue • Tarnishes silver and copper • Darkens lead pigments • Blackens copper, damages silver, reacts with bronze and lead, and corrodes zinc (synergetic effect with NO_2) • Damages ceramics, stone and leather
	Inside	• Mineral specimens that contain pyrite • Adhesives and wool carpets	
Nitrogen dioxide (NO_2)	Outside	• Combustion of fuels by vehicles, power plants and industrial activities • Fireworks	• Enhances deterioration effects of sulphur dioxide on leather, metals and stone, among others • Corrodes copper-rich silver • Fades dyestuffs, certain inks and organic pigments • Degrades fibres made from rayon, silk, wool, and nylon by causing its yellowing and embrittlement • Corrodes zinc and affects the tarnishing of copper and silver
	Inside	• Stoves, heaters, fireplaces, among others • Tobacco smoke • Dry-process photocopiers • Degradation of cellulose nitrate objects • Formation of acids	

Ozone (O_3)	Outside	• Photochemical smog	• Fades dyes and piments • Embrittles fabrics, textiles and cellulose materials • Enhance the tarnishing of silver • Affects animal skins • Discolours photographies
	Inside	• Building's electronical equipment	
Sulphur dioxide (SO_2)	Outside	• Combustion of fossil fuels that contain sulphur, such as coal, gasoline and diesel fuel • Pulp-and-paper, cement and petroleum industries • Fireworks	• Hydrolyses to H_2SO_4 when absorbed by cellulose materials • Breaks the molecular structure of animal skins, e.g. leather and parchment • Non-reversible colour changes of acid-sensitive pigments and dyestuffs fading • Corrodes most metals • Photography's darkening due to the attacks to the silver salts • Attacks carbonate rocks, as well as calcareous materials
	Inside	• Combustion of fuels containing sulphur for cooking and heating • Firewood used to cook and heat • Propane or gasoline powered machines	
Water-vapour (H_2O)*	Outside	• Atmosphere • Bodies of water	• Causes damage to cellulose-based materials, e.g. books and paper artworks, and other organic objects, since it increases hydrolysis reactions • Increases the effect of nitrogen oxides on photographies • Increases hydrogen sulphide corrosion of copper and silver • Main parameter that governs the "bronze disease" • Increases the deterioration of materials • Increases fading of dyestuffs
	Inside	• Fountains • Humidifiers • People • Cleaning activities	

Fine ($PM_{2.5}$) and coarse ($PM_{2.5}$) particles	General: Atomizing humidifier, burning candles, cooking, laser printers, spray cans, shedding from clothing, carpets, industrial activities, outdoor building construction and soil, among others Biological and organic compounds: microorganisms, degradation of materials and objects, visitors and construction activities Soot: burning candles and incense, fires, coal combustion and vehicle exhaustion Ammonium salts: reaction of ammonia with SO_2 or NO_2 inside or outside or on solid surfaces	General: • Abrasion of surfaces • Disfiguration of objects • Can initiate or increase corrosion processes • Can initiate catalysis with the forming of reactive gases Soot: • Soil of porous surfaces (e.g. paintings, frescos, statues, books, textiles) • Increase of metals corrosion rates

*- Although several guidelines recommend ranges of RH with the purpose of mitigating the physical damages caused by RH, water-vapour is also considered as a pollutant due to its capacity to increase both corrosion and other decay rates, as well as because it is involved in most chemical reactions [5].

Annex E. Airborne pollutants limit-values and target-values

Table E.1 – Limit values for Sulphur dioxide (SO_2), Nitrogen dioxide (NO_2), Coarse particle matter (PM_{10}) and Fine particle matter ($PM_{2.5}$). Note that the 20 μg/m^3 limit value for $PM_{2.5}$ is only from 2020 onward [202]. Table adapted from Ref. [202]

Pollutant	Period	Limit-value
Sulphur dioxide (SO_2)	1 hour	**350 μg/m^3**, which must not be exceeded more than **24** times in each calendar year
	1 day	**125 μg/m^3**, which must not be exceeded more than **3** times in each calendar year
Nitrogen dioxide (NO_2)	1 hour	**200 μg/m^3**, which must not be exceeded more than **18** times in each calendar year
	1 year	**40 μg/m^3**
Coarse particle matter (PM_{10})	1 day	**50 μg/m^3**, which must not be exceeded more than **35** times in each calendar year
	1 year	**40 μg/m^3**
Fine particle matter ($PM_{2.5}$)	1 year	**25 μg/m^3**

Table E.2 – Target-value for Ozone (O_3). Table adapted from Ref. [202]

Pollutant	Period	Target-value
Ozone (O_3)	Maximum daily eight-hour mean	**1250 μg/m^3**, which must not be exceeded more than **25** days per calendar year averaged over three years

Annex F. Emissions and concentrations GHGs for AR4 and AR5

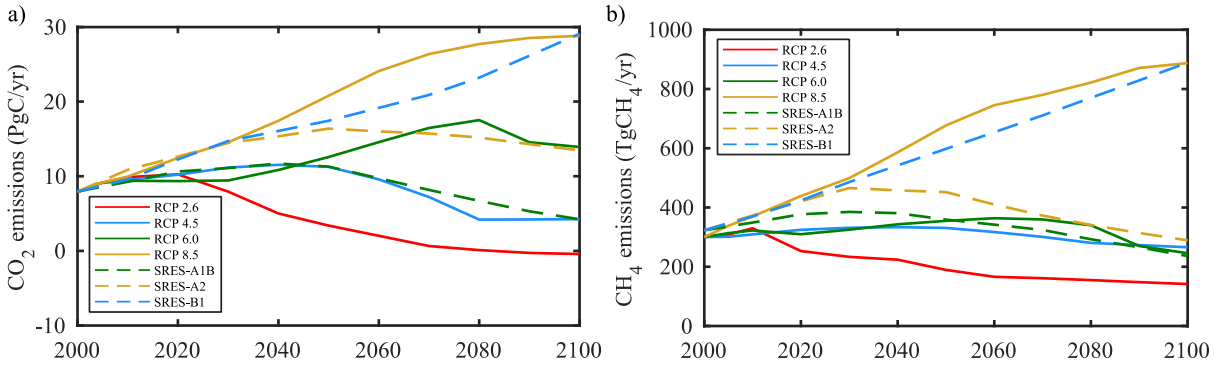

Figure F.1 – CO_2 (a) and CH_4 (b) emissions for the three SRES scenarios – A1B, A2 and B1 – and the four RCPs scenarios – RCP 2.6, RCP 4.5, RCP 6.0 and RCP 8.5 [219,135]

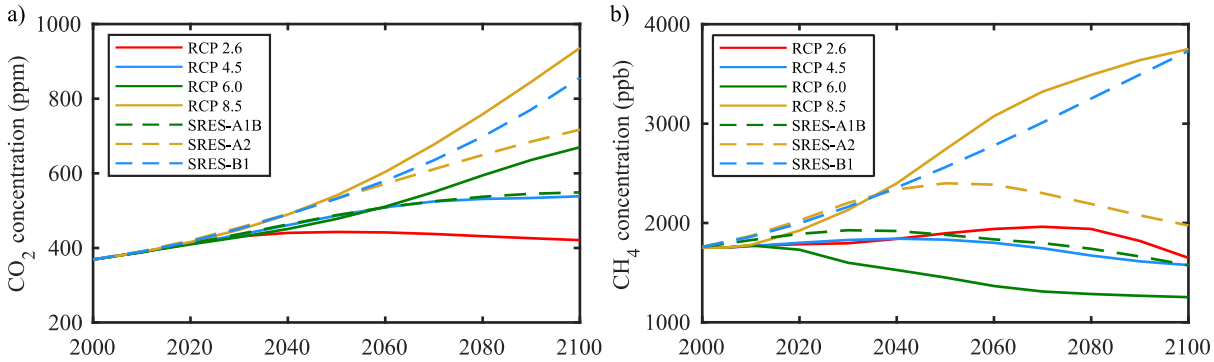

Figure F.2 – CO_2 (a) and CH_4 (b) atmospheric concentrations for the three SRES scenarios – A1B, A2 and B1 – and the four RCPs scenarios – RCP 2.6, RCP 4.5, RCP 6.0 and RCP 8.5 [219,135]

Annex G. St. Cristóvão church plan and photographs for each zone of the building

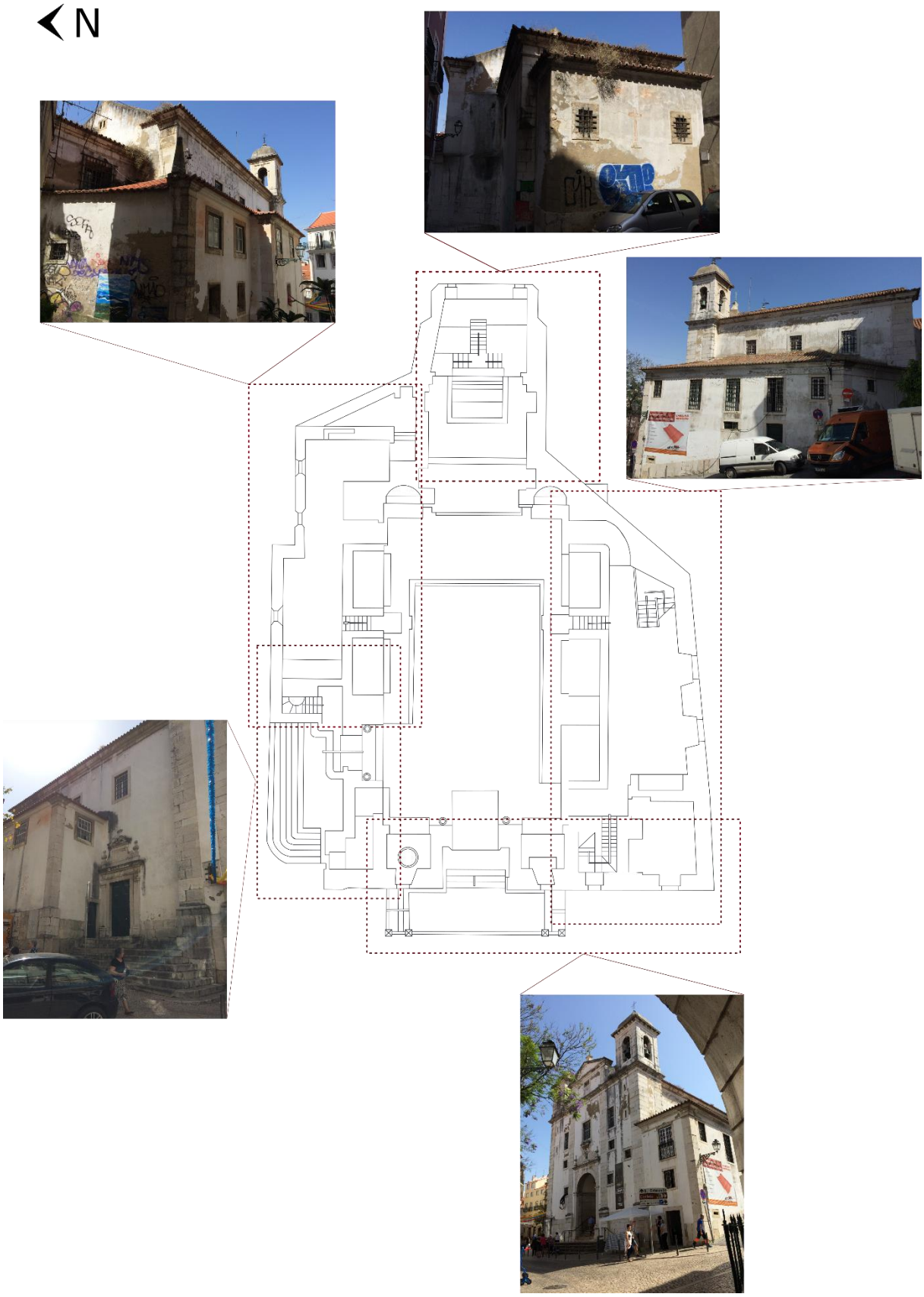

Figure G.1 – St. Cristóvão church plan with photographs for each zone of the building

Annex H. Electricity price for industrial users

The following tables present the electricity price (€/kWh) for industrial users that includes all taxes and levies between 2007-2019 for the 7 bands with different consumptions, namely: *band-IA* with an annual consumption below 20 MWh, *band-IB* with an annual consumption between 20 and 500 MWh, *band-IC* with an annual consumption between 500 and 2,000 MWh, *band ID* with an annual consumption between 2,000 and 20,000 MWh, *band-IE* with an annual consumption between 20,000 and 70,000 MWh, *band-IF* with an annual consumption between 70,000 and 150,000 MWh and *band-IG* with an annual consumption higher than 150,000 MWh [103]. This information is also present in Figure 6.5.

Table H.1 – Electricity price (€/kWh) for industrial users that includes all taxes and levies between 2007-2019 for Czech Republic for band IA, IB, IC, ID, IE, IF and IG [102]

	Czech Republic – Electricity price (€/kWh)						
	Band IA	Band IB	Band IC	Band ID	Band IE	Band IF	Band IG
2007S2	0.141	0.109	0.095	0.078	0.067	0.067	
2008S1	0.164	0.131	0.110	0.091	0.081	0.083	
2008S2	0.167	0.134	0.111	0.093	0.083	0.084	
2009S1	0.162	0.132	0.106	0.093	0.086	0.086	
2009S2	0.171	0.139	0.111	0.097	0.090	0.091	
2010S1	0.170	0.134	0.102	0.093	0.089	0.089	
2010S2	0.176	0.138	0.107	0.096	0.092	0.092	
2011S1	0.184	0.145	0.110	0.098	0.101	0.096	
2011S2	0.180	0.141	0.107	0.096	0.098	0.094	
2012S1	0.187	0.144	0.103	0.096	0.093	0.098	
2012S2	0.187	0.145	0.102	0.096	0.092	0.099	
2013S1	0.185	0.147	0.101	0.096	0.095	0.100	
2013S2	0.182	0.146	0.098	0.094	0.093	0.097	
2014S1	0.158	0.124	0.082	0.077	0.079	0.079	
2014S2	0.157	0.124	0.081	0.076	0.079	0.078	
2015S1	0.154	0.120	0.076	0.071	0.073	0.075	
2015S2	0.157	0.121	0.077	0.071	0.074	0.076	
2016S1	0.160	0.116	0.072	0.063	0.065	0.067	
2016S2	0.160	0.116	0.072	0.062	0.064	0.067	
2017S1	0.162	0.111	0.068	0.061	0.060	0.063	
2017S2	0.168	0.118	0.070	0.062	0.061	0.064	
2018S1	0.177	0.124	0.072	0.063	0.062	0.063	0.062
2018S2	0.177	0.128	0.071	0.063	0.064	0.063	
2019S1	0.188	0.136	0.076	0.072	0.073	0.069	

Table H.2 – Electricity price (€/kWh) for industrial users that includes all taxes and levies between 2007-2019 for Spain for band IA, IB, IC, ID, IE, IF and IG [102]

Spain – Electricity price (€/kWh)							
	Band IA	Band IB	Band IC	Band ID	Band IE	Band IF	Band IG
2007S2	0.151	0.111	0.091	0.079	0.066	0.053	0.039
2008S1	0.131	0.111	0.092	0.080	0.068	0.057	0.042
2008S2	0.131	0.120	0.102	0.085	0.074	0.069	0.049
2009S1	0.158	0.125	0.110	0.091	0.079	0.069	0.051
2009S2	0.168	0.127	0.107	0.089	0.078	0.068	0.048
2010S1	0.172	0.133	0.111	0.088	0.072	0.064	0.049
2010S2	0.178	0.132	0.104	0.085	0.073	0.064	0.049
2011S1	0.164	0.131	0.108	0.087	0.075	0.068	0.050
2011S2	0.192	0.139	0.110	0.089	0.077	0.069	0.050
2012S1	0.195	0.146	0.116	0.097	0.083	0.072	0.053
2012S2	0.204	0.148	0.114	0.095	0.084	0.073	0.054
2013S1	0.223	0.143	0.117	0.100	0.082	0.066	0.054
2013S2	0.238	0.146	0.114	0.103	0.083	0.072	0.063
2014S1	0.261	0.152	0.119	0.099	0.075	0.068	0.051
2014S2	0.278	0.148	0.111	0.098	0.079	0.074	0.065
2015S1	0.260	0.150	0.112	0.092	0.079	0.072	0.064
2015S2	0.257	0.144	0.108	0.091	0.078	0.076	0.072
2016S1	0.236	0.140	0.105	0.086	0.070	0.064	0.052
2016S2	0.235	0.134	0.098	0.082	0.072	0.067	0.059
2017S1	0.244	0.130	0.101	0.084	0.075	0.069	0.066
2017S2	0.198	0.132	0.098	0.082	0.073	0.067	0.064
2018S1	0.271	0.114	0.101	0.094	0.087	0.069	0.063
2018S2	0.233	0.135	0.105	0.090	0.081	0.079	0.074
2019S1	0.228	0.141	0.109	0.092	0.082	0.074	0.065

Table H.3 – Electricity price (€/kWh) for industrial users that includes all taxes and levies between 2007-2019 for Portugal for band IA, IB, IC, ID, IE, IF and IG [102]

Portugal – Electricity price (€/kWh)							
	Band IA	Band IB	Band IC	Band ID	Band IE	Band IF	Band IG
2007S2	0.095	0.090	0.073	0.064	0.055	0.050	
2008S1	0.111	0.083	0.078	0.070	0.057	0.050	
2008S2	0.114	0.083	0.078	0.070	0.058	0.051	
2009S1	0.137	0.103	0.092	0.083	0.067	0.064	
2009S2	0.147	0.106	0.093	0.082	0.068	0.052	
2010S1	0.112	0.095	0.090	0.076	0.065	0.050	
2010S2	0.108	0.092	0.087	0.076	0.065	0.056	
2011S1	0.106	0.092	0.090	0.084	0.066	0.061	
2011S2	0.108	0.094	0.090	0.083	0.068	0.060	
2012S1	0.121	0.102	0.105	0.099	0.082	0.079	
2012S2	0.125	0.105	0.099	0.090	0.080	0.075	
2013S1	0.128	0.115	0.102	0.091	0.080	0.075	
2013S2	0.127	0.112	0.101	0.097	0.082	0.077	
2014S1	0.160	0.129	0.103	0.089	0.073	0.063	
2014S2	0.159	0.127	0.105	0.089	0.077	0.070	
2015S1	0.170	0.125	0.099	0.090	0.074	0.066	
2015S2	0.168	0.123	0.100	0.091	0.075	0.071	
2016S1	0.159	0.124	0.094	0.086	0.068	0.049	
2016S2	0.158	0.124	0.095	0.086	0.070	0.060	
2017S1	0.129	0.108	0.084	0.077	0.067	0.064	0.060
2017S2	0.129	0.106	0.084	0.078	0.067	0.065	0.058
2018S1	0.123	0.100	0.078	0.074	0.064	0.059	0.051
2018S2	0.119	0.100	0.081	0.077	0.069	0.063	0.059
2019S1	0.105	0.100	0.087	0.078	0.071	0.063	0.060

Table H.4 – Electricity price (€/kWh) for industrial users that includes all taxes and levies between 2007-2019 for United Kingdom for band IA, IB, IC, ID, IE, IF and IG [102]

United Kingdom – Electricity price (€/kWh)							
	Band IA	Band IB	Band IC	Band ID	Band IE	Band IF	Band IG
2007S1	0.140	0.113	0.106	0.098	0.093	0.087	0.082
2007S2	0.143	0.121	0.108	0.094	0.089	0.085	0.071
2008S1	0.127	0.107	0.094	0.084	0.083	0.086	0.076
2008S2	0.131	0.113	0.105	0.098	0.095	0.097	0.085
2009S1	0.132	0.114	0.108	0.099	0.097	0.095	0.082
2009S2	0.134	0.112	0.097	0.087	0.084	0.084	0.077
2010S1	0.138	0.112	0.095	0.084	0.081	0.079	0.082
2010S2	0.142	0.115	0.096	0.085	0.077	0.077	0.077
2011S1	0.129	0.111	0.094	0.086	0.082	0.081	0.078
2011S2	0.144	0.115	0.100	0.089	0.083	0.079	0.082
2012S1	0.147	0.125	0.110	0.099	0.098	0.089	0.095
2012S2	0.155	0.130	0.115	0.105	0.103	0.100	0.101
2013S1	0.142	0.125	0.112	0.103	0.103	0.103	0.097
2013S2	0.159	0.130	0.116	0.108	0.105	0.102	0.101
2014S1	0.162	0.139	0.125	0.114	0.115	0.111	0.108
2014S2	0.173	0.145	0.129	0.118	0.118	0.115	0.113
2015S1	0.151	0.133	0.118	0.110	0.107	0.105	0.101
2015S2	0.147	0.135	0.121	0.111	0.108	0.106	0.103
2016S1	0.128	0.116	0.104	0.095	0.093	0.091	0.089
2016S2	0.114	0.108	0.097	0.088	0.086	0.085	0.083
2017S1	0.130	0.114	0.094	0.096	0.100	0.100	0.089
2017S2	0.127	0.109	0.089	0.091	0.096	0.095	0.085
2018S1	0.136	0.118	0.097	0.099	0.095	0.092	0.086
2018S2	0.143	0.121	0.101	0.102	0.098	0.092	0.091
2019S1	0.136	0.122	0.100	0.093	0.087	0.083	0.080

Table H.5 – Electricity price (€/kWh) for industrial users that includes all taxes and levies between 2007-2019 for United Kingdom for band IA, IB, IC, ID, IE, IF and IG [102]

Norway – Electricity price (€/kWh)							
	Band IA	Band IB	Band IC	Band ID	Band IE	Band IF	Band IG
2007S2	0.071	0.064	0.063	0.051	0.041	0.020	
2008S1	0.074	0.066	0.065	0.053	0.040	0.023	
2008S2	0.085	0.075	0.075	0.055	0.051	0.034	
2009S1	0.070	0.068	0.067	0.057	0.047	0.030	
2009S2	0.071	0.067	0.067	0.055	0.044	0.031	
2010S1	0.105	0.093	0.089	0.075	0.068	0.046	
2010S2	0.092	0.081	0.080	0.065	0.057	0.033	
2011S1	0.105	0.099	0.096	0.082	0.071	0.045	
2011S2	0.082	0.077	0.076	0.062	0.049	0.041	
2012S1	0.078	0.079	0.077	0.059	0.046	0.035	
2012S2	0.073	0.071	0.071	0.054	0.044	0.036	
2013S1	0.079	0.083	0.081	0.063	0.051	0.042	
2013S2	0.073	0.073	0.072	0.057	0.046	0.042	
2014S1	0.068	0.066	0.065	0.050	0.037	0.032	
2014S2	0.068	0.067	0.066	0.051	0.040	0.036	
2015S1	0.063	0.062	0.061	0.046	0.034	0.028	
2015S2	0.053	0.054	0.053	0.039	0.030	0.028	
2016S1	0.057	0.058	0.057	0.044	0.035	0.031	
2016S2	0.063	0.064	0.064	0.051	0.040	0.036	
2017S1	0.066	0.062	0.061	0.049	0.040	0.036	0.0403
2017S2	0.065	0.061	0.060	0.048	0.040	0.036	
2018S1	0.073	0.069	0.068	0.056	0.049	0.041	
2018S2	0.084	0.079	0.077	0.065	0.060	0.051	
2019S1	0.086	0.074	0.073	0.062	0.054	0.046	

Annex I. Heating, cooling, humidification and dehumidification energy demands

In these three tables, the green colour means that the energy consumption diminishes, whilst the red colour means that the energy consumption increases. Plus, the value of the colour translates the magnitude of the decrease or increase in relation to the respective reference value, i.e. the light green means that the decrease is small and the dark green means that the decrease is substantial, while the light red means that the increase is small and the dark red means that the increase is substantial.

Table I.1 – Heating, cooling, humidification and dehumidification energy demand (kWh) for Thomson's methodology for IPCC scenario A1B and A2 between 1990 (reference case) and 2100 for Lisbon, Seville, Prague, Oslo and London

Climate		Ref	2020	2030	2040	2050	2060	2070	2080	2090	2100
Lisbon	Heat	**48,897**	43,958	40,940	39,080	36,245	34,844	32,599	31,755	29,708	29,713
			43,736	41,064	39,512	36,830	35,133	32,033	30,054	27,174	27,522
	Cooling	**392**	915	1,437	1,694	2,272	2,565	3,287	3,862	4,716	4,841
			934	1,278	1,647	2,071	2,732	3,840	4,937	6,542	6,762
	Humid.	**15**	3	1	0	0	0	0	0	0	0
			0	0	0	0	0	0	0	0	0
	Dehumid	**3,627**	4,862	5,524	6,176	6,945	7,563	8,372	8,879	9,647	9,916
			4,671	5,436	5,977	6,934	7,439	8,657	10,031	11,447	11,446
Seville	Heat	**49,958**	43,723	40,356	38,250	34,856	33,397	30,943	30,043	27,720	28,206
			43,134	40,125	38,469	35,728	33,900	30,357	28,466	25,389	25,809
	Cooling	**7,655**	12,452	14,407	16,615	18,820	21,161	23,188	25,752	27,919	28,464
			12,381	14,088	16,220	18,174	20,990	24,414	28,549	32,459	33,688
	Humid.	**345**	81	80	50	31	23	3	1	2	2
			55	75	54	35	15	7	1	1	0
	Dehumid	**4,343**	6,636	7,730	8,793	10,653	11,655	12,973	14,193	15,589	15,537
			6,923	8,080	8,999	9,933	11,686	13,601	15,691	18,124	18,570
Prague	Heat	**170,305**	155,830	151,078	146,907	142,198	138,805	135,164	132,054	128,344	128,341
			156,803	152,320	148,641	143,761	139,712	134,463	130,289	125,088	124,869
	Cooling	**0**	0	0	0	0	0	0	5	13	20
			0	0	0	0	0	3	20	97	171
	Humid.	**9,495**	8,272	7,856	7,410	6,906	6,551	6,213	5,821	5,486	5,445
			8,338	7,920	7,469	7,093	6,607	6,206	5,583	5,083	5,172
	Dehumid	**1,139**	1,820	1,965	1,869	2,258	2,739	2,507	3,137	3,522	3,166
			1,290	1,715	1,937	2,304	2,523	2,906	3,284	3,736	3,851
Oslo	Heat	**251,316**	229,359	223,466	218,024	212,166	207,005	202,130	197,765	192,944	191,864
			232,738	226,234	219,372	212,996	206,889	200,392	194,626	188,213	187,556
	Cooling	**0**	0	0	0	0	0	0	0	0	0
			0	0	0	0	0	0	0	0	0
	Humid.	**14,963**	12,970	12,400	11,947	11,380	10,869	10,377	9,810	9,518	9,462
			13,273	12,652	12,115	11,311	10,886	10,346	9,700	9,072	8,902
	Dehumid	**425**	411	693	734	799	1,083	1,193	1,433	1,691	1,581
			655	474	909	747	778	1,168	1,081	1,554	1,173

London	Heat	**145,903**	134,247	130,422	127,220	123,645	121,020	117,484	115,276	111,913	111,555
			136,019	132,150	129,018	125,215	121,960	117,682	114,343	109,942	109,938
	Cooling	**0**	0	0	0	0	0	0	0	0	0
			0	0	0	0	0	0	0	0	0
	Humid.	**4,927**	3,961	3,743	3,385	3,137	2,841	2,486	2,266	2,023	1,914
			4,168	3,768	3,502	3,220	2,999	2,616	2,331	1,974	2,028
	Dehumid	**1,503**	2,043	2,426	2,670	2,858	3,084	3,747	3,821	4,093	4,346
			1,882	2,403	2,569	2,759	2,936	3,436	4,035	4,638	4,413

Table I.2 – Heating, cooling, humidification and dehumidification energy demand (kWh) for ASHRAE's methodology for IPCC scenario A1B and A2 between 1990 (reference case) and 2100 for Lisbon, Seville, Prague, Oslo and London

Climate		Ref	2020	2030	2040	2050	2060	2070	2080	2090	2100
Lisbon	Heat	**1,770**	1,120	859	589	443	273	254	153	118	93
			1,091	839	600	482	271	204	111	62	29
	Cooling	**0**	0	0	0	0	0	0	0	0	0
			0	0	0	0	0	0	0	0	0
	Humid.	**13**	15	19	8	27	8	20	12	4	5
			0	22	3	42	9	4	3	9	5
	Dehumid	**124**	68	166	123	214	139	122	140	150	82
			108	126	92	168	55	144	156	172	170
Seville	Heat	**3,362**	2,067	1,442	1,117	754	535	396	278	224	191
			1,968	1,321	1,210	844	613	386	235	100	129
	Cooling	**0**	0	0	0	0	0	0	0	0	0
			0	0	0	0	0	0	0	0	0
	Humid.	**127**	77	77	74	154	187	131	135	87	50
			114	154	166	80	163	140	120	143	130
	Dehumid	**425**	286	224	309	464	359	330	448	291	221
			507	317	466	260	504	268	416	386	312
Prague	Heat	**80,037**	69,977	66,245	63,537	60,128	57,675	55,042	53,057	50,312	50,235
			70,704	67,309	64,496	61,377	58,554	54,800	51,921	47,873	48,049
	Cooling	**0**	0	0	0	0	0	0	0	0	0
			0	0	0	0	0	0	0	0	0
	Humid.	**208**	208	269	177	208	236	214	257	273	202
			258	226	201	279	204	261	227	276	229
	Dehumid	**290**	353	439	240	266	526	223	540	348	370
			294	380	324	316	345	301	304	219	398
Oslo	Heat	**144,827**	127,626	122,828	118,698	113,952	110,165	106,150	102,827	99,093	98,306
			130,689	125,085	120,121	114,751	110,454	105,115	100,606	95,432	95,167
	Cooling	**0**	0	0	0	0	0	0	0	0	0
			0	0	0	0	0	0	0	0	0
	Humid.	**330**	298	344	289	309	286	335	313	392	359
			279	313	301	325	293	316	309	392	324
	Dehumid	**478**	226	322	249	220	378	248	244	358	234
			398	156	386	197	132	296	253	363	134

London	Heat	**53,933**	46,768	44,100	42,220	39,688	38,140	35,789	34,591	32,287	32,331
			47,731	45,054	43,382	40,750	38,855	36,120	34,284	31,331	31,593
	Cooling	**0**	0	0	0	0	0	0	0	0	0
			0	0	0	0	0	0	0	0	0
	Humid.	**13**	13	44	21	21	29	35	38	33	100
			38	52	21	39	51	36	79	52	53
	Dehumid	**104**	92	164	186	156	141	182	157	197	193
			92	174	81	125	119	96	180	128	137

Table I.3 – Heating, cooling, humidification and dehumidification energy demand (kWh) for FCT-UNL methodology for IPCC scenario A1B and A2 between 1990 (reference case) and 2100 for Lisbon, Seville, Prague, Oslo and London

Climate		Ref	2020	2030	2040	2050	2060	2070	2080	2090	2100
Lisbon	Heat	**2,011**	1,260	1,150	764	738	468	549	373	443	314
			1,272	1,109	850	719	480	560	413	504	362
	Cooling	**1,176**	1,326	1,172	1,299	1,129	1,254	1,183	1,447	1,187	1,373
			1,269	1,079	1,258	1,290	1,340	1,155	1,324	1,207	1,243
	Humid.	**161**	153	81	153	161	116	130	213	152	163
			33	139	107	165	168	91	90	83	101
	Dehumid	**525**	694	880	978	1,071	1,283	1,191	1,377	1,382	1,456
			819	783	967	919	1,032	1,239	1,564	1,683	1,731
Seville	Heat	**4,046**	2,712	2,201	1,654	1,383	1,063	1,106	826	896	835
			2,587	2,083	1,808	1,535	1,258	1,035	738	883	852
	Cooling	**951**	1,013	916	1,241	870	1,144	1,019	1,165	1,045	1,166
			999	852	1,162	1,012	1,167	1,017	1,318	963	1,094
	Humid.	**71**	145	119	135	160	243	184	234	232	173
			81	327	241	170	220	252	111	227	286
	Dehumid	**636**	609	613	731	1,148	1,071	1,134	1,423	1,564	1,491
			662	566	781	816	1,101	1,177	1,518	1,766	1,855
Prague	Heat	**80,231**	70,143	66,384	63,726	60,362	57,850	55,242	53,179	50,474	50,324
			70,812	67,498	64,770	61,495	58,695	54,932	52,134	48,056	48,170
	Cooling	**329**	268	313	424	354	393	355	656	343	613
			564	416	492	373	493	520	528	561	891
	Humid.	**815**	735	815	653	721	614	660	673	702	578
			795	768	674	804	619	745	675	771	664
	Dehumid	**1,027**	1,018	1,099	790	765	1,115	761	1,078	951	825
			777	966	886	1,006	1,027	877	813	730	975
Oslo	Heat	**144,809**	127,641	122,849	118,689	113,947	110,166	106,200	102,877	99,197	98,409
			130,729	125,092	120,108	114,744	110,446	105,117	100,709	95,633	95,293
	Cooling	**161**	149	70	77	55	73	59	87	32	88
			123	94	76	40	113	16	163	31	83
	Humid.	**1,182**	1,024	1,098	1,031	1,030	955	1,036	1,012	1,079	1,036
			1,058	1,105	1,055	997	974	966	945	1,021	941
	Dehumid	**1,438**	1,045	1,125	1,085	998	1,091	1,077	1,111	1,176	995
			1,275	1,024	1,281	956	863	995	804	996	732

London	Heat	**54,026**	46,811	44,159	42,334	39,738	38,177	35,925	34,627	32,394	32,358
			47,772	45,103	43,476	40,829	38,897	36,172	34,349	31,496	31,662
	Cooling	**275**	347	345	241	262	356	250	328	372	360
			328	291	375	319	438	235	292	322	432
	Humid.	**221**	259	238	199	164	209	227	202	188	229
			229	236	197	226	228	237	204	261	203
	Dehumid	**383**	309	387	434	383	378	453	469	542	504
			279	397	299	321	313	350	502	512	512

Annex J. Skartveit and Olseth model

There are several models in literature that split the global radiation into direct and diffuse radiation – e.g. BRL model [223], Perez model [211] and *Skartveit and Olseth* model [255]. Lanini [166] compared the performance of several of these models and determined that the best performance was achieved by the *Skartveit and Olseth* model. Hence, this annex describes the methodology behind this model.

The *Skartveit and Olseth* model was firstly developed in 1986 [254] and then updated in 1998 [255]. This model splits the direct and diffuse components based on the diffuse faction and solar elevation concepts. However, since it was found to overestimate the diffuse faction under cloudless sky conditions, the 1998 update brought two new parameters, the regional surface albedo and the *hourly variability index* (σ_3), which is obtained through the following equations:

$$\sigma_3 = \left(\frac{(\rho_i - \rho_{i-1})^2 + (\rho_i - \rho_{i+1})^2}{2} \right)^{0.5} \quad \text{J.1}$$

Where σ_3 is the hourly variability index, ρ_i is the clear sky index for timestep *i*, ρ_{i-1} is the clear sky index for the timestep prior to *i* and ρ_{i+1} is the clear sky index for the timestep after *i*. Note that for the initial and last values, equation J.1 is simplified to the following form:

$$\sigma_3 = |\rho_i - \rho_{i\pm1}| \quad \text{J.2}$$

Where σ_3 is the hourly variability index, ρ_i is the clear sky index for timestep *i*, $\rho_{i\pm1}$ is the clear sky index for the timestep prior or after timestep *i* dependent to which σ_3 refers to. Equation J.2 is dependent on the data that is missing, which means that for the initial value the hourly variability index is $\rho_i - \rho_{i+1}$, whilst for the last value the hourly variability index is $\rho_i - \rho_{i-1}$. The *clear sky index* is determined using the following equation:

$$\rho_i = \frac{k}{k_1} \quad \text{J.3}$$

Where ρ_i is the clear sky index for timestep *i*, *k* is the clearness index and k_1 is the cloudless clearness index (which is obtained using equation J.10). The *clearness index* is obtained using the following equation:

$$k = \frac{H_g}{H_{ex}} \quad \text{J.4}$$

Where *k* is the clearness index, H_g is the surface global irradiance and H_{ex} is the extraterrestrial global irradiance (which is obtained using equation I.24). A low σ_3 is associated either with overcast ($\rho_i \approx 0$) or nearly cloudless sky ($0.9 < \rho_i < 1.0$). Consequently, the model is subdivided into the four situations depending on the clearness index (*k*). For low variability index values ($\sigma_3 \approx 0$), the diffuse fraction *d* is

calculated using the following equation system:

$$d = 1.00 \qquad k \leq 0.22 \qquad \text{J.5}$$

$$d = \int (k,h) = 1.00 - (1.00 - d_1) \cdot \left(0.11 \cdot \sqrt{K} + 0.15 \cdot K + 0.74 \cdot K^2\right) \qquad 0.22 \leq k \leq k_2 \qquad \text{J.6}$$

$$d = d_2 \cdot k_2 \cdot \frac{(1-k)}{\left(k \cdot (1-k_2)\right)} \qquad k_2 \leq k \leq k_{max} \qquad \text{J.7}$$

$$d = 1.00 - k_{max} \cdot \frac{(1-d_{max})}{k} \qquad k \geq k_{max} \qquad \text{J.8}$$

K in equation J.6 is calculated using the following equation system:

$$K = 0.5 \cdot \left(1 + sin\left(\frac{(k-0.22)}{(k_1-0.22)} \cdot \pi - \frac{\pi}{2}\right)\right) \qquad \text{J.9}$$

$$k_1 = 0.83 - 0.56 \cdot exp(-0.06 \cdot h) \qquad \text{J.10}$$

$$k_2 = 0.95 \cdot k_1 \qquad \text{J.11}$$

$$d_1 = 0.07 + 0.046 \cdot \frac{(90-h)}{(h+3)} \qquad \text{J.12}$$

Where *h* is the solar elevation (º). Note that d_1 has a unitary value if h ≤ 1.4º [255]. The $d_2 = \int(k_2,h)$ in equation J.7 is calculated using J.6, J.9, J.10, J.11 and J.12. In turn, the k_{max} is calculated using the following equation system:

$$k_{max} = \frac{\left(k_{b,max} + \frac{d_2 \cdot k_2}{(1-k_2)}\right)}{\left(1 + \frac{d_2 \cdot k_2}{(1-k_2)}\right)} \qquad \text{J.13}$$

$$k_{b,max} = 0.81^{\alpha} \qquad \text{J.14}$$

$$\alpha = \left(\frac{1}{\sin(h)}\right)^{0.6} \qquad \text{J.15}$$

Where *h* is the solar elevation (º). In turn, the d_{max} is calculated using the following equation:

$$d_{max} = d_2 \cdot k_2 \left(\frac{(1-k_{max})}{k_{max} \cdot (1-k_2)}\right) \qquad \text{J.16}$$

On the other hand, for higher variability index values ($\sigma_3 > 0$) it is necessary to add a $\Delta(k, h, \sigma_3)$ term to equation J.5, J.6, J.7 and J.8 so that the effect of variable/inhomogeneous clouds is accounted for [255]:

$$\Delta(k,h,\sigma_3) = 0 \qquad k \leq 0.14 \qquad \text{J.17}$$

$$\Delta(k,h,\sigma_3) = -3k_L^2 \cdot (1-k_L) \cdot \sigma_3^{1.3} \qquad 0.14 \leq k \leq k_x \qquad \text{J.18}$$

$$\Delta(k,h,\sigma_3) = 3k_R \cdot (1-k_R)^2 \cdot \sigma_3^{0.6} \qquad k_x \leq k \leq k_x + 0.71 \qquad \text{J.19}$$

$$\Delta(k,h,\sigma_3) = 0 \qquad k \geq k_x + 0.71 \qquad \text{J.20}$$

Where the k_x, k_L and k_R are calculated using equation J.21, J.22 and J.23, respectively:

$$k_x = 0.56 - 0.32 \cdot exp(-0.06 \cdot h) \qquad \text{J.21}$$

$$k_L = \frac{(k-0.14)}{(k_x - 0.14)} \qquad \text{J.22}$$

$$k_R = \frac{(k-k_x)}{0.71} \qquad \text{J.23}$$

Where h is the solar elevation (º) and k is the clearness index. Figure 2, figure 3a and figure 3b of Ref. [255] were recreated using the code developed for this thesis to validate the developed code. Figure J.1 presents the obtained results that, when compared with the respective figures in Ref. [255], show that the obtained results perfectly overlay the values presented in Ref. [255], thus validating the code.

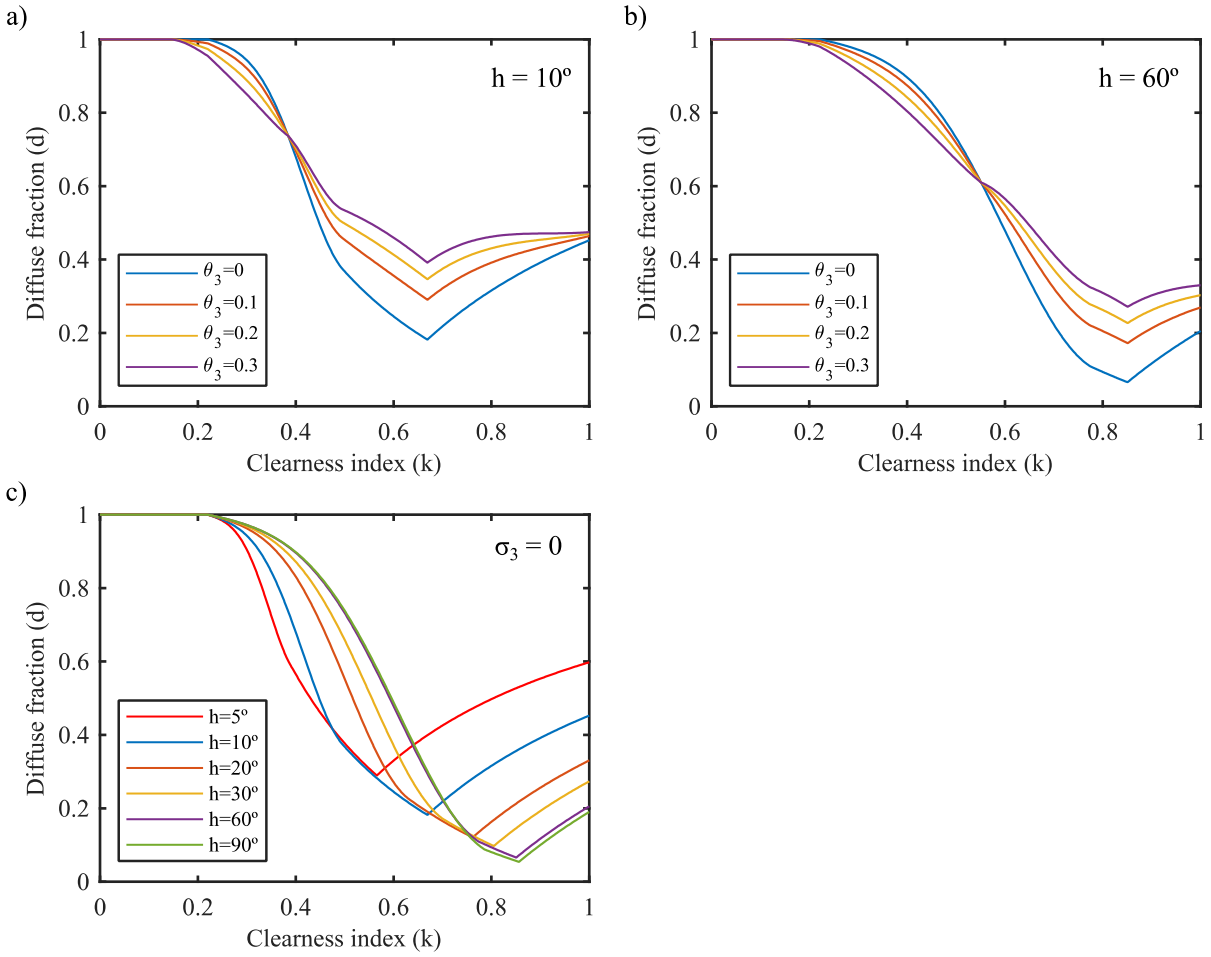

Figure J.1 – Diffuse fraction vs clearness index for four variability indices for solar elevation of 10º (a) and 60º (b), and

diffuse fraction vs clearness index for six solar elevations for invariable hours (c)

The extraterrestrial solar radiation (H_{ex}, W/m^2) variance can be obtained using the following equation:

$$H_{ex} = G_{sc}\left(1 + 0.033\cos\frac{360 \cdot n}{365}\right) \qquad \text{J.24}$$

G_{sc} is the *solar constant* (1367 w/m^2 [78]) and n is the nth day of the year. The application of this equation results in the variance depicted in Figure J.2. According to *Duffie and Beckman* [78], this equation is suitable to determine the variance of the extraterrestrial radiation throughout the year for most engineering problems, but for a more accurate analysis *Iqbal* [143] supports the use of the equation developed by *Spencer* [257].

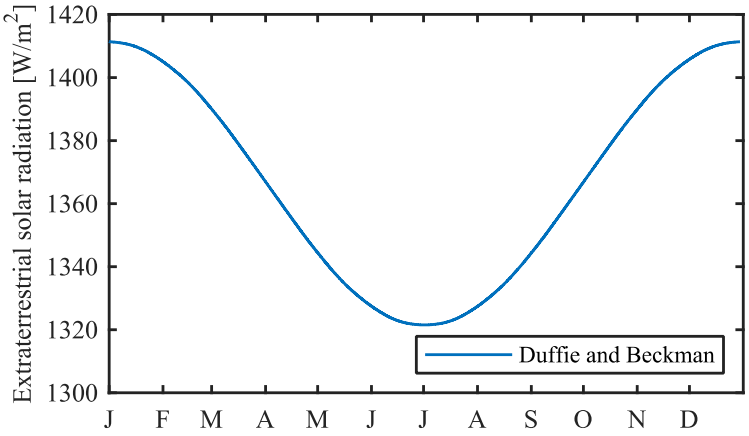

Figure J.2 – Variance of the extreterrestrial solar radiation through the year

The solar elevation (h,º) was obtained using the MATLAB code developed by *Mikofski* [189], which suffered adaptations to serve the aims of this thesis more adequately. This code is based on the equations that calculate the solar zenith angle and the solar azimuth angle depending on the angle of incidence, the declination and the hour angle, which is described for example in *Duffie and Beckman* [78] by equations 1.6.5 and 1.6.6, respectively. For the code to run it is necessary to input the location (latitude and longitude, in degrees), timezone (offset relative to the UTC in hours) and rotation (in degrees). Its outputs are the solar zenith and azimuth for the selected location throughout the selected period of time. Solar elevation angle (h) and the solar zenith angle (z) are complementary angles (Figure J.3).

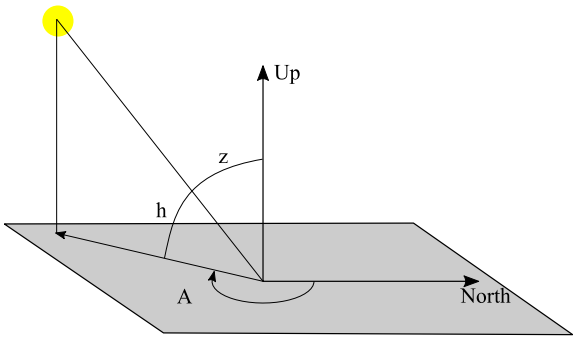

Figure J.3 – Graphical representation of the solar elevation angle (h), solar zenith angle (z) and solar azimuth angle (A) (figure adapted from Ref. [198])

This code's performance can easily be compared with, for example, a reliably online solar position calculator [199]. This was performed for Lisbon – i.e. longitude: -9.13333º, latitude: 38.71667º, timezone: 0 h and rotation: 0º. The presented results show that the values obtained from the MATLAB code are very similar to the values obtained from NOAA ESRL's solar position calculator (Table J.1).

Table J.1 – Solar zenith (º), solar elevation (º) and sun azimuth (º) values for Lisbon in 16/6/2019 between 6h00–19h00, which were obtained using NOAA ESRL calculator [199] and the MATLAB code [189]

Date	NOAA ESRL			MATLAB code		
	Solar zenith [º]	Solar elevation [º]	Sun azimuth [º]	Solar zenith [º]	Solar elevation [º]	Sun azimuth [º]
16/6/19 6:00	82.292	7.708	66.092	82.362	7.638	66.114
16/6/19 7:00	71.345	18.655	74.585	71.347	18.653	74.608
16/6/19 8:00	59.896	30.104	82.964	59.877	30.123	82.989
16/6/19 9:00	48.227	41.773	92.003	48.197	41.803	92.035
16/6/19 10:00	36.643	53.357	103.099	36.607	53.393	103.146
16/6/19 11:00	25.733	64.268	119.560	25.697	64.303	119.646
16/6/19 12:00	17.285	72.715	150.060	17.264	72.736	150.239
16/6/19 13:00	16.114	73.886	199.176	16.137	73.863	199.386
16/6/19 14:00	23.358	66.642	234.911	23.410	66.590	235.021
16/6/19 15:00	33.925	56.075	253.653	33.992	56.008	253.715
16/6/19 16:00	45.421	44.579	265.612	45.497	44.503	265.656
16/6/19 17:00	57.101	32.899	274.979	57.188	32.812	275.016
16/6/19 18:00	68.624	21.376	283.433	68.728	21.272	283.469
16/6/19 19:00	79.722	10.278	291.844	79.871	10.129	291.882

Annex K. Reference year weather files

Standard EN 15927-4 [89] describes a two-step procedure to construct a representative year that is based on multi-year records of, at least, four meteorological variables. The following four meteorological variables in hourly values are used to develop such representative years:

- Temperature (ºC)
- Relative humidity (%)
- Global radiation (W/m^2)
- Wind speed at a height of 10 m above ground (m/s)

Note that this standard also accounts for the use of more than these four meteorological variables, which is normal in most cases of hygrothermal simulations (see subchapter 3.2.1). The following steps thoroughly describe this procedure:

1st step: Select the best representative month from the multi-year records. Perform this selection for each of the twelve months that compose a year, i.e. January, February, March, April, May, June, July, August, September, October, November and December; which is based, at least, on a 10-year worth of records. The temperature, relative humidity and global radiation are designated as primary parameters (ρ) and the wind speed is designated as secondary parameter, which is used in step *f* of this procedure:

a. Determine the *daily means* for each of the three primary parameters

b. For each month determine the *cumulative distribution function* of the daily means of all years of the selected dataset by sorting all values in increasing order. Lastly, the following equation is used:

$$\Phi(p,m,i) = \frac{K(i)}{N+1} \qquad \text{K.1}$$

Where $\Phi(p,m,i)$ is the cumulative distribution function, $K(i)$ is the rank of the i value of the daily mean for the respective primary parameter within that calendar month in the whole data set, and N is the number of days in each calendar month in the whole data set (e.g. for a 10-year data set January has an overall day count of 310 days)

c. Determine the *cumulative distribution function* of the daily means within each calendar month for each year of the dataset by sorting all the values for that month and that year in increasing order. Lastly, the following equation is used:

$$\mathrm{F}(p,y,m,i) = \frac{J(i)}{n+1} \qquad \text{K.2}$$

Where $F(p,y,m,i)$ is the cumulative distribution function of the daily means within each calendar

month for each year, *J(i)* is the rank of the *i* value of the daily mean for the respective primary parameter within that calendar month and that year, and *n* number of days in each month.

d. Determine the *Finkelstein-Schafer statistic* for each calendar month of each year using the following equation:

$$F_S(p,y,m) = \sum_{i=1}^{n} |\mathrm{F}(p,y,m,i) - \Phi(p,m,i)| \qquad \text{K.3}$$

Where $F_s(p,y,m)$ is the Finkelstein-Schafer statistic, $F(p,y,m,i)$ is the cumulative distribution function of the daily means within each calendar month for each year, and $\Phi(p,m,i)$ is the cumulative distribution function

e. Rank each month from the data set in increase order according to its Finkelstein-Schafer statistic. This procedure is performed for each of the twelve calendar months, i.e. January, …, December

f. Sum the three rankings for each calendar month. For the three-lowest overall ranking months calculate the deviation between the monthly mean wind speed and the multi-year calendar-month mean. Lastly, select the month with the lowest wind speed deviation

2nd step: In order to smooth the transaction between the selected months, submit the last eight hours of the prior month and the first eight hours of the posterior month to an interpolation process. Note that December and January should also be submitted to this interpolation process since hygrothermal simulation tend to be run for more than one year

Annex L. Recommend thicknesses ranges and MRF for ceilings/roofs for Lisbon and Seville

Table L.1 – Thickness range (cm) that outperforms the case-study without any retrofit measure (WR) for Lisbon and Seville for future conditions – RCP 4.5 and RCP 8.5

Climate	Scenario	Parameter	W1 (2-20)		W2 (2-20)		W3 (2-20)		W4 (2-20)		W5 (1.5-5.0)		R1 (2-10)		R2 (2-10)		C1 (2-10)		C2 (2-10)	
Lisbon	RCP 4.5	MRF	7	20	2	20	4	20	2	20	1.5	5.0	2	10	2	10	2	10	3	10
		eLM	0	0	0	0	0	0	0	0	1.5	3.0	0	0	0	0	0	0	2	3
		Furniture	2	20	2	20	2	20	2	20	1.5	5.0	2	10	2	10	2	10	2	10
		Sculpture	0	0	0	0	0	0	0	0	0	0	2	10	2	10	2	10	4	10
		Base layer	2	20	2	20	2	20	2	20	1.5	5.0	2	10	2	10	2	10	3	10
		Pictorial layer	2	20	2	20	2	20	2	20	1.5	5.0	8	10	0	0	2	10	2	10
		Thermal comfort	2	20	2	20	2	20	2	20	2.2	5.0	2	10	2	10	2	10	4	10
	RCP 8.5	MRF	15	20	2	20	6	20	2	20	1.5	5.0	2	10	2	10	2	10	3	10
		eLM	0	0	0	0	0	0	0	0	1.5	3.5	0	0	0	0	0	0	2	3
		Furniture	2	20	2	20	2	20	2	20	1.5	5.0	2	10	2	10	2	10	2	10
		Sculpture	0	0	0	0	0	0	0	0	0	0	2	10	2	10	0	0	0	0
		Base layer	2	20	2	20	2	20	2	20	1.5	5.0	2	10	2	10	2	10	3	10
		Pictorial layer	3	20	2	20	2	20	2	20	1.5	5.0	0	0	0	0	2	10	2	10
		Thermal comfort	2	20	2	20	2	20	2	20	1.5	5.0	2	10	2	10	2	10	4	10
Seville	RCP 4.5	MRF	18	20	7	20	11	20	2	20	1.5	5.0	2	10	2	10	2	10	3	10
		eLM	2	20	2	20	2	20	2	20	1.5	5.0	0	0	0	0	2	10	2	7
		Furniture	2	20	2	20	2	20	2	20	1.5	5.0	2	10	2	10	2	10	2	10
		Sculpture	0	0	0	0	0	0	0	0	1.5	5.0	2	10	2	10	2	10	4	10
		Base layer	2	20	2	20	2	20	2	20	1.5	5.0	2	10	2	10	2	10	2	10
		Pictorial layer	2	20	2	20	2	20	2	20	1.5	5.0	2	10	2	10	2	10	2	10
		Thermal comfort	2	20	2	6	2	8	2	20	0	0.0	2	10	2	10	2	10	4	9
	RCP 8.5	MRF	0	0	10	20	0	0	2	20	1.5	5.0	2	10	2	10	2	10	4	10
		eLM	2	20	2	20	2	20	2	20	1.5	5.0	0	0	0	0	2	10	2	6
		Furniture	2	20	2	20	2	20	2	20	1.5	5.0	2	10	2	10	2	10	2	10
		Sculpture	0	0	0	0	0	0	0	0	0	0	0	0	0	0	0	0	0	0
		Base layer	4	20	2	20	2	20	2	20	1.6	5.0	2	10	2	10	2	10	3	10
		Pictorial layer	2	20	2	20	2	20	2	20	1.5	5.0	4	10	5	10	2	10	2	10
		Thermal comfort	0	0	0	0	0	0	0	0	0	0	2	10	2	10	0	0	0	0

Table L.2 – Thickness range (cm) that outperforms the case-study without any retrofit measure (WR) for Prague and Oslo for future conditions – RCP 4.5 and RCP 8.5

Climate	Scenario	Parameter	W1 (2-20)		W2 (2-20)		W3 (2-20)		W4 (2-20)		W5 (1.5-5)		R1 (2-10)		R2 (2-10)		C1 (2-10)		C2 (2-10)	
Prague	RCP 4.5	MRF	8	20	2	20	6	20	2	20	0	0	0	0	2	10	2	10	3	10
		eLM	0	0	0	0	0	0	0	0	1.5	1.6	0	0	0	0	0	0	2	2
		Furniture	2	20	2	20	2	20	2	20	1.5	5.0	2	10	2	10	2	10	2	10
		Sculpture	0	0	8	20	0	0	7	20	2.0	5.0	2	4	4	4	0	0	0	0
		Base layer	2	20	2	20	2	20	2	20	0	0	2	10	2	10	2	10	3	10
		Pictorial layer	0	0	0	0	0	0	0	0	0	0	0	0	0	0	0	0	0	0
		Thermal comfort	2	20	2	20	2	20	2	20	1.5	5.0	2	10	2	10	2	10	3	10
	RCP 8.5	MRF	0	0	10	20	0	0	4	20	0	0	2	10	2	10	2	10	4	10
		eLM	0	0	0	0	0	0	0	0	1.5	2.0	0	0	0	0	0	0	2	2
		Furniture	2	20	2	20	2	20	2	20	1.5	5.0	2	10	2	10	2	10	2	10
		Sculpture	0	0	0	0	0	0	0	0	0	0	0	0	0	0	0	0	0	0
		Base layer	3	20	2	20	2	20	2	20	0	0	2	10	2	10	2	10	3	10
		Pictorial layer	0	0	0	0	0	0	0	0	0	0	2	2	2	3	0	0	0	0
		Thermal comfort	2	20	2	20	2	20	2	20	2.2	3.4	2	10	2	10	2	10	3	10
Oslo	RCP 4.5	MRF	4	20	2	20	3	20	2	20	0	0	0	0	2	10	2	10	3	10
		eLM	0	0	0	0	0	0	0	0	0	0	0	0	0	0	0	0	2	2
		Furniture	2	20	2	20	2	20	2	20	1.5	5.0	2	10	2	10	2	10	2	10
		Sculpture	0	0	0	0	0	0	0	0	2.0	2.0	0	0	0	0	0	0	0	0
		Base layer	2	20	2	20	2	20	2	20	2.3	5.0	2	10	2	10	2	10	2	10
		Pictorial layer	0	0	0	0	0	0	0	0	0	0	0	0	2	2	0	0	0	0
		Thermal comfort	2	20	2	20	2	20	2	20	1.7	5.0	2	10	2	10	2	10	3	10
	RCP 8.5	MRF	5	20	2	20	3	20	2	20	0	0	2	10	2	10	2	10	3	10
		eLM	0	0	0	0	0	0	0	0	0	0	0	0	0	0	0	0	2	2
		Furniture	2	20	2	20	2	20	2	20	1.5	5.0	2	10	2	10	2	10	2	10
		Sculpture	0	0	0	0	0	0	0	0	2.0	2.0	0	0	0	0	0	0	0	0
		Base layer	2	20	2	20	2	20	2	20	1.8	5.0	2	10	2	10	2	10	2	10
		Pictorial layer	0	0	0	0	0	0	0	0	0	0	0	0	0	0	0	0	0	0
		Thermal comfort	2	20	2	20	2	20	2	20	1.5	5.0	2	10	2	10	2	10	3	10

Table L.3 – Thickness range (cm) that outperforms the case-study without any retrofit measure (WR) for London for future conditions – RCP 4.5 and RCP 8.5

Climate	Scenario	Parameter	W1 (2-20)		W2 (2-20)		W3 (2-20)		W4 (2-20)		W5 (1.5-5)		R1 (2-10)		R2 (2-10)		C1 (2-10)		C2 (2-10)	
London	RCP 4.5	MRF	7	20	2	20	5	20	2	20	0	0	2	10	2	10	2	10	3	10
		eLM	0	0	0	0	0	0	0	0	0	0	0	0	0	0	0	0	2	2
		Furniture	2	20	2	20	2	20	2	20	1.5	5.0	2	10	2	10	2	10	2	10
		Sculpture	0	0	0	0	0	0	2	20	0	0	0	0	0	0	0	0	0	0
		Base layer	2	20	2	20	2	20	2	20	1.7	5.0	2	10	2	10	2	10	2	10
		Pictorial layer	2	20	2	20	2	20	2	20	0	0	3	10	3	10	2	10	2	10
		Thermal comfort	2	20	2	20	2	20	2	20	2.0	5.0	2	10	2	10	2	10	3	10
	RCP 8.5	MRF	5	20	2	20	3	20	2	20	2.7	5.0	2	10	2	10	2	10	3	10
		eLM	0	0	0	0	0	0	0	0	0	0	0	0	0	0	0	0	2	2
		Furniture	2	20	2	20	2	20	2	20	1.5	5.0	2	10	2	10	2	10	2	10
		Sculpture	0	0	0	0	0	0	0	0	0	0	0	0	0	0	0	0	0	0
		Base layer	2	20	2	20	2	20	2	20	1.8	5.0	2	10	2	10	2	10	2	10
		Pictorial layer	0	0	0	0	0	0	20	20	0	0	0	0	0	0	0	0	0	0
		Thermal comfort	2	20	2	20	2	20	2	20	3.0	5.0	2	10	2	10	2	10	3	10

Table L.4 – Thickness range (cm) in which the indoor climate is in ideal conditions (IC) for the five climates in future conditions – RCP 4.5 and RCP 8.5

Climate	Scenario	Parameter	W1 (2-20)		W2 (2-20)		W3 (2-20)		W4 (2-20)		W5 (1.5-5)		R1 (2-10)		R2 (2-10)		C1 (2-10)		C2 (2-10)	
Lisbon	RCP 4.5	MRF	0	0	8	20	0	0	4	20	4.0	5.0	2	10	2	10	0	0	0	0
		eLM	0	0	0	0	0	0	0	0	0	0	0	0	0	0	0	0	0	0
	RCP 8.5	MRF	0	0	0	0	0	0	0	0	0	0	0	0	0	0	0	0	0	0
		eLM	0	0	0	0	0	0	0	0	0	0	0	0	0	0	0	0	0	0
Seville	RCP 4.5	MRF	2	20	2	20	2	20	2	20	1.5	5.0	2	10	2	10	2	10	2	10
		eLM	0	0	0	0	0	0	0	0	0	0	0	0	0	0	0	0	0	0
	RCP 8.5	MRF	0	0	0	0	0	0	0	0	0	0	0	0	0	0	0	0	0	0
		eLM	0	0	0	0	0	0	0	0	0	0	0	0	0	0	0	0	0	0
Prague	RCP 4.5	MRF	2	20	2	20	2	20	2	20	1.5	5.0	2	10	2	10	2	10	2	10
		eLM	2	20	2	20	2	20	2	20	1.5	5.0	2	10	2	10	2	10	2	10
	RCP 8.5	MRF	0	0	0	0	0	0	0	0	0	0	0	0	0	0	0	0	0	0
		eLM	2	20	2	20	2	20	2	20	1.5	5.0	2	10	2	10	2	10	2	10
Oslo	RCP 4.5	MRF	2	20	2	20	2	20	2	20	1.5	5.0	2	10	2	10	2	10	2	10
		eLM	2	20	2	20	2	20	2	20	1.5	5.0	2	10	2	10	2	10	2	10
	RCP 8.5	MRF	0	0	0	0	0	0	0	0	0	0	0	0	0	0	0	0	0	0
		eLM	2	20	2	20	2	20	2	20	1.5	5.0	2	10	2	10	2	10	2	10
London	RCP 4.5	MRF	2	20	2	20	2	20	2	20	1.5	5.0	2	10	2	10	2	10	2	10
		eLM	2	20	2	20	2	20	2	20	1.5	5.0	2	10	2	10	2	10	2	10
	RCP 8.5	MRF	2	20	2	20	2	20	2	20	1.5	5.0	2	10	2	10	2	10	2	10
		eLM	2	20	2	20	2	20	2	20	1.5	5.0	2	10	2	10	2	10	2	10

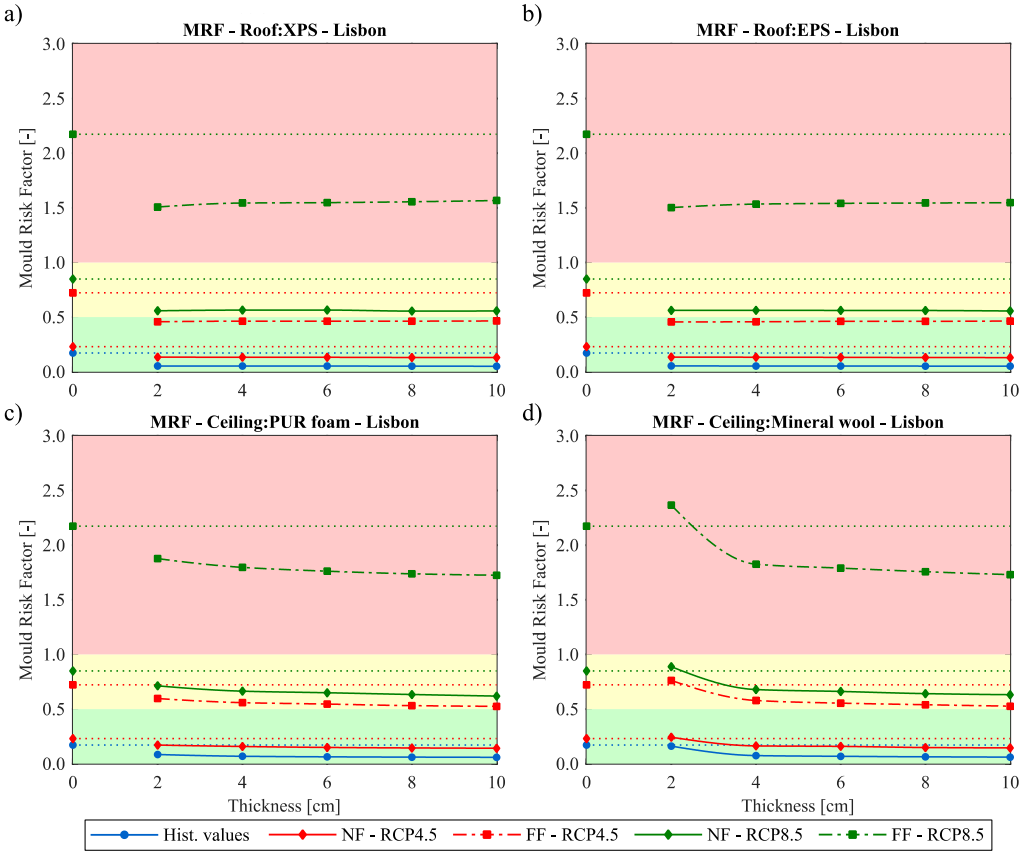

Figure L.1 – Mould risk factor (MRF) assessment for the ceilings/roofs retrofits for Lisbon

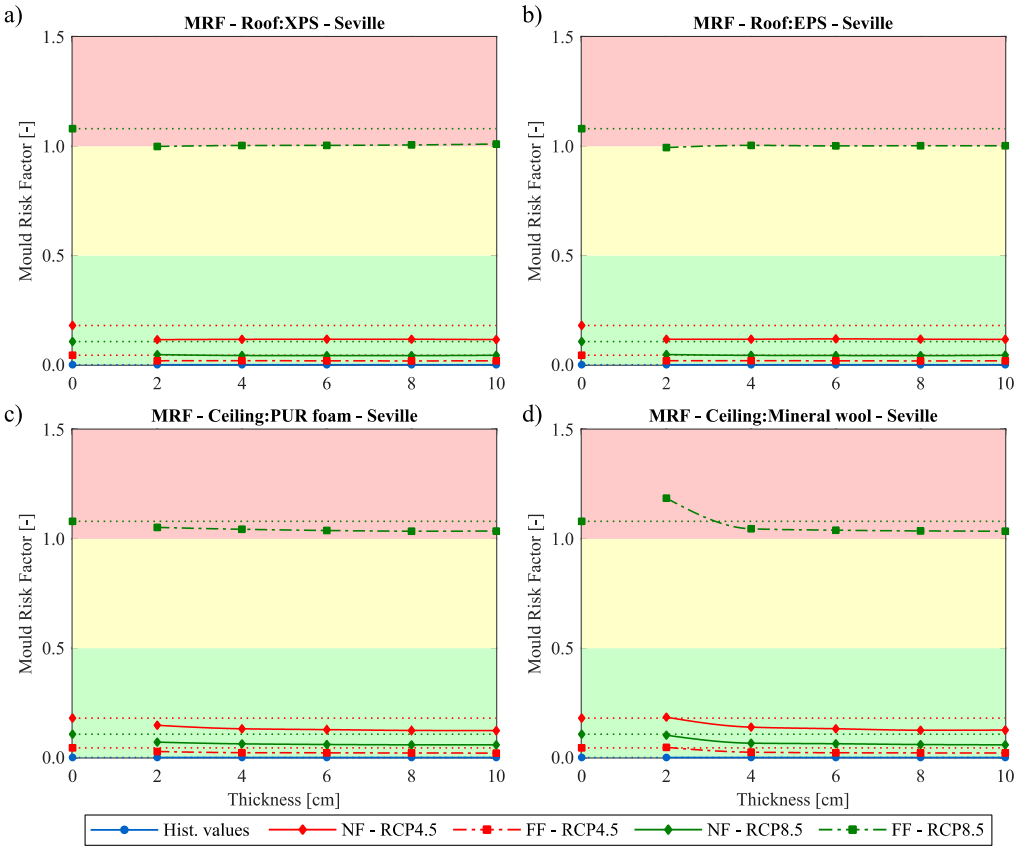

Figure L.2 – Mould risk factor (MRF) assessment for the ceilings/roofs retrofits for Seville